Faculté des Sciences

UNIVERSITÉ DE NEUCHÂTEL

Institut de Chimie

Synthesis, characterization and exploration of the catalytic, supramolecular and biological applications of dinuclear complexes

Thèse présentée à la Faculté des Sciences de l`Université de Neuchâtel

Pour l`obtention du grade de Docteur ès Sciences par

Justin Paul Raj Johnpeter

Master of Science (General Chemistry), St. Joseph`s College, Bharathidasan University, Tiruchirappalli, India

Directeur de thèse: **Prof. Bruno Therrien**

Membres du jury:

Prof. Bruno Therrien	Directeur de thèse, Université de Neuchâtel, Suisse
Prof. Robert Deschenaux	Rapporteur interne, Université de Neuchâtel, Suisse
Prof. Stefano Brenna	Rapporteur externe, University of Insubria, Italy

22.10.2013

UNIVERSITÉ DE NEUCHÂTEL

Faculté des sciences
Secrétariat-décanat de Faculté
Rue Emile-Argand 11
2000 Neuchâtel - Suisse
Tél: + 41 (0)32 718 2100
E-mail: secretariat.sciences@unine.ch

IMPRIMATUR POUR THESE DE DOCTORAT

La Faculté des sciences de l'Université de Neuchâtel autorise l'impression de la présente thèse soutenue par

Monsieur Justin Paul Raj JOHNPETER

Titre: "Synthesis, charactererization and exploration of the catalytic, supramolecular and biological applications of dinuclear complexes"

sur le rapport des membres du jury:

- Prof. ass. Bruno Therrien, Université de Neuchâtel, directeur de thèse
- Prof. Robert Deschenaux, Université de Neuchâtel
- Dr Stefano Brenna, Università degli studi dell'insubria, Como, Italie

Neuchâtel, le 28 octobre 2013

Le Doyen, Prof. P. Kropf

Table of contents

Acknowledgments

The work presented in this thesis has been done in the laboratoire de chimie organométallique et de catalyse moléculaire, Institut de chimie, Université de Neuchâtel, Switzerland, under the direction of Prof. Bruno Therrien.

First and foremost, I would like to express my sincere thanks to my research advisor Prof. Bruno Therrien for offering me the opportunity to work in his group. I have learned a lot during these years, thank you very much for your guidance and support.

Prof. Stefano Brenna and Prof. Robert Deschenaux, thank you for taking interest in my work and accepting to be in members of jury.

I owe my special thanks to all my collaborators, Dr. L. Plasseraud, Dr. N. Armaroli, Dr. F. Schmitt and Dr. N. Nagesh, for their contribution in my work.

I want to thank all the members (past and present) in my group, Prof. Georg Süss-Fink, Dr. Johan Mattason, Dr. Michaël Gras, Dr. Nicolas Barry, Dr. Trieu-Tien Thai, Dr. Farooq-Ahmad Khan, Dr. Julien Freudenreich, Anne-Flore Ibao, Dr. Mona Anca Furrer, Dr. M. Ulaganatha Raja, Dr. Gajendra Gupta, Dr. Nandhagopal Raja, Amine Garci, Sun Bing, Emmanuel Denoyelle, Thomas Cheminel, David Stibal, Minghui Yuan for all the good moments that we have shared and for their collaboration.

I must thank the technical staffs Dr. Claudio Dalvit and Dr. Armelle vallet for their help in NMR and Mass spectroscopic experiments. Special thanks to Mrs. Tissot for aid in administrative issues.

My special thanks to my beloved akka Dr. M. Baby Mariyatra for introducing me chemistry. Especially, for your moral support and encouragement in all the times from my childhood, without you I would not be where I am today with all the great experiences that I have had. A big thanks to my cousin-in-law Dr. Mothi, for teaching me chemistry. Very special thanks to my best friends, Dr. John Mohanraj and Dr. Percia for their constant help and support. I would like to extend my thanks to all my friends who encouraged and supported me throughout my PhD time.

I must thank my family members for their encouragement, prayers and unselfish support throughout my life.

Last but not least: I thank the GOD almighty for providing me enough physical and intellectual strength to carry out my research successfully and to achieve this position.

Summary

The work presented in this thesis involves the synthesis and characterization of dinuclear ruthenium, rhodium and iridium complexes. The catalytic, supramolecular and biological applications of these dinuclear complexes will be discussed. In the first part, the synthesis of sawhorse-type diruthenium tetracarbonyl complexes and their catalytic applications in the supercritical carbon dioxide ($scCO_2$) are presented. Synthesis of sawhorse-type molecular tweezers derived from pyrenyl and porphyrin carboxylic derivatives are presented in the second part. The host-guest interactions between the sawhorse-type molecular tweezers with different guest molecules will be discussed. In the final part, the anticancer potential of dinuclear ruthenium, rhodium and iridium complexes are evaluated with different cancer cell lines.

Keywords

Carbonyl ligands, Carboxylato bridges, Fatty acids, Dinuclear complexes, Ruthenium, Rhodium, Iridium, Fluorinated fatty acids, Supercritical carbon dioxide, Molecular recognition, Porphyrin tweezers, Pyrene tweezers, Supramolecular chemistry, Multinuclear complexes, Photosensitizers, Porphyrin ligand, Bio-organometallic, Photodynamic therapy, Biologically active acids.

DEDICATED TO MY PARENTS

Chapter 1:

General Introduction

1. General Introduction

1.1. Metal carbonyl complexes

Families of metal carbonyls are well known for their interesting structural features and for their versatile applications not only in the field of catalysis like Monsanto and Cativa processes but also in biological and supramolecular chemistry. The remarkable stability of metal carbonyl complexes is achieved by the "π back-bonding" involvement of the metal d-orbitals and carbonyl ligands (Fig. 1).

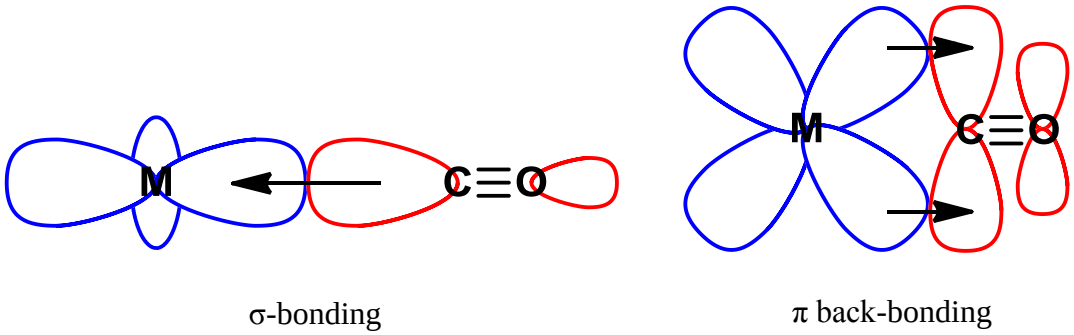

Fig. 1. *The p-orbital of carbonyl ligand gives an unshared pair of electrons to the vacant d-orbital of the metal through σ-bonding. The filled d-orbital of the metal gives back an electron to the anti-bonding p-orbital of CO through π back-bonding (dπ → pπ*). (Picture taken from[1])*

Two different kinds of metal carbonyls exist, namely the homoleptic and the heteroleptic. The homoleptic is metal carbonyl complexes containing identical ligands for example, $Ni(CO)_4$, $Fe(CO)_5$, $Cr(CO)_6$, $Fe_3(CO)_{12}$, $Ru_3(CO)_{12}$ and $Os_3(CO)_{12}$. The heteroleptic is metal carbonyl complexes containing more than one type of ligands for example, $Re(CO)_3$(2,2'-bpy)Cl (bpy = 2,2'-bipyridine) and $IrCl(CO)_2$.

The most straightforward way to synthesize metal carbonyls is through reduction of the corresponding metallic salt under a high pressure of carbon monoxide. Among the transition metal catalysts, ruthenium carbonyl clusters have played an important role in catalysis due to the plethora of applications that were made since its discovery. The production of the ruthenium carbonyl cluster, dodecacarbonyltriruthenium $\{Ru_3(CO)_{12}\}$, involves high temperature and high pressure (120 ºC, 65 bar of CO), which yields modest

amounts of $Ru_3(CO)_{12}$.[2] Fauré *et al*.[3] have produced $Ru_3(CO)_{12}$ in one pot in ethylene glycol under milder conditions with a relatively moderate yield. Since then, other methods have also been reported for the synthesis of $Ru_3(CO)_{12}$.[4] Notably, the recent method using microwave gave very high yield up to 90 % of $Ru_3(CO)_{12}$ even under very low CO pressure (3.5 bar).[5] $Ru_3(CO)_{12}$ was characterized by IR spectroscopy which showed the corresponding CO absorption bands [$\nu_{(CO)}$, 2011 (m), 2030 (s), 2060 (vs) cm^{-1}].[3] X-ray structure of $Ru_3(CO)_{12}$ was reported by Mason *et al*.[6] which demonstrated that the trinuclear ruthenium was coordinated to 12 carbonyl ligands in terminal positions to form a symmetrical ruthenium cluster (Fig. 2).

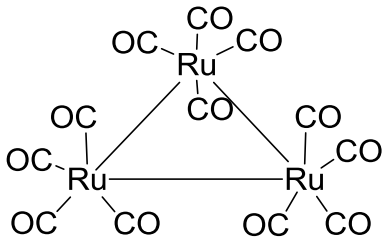

Fig. 2. *Structural representation of dodecacarbonyltriruthenium $Ru_3(CO)_{12}$.*

1.2. Sawhorse-type diruthenium tetracarbonyl complexes

Among ruthenium carbonyls, complexes having $Ru_2(CO)_4$ backbone with a typical sawhorse-type geometry are well known for their applications in catalysts, liquid crystals, bioactive substances and also as supramolecular materials.[7] Sawhorse-type diruthenium tetracarbonyl complexes are synthesized from the precursor $Ru_3(CO)_{12}$. In 1969, Lewis *et al*.[8] introduced a method for the synthesis of sawhorse-type diruthenium tetracarbonyl complexes. Refluxing $Ru_3(CO)_{12}$ with carboxylic acids, RCOOH (R = H, CH_3, C_2H_4 or n-C_9H_{19}) gave yellow-orange polymeric material, $[Ru_2(CO)_4(OOCR)_2]_n$ (R = H, CH_3, C_2H_4 or n-C_9H_{19}). Depolymerization of this material can be achieved using coordinating solvents {tetrahydrofuran (thf) or acetonitrile}. Addition of monodentate ligands such as pyridine, acetonitrile or phosphine affords stable dinuclear tetracarbonyl complexes (Fig. 3).

$$2/3\ Ru_3(CO)_{12} + 2\ RCOOH + 2\ L \rightarrow Ru_2(CO)_4(OOCR)_2L_2 + 4\ CO + H_2 \qquad \text{(eq. 1)}$$

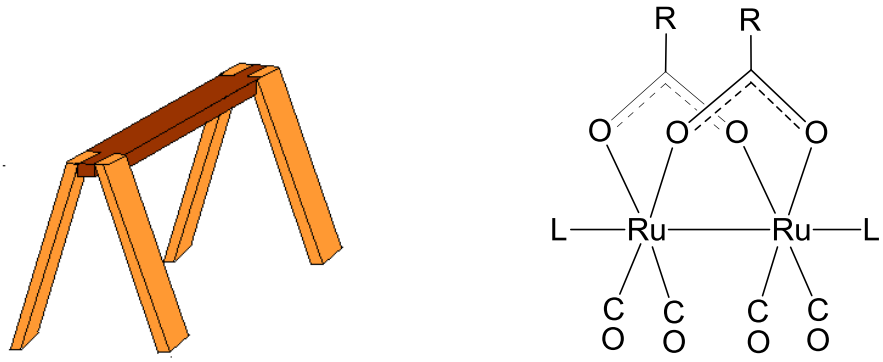

Fig. 3. *The sawhorse geometry of $[Ru_2(CO)_4(OOCR)_2L_2]$ complexes.*

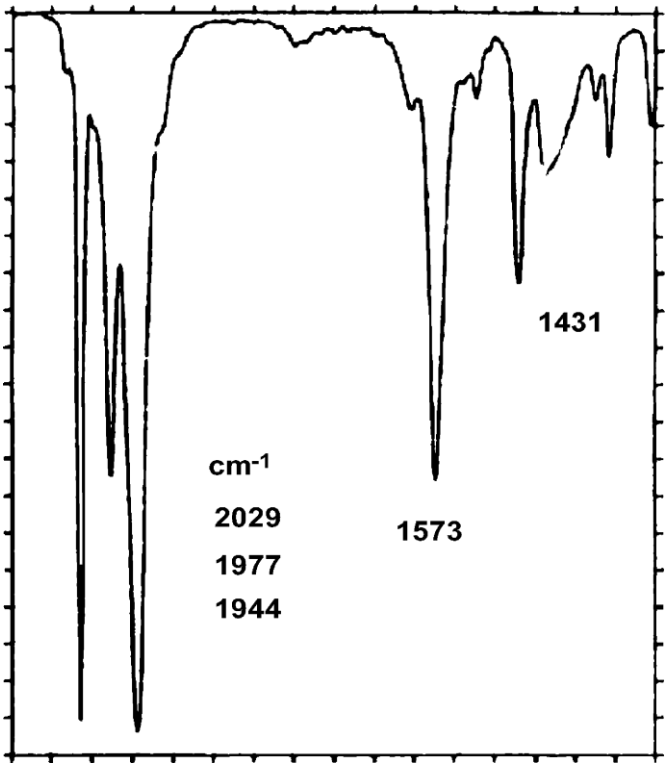

Fig. 4. *IR-spectrum of $Ru_2(CO)_4(OOCEt)_2(N_2C_3H_4)_2$. (Picture taken from[7])*

The structure of $Ru_2(CO)_4$ sawhorse-type complexes can be easily recognized by their characteristic three IR band patterns (very strong-medium-very strong) between 1900 to 2050

cm^{-1}. Asymmetric and symmetric absorption stretching frequencies of the bridging μ_2-η^2-O,O carboxylato groups are observed between 1550 and 1400 cm^{-1} (Fig. 4).

In 1977, Schumann *et al.*[9] reported the single crystal X-ray structure of tri(*t*-butyl)phosphine derivative of the sawhorse-type complex, $Ru_2(CO)_4(OOCBu^n)_2(PBu^t_3)_2$, which clearly showed the dinuclear ruthenium-ruthenium backbone, and each ruthenium atom having two carbonyl ligands in the remaining equatorial positions. The $Ru_2(CO)_4$ unit carries two μ_2-η^2-O,O carboxylato groups coordinated in four equatorial positions of the two ruthenium atoms and the two tri(*t*-butyl)phosphine ligands are coordinated in the axial position of ruthenium atoms. Later, Jones and co-workers[10] also obtained the crystal structure of di(*t*-butyl)phosphine derived diruthenium tetracarbonyl complex, $Ru_2(CO)_4(OOCMe)_2$-$(PBu^t_2H)_2$ which displayed a similar structure as $Ru_2(CO)_4(OOCBu^n)_2(PBu^t_3)_2$ (Fig. 5).

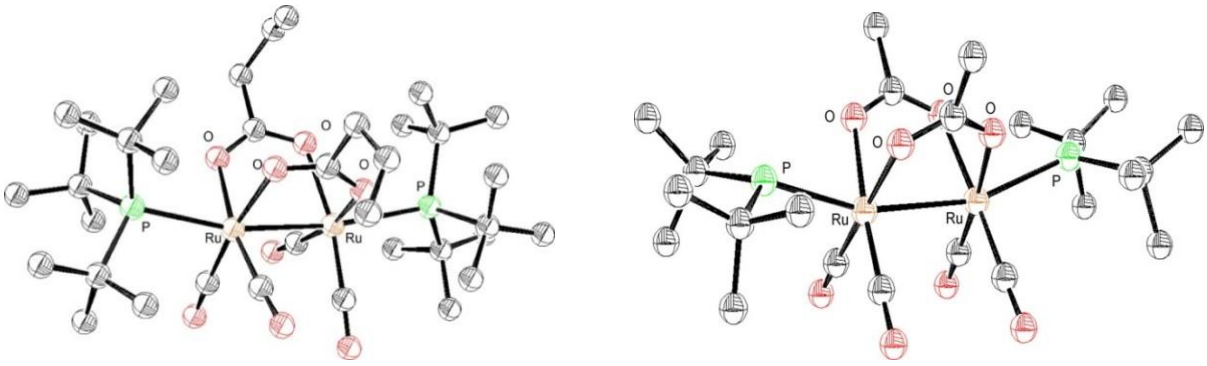

$[Ru_2(CO)_4(OOCBu^n)_2(PBu^t_3)_2]$ $[Ru_2(CO)_4(OOCMe)_2(PBu^t_2H)_2]$

Fig. 5. *ORTEP representation of diruthenium complexes* $Ru_2(CO)_4(OOCBu^n)_2(PBu^t_3)_2$,[7,9] *and* $Ru_2(CO)_4(OOCMe)_2(PBu^t_2H)_2$.[7,10] *(Picture taken from*[7]*)*

In 1985, Süss-Fink and co-workers[11] analysed the polymeric propionato dinuclear tetracarbonyl material derived from propionic acid on refluxing with $Ru_3(CO)_{12}$ in thf medium. Infrared and raman spectroscopic analyses showed that diruthenium unit coordinates with propionato ligand in equatorial position and the dinuclear units were held together by a strong interaction between an oxygen atom of carboxylato bridge and a ruthenium atom of the neighboring dinuclear unit (Ru-O) (Fig. 6). This model is widely accepted for the polymeric nature of $[Ru_2(CO)_4(OOCR)_2]_n$.

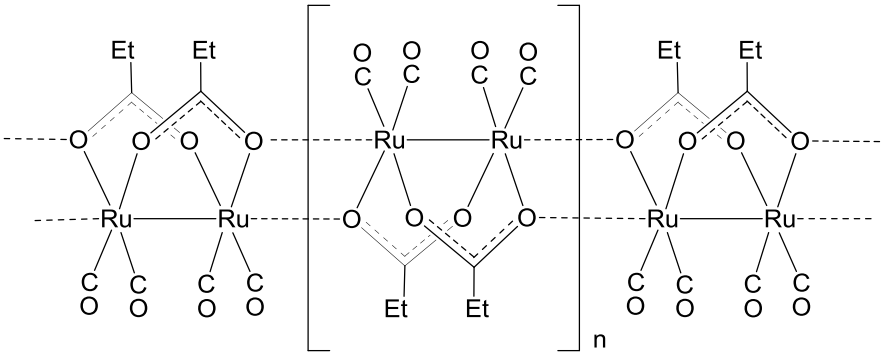

Fig. 6. *The polymeric chain of sawhorse units* $[Ru_2(CO)_4(OOCEt)_2]_n$.[7]

Süss-Fink and co-workers[12] have used a variety of carboxylic acids for the synthesis of sawhorse-type diruthenium complexes from $Ru_3(CO)_{12}$. All reactions were carried out in a pressure Schlenk tube at 120 ºC using thf as solvent. They further extended their synthesis to other ligands such as carboamido ($RCONH_2$),[13] pyrazolato ($C_3R_1R_2R_3N_2H$),[14] oxinato (R_1R_2CNOH)[15] and sulfanato (R_2SO_3H)[16] derivatives to get access to other sawhorse-type diruthenium complexes. The only drawback of this method is that, for the high temperature reactions (120 ºC) in the presence of low boiling solvent like thf (b.p. 66 ºC), a pressure Schlenk tube or an autoclave is required, which is not always readily available in most synthetic laboratories. This difficulty could be overcome by performing the reaction in anhydrous methanol, which requires only reflux conditions. It was observed that even under these mild conditions, the yields of the reaction were almost identical to those of the reaction at high temperature in a pressure Schlenk tube.[12a,12d]

$$2\ [Ru(CO)_2Cl_2]_n + 4\ RCOONa + 2\ L \rightarrow [Ru(CO)_2(OOCR)L]_2 + CO_2 + 4\ NaCl \qquad \text{(eq. 2)}$$

Spiccia and co-workers[17] reported a benign and efficient alternative method for the synthesis of sawhorse-type diruthenium complexes. Refluxing ruthenium trichloride hydrate ($RuCl_3 \cdot xH_2O$) with formic acid, which provided a polymeric ruthenium dichloride $[Ru(CO)_2Cl_2]_n$ material[18] that can be isolated. Addition of sodium carboxylate and a two-electron donor ligand to this material in methanol at reflux condition for 2.5 h afforded diruthenium complexes $[Ru_2(CO)_4(OOCR)_2(L)_2]$ (eq. 2). Notably, the yields were found to be lower than those obtained from $Ru_3(CO)_{12}$. However this method was found to have more advantageous, for example, the starting precursor $RuCl_3 \cdot xH_2O$ is less expensive than

$Ru_3(CO)_{12}$ and shorter reaction time and milder synthesis conditions are surely interesting enough to consider this as an effective alternative method.

1.3. Catalytic activity of sawhorse-type diruthenium tetracarbonyl complexes

Diruthenium tetracarbonyl complexes of the type $[Ru_2(CO)_4(OOCR)_2L_2]$ and their polymeric derivatives $[Ru_2(CO)_4(OOCR)_2]_n$ have been extensively studied for hydrogenation,[19] isomerization,[20] carbonylation,[21] carbon-carbon[22] and carbon-oxygen coupling[23] reactions. Recent review from Therrien *et al.*[7] summarized all the different catalytic applications of the sawhorse-type $Ru_2(CO)_4$ complexes.

Frediani *et al*.[19a] reported the hydrogenation of hex-1-ene using dinuclear catalyst $[Ru_2(CO)_4(OOCCH_3)_2(biisoq)_2][CH_3COO]$ (biisoq = 1,1'-biisoquinoline) (Fig. 7) under H_2 (100 bar) in a methanol/water mixture (catalyst/substrate ratio of 1:1000 at 60 ºC for 6 h) resulted in 87 % of hexane (eq. 3). Similar type of catalyst $[Ru_2(CO)_4(OOCCH_3)(bpy)_2]$-$[CH_3COO]$ (bpy = 2,2'-bipyridine) was used for the catalytic hydrogenation of acetone under 100 bar pressure of H_2 {100 ºC, methanol/water (2:1), catalyst/substrate (1:3800)} with catalytic turnover frequencies (TOF) up to 142 h^{-1} and provided 89 % yield of isopropanol.[19b]

The dinuclear complexes such as $[Ru_2(CO)_4(OOCCH_3)_2(PBu_3)_2]$ and $[Ru_2(CO)_4$-$\{OOCCH(OH)CH(OH)COO\}(bipy)_2]$ were reported as catalysts for hydrogenation of cyclohexene and of styrene, respectively. In the first case, catalyst $[Ru_2(CO)_4$-$(OOCCH_3)_2(PBu_3)_2]$ reduced cyclohexene under 130 bar of H_2 at 60 ºC for 22 h with a catalyst/substrate ratio of 1:2300 to provide cyclohexane with 22 % yield.[24] The same catalyst is also efficient for the hydrogenation of ketone to alcohol for example, 1-phenylethanol was prepared from acetophenone at 120 ºC with 66 % conversion (catalyst/substrate 1:2300, H_2 = 130 atm).[24] In the second case, the catalyst $[Ru_2(CO)_4\{OOCCH(OH)CH(OH)COO\}(bipy)_2]$ gave ethyl benzene by the hydrogenation of styrene with a catalyst/substrate ratio of 1:100 under 100 bar of H_2 using methanol/water as solvent at 100 ºC for 6 h with 91 % yield.[25]

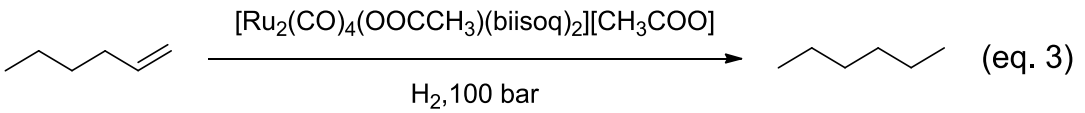

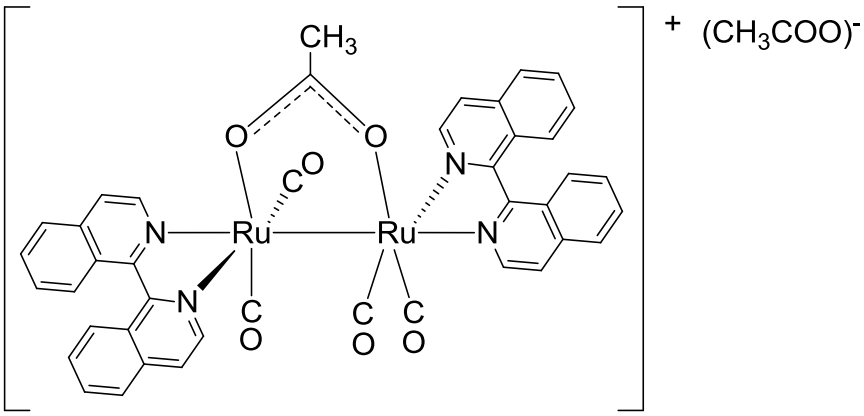

Fig. 7. *Suggested chemical structure of catalyst $[Ru_2(CO)_4(OOCCH_3)(biisoq)_2][CH_3COO]$.*

In 1989, Süss-Fink and co-workers[26] synthesized dinuclear $Ru_2(CO)_4$ complexes using bisphosphines such as dppe {1,2-bis(diphenylphosphino)ethane} (**i**), cyclop {1,2-bis(diphenylphosphinomethyl)cyclohexane} (**ii**), diop {4,5-bis(diphenyl-phosphinomethyl)-2,2-dimethyl-1,3-dioxolane} (**iii**) (Fig. 8) which were used for hydrogenation of hydroxyacetone. These chiral catalysts showed satisfactory catalytic turnovers, but with very low enantioselectivity.

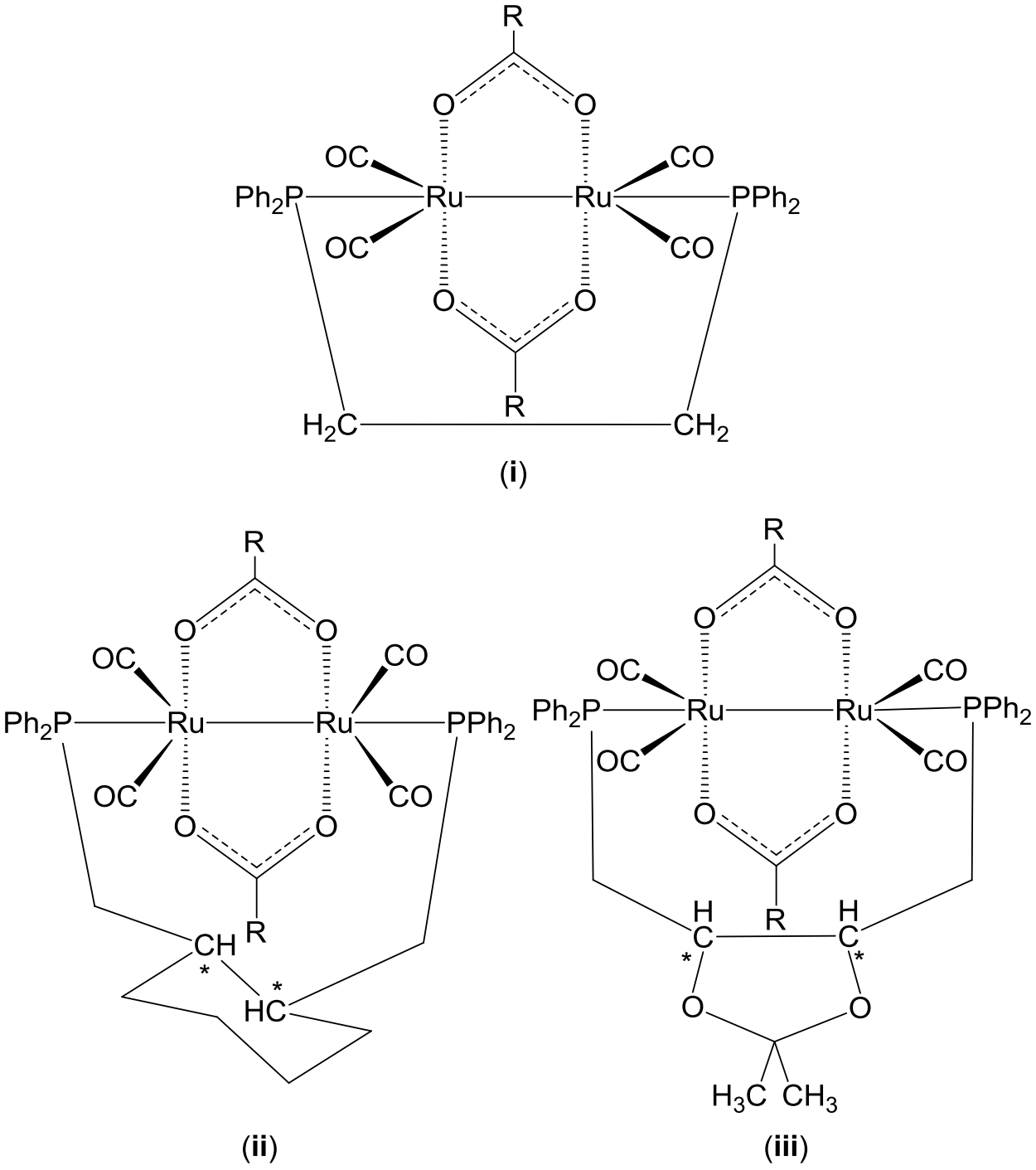

Fig. 8. *Chiral bis-phosphine derived sawhorse-type $Ru_2(CO)_4$ complexes.*

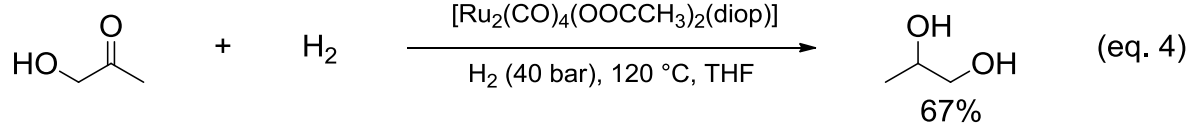

(eq. 4)

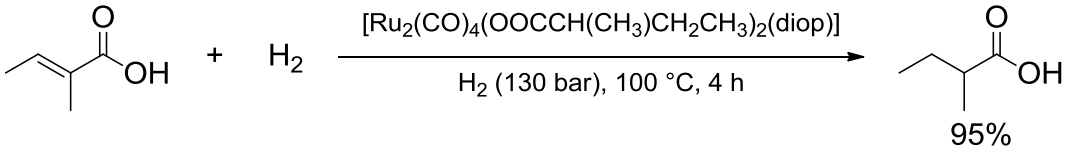

(eq. 5)

The chiral dinuclear complex $[Ru_2(CO)_4(OOCCH_3)_2(diop)]$ converts hydroxyacetone to 1,2-propanediol (eq. 4) under 40 bar of H_2 in tetrahydrofuran at 120 ºC, which results in 14 % enantiomeric exess with 67 % conversion (catalyst/substrate ratio 1:1000).[27] 2-Methyl-butanoic acid was obtained by the hydrogenation of tiglic acid in the presence of $[Ru_2(CO)_4(OOCCH(CH_3)CH_2CH_3)_2(diop)]$ as catalyst (eq. 5). The hydrogenation reaction was carried out under a H_2 pressure of 130 atm, in toluene/ethanol (1:1) as solvent mixture at 100 ºC for 4 h with catalyst/substrate ratio 1:655, providing 95 % conversation with 37 % of optical purity.[28]

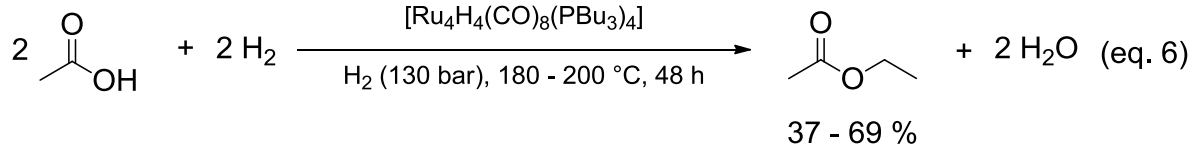

(eq. 6)

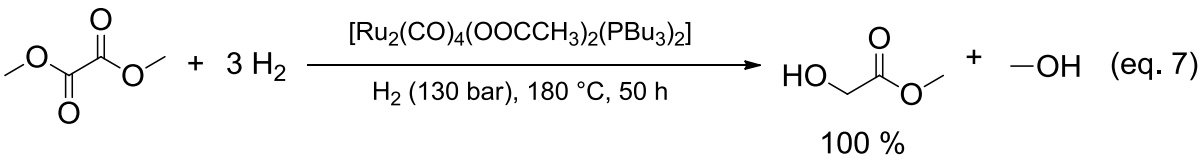

(eq. 7)

Diruthenium carbonyl complexes efficiently catalyze the reduction of saturated aliphatic carboxylic acids, which are one of the industrially important bulk chemicals. $[Ru_4H_4(CO)_8(PBu_3)_4]$ could reduce the easily available acetic acid to ethyl acetate (eq. 6) under H_2 (130 atm) at 180 ºC for 48 h with 37 % conversion; while the conversion has been

increased up to 69 % with an increase in temperature to 200 ºC also with the formation of ethyl alcohol as a side product.[29] The phosphine-substituted ruthenium carbonyl carboxylate $[Ru_2(CO)_4(OOCCH_3)_2(PBu_3)_2]$ catalyzed the hydrogenation of dimethyl oxalate under H_2 (130 atm) at 180 ºC for 50 h affording 100 % conversion to methyl glycolate in benzene (eq. 7).[30]

1.4. Arene ruthenium complexes

In 1967, Winkhaus and Singer discovered the first arene ruthenium complex by dehydrogenation of 1,3-cyclohexadiene (C_6H_8) with ruthenium trichloride hydrate ($RuCl_3 \cdot xH_2O$) in ethanolic medium under reflux condition. The obtained orange-red precipitate of the neutral diamagnetic complex was considered to be a polymeric material and they proposed an empirical formula for the polymeric structure $[(C_6H_6)RuCl_2]_n$ (eq. 8).[31]

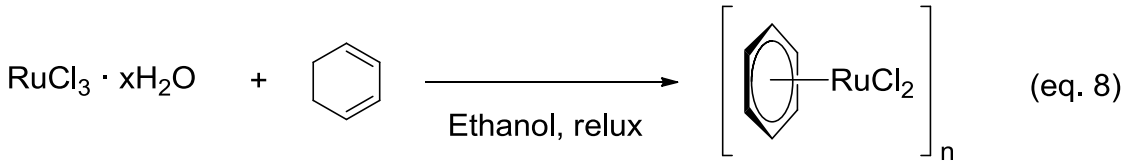

However, the structure was considered to be a polymer until Baird[32] and Bennett[33] revealed that the proposed polymeric structure was erroneous and showed that this complex actually had a dimeric structure $[(\eta^6\text{-}C_6H_6)Ru(\mu\text{-}Cl)Cl]_2$, where each ruthenium atom is in +2 oxidation state. The arene hapticity (η) is six and two units of $(C_6H_6)RuCl$ are linked by the chloro bridge. Later, Canivet *et al.*[34] showed the X-ray crystal structure of di-μ-chloro-bis[(η^6-benzene)chlororuthenium(II)] (Fig. 9).

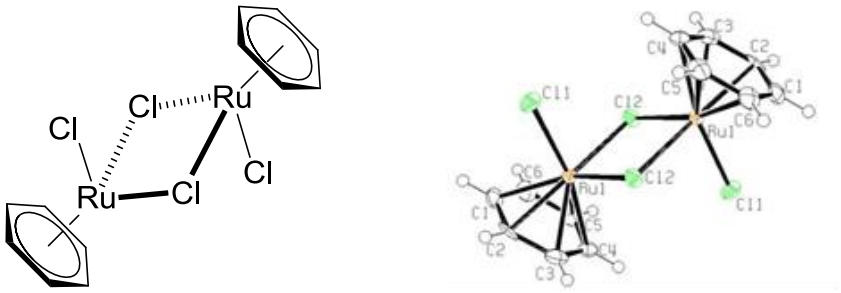

Fig. 9. *Structure of [(η^6-C_6H_6)Ru(μ-Cl)Cl]$_2$. (*crystal structure *taken from*[34]*)*

After the discovery of the of arene ruthenium dimeric structure, a remarkable number of arene ruthenium complexes has been synthesized. The dimeric *p*-cymene di-ruthenium complex [(η^6-*p*-$MeC_6H_4Pr^i$)Ru(μ-Cl)Cl]$_2$ was synthesized by the dehydrogenation of the electron poor diene (α)-phellandrene with ruthenium(III) trichloride hydrate in refluxing ethanol (eq. 9).[33,35]

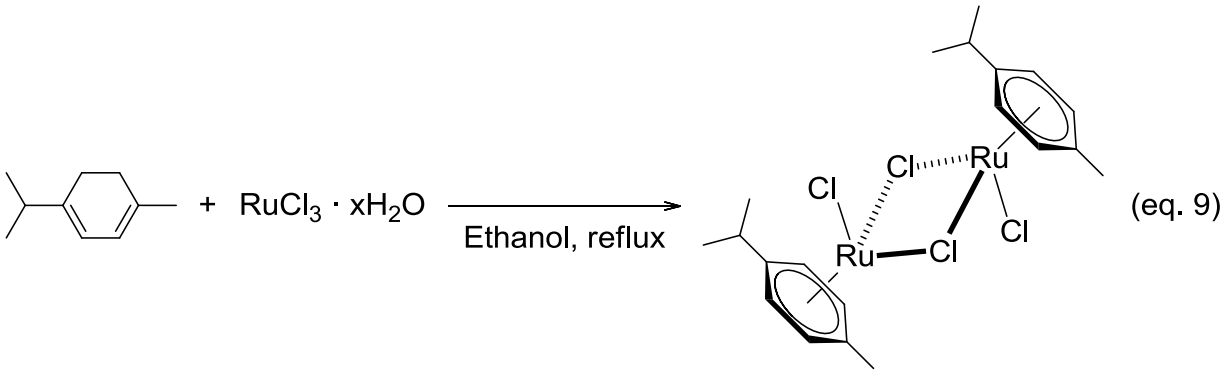

(eq. 9)

1.5. Pentamethylcylopentadienyl rhodium and iridium complexes

Kang *et al.*[36] showed the synthesis of dichloro(η^5-pentamethylcyclopentadienyl)-rhodium and iridium dimers from methanol solution of rhodium trichloride hydrate ($RhCl_3 \cdot xH_2O$) or iridium trichloride hydrate ($IrCl_3 \cdot xH_2O$) with hexamethylbicyclo[2,2,0]hexadiene (HMDB). The HMDB undergoes ring-contraction under acidic condition and leads to the formation of pentamethylcyclopentadienylrhodium and iridium dimers (eq. 10). Subsequently, White *et al.* [37] developed another synthetic route to prepare Rh(III) and Ir(III) dimers by the reaction of pentamethylcyclopentadiene with metal hydrates in reagent-grade

methanol under nitrogen atmosphere for 48 h which resulted in air stable red crystalline powders $[(\eta^5\text{-}C_5Me_5)M(\mu\text{-}Cl)Cl]_2$ (M = Rh and Ir)] (eq. 11).

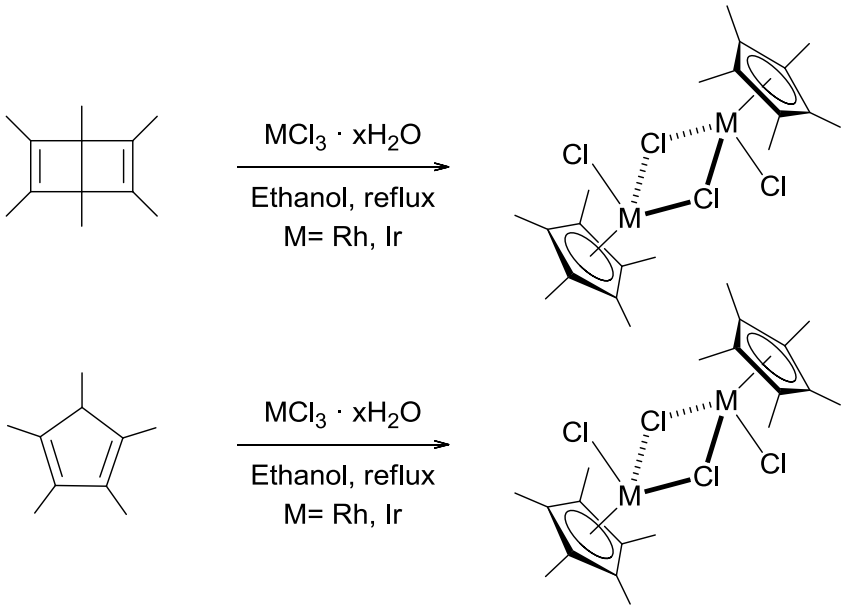

1.6. Reactivity of dinuclear Ru, Rh and Ir sulfur bridged complexes

Transition metal complexes with sulfur ligands especially thiol derivatives, have interesting structural properties and excellent reactivity.[38] The thiolato bridged dinuclear cationic complexes are synthesized from the starting precursors, such as $[(\eta^6\text{-}p\text{-}MeC_6H_4Pr^i)Ru(\mu\text{-}Cl)Cl]_2$ or $[(\eta^5\text{-}C_5Me_5)M(\mu\text{-}Cl)Cl]_2$ (M = Rh and Ir)]. The dimeric arene-ruthenium dichloride complexes were found to react with thiols to give cationic thiolato-bridged arene-ruthenium complexes of the type $[(\eta^6\text{-arene})_2Ru_2(\mu\text{-}SR)_3]^+$. Schacht *et al.*[39] reported the first thiolato-bridged complex $[(\eta^6\text{-}C_6Me_6)_2Ru_2(\mu\text{-}SC_6H_5)_3]^+$, which was derived from hexamethylbenzene ruthenium dimer $[(\eta^6\text{-}C_6Me_6)Ru_2(\mu\text{-}Cl)Cl]_2$ (Fig. 10). Mashima *et al.*[40] reported another complex of this type $[(\eta^6\text{-}p\text{-}MeC_6H_4Pr^i)_2Ru_2(\mu\text{-}SC_6H_5)_3]^+$ derived from *p*-cymene ruthenium dimer (Fig. 10).

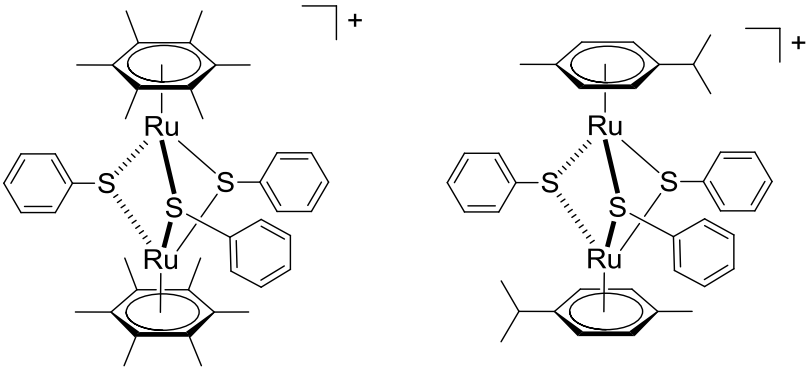

Fig. 10. *Structures of cationic $[(\eta^6\text{-}C_6Me_6)_2Ru_2(\mu\text{-}SC_6H_5)_3]^+$ (left) and $[(\eta^6\text{-}p\text{-}MeC_6H_4Pr^i)_2Ru_2(\mu\text{-}SC_6H_5)_3]^+$ (right) complexes.*

Similarly, Nishio *et al.*[41] reported the neutral $[(\eta^5\text{-}C_5Me_5)Ir(\mu\text{-}SCH_2C_6H_5)Cl]_2$ (Fig. 11) and the cationic $[(\eta^5\text{-}C_5Me_5)_2Ir_2(\mu\text{-}SCH_2CH_3)_3]^+$ (Fig. 11) dinuclear Ir complexes containing bridging thiolato ligands. Complex $[(\eta^5\text{-}C_5Me_5)Ir(\mu\text{-}SCH_2C_6H_5)Cl]_2$ was synthesized from the reaction of $[(\eta^5\text{-}C_5Me_5)Ir(\mu\text{-}Cl)Cl]_2$ with benzyl mercaptan ($C_6H_5CH_2SH$) in CH_2Cl_2 at room temperature for 12 h. While, $[(\eta^5\text{-}C_5Me_5)Ir(\mu\text{-}Cl)Cl]_2$ reacted with ethanethiol (CH_3CH_2SH) in CH_2Cl_2 at room temperature for 6 h to give the cationic complex $[(\eta^5\text{-}C_5Me_5)_2Ir_2(\mu\text{-}SCH_2CH_3)_3]^+$.

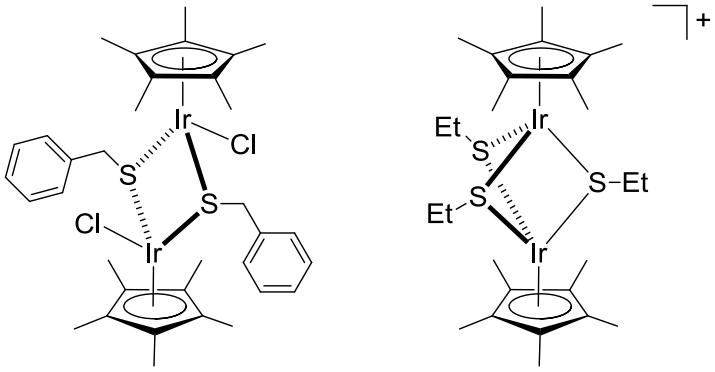

Fig. 11. *Structures of dinuclear Ir complexes $[(\eta^5\text{-}C_5Me_5)_2Ir_2(\mu\text{-}SCH_2Ph)_2Cl_2]$ (left) and $[(\eta^5\text{-}C_5Me_5)_2Ir_2(\mu\text{-}SCH_2CH_3)_3]^+$(right).*

Süss-Fink and co-workers[42] reported the star-like tris-thiobromo dinuclear(II) cationic complexes $[(\eta^6\text{-}p\text{-}MeC_6H_4Pr^i)_2Ru_2(\mu\text{-}SC_6H_4\text{-}p\text{-}Br)_3]^+$ (Fig. 12) and $[(\eta^5\text{-}C_5Me_5)_2Rh_2(\mu\text{-}SC_6H_4\text{-}p\text{-}Br)_3]^+$ synthesized from ruthenium $[(\eta^6\text{-}p\text{-}MeC_6H_4Pr^i)Ru(\mu\text{-}Cl)Cl]_2$ and rhodium $[(\eta^5\text{-}C_5Me_5)Rh(\mu\text{-}Cl)Cl]_2$ dimers, respectively. The star-like trisbromo cationic complexes undergo a triple Suzuki coupling with oligophenylene boronic acids (thiophene boronic acids) to give $[(\eta^6\text{-}p\text{-}MeC_6H_4Pr^i)_2Ru_2(\mu\text{-}SC_6H_4\text{-}p\text{-}C_4H_3S)_3]^+$ and $[(\eta^5\text{-}C_5Me_5)_2Rh_2(\mu\text{-}SC_6H_4\text{-}p\text{-}C_4H_3S)_3]^+$ (Fig. 12). The electrochemical and optical properties of these complexes have been studied.

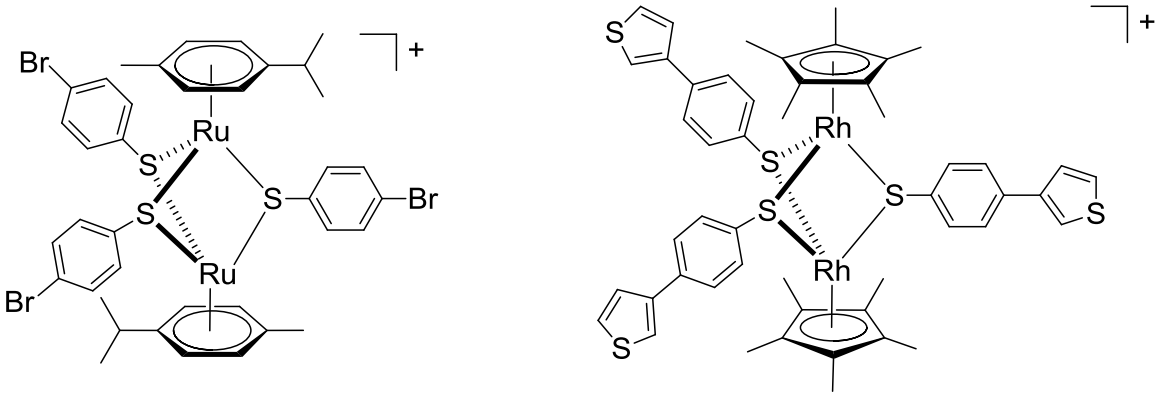

Fig. 12. *Structures of star-like cationic $[(\eta^6\text{-}p\text{-}MeC_6H_4Pr^i)_2Ru_2(\mu\text{-}SC_6H_4\text{-}p\text{-}Br)_3]^+$ (left) and $[(\eta^5\text{-}C_5Me_5)_2Rh_2(\mu\text{-}SC_6H_4\text{-}p\text{-}C_4H_3S)_3]^+$ (right) complexes.*

They also reported a series of cationic diruthenium trithiolato complexes $[(\eta^6\text{-arene})_2Ru_2(\mu\text{-}SR)_3]^+$ which were tested for anticancer activity. The water soluble cationic trithiolato complexes showed high cytotoxicity against human ovarian cancer cells even in the submicromolar range. From the *in vitro* studies, it was shown that the cationic complex $[(\eta^6\text{-}p\text{-}MeC_6H_4Pr^i)_2Ru_2(\mu\text{-}SC_6H_4\text{-}CH_3)_3]^+$ (Fig. 13) has IC_{50} of 0.13 μM on A7280 and 0.08 μM on A2780cisR ovarian cancer cell lines.[43] The neutral dithiolato complexes were also obtained from the reaction of $[(\eta^6\text{-}p\text{-}MeC_6H_4Pr^i)Ru(\mu\text{-}Cl)Cl]_2$ with thiolates at 0 ºC in technical-grade ethanol. The antiproliferative activities of the dithiolato complexes were evaluated against human ovarian cancer cell lines. Following *in vitro* studies, the neutral dithiolato complex $[(\eta^6\text{-}p\text{-}MeC_6H_4Pr^i)_2Ru_2(\mu\text{-}SCH_2CH_2Ph)_2Cl_2]$ (Fig. 13) has shown very

high cytotoxicity (IC_{50} values of 0.02 µM on A2780 and 0.31 µM on A2780cisR ovarian cancer cell lines).[38a]

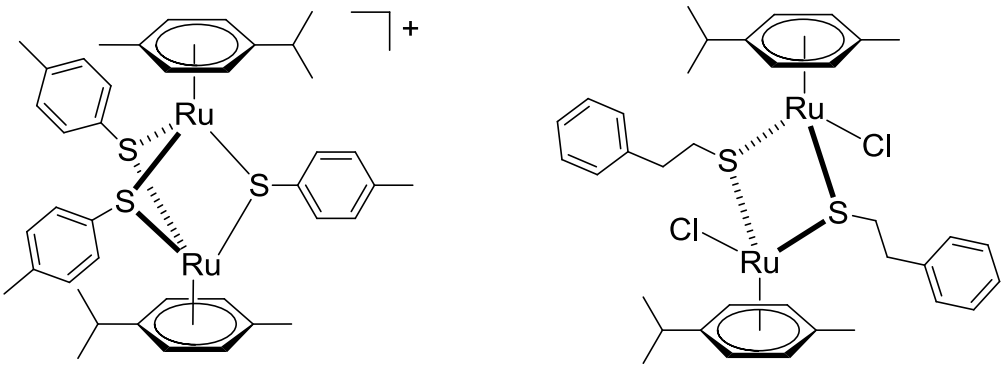

Fig. 13. *Highly cytotoxic thiolato complexes $[(\eta^6\text{-}p\text{-}MeC_6H_4Pr^i)_2Ru_2(\mu\text{-}SC_6H_4\text{-}CH_3)_3]^+$ (left) and $[(\eta^6\text{-}p\text{-}MeC_6H_4Pr^i)_2Ru_2(\mu\text{-}SCH_2CH_2Ph)_2Cl_2]$ (right).*

1.7. Aim of the present work

The aim of this thesis was to develop a novel series of dinuclear metal complexes, for catalytic, supramolecular and biological applications. The first part of the work deals with the synthesis, characterization and exploration of the hydrogenation potential of sawhorse-type diruthenium tetracarbonyl complexes in supercritical carbon dioxide ($scCO_2$) medium. The second part of the thesis highlights the possible supramolecular applications of sawhorse-type diruthenium complexes, and in the final part we explored the anticancer activity of dinuclear Ru, Rh and Ir complexes.

The catalytic activity in $scCO_2$ was studied in collaboration with Dr. L. Plasseraud, UMR CNRS 6302, Université de Bourgogne, France. During a collaboration with Dr. N. Armaroli at the CNR-ISOF, Bologna, Italy, molecular tweezer applications of dinuclear complexes were explored. Dr. F. Schmitt from the CHUV in Lausanne, Switzerland and Dr. N. Nagesh from CCMB, Hyderabad, India helped us with the biological studies and related applications.

Chapter 2: Catalytically active dinuclear ruthenium complexes

2. Catalytically active dinuclear ruthenium complexes

2.1. Supercritical carbon dioxide in catalysis

Supercritical carbon dioxide ($scCO_2$) is an interesting reaction medium for homogenous catalysis due to its inertness to most catalytic reactions, whilst in some cases it has also been employed as a reactant. Supercritical fluid is one of the best ecologically friendly alternatives to conventional solvents and it attracted the attention of chemists due to its abundance in nature, its non-toxicity, non-flammability, non-corrosive nature, it is also inexpensive, readily available and it could be easily removed from the reaction mixture.[44] Normally, in a standard temperature and pressure (STP) it behaves as a gas, while at pressure of (P_c) 72.9 bar at (T_c) 31.0 ºC, the gas converted into a fluid called supercritical fluid (Fig. 14).[44]

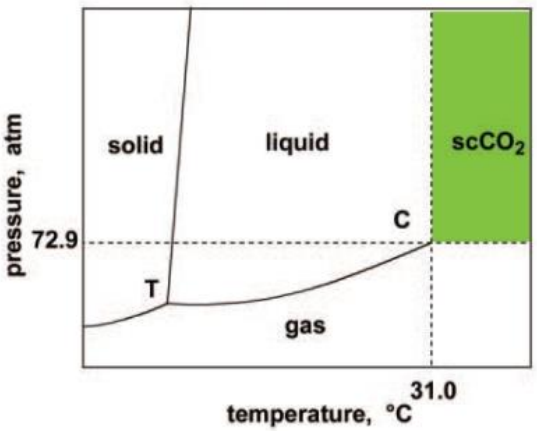

Fig. 14. *Schematic phase diagram of carbon dioxide fluid (T: triple point, C: critical point). Picture taken from.*[45]

Noyori and co-workers[46] showed that transition metal complexes of trialkylphosphine derivatives were highly soluble in $scCO_2$ with an excellent catalytic activity for the homogenous hydrogenation of CO_2 in the supercritical state. The catalysts $RuH_2\{P(C_6H_5)_3\}_4$, $RuH_2\{P(CH_3)_3\}_4$, $RuCl_2\{P(CH_3)_3\}_4$, $RuCl(O_2CCH_3)\{P(CH_3)_3\}_4$, *trans*-$RuCl_2(dmpe)_2$, *trans*-$RuHCl(dmpe)_2$ {dmpe = $(CH_3)_2P(CH_2)_2P(CH_3)_2$} and $Ru_3(CO)_{12}$ have been studied for hydrogenation of $scCO_2$ to formic acid, alkyl formate and formamides. Among these

catalysts, the more active catalyst precursors are shown in Fig. 15, and the catalyst $[RuCl_2\{P(CH_3)_3\}]_4$ showed excellent catalytic activities (eq 12-14).

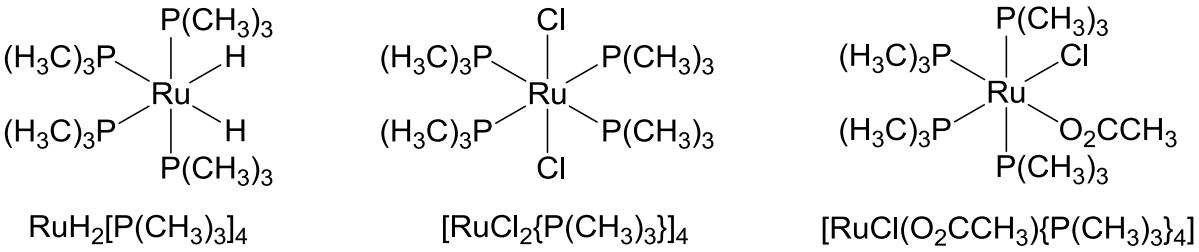

Fig. 15. *Catalytically active transition metal trialkylphosphine complexes.*[46]

$$CO_2 + H_2 \xrightarrow[N(C_2H_5)_3,\ 50\ ^\circ C]{[RuCl_2\{P(CH_3)_3\}_4]} HCO_2H \quad 7{,}200\ TON \qquad \text{(eq. 12)}$$

$$CO_2 + H_2 + CH_3OH \xrightarrow[N(C_2H_5)_3,\ 80\ ^\circ C]{[RuCl_2\{P(CH_3)_3\}_4]} HCO_2CH_3 + H_2O \quad 3{,}500\ TON \qquad \text{(eq. 13)}$$

$$CO_2 + H_2 + NH(CH_3)_2 \xrightarrow[100\ ^\circ C]{[RuCl_2\{P(CH_3)_3\}_4]} HC(=O)N(CH_3)_2 + H_2O \quad 370{,}000\ TON \qquad \text{(eq. 14)}$$

The Ru(II)phosphine catalyst $[RuCl_2\{P(CH_3)_3\}_4]$ promoted the hydrogenation of $scCO_2$ to formic acid (eq. 12) in the presence of triethylamine under a supercritical mixture {80 atm of H_2 and 130 atm CO_2} at 50 ºC with a turn over number (TON) up to 7,200.[46-47] With methanol as additive in the presence of triethylamine at 80 ºC, the same catalyst converted formic acid into methyl formate (eq. 13) by dehydration (80 atm of H_2 and 130 atm of CO_2) and with a TON up to 3,500.[46] While replacing the base from triethylamine to dimethylamine, the catalyst efficiently produced dimethylformamide (DMF) with a very high turnover number 370,000 {under 80 atm of H_2 and 130 atm of CO_2} at 100 ºC in supercritical fluid (eq. 14).[45,48]

One of the major obstacles in green catalysis is the poor solubility of metal complexes in $scCO_2$ and this problem has been circumvented by the addition of fluorinated alcohols to

the reaction mixture.[45,49] Introducing fluorinated counter-anions such as tetrakis-{3,5-bis(trifluoromethyl)phenyl}borate (BARF) or trifluoromethanesulfonate (CF_3SO_3) with cationic catalyst[44] or ligand modifications using "fluorous ponytails" (perfluroalkyl-substituted) in transition metal catalyst,[50] has improved the solubility of metal complexes in $scCO_2$ as well as increased the catalytic activity.

Noyori and co-workers[49] showed the hydrogenation of α,β-unsaturated carboxylic acid in $scCO_2$ medium in the presence of optically active catalyst [Ru(OOCCH$_3$)$_2$\{(*S*)-H$_8$-binap\}] {binap = 2,2'-bis(diphenylphosphino)-1,1'-binaphthyl} (Fig. 16). For example, hydrogenation of tiglic acid to (*S*)-2-methylbutanoic acid in the presence of catalyst in $scCO_2$ (33 atm H_2 and 175 atm CO_2) afforded 99 % conversion with 81 % ee at 50 ºC. While introducing the fluorinated additive like pentadecafluoro-1-octanol {$CF_3(CF_2)_6CH_2OH$} significantly increased the catalyst solubility in $scCO_2$ with enantioselectivities up to 89 % even under a very low (5 atm) H_2 pressure (eq. 15).

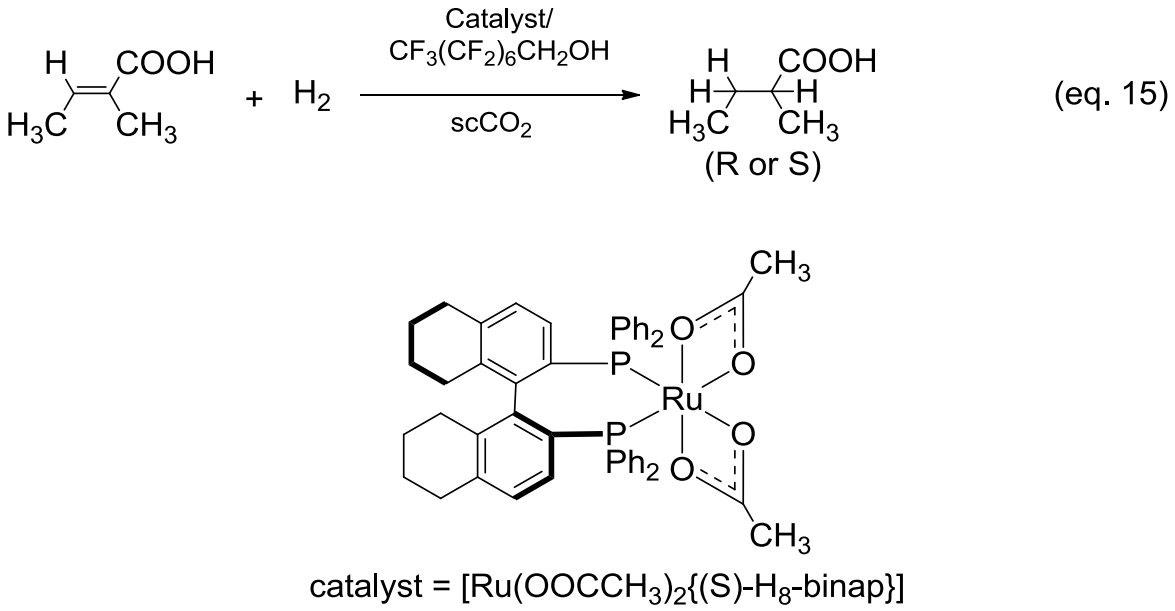

Fig. 16. *Molecular structure of catalyst* [Ru(OOCCH$_3$)$_2$\{(*S*)-H$_8$-binap\}].

Burk and Tumas[44] employed the highly lipophilic fluorinated counter-anion [B\{3,5-$(CF_3)_2C_6H_3$\}$_4$]$^-$ {tetrakis-(3,5-bis(trifluoromethyl)phenyl)borate (BARF)} with cationic

rhodium catalysts in order to improve the solubility in $scCO_2$ (Fig. 17). This strategy was successfully used for asymmetric catalytic hydrogenation.

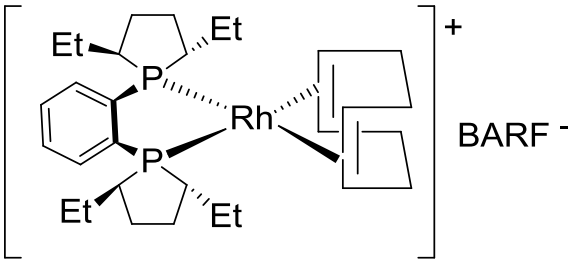

Fig. 17. *Cationic rhodium catalyst employed with fluorinated counter-anion.*[44]

Later, Leitner and co-workers[50] showed an alternative approach to improve the solubility of transition metal complexes in supercritical fluid by introducing "fluoro-ponytails" at the periphery of *bis*-arylphosphanes ligands (Fig. 18). The CO_2-philic or fluorophilic long perfluroalkyl-substituted chain {m-$(CH_2)_2(CF_2)_nCF_3$} directly attached to a bidentate chelating arylphosphane of transition metal complexes remarkably increased the solubility in $scCO_2$ without changing their catalytic properties.

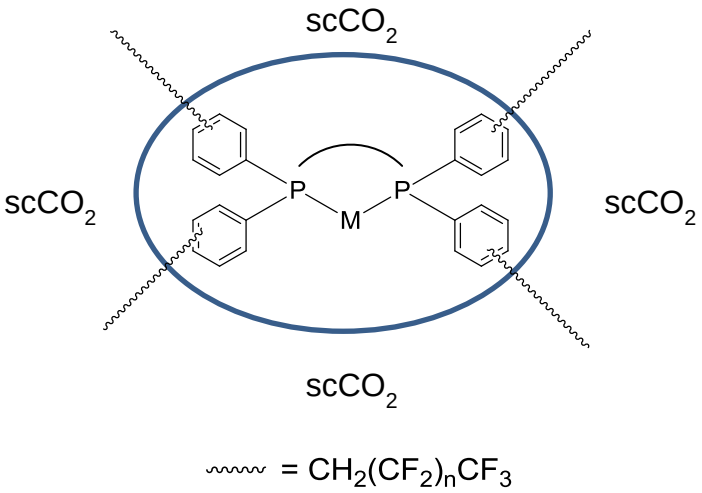

Fig. 18. *Transition metal complexes attached with "Fluoro-ponytails".*[50]

The complex $RuCl_2(dppe)_2$ {dppe = $(C_6H_5)_2P(CH_2)_2P(C_6H_5)_2$} is an active catalyst showing very high turnover number (up to 740,000) for dimethylformamide (DMF) productions (H_2 = 84 atm, CO_2 = 128 atm, T = 99 ºC, additive = dimethylamine). Though, catalyst $RuCl_2(dppe)_2$ is not soluble in $scCO_2$; the dimethylammonium dimethylcarbamate formation from additive (dimethylamine) in $scCO_2$ in the reaction medium influenced the catalyst solubility.[51] Berven *et al.*[51b] have improved the catalyst ($RuCl_2(dppe)_2$) solubility by attaching fluoro-ponytail of $(CF_2)_5CF_3$ to dppe. The incorporation of eight perfluoroalkyl "ponytails" {$(CF_2)_5CF_3$} enhanced the solubility of the metal complex in $scCO_2$ when compared to the insoluble parent compound. They suggested that, the highly CO_2-philic complex of ruthenium $RuCl_2(dfppe)_2$ {dfppe = $\{CF_3(CF_2)_5(p\text{-}C_6H_4)\}_2P(CH_2)_2P\{(p\text{-}C_6H_4)\text{-}(CF_2)_5CF_3\}_2$ could be a potential catalyst in supercritical fluids (Fig. 19) for DMF productions.[51b]

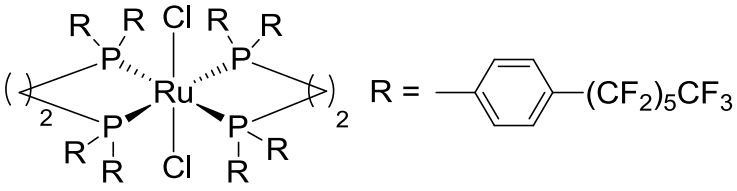

Fig. 19. *Ruthenium chloro complex attached with di-phosphine ligand of "Fluoro-ponytail".*[51b]

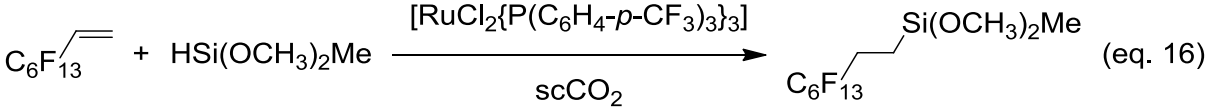

(eq. 16)

Sakakura and co-workers[52] reported the hydrosilation of polyfluoroolefin in the presence of the catalyst $RuCl_2\{P(C_6H_4\text{-p-}CF_3)_3\}_3$, which resulted in high yield (74 %) with high selectivity (98 %) in $scCO_2$ under 300 atm of CO_2, at 90 ºC for 24 h (catalyst/substrate ratio 1:200) (eq. 16). The high conversion and selectivity were achieved because of the remarkable solubility of the catalyst in $scCO_2$.

2.2. Sawhorse-type complexes containing μ_2-η^2 carboxylato ligands derived from saturated fatty acids and fluorinated fatty acids

Since the discovery of sawhorse-type diruthenium complexes, a considerable number of complexes with carboxylato bridges have been synthesized and they have been studied for different catalytic applications. Recent review gave a detailed view of the chemistry of sawhorse-type ruthenium complexes.[7] Herein, we report the synthesis and characterization of several new $Ru_2(CO)_4$ sawhorse-type complexes containing carboxylato ligands derived from saturated fatty acids such as butyric, heptanoic, nonanoic, decanoic, dodecanoic, tridecanoic, tetradecanoic, heptadecanoic and octadecanoic acids as well as fluorinated fatty acids such as perfluorobutyric and perfluorododecanoic acids with a variety of axial ligands (pyridine, triphenylphosphine or 1,3,5-triaza-7-phosphatricyclo[3.3.1.1]decane). Sawhorse-type diruthenium tetracarbonyl complexes derived from perfluoroalkyl ponytails (fluorinated fatty acids) showed good solubility in $scCO_2$, which have motivated us to test them as catalysts for the hydrogenation of styrene under $scCO_2$ condition.

2.2.1. Synthesis of sawhorse-type diruthenium tetracarbonyl complexes

Dodecacarbonyltriruthenium reacts with the appropriate carboxylic acid [heptanoic, $CH_3(CH_2)_5COOH$; nonanoic, $CH_3(CH_2)_7COOH$; decanoic, $CH_3(CH_2)_8COOH$; tridecanoic, $CH_3(CH_2)_{11}COOH$; tetradecanoic, $CH_3(CH_2)_{12}COOH$; heptadecanoic, $CH_3(CH_2)_{15}COOH$; octadecanoic, $CH_3(CH_2)_{16}COOH$; perflurorobutyric, $CF_3(CF_2)_2COOH$; and perfluorododecanoic, $CF_3(CF_2)_{10}COOH$; in thf at reflux under high pressure to yield a solution containing the thf intermediates $Ru_2(CO)_4(\mu_2\text{-}\eta^2\text{-}O_2C(CH_2)_5CH_3)_2(thf)_2$, $Ru_2(CO)_4(\mu_2\text{-}\eta^2\text{-}O_2C(CH_2)_7CH_3)_2(thf)_2$, $Ru_2(CO)_4(\mu_2\text{-}\eta^2\text{-}O_2C(CH_2)_8CH_3)_2(thf)_2$, $Ru_2(CO)_4(\mu_2\text{-}\eta^2\text{-}O_2C(CH_2)_{11}CH_3)_2(thf)_2$, $Ru_2(CO)_4\text{-}(\mu_2\text{-}\eta^2\text{-}O_2C(CH_2)_{12}CH_3)_2(thf)_2$, $Ru_2(CO)_4(\mu_2\text{-}\eta^2\text{-}O_2C(CH_2)_{15}CH_3)_2(thf)_2$, $Ru_2(CO)_4(\mu_2\text{-}\eta^2\text{-}O_2C(CH_2)_{16}CH_3)_2(thf)_2$, $Ru_2(CO)_4(\mu_2\text{-}\eta^2\text{-}O_2C(CF_2)_2CF_3)_2(thf)_2$ and $Ru_2(CO)_4(\mu_2\text{-}\eta^2\text{-}O_2C(CF_2)_{10}CF_3)_2(thf)_2$, respectively. These labile dinuclear thf intermediates further react with two-electron donor ligands (L), such as pyridine (NC_5H_5) (**a**), triphenylphosphine (PPh_3) (**b**) or 1,3,5-triaza-7-phosphatricyclo[3.3.1.1]decane (PTA) (**c**) to generate the stable dinuclear complexes $Ru_2(CO)_4(\mu_2\text{-}\eta^2\text{-}O_2C(CH_2)_5CH_3)_2(L)_2$ (**1a**, L = C_5H_5N; **1b**, L = PPh_3), $Ru_2(CO)_4(\mu_2\text{-}\eta^2\text{-}$

$O_2C(CH_2)_7CH_3)_2(L)_2$ (**2a**, L = C_5H_5N; **2b**, L = PPh_3), $Ru_2(CO)_4(\mu_2\text{-}\eta^2\text{-}O_2C(CH_2)_8CH_3)_2(L)_2$ (**3a**, L = C_5H_5N; **3b**, L = PPh_3), $Ru_2(CO)_4(\mu_2\text{-}\eta^2\text{-}O_2C(CH_2)_{11}CH_3)_2(L)_2$ (**4a**, L = C_5H_5N; **4b**, L = PPh_3), $Ru_2(CO)_4(\mu_2\text{-}\eta^2\text{-}O_2C(CH_2)_{12}CH_3)_2(L)_2$ (**5a**, L = C_5H_5N; **5b**, L = PPh_3), $Ru_2(CO)_4(\mu_2\text{-}\eta^2\text{-}O_2C(CH_2)_{15}CH_3)_2(L)_2$ (**6a**, L = C_5H_5N; **6b**, L = PPh_3), $Ru_2(CO)_4(\mu_2\text{-}\eta^2\text{-}O_2C(CH_2)_{16}CH_3)_2(L)_2$ (**7a**, L = C_5H_5N; **7b**, L = PPh_3), $Ru_2(CO)_4(\mu_2\text{-}\eta^2\text{-}O_2C(CF_2)_2CF_3)_2(L)_2$ (**8a**, L = C_5H_5N; **8b**, L = PPh_3; **8c**, L = PTA) and $Ru_2(CO)_4(\mu_2\text{-}\eta^2\text{-}O_2C(CF_2)_{10}CF_3)_2(L)_2$ (**9a**, L = C_5H_5N; **9b**, L = PPh_3; **9c**, L = PTA), in reasonable yields (see Scheme 1). Within the saturated fatty acids series **1**-**7**, the complex containing axial pyridine and triphenylphosphine ligands were isolated in good yield (Scheme 1).

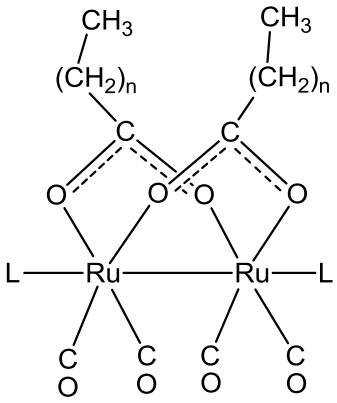

(**1-7**)

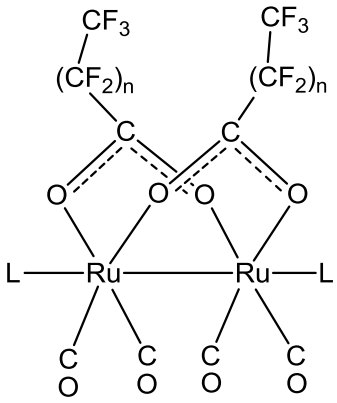

(**8-9**)

L	n = 5	n = 7	n = 8	n = 11	n = 12	n = 15	n = 16	n = 2	n = 10
C_5H_5N	**1a**	**2a**	**3a**	**4a**	**5a**	**6a**	**7a**	**8a**	**9a**
PPh_3	**1b**	**2b**	**3b**	**4b**	**5b**	**6b**	**7b**	**8b**	**9b**
PTA	-	-	-	-	-	-	-	**8c**	**9c**

***Scheme 1**. Synthesis of the dinuclear complexes $Ru_2(CO)4(\mu_2\text{-}\eta^2\text{-}O_2C(CX_2)_nCX_3)_2(L)_2$; X = H, F (**1-9**).*

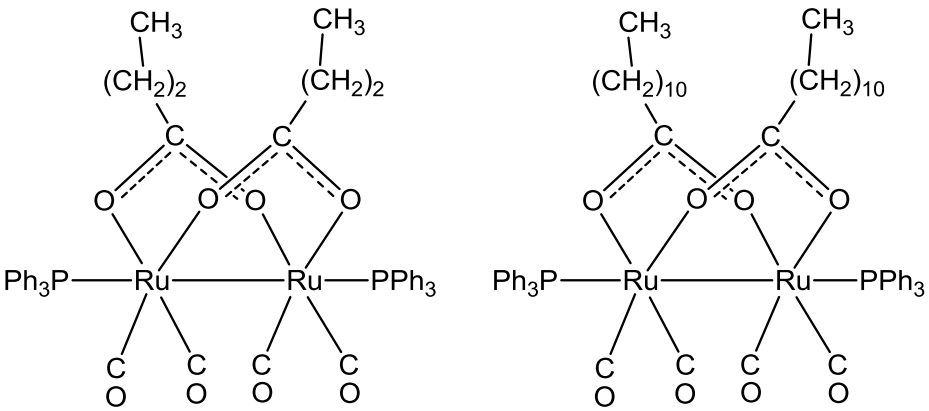

Fig. 20. *Molecular structure of the dinuclear complexes $Ru_2(CO)_4(\mu_2\text{-}\eta^2\text{-}O_2C(CH_2)_2CH_3)_2(PPh_3)_2$ (**10**); $Ru_2(CO)_4(\mu_2\text{-}\eta^2\text{-}O_2C(CH_2)_{10}CH_3)_2(PPh_3)_2$ (**11**).*

The same synthetic method was followed to prepare the complexes $Ru_2(CO)_4(\mu_2\text{-}\eta^2\text{-}O_2C(CH_2)_2CH_3)_2(PPh_3)_2$ (**10**); $Ru_2(CO)_4(\mu_2\text{-}\eta^2\text{-}O_2C(CH_2)_{10}CH_3)_2(PPh_3)_2$ (**11**). The catalytic activity of complexes **8** and **9** were compared with the parent complexes **10** and **11** (Fig. 20) as well as with the starting precursor $Ru_3(CO)_{12}$. The catalytic activity of these complexes will be discussed at the end of this chapter.

The sawhorse-type dinuclear tetracarbonyl complexes are air-stable yellow crystalline powders and have been completely characterized by infrared (IR), NMR and mass spectrometry as well as by their micro-analytical data. All compounds exhibit the characteristic pattern of the $Ru_2(CO)_4$ sawhorse unit in the $\nu_{(CO)}$ region of the IR spectra, which consist of three bands (very-strong; medium; very-strong) between 2100 and 1900 cm^{-1}, and the strong and broad band for symmetric and asymmetric $\nu_{(OCO)}$ vibrations of the bridging carboxylato groups around 1560 cm^{-1}.[7] In the fluorinated derivatives **8** and **9**, this asymmetric $\nu_{(OCO)}$ vibration band is observed at 1660 cm^{-1}. The PPh_3 derivatives **1b**-**9b, 10** and **11** showed a sharp singlet at ≈ 15 ppm in their ^{31}P NMR spectra ($CDCl_3$, 23 °C), while PTA derivatives **8c** and **9c** shown a signal at ≈ -54 ppm, both in accordance with coordination of PTA and PPh_3 in the axial positions of sawhorse-type diruthenium tetracarbonyl complexes.[12a,b,53] In **1**-**11**, all ^1H NMR spectra ($CDCl_3$, 23 °C) showed the expected resonances for the axial ligands. For example, in complexes **1a**-**9a** the protons of the pyridyl ligands appeared at δ = 7.5, 7.9 and 8.7 ppm in a 2:1:2 integration ratio, while for the PTA

derivative **8c** and **9c** two multiplets of equal integrations at 4.3 and 4.6 ppm were observed. In complexes **1b-9b**, **10** and **11** the axial PPh_3 ligands showed two multiplets in the aromatic region. In the ^{19}F NMR spectra ($CDCl_3$, 23 °C) of complexes **8**, three distinct signals were observed and easily assigned, while for complexes **9** several additional signals corresponding to median CF_2 groups appeared between -120 and -125 ppm.

2.2.2. Single-crystal X-ray structures of sawhorse-type diruthenium tetracarbonyl complexes derived from saturated fatty acid

The single-crystals of **1b**, **2a**, **3a**, **4a** and **5a** were obtained by slow diffusion of pentane into a dichloromethane solution of the corresponding complex. The single-crystal structure analysis of **1b** showed a $Ru_2(CO)_4$ sawhorse backbone with the two PPh_3 ligands in the axial positions and the carboxylato bridges in the equatorial positions, as expected (Fig. 21). The Ru-Ru distance [2.7239(5) Å] is in the range of a ruthenium-ruthenium single bond, as it was also observed in analogous complexes containing triphenylphosphine axial ligands.[12a,12d,54] The P-Ru-Ru-P torsion angle is 40.4(2)°, which is comparable to those observed in $Ru_2(CO)_4\{O_2CCH_2O\text{-}C_6H_2Cl_2\text{-}COC(CH_2)C_2H_5\}_2(PPh_3)_2$[12a] and $Ru_2(CO)_4\text{-}(O_2CC_5H_4FeC_5H_5)_2(PPh_3)_2$.[54]

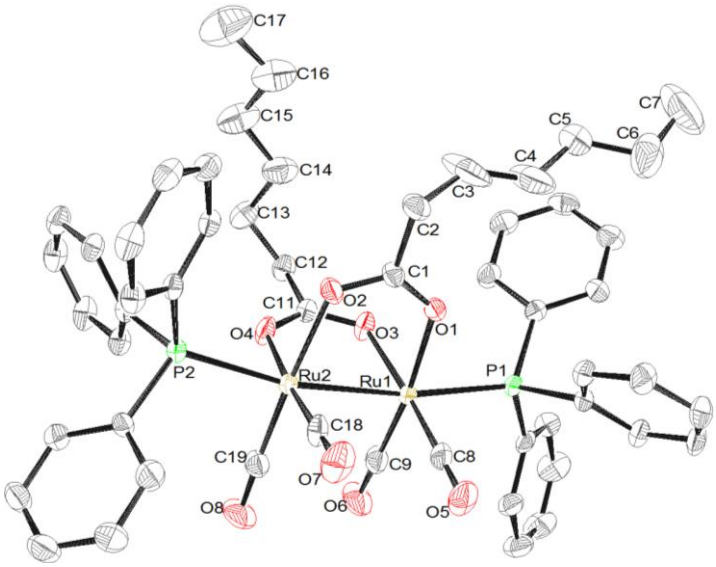

Fig. 21. *ORTEP drawing of* ***1b*** *with ellipsoids at the 35 % probability level.*

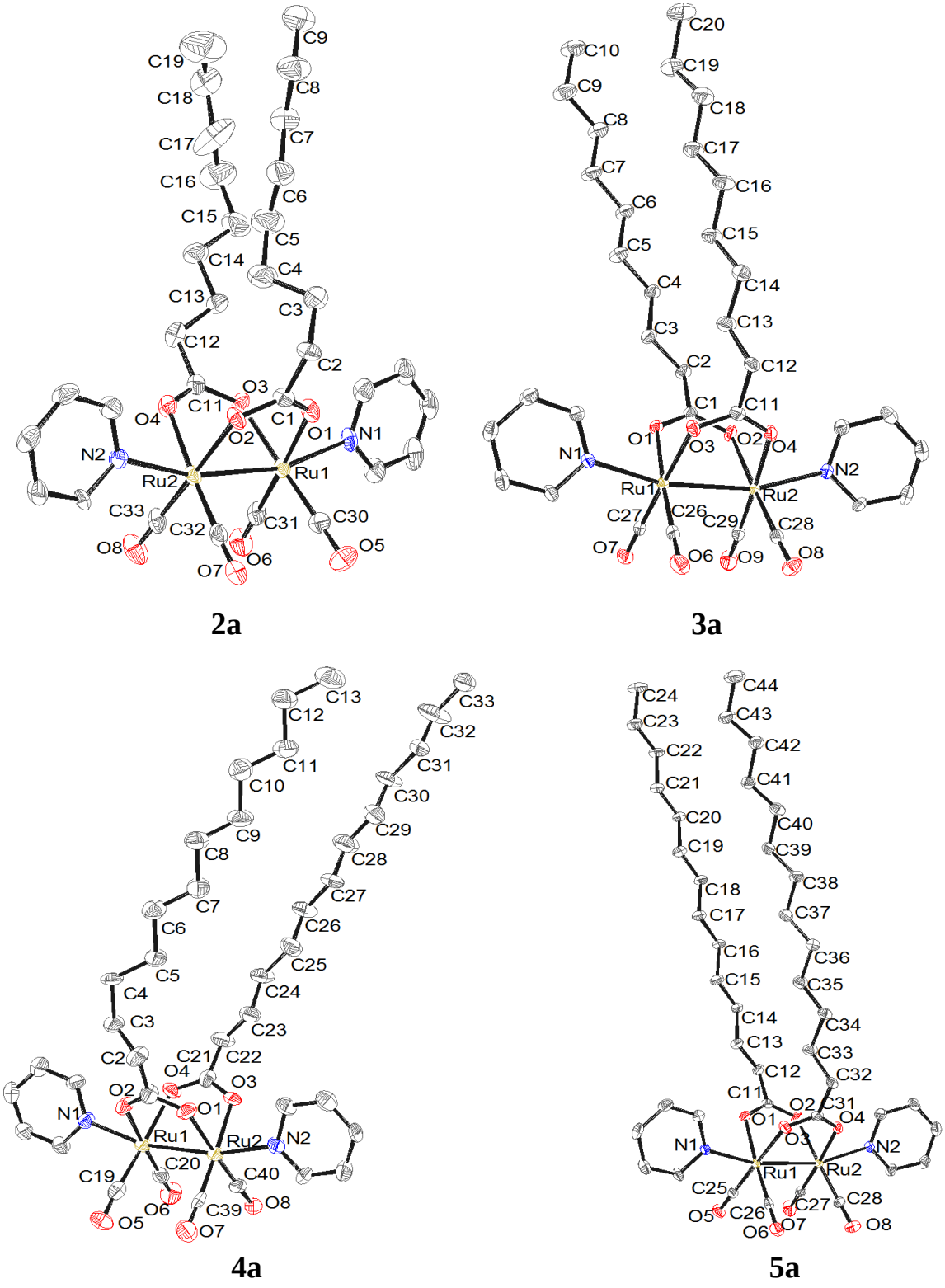

Fig. 22. *ORTEP drawings of* ***2a***, ***3a***, ***4a*** *and* ***5a*** *with ellipsoids at the 35 % probability level.*

Table 1. Selected bond lengths (Å) and angles (º) for **1b**, **2a**, **3a**, **4a** and **5a**.

	1b	**2a**	**3a**	**4a**	**5a**
Distances (Å)					
Ru-Ru	2.7239(5)	2.6804(8)	2.6817(5)	2.6793(14)	2.6829(5)
Ru-P_{PPh3}	2.4566(11)				
Ru-P_{PPh3}	2.4296(11)				
Ru-$N_{pyridine}$		2.223(6)	2.224(3)	2.246(9)	2.215(4)
Ru-$N_{pyridine}$		2.211(6)	2.209(3)	2.206(9)	2.216(4)
Ru-$O_{carboxylato}$	2.123(3)	2.128(6)	2.148(3)	2.122(8)	2.150(3)
Ru-$O_{carboxylato}$	2.114(3)	2.120(5)	2.115(3)	2.123(8)	2.118(3)
Ru-$O_{carboxylato}$	2.138(3)	2.131(6)	2.126(3)	2.136(8)	2.125(4)
Ru-$O_{carboxylato}$	2.114(3)	2.124(6)	2.127(3)	2.132(8)	2.121(4)
Angles (º)					
$O_{carboxylato}$					
O-Ru-O	85.06(14)	83.3(2)	82.81(12)	81.4(4)	82.82(15)
O-Ru-O	84.32(12)	83.7(2)	83.22(12)	82.3(3)	83.47(16)
$C_{carbonyl}$					
C-Ru-C	90.2(2)	88.5(4)	88.3(2)	86.7(6)	88.3(2)
C-Ru-C	88.4(2)	89.4(4)	89.3(2)	88.4(5)	89.4(2)
Torsion angles (°)					
L-Ru-Ru-L	40.4(2)	-6.5(11)	10.2(5)	-6.1(16)	9.0(6)

Similarly, the single-crystal structure analyses of **2a**, **3a**, **4a** and **5a** exhibit the $Ru_2(CO)_4$ sawhorse backbone with the two pyridyl ligands in the axial positions and the carboxylato bridges in the equatorial positions (Fig. 22). Selected geometrical parameters are given in Table 1. The Ru-Ru distances [**2a**: 2.6804(8) Å, **3a**: 2.6817(5) Å, **4a**: 2.6793(14) Å, **5a**: 2.6829(5) Å] are as well in the range of a ruthenium-ruthenium single bond but they are considerably shorter than the one observed in the triphenylphosphine derivative **1b** (Table 1). This difference in the metal-metal distance can be associated to an increase in electron

density between the metal atoms as a result of the lack of back-bonding to the pyridyl ligands.

In the crystal packing of **2a**, closed parallel π-π stacking interactions is observed between pyridyl groups of two adjacent dinuclear complexes (Fig. 23). The centroid-centroid separation is 3.73 Å and agreed well with the theoretical value calculated from this π stacking mode.[55]

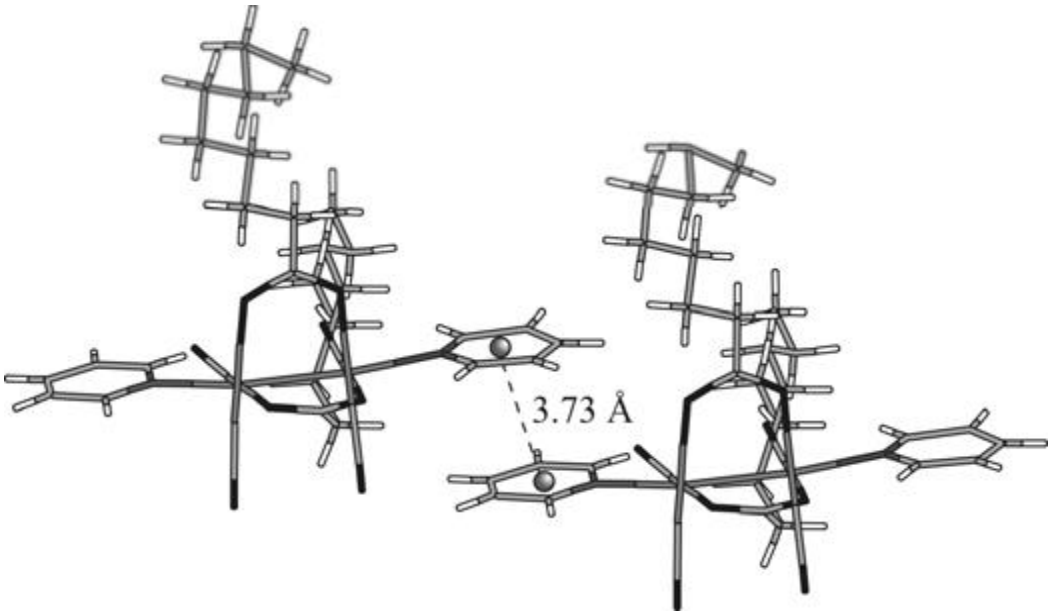

Fig. 23. *Parallel π-stacking interaction observed in the crystalline packing of* ***2a.***

Similarly, in the crystal packing of **3a**, **4a** and **5a** parallel π stacking interactions are observed between neighboring pyridyl moieties of adjacent sawhorse complexes, however, the centroid-centroid separations are slightly shorter in these crystals (**3a**: 3.64 Å, **4a**: 3.63 Å, **5a**: 3.64 Å). The presence of longer alkyl chains in **3a**, **4a** and **5a** induces a different packing arrangement as compared to **2a**. Indeed, to maximize van der Waals and electrostatic interactions between alkyl chains, and to optimize packing density, the two alkyl chains of the sawhorse-type complex adopt a parallel arrangement. Moreover, these parallel pair of alkyl chains interacts with neighboring parallel pair of alkyl chains from symmetry related molecules to generate layers of alkyl chains. As an example, the head-to-tail arrangement of parallel alkyl chains observed in **5a** is presented in Fig. 24. The width of these layers is approximately 14.0 Å in **3a** [Ru-Ru separation], while in **4a** it reaches 17.6 Å and in 5a it is greater than 25.0 Å.

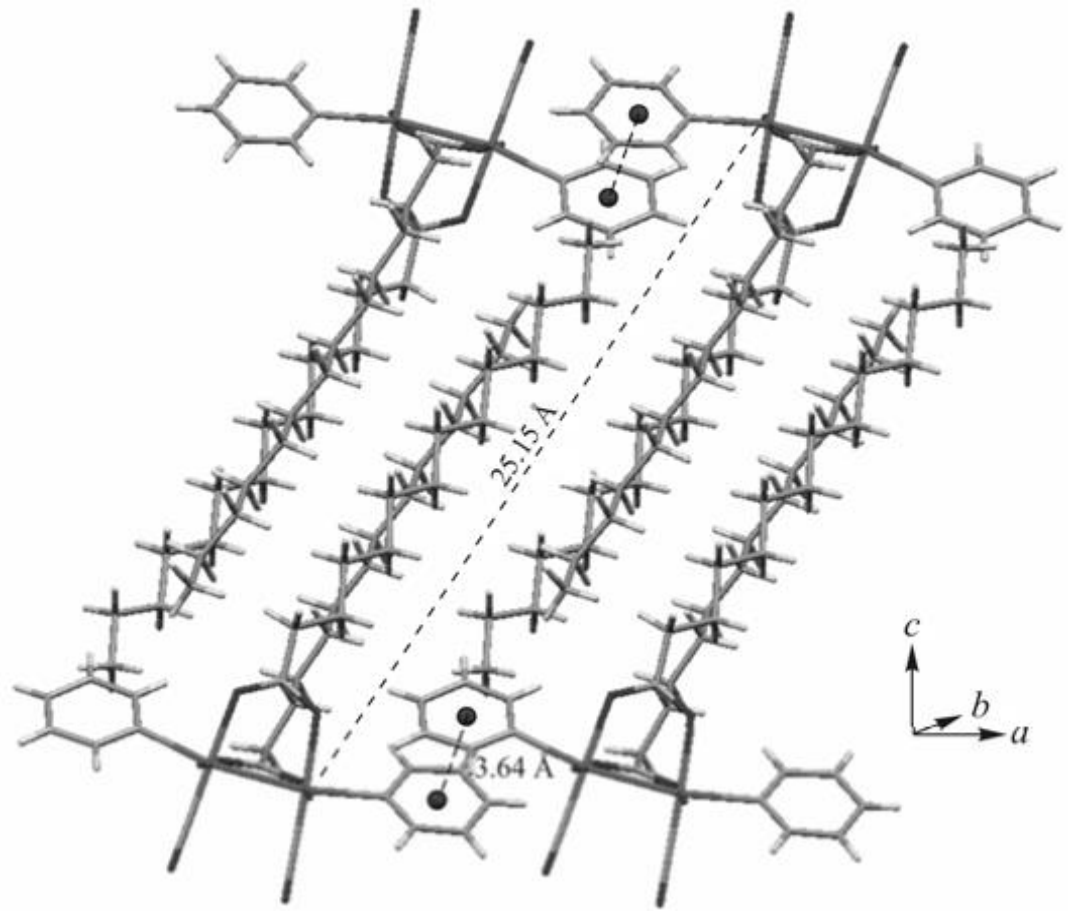

Fig. 24. *Main interactions involved in the crystalline packing of* ***5a****, π-stacking interactions between adjacent pyridyl groups and van der Waals interactions between parallel alkyl chains.*

2.2.3. Comparing X-ray structures of saturate fatty acid with non-fatty acid derivative (**8a** and **10**)

Crystals of **8a** and **10** were obtained by slow diffusion of pentane into a dichloromethane solution of the corresponding complex. The single-crystal structure analyses of **8a** and **10** showed the $Ru_2(CO)_4$ sawhorse backbone with the two pyridine (**8a**) or triphenylphosphine (**10**) ligands in the axial positions and the carboxylato bridges in the equatorial positions (Fig. 25). The Ru-Ru distances [**8a**: 2.694(1) Å, **10**: 2.7477(5) Å] are

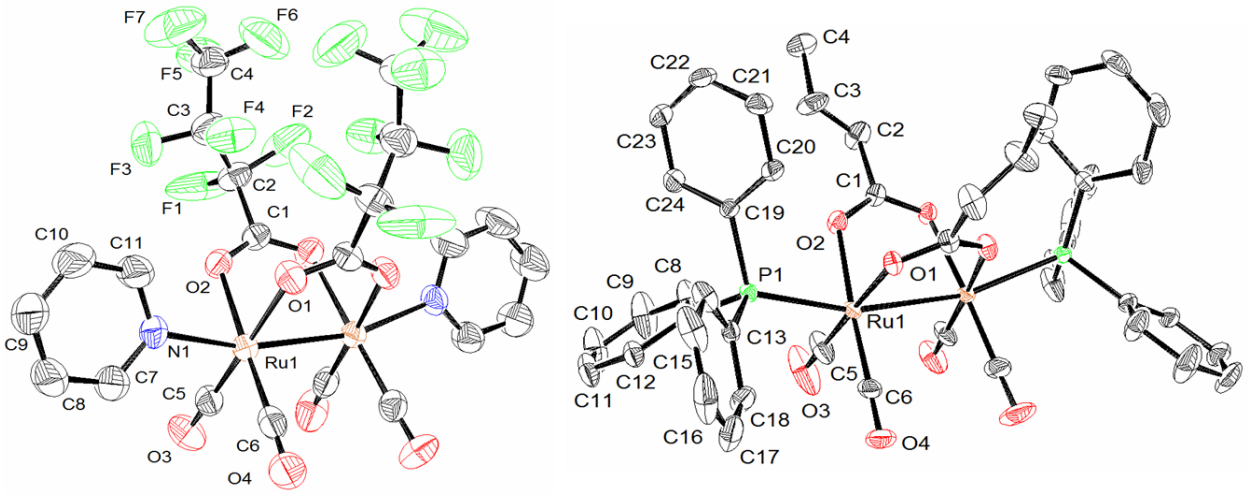

Fig. 25. *ORTEP representation of complexes* ***8a*** *and* ***10*** *showing ellipsoids at the 35 % probability level with hydrogen atoms omitted for clarity (symmetry code: i = -x, y, ½-z).*

Table 2. Selected bond lengths (Å) and angles (°)

8a		**10**	
Ru1-Ru1^{i}	2.694(1)	Ru1-Ru1^{i}	2.7477(5)
Ru1-N1	2.218(4)	Ru1-P1	2.4524(8)
Ru1-O1	2.151(4)	Ru1-O1	2.130(2)
Ru1-O2	2.149(4)	Ru1-O2	2.124(2)
O1-C1-O2^{i}	129.2(5)	O1-C1-O2^{i}	125.3(3)
N1-Ru1-Ru1^{i}	165.79(13)	P1-Ru1-Ru1^{i}	163.97(2)
O1-Ru1-O2	83.52(18)	O1-Ru1-O2	87.66(10)

in the range of a ruthenium-ruthenium single bond, as it was also observed in analogous complexes.[12a,53a] The OCO bond angles of the carboxylato bridges [**8a**: 129.2(5)°, **10:** 125.3(3)°] differ only slightly from those observed in other $Ru_2(CO)_4(\mu_2\text{-}\eta^2\text{-}O_2CR)_2L_2$ complexes.[12a] In **10**, the Ru-P distance is 2.4524(8) Å, consistent with the Ru-P distances observed in analogous complexes.[12a,53a] The remaining structural parameters appear to be normal for this type of complexes.[7] Selected bond lengths and angles for **8a** and **10b** are listed in Table 2.

2.3. Catalytic evaluation of sawhorse-type diruthenium tetracarbonyl complexes

Quantitative yields of such new complexes containing in particular carboxylato ligands derived from saturated fluorinated fatty acids motivated us to evaluate their catalytic properties under supercritical conditions of carbon dioxide. Indeed, ligand modifications with perfluoroalkyl ponytails are known to exhibit a great CO_2-philic character, and thus they have been used to increase the solubility of homogeneous catalysts in $scCO_2$.[56] In this preliminary catalytic study, selected sawhorse-type diruthenium complexes with short (**8b** and **8c**) and long (**9b**) fluorinated alkyl chains were considered as catalyst for the hydrogenation of styrene in $scCO_2$ conditions (eq. 17), and their activities were also compared with those obtained with non-fluorinated analogues **10**, **11** and $Ru_3(CO)_{12}$.

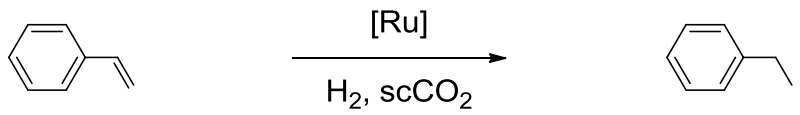

eq. 17

Catalytic data are summarized in Table 3. It appears that the sawhorse-type diruthenium complexes are very poor catalysts for the hydrogenation of styrene. The conversions of styrene into ethyl benzene are always below 15 % regardless of the length of the fluorinated alkyl chains and the nature of the axial ligands (PPh_3 axial ligands seem to be the most suitable). In addition, the yield in ethyl benzene is not exalted by the supercritical conditions of carbon dioxide (entries 2 and 4). The incorporation of fluorinated alkyl chains showed a modest improvement. In previous studies, the addition of a co-solvent, such as methanol, has been reported to be helpful for increasing the catalytic activity of transition metal catalysts under $scCO_2$ conditions.[57] Herein, for the same complex (**8b**), we only observe a weak positive effect with the presence of methanol (entries 2 and 3). In fact, the best conversion was obtained using $Ru_3(CO)_{12}$ as catalyst (entry 9). Enhancement in the conversion was observed when the reaction was carried out in the presence of H_2 (entries 10 and 11). However, the degradation of the catalyst was also observed, leading to a final black precipitate suspected to be ruthenium nanoparticles.[58] Thus, the low activity recorded with these sawhorse-type diruthenium tetracarbonyl complexes can be rationalized by the stability and preservation of the starting ruthenium species in the $scCO_2$ reaction medium.

Table 3. Hydrogenation of styrene under supercritical carbon dioxide conditions to ethylbezene.

Entry	Catalyst	Medium	Conversion(%)
1	**10**	H_2[a]/CO_2[b]	7
2	**8b**	H_2[a]/CO_2[b]	6
3	**8b**	H_2[a]/CO_2[b]/CH_3OH[c]	10
4	**8b**	H_2[a]	12
5	**8c**	H_2[a]/CO_2[b]	4
6	**11**	H_2[a]/CO_2[b]/CH_3OH[c]	3
7	**9b**	H_2[a]/CO_2[b]/CH_3OH[c]	6
8	**9b**	H_2[a]	6
9	$Ru_3(CO)_{12}$	H_2[a]/CO_2[b]	22
10	$Ru_3(CO)_{12}$	H_2[a]	71
11	recovery of entry 10	H_2[a]	95

Reaction conditions: Amount of catalyst = 0.02 mmol, substrate/catalyst = 500/1, T = 65 °C, reaction time = 16 h. [a] P_{H_2} = 10 bar. [b] P_{total} = 120 bar. [c] 1 mL.

In conclusion, we have synthesized and characterized a series of sawhorse-type complexes containing carboxylates derived from fluorinated and non-fluorinated fatty acids. The single-crystal structure analyses of **2a**, **3a**, **4a** and **5a** revealed that for $n \geq 8$, the packing of the non-fluorinated alkyl chains and the π-π interactions between pyridyl groups dominated, while for $n \leq 7$, only the arrangement of the axial pyridyl ligands played a significant role in the crystalline packing of these sawhorse-type complexes. Complexes **8**, **9**, **10** and **11** were evaluated as catalyst for the hydrogenation of styrene under $scCO_2$. All these catalysts gave a very poor conversion.

Chapter 3: Supramolecular properties of dinuclear ruthenium complexes

3. Supramolecular properties of dinuclear ruthenium complexes

3.1. Molecular Tweezers

The term molecular tweezer has been introduced by Whitlock[59] and was popularized by Zimmerman.[60] Molecular tweezers are synthetic macrocyclic receptors with an interactive site able to bind with a substrate. These interactive sites are often obtained by coupling two functional groups to a rigid or a semi-rigid spacer (Fig. 26). The interactions between the functional groups of the receptor and the substrate can be of different natures, hydrogen bonds, metal-coordinations, hydrophobic forces, solvophobic effects, π-π stacking or van der Waals interactions.[61]

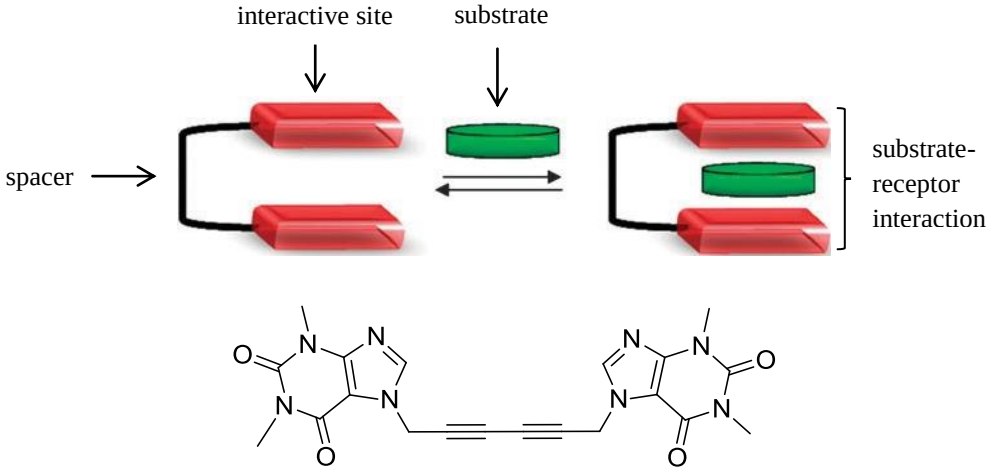

Fig. 26. *Cartoon representation of molecular tweezer (picture taken from[61b]) and the first molecular tweezer described by the Whitlock group.[59]*

These kinds of substrate-receptor recognition processes play important roles in biology, for example for energy transduction in organisms, to control metabolic processes via participation in various enzymatic reactions, in DNA polymerizations, for transportation of neutral and ionic species through membranes and also in the transformation of genetic information during cell metabolism.[62] To better understand and to mimic some of these fundamental recognition processes operating in living organisms, chemists have designed artificial molecular tweezers.

3.2. Organic, inorganic and organometallic molecular tweezer

Pyrene is the smallest peri-fused polycyclic aromatic hydrocarbon and it is obtained during the combustion of organic compounds.[63] The pyrene molecule is highly symmetrical and despite having 16 π electrons and not following the Hückel's (4*n* + 2) rule, pyrene is aromatic.[64] These features provide to pyrene some interesting electronic properties,[65] which can be exploited for the preparation of chemosensors. The large planar π-conjugated surface of pyrene generates a high fluorescence quantum yield and pyrene shows a strong excimer emission with itself or with pyrene analogues. The face-to-face arrangement of pyrenes bound with a spacer associated with an intramolecular excimer formation has been widely utilized to detect the presence and absence of guest molecules. The preparation of pyrenyl-containing chemosensors has been mainly designed around organic spacers.[66] Two pyrene units have been covalently bonded to 1,5-bis(2-aminophenoxy)-3-oxopentane to generate a tweezer for metal ions (Fig. 27; **A**).[67] A bis-pyrenyl derivative (Fig. 27; **B**), which possesses the ability to form π-π stacking interactions and hydrogen bonds, has been synthesized by Colquhoun and Zhu.[68] Biomolecules, such as sugar[69] or bile acid[70] (Fig. 27; **C**) have also been used as scaffolds to form bis-pyrenyl tweezers. Similarly, two pyrenyl units have been coupled to cyclodextrin[71] and calix[4]arene[72] to generate supramolecular tweezers. These examples, among others, illustrate the diversity and popularity of organic spacers in the design of pyrenyl-based tweezers.

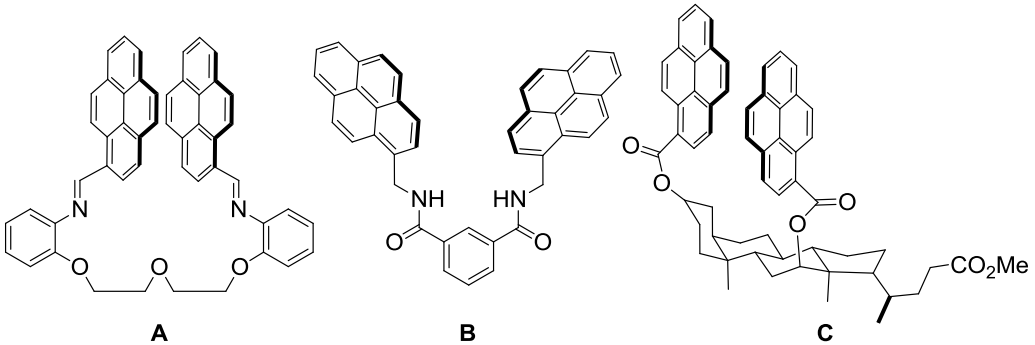

Fig. 27. *Examples of organic bis-pyrenyl tweezers* ***A***, ***B*** *and* ***C****.*

Despite being scarce, example of pyrenyl-based tweezers obtained from coordination chemistry can be found in the literature. Inorganic tweezers such as Cu- and Rh-based tweezers (Fig. 28 ; **D**) able to trap chloride in their cavities have been prepared by Mirkin.[73] A NCN-pincer type palladium aqua complex with an appended pyrenyl group (Fig. 28; **E**) has been designed by van Koten.[74] This organometallic complex interacts with picric acid in solution and catalyzes aldol condensation. In the presence of pyrophosphate, two mono-pyrenyl zinc cations have been assembled (Fig. 28; **F**) to generate a molecular tweezer.[75] In water, this di-zinc pyrophosphate complex showed high fluorescence due to the formation of an excimer. Similar excimeric emission was obtained by coordinating two (diphenylphosphino)pyrene ligands to silver.[76] These examples are, to the best of our knowledge, the only examples in which metals were used to assemble pyrenyl-based tweezers, despite the versatility of coordination chemistry.

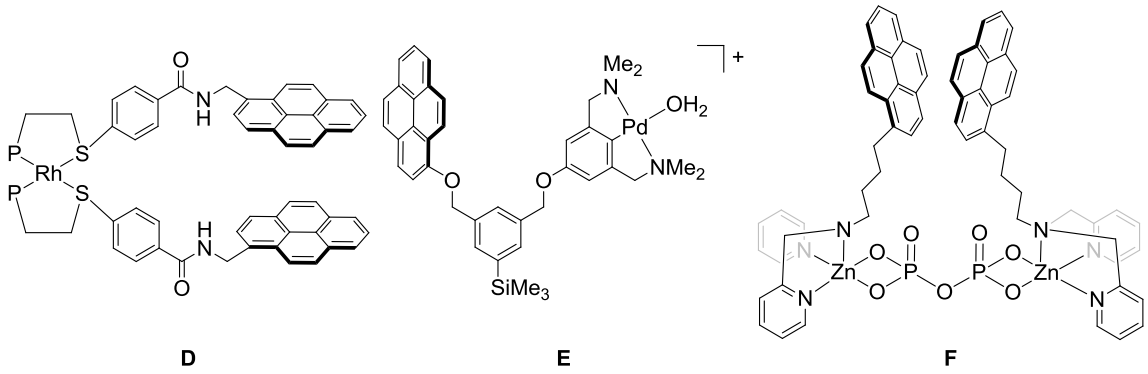

Fig. 28. *Examples of inorganic and organometallic pyrenyl appended molecular tweezers **D**, **E** and **F**.*

Similarly, porphyrins were also used to design molecular tweezers because of their planar aromatic nature. The large aromatic surface provided by the tetrapyrrol core allows π-stacking interactions with guest molecules,[77] while inserting zinc in the porphyrin core gives an additional coordination site for additional bonding.[78] In fact, the Zn(II) center is easily five coordinated and interact strongly with N-donor ligands. Strategies to connect two porphyrin units involve either organic chemistry,[79] definitely the most common strategy, or coordination chemistry. Among inorganic connectors, Reed and Boyd have used dichloro-palladium metal center and two mono-pyridyl porphyrin derivatives to generate a molecular

tweezer (Fig. 29, **G**), which shows excellent affinity for C_{60} and C_{70}.[80] Similarly, Shinkai reported on-off switchable tweezers for C_{60} using palladium-dppp metal center (dppp = 1,3-bis(diphenylphosphino)propane) and two mono-pyridyl-functionalized zinc metallo-porphyrin derivatives (Fig. 29, **H**).[81] Despite these examples and the versatility of metal centers to build two and three dimensional assemblies,[82] coordination chemistry has scarcely been used to assemble two porphyrin panels to generate molecular tweezers.[83]

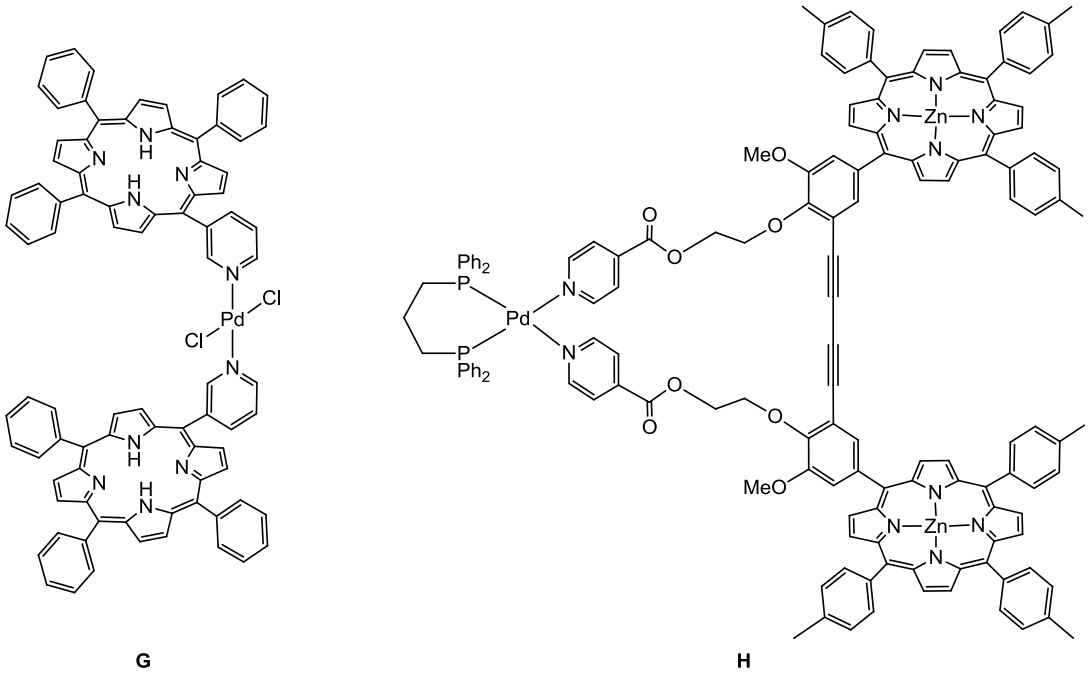

Fig. 29. *Examples of porphyrin appended inorganic molecular tweezers* ***G*** *and* ***H****.*

Since the discovery of sawhorse-type diruthenium tetracarbonyl complexes,[8] a tremendous number of such complexes with carboxylato bridges have been synthesized and studied (more information can be read in general introduction) for different applications.[7] However, to the best of our knowledge, sawhorse units have never been used to build molecular tweezers. Herein we report the synthesis of sawhorse-type diruthenium tetracarbonyl molecular tweezers containing pyrenyl or porphyrinyl group in the equatorial position of the sawhorse backbone and evaluate their ability to act as molecular tweezers with guest molecules such as fullerene (C_{60}), pyridine (pyr), 4,4'-bipyridine (bpy), 1,2-bis(4-pyridyl)ethylene (bpe), and photoactive guests, like 5,10-bis(4-pyridyl)-15,20-di-phenyl-

21H,23H-porphyrin (5,10-dpp), and 5,15-bis(4-pyridyl)-10,20-diphenyl-21H,23H-porphyrin (5,15-dpp) (Fig. 38).

3.3. Sawhorse-type molecular tweezers derived from pyrenyl-carboxylic acids

$Ru_3(CO)_{12}$ reacts with an excess of the pyrenyl-carboxylic acid derivatives, 1-pyrenecarboxylic acid ($C_{16}H_9COOH$), 1-pyreneacetic acid ($C_{16}H_9CH_2COOH$) and 1-pyrenebutyric acid {$C_{16}H_9(CH_2)_3COOH$}, under high pressure conditions to yield a solution containing the thf intermediates $Ru_2(CO)_4(\mu_2\text{-}\eta^2\text{-}OOCC_{16}H_9)_2(thf)_2$, $Ru_2(CO)_4(\mu_2\text{-}\eta^2\text{-}OOCCH_2C_{16}H_9)_2(thf)_2$ and $Ru(CO)\{\mu_2\text{-}\eta^2\text{-}OOC(CH_2)_3C_{16}H_9\}(thf)_2$, respectively. These labile thf intermediates further react with two-electron donor ligands (L), such as pyridine (NC_5H_5) (**a**) and triphenylphosphine (PPh_3) (**b**), to generate in reasonable yields the stable dinuclear tetracarbonyl complexes $Ru_2(CO)_4(\mu_2\text{-}\eta^2\text{-}OOCC_{16}H_9)_2(L)_2$ (**12a**, L = C_5H_5N; **12b**, L = PPh_3), $Ru_2(CO)_4(\mu_2\text{-}\eta^2\text{-}OOCCH_2C_{16}H_9)_2(L)_2$ (**13a**, L = C_5H_5N; **13b**, L = PPh_3) and $Ru(CO)\{\mu_2\text{-}\eta^2\text{-}OOC(CH_2)_3C_{16}H_9\}(L)_2$ (**14a**, L = C_5H_5N; **14b**, L = PPh_3) (Fig. 30).

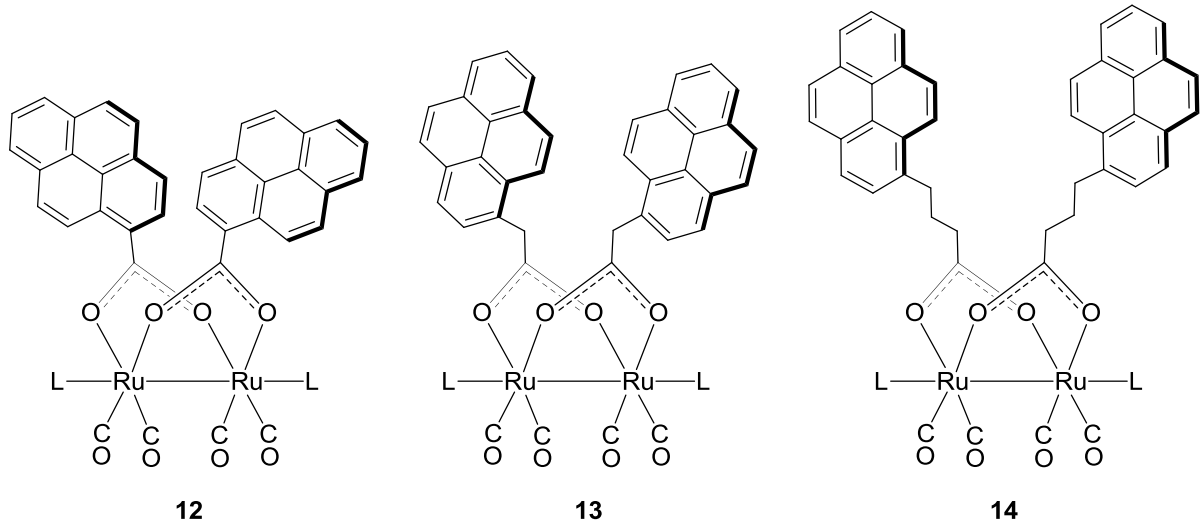

Fig. 30. *Structures of the sawhorse-type diruthenium tetracarbonyl complexes **12**, **13** and **14** (**a**, L = NC_5H_5; **b**, L = PPh_3).*

All complexes are yellow crystalline powders, stable in air, and they have been fully characterized by IR, NMR, UV-Vis, mass spectrometry and by elemental analysis.

In the infrared spectra, the complexes show the characteristic three band pattern (very strong - medium - very strong) at around 1945, 1970 and 2020 cm^{-1}, together with a strong and broad band for the symmetric and asymmetric ν(OCO) vibrations of the two bridging carboxylato groups around 1570 cm^{-1}. For **12b**, **13b** and **14b**, the $^{31}P\{^{1}H\}$ NMR spectra show a sharp singlet at $\delta \approx 15$ ppm which correspond to the PPh_3 axial ligands. In the ^{1}H NMR spectra, complexes **13a** and **13b** show a singlet at $\delta = 3.68$ and 4.17 ppm respectively, associated with the CH_2 of the pyrenyl-carboxylato ligands, while for complexes **14a** and **14b** two triplets and one quintet are observed between 1.68 and 3.19 ppm. These signals correspond to the aliphatic protons of the butyl chains in **14**.

The electronic absorption spectra of the sawhorse-type diruthenium tetracarbonyl complexes **12**–**14** and of the free pyrenyl-carboxylic acids (A1 = 1-pyrenecarboxylic acid, A2 = 1-pyreneacetic acid, A3 = 1-pyrenebutyric acid) show bands from 278 to 383 nm (Fig. 31). The complexes **12b**, **13b** and **14b** show an additional absorption at 383 nm which is due to the presence of the axial PPh_3 ligands. Notably, the absorption bands of the uncoordinated pyrenyl-carboxylic acids and those of the complexes **12**–**14** remain unchanged, suggesting the absence of sizeable ground-state inter-pyrene electronic interactions.

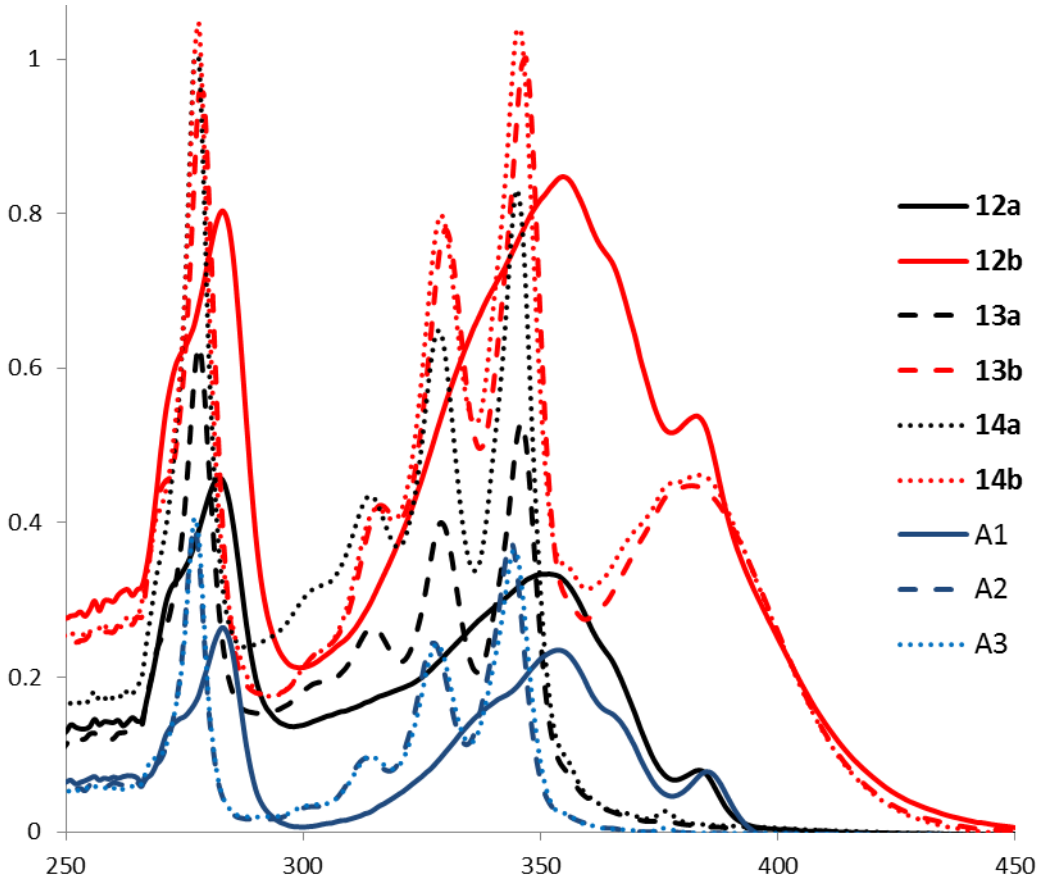

Fig. 31. *The UV-Vis spectra of complexes* ***12***–***14****, 1-pyrenecarboxylic acid (A1), 1-pyreneacetic acid (A2) and 1-pyrenebutyric acid (A3) at* 10^{-5} *M concentration in* CH_2Cl_2 *at room temperature.*

The molecular structures of **12b**, **13b** and **14b** have been determined by single-crystal X-ray structure analysis (Fig. 32 - Fig. 34). Selected bond lengths and angles are reported in Table 4. All complexes show a typical diruthenium backbone with the pyrenyl-carboxylato ligands being in the equatorial positions and bridging the two ruthenium atoms, while the triphenylphosphine ligands occupy the axial coordination sites. As often encountered in such complexes, the Ru-Ru distances [2.7098(9) Å (**12b**); 2.7036(3) Å (**13b**); 2.7502(5) Å (**14b**)] remain in the range of a metal-metal single bond,[7] and the P-Ru-Ru-P axes deviate significantly from linearity, the Ru-Ru-P angles being comprised between 162° and 167°. Overall, the geometrical parameters observed in **12b**, **13b** and **14b** are comparable to those found in analogous diruthenium tetracarbonyl complexes with triphenylphosphine axial ligands.[12a]

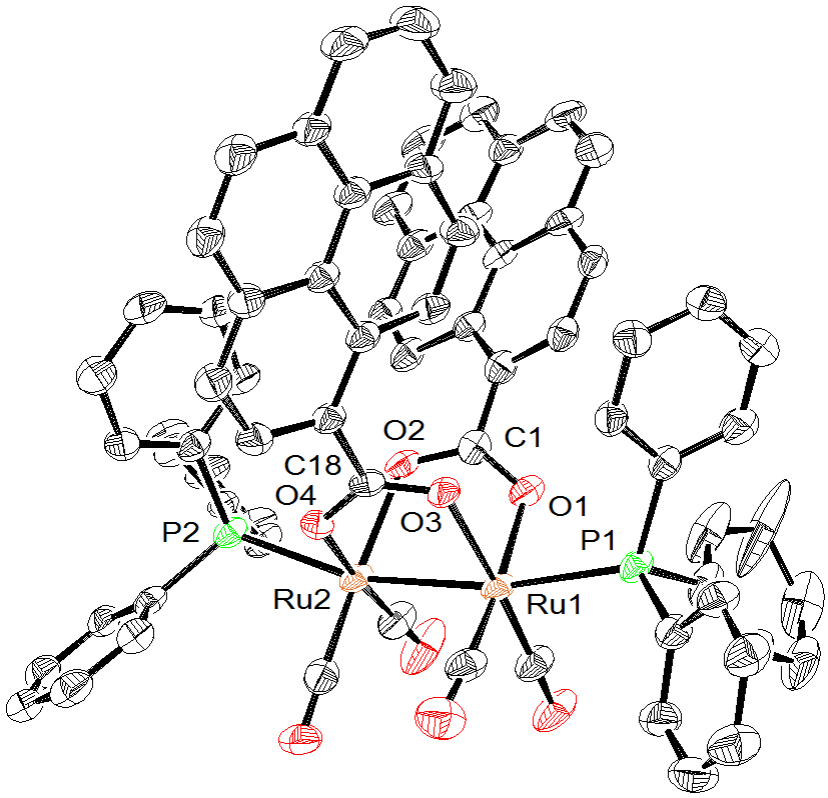

Fig. 32. *ORTEP drawing of complex* ***12b*** *with ellipsoids at the 35 % probability level.*

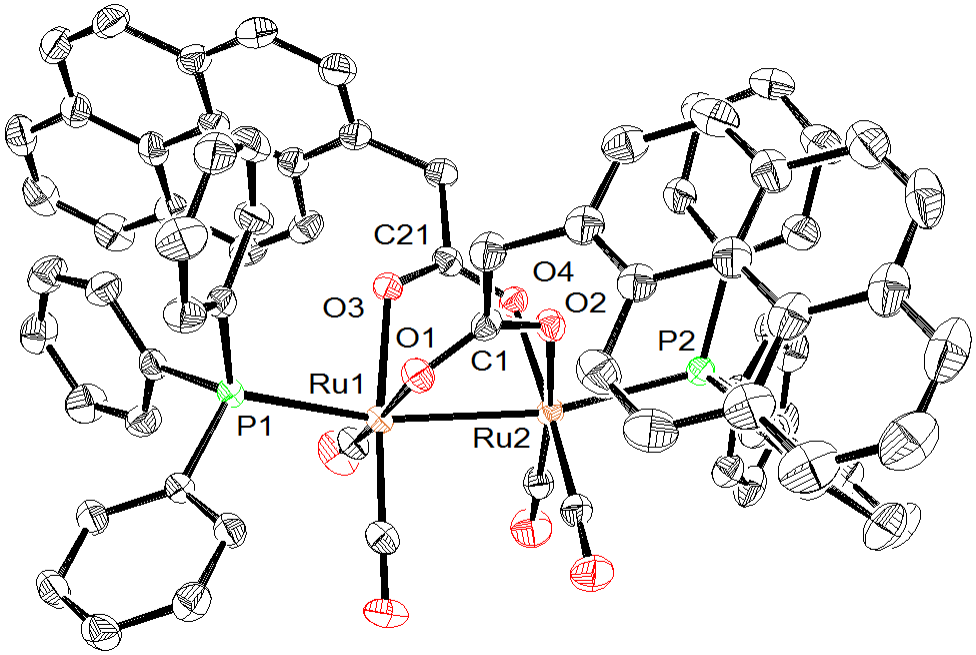

Fig. 33. *ORTEP drawing of complex* ***13b*** *with ellipsoids at the 35 % probability level.*

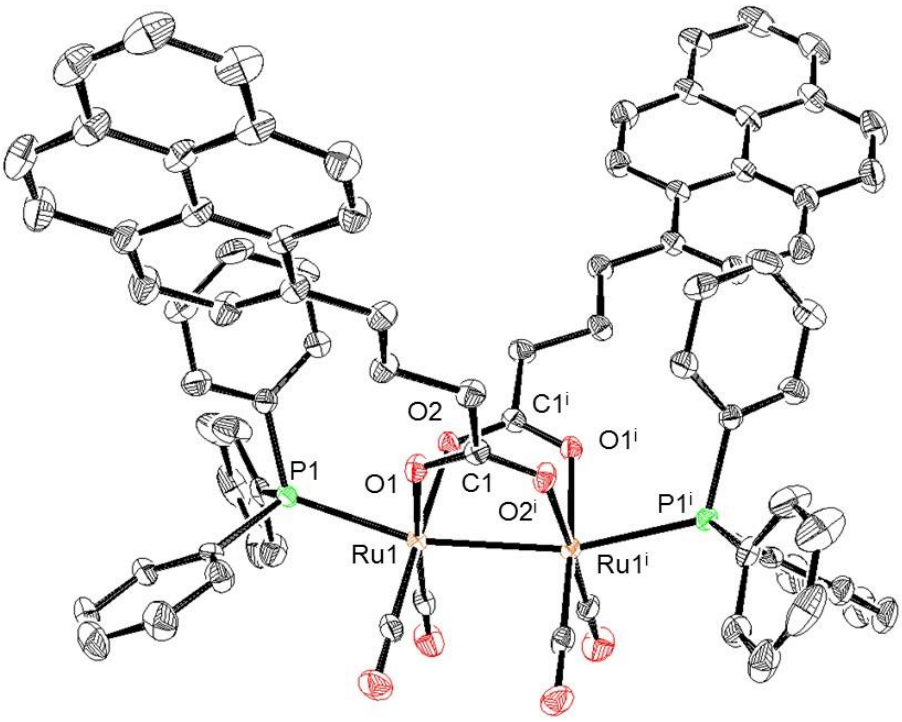

Fig. 34. *ORTEP drawing of complex* ***14b*** *with ellipsoids at the 35 % probability level (symmetry code i = -x, y, ½-z).*

Interestingly, in the crystal packing of **14b**, the complex crystallizes with two molecules of toluene. These toluene molecules fill the voids left between the pyrenyl-butyric moieties, and they interact weakly with either the pyrenyl groups through π-π stacking interactions or with the phenyl groups of the PPh_3 ligands. In **13b**, strong intermolecular pyrenyl-pyrenyl interactions are observed between neighboring sawhorse complexes (Fig. 35). The distance between the two symmetry related pyrenyl-planes is only 3.49 Å, the typical distance for a slipped-parallel π- stacking interaction.[55]

Table 4. Selected bond lengths (Å) and angles (º) for **12b**, **13b** and **14b**

	12b	**13b**	**14b**
Distances (Å)			
Ru-Ru	2.7098(9)	2.7036(3)	2.7502(5)[a]
Ru1-P1	2.452(2)	2.4350(7)	2.4674(7)
Ru2-P2	2.452(2)	2.4512(7)	
Ru1-O1	2.111(6)	2.132(2)	2.123(2)
Ru1-O3	2.161(5)	2.136(2)	2.126(2)
Ru2-O2	2.167(6)	2.137(2)	
Ru2-O4	2.110(5)	2.136(2)	
Angles (°)			
Ru-Ru-P1	167.45(6)	164.01(2)	164.09(2)
Ru-Ru-P1	161.92(5)	165.99(2)	
O1-Ru-O3	82.6(2)	84.58(7)	85.90(7)
O2-Ru-O4	85.8(2)	83.80(7)	
O1-C-O2	125.1(8)	125.8(2)	125.6(2)
O3-C-O4	125.2(6)	126.0(2)	
C_{CO}-Ru1-C_{CO}	89.2(4)	89.6(4)	86.2(1)
C_{CO}-Ru2-C_{CO}	89.7(4)	87.2(1)	

[a] *symmetry code -x, y, ½-z*

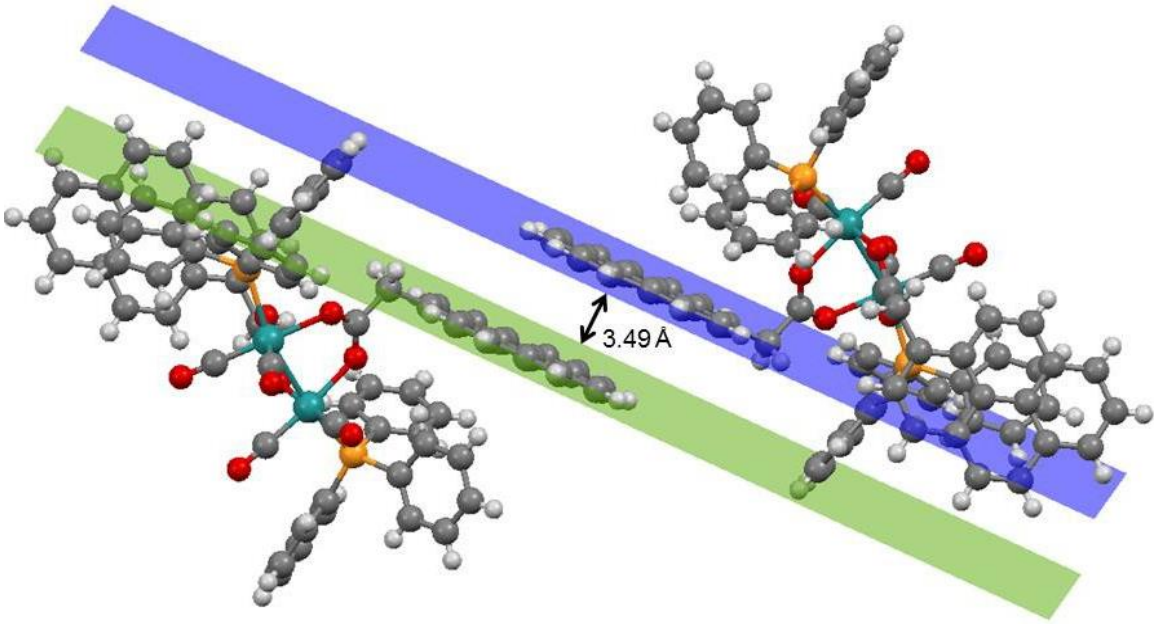

Fig. 35. *Intermolecular pyrenyl-pyrenyl interactions observed in the crystal packing of* ***13b****.*

After confirming the molecular structures of complexes **12**–**14**, the ability for these complexes to act as molecular tweezers in solution was studied. Fullerene (C_{60}) was selected as a guest to evaluate the hosting potential of the bis-pyrenyl derivatives. Planar aromatic moieties are known to interact with C_{60} through π-π stacking interactions.[84] Upon addition of increasing amounts of C_{60} (up to 4 equiv.) to a solution of complexes **12**, **13** and **14** (**12b**: 3.3 x 10^{-6} M in toluene; **13b**: 2.3 x 10^{-6} M in toluene, **14a**: 5.4 x 10^{-6} M in toluene, **14b**: 6.5 x 10^{-6} M in cyclohexane), no changes were observed in the UV-Vis spectra. Fluorescence measurements also suggest no interaction between **14** and C_{60}, showing no spectral changes during the titration experiments (toluene, 4.5 x 10^{-6} M concentrations, up to 5 equiv. of C_{60}, λ_{exc} = 345 nm). Finally, upon addition of increasing amounts of complex **14b** to a toluene-d_8 solution of C_{60}, no chemical shift was observed for the ^{13}C NMR signal of C_{60}. Therefore, to rationalize this lack of host-guest interaction between the complexes and C_{60}, molecular modeling was performed.

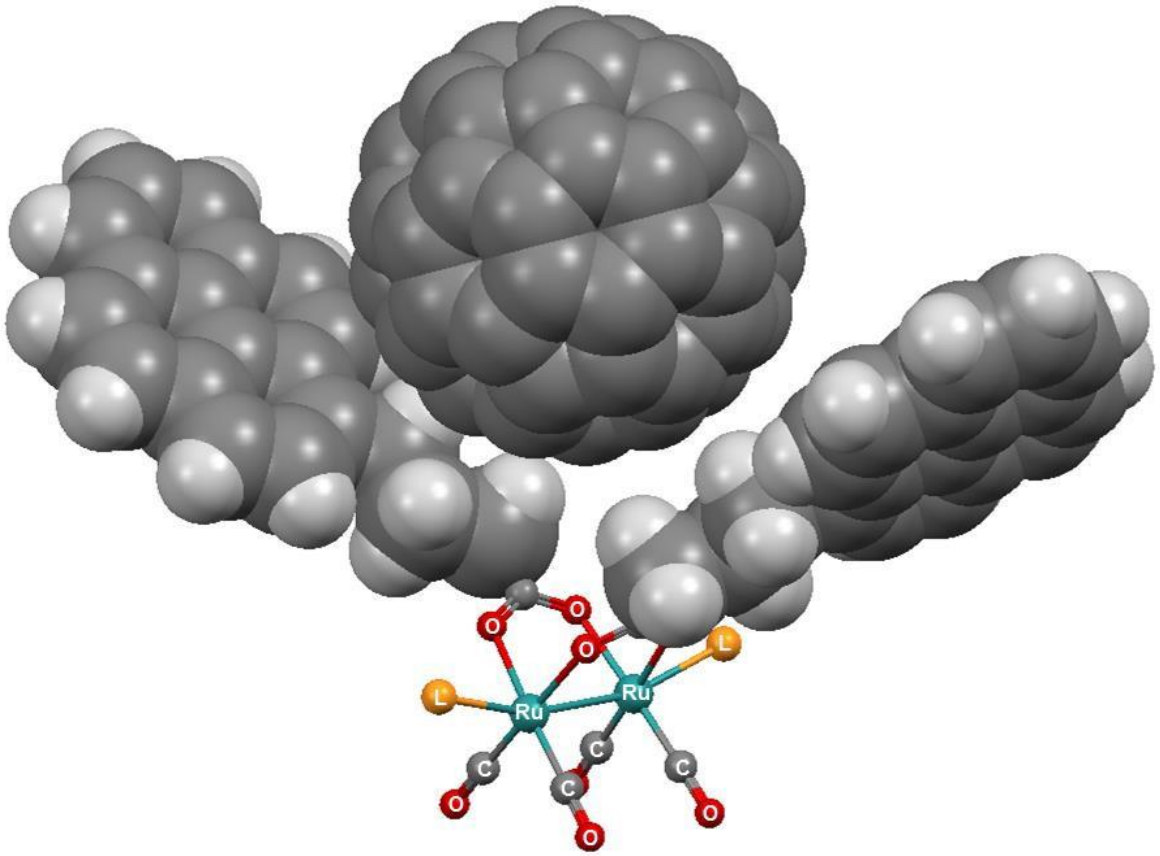

Fig. 36. *Chem3D model showing a fullerene molecule between the two pyrenyl groups of* ***14****.*

The Chem3D software was used to place a fullerene molecule in the cavity of the bis-pyrenyl complexes **12**–**14**. In **12**, the rigidity and limited flexibility of the two pyrenyl groups did not allow the fullerene to interact significantly with pyrene, while with **13**, fullerene fits better but the π-stacking interaction is not optimal. On the other hand, with complex **14**, the flexibility provided by the butyl chains seems to offer an appropriate cavity between the pyrenyl groups to interact with fullerene (Fig. 36). Yet, no meaningful interaction was observed in solution between **14** and fullerene (C_{60}).

3.4. Porphyrin derived sawhorse-type molecular tweezers

In a similar fashion, π-conjugated aromatic porphyrin moieties were also used for the synthesis of sawhorse-type diruthenium tetracarbonyl tweezers. Their binding ability with different guest molecules in solution was evaluated by using optical spectroscopic methods.

Herein, we report the synthesis and the binding affinity of the sawhorse-type dinuclear ruthenium complex $[Ru_2(CO)_4(O_2CC_{44}H_{29}N_4)_2(PPh_3)_2]$ (**15**), which was previously evaluated as photosensitizer for cancer cells,[12b] and the new tetranuclear ruthenium complex, $[\{Ru_2(CO)_4(PPh_3)_2\}_2(O_2CC_{44}H_{28}N_4CO_2)_2]$ (**16**), which is composed of two sawhorse units connected by di-carboxylic porphyrin bridges. In addition, the corresponding zinc(II)-porphyrin derivatives $[Ru_2(CO)_4(O_2CC_{44}H_{27}N_4Zn)_2(PPh_3)_2]$ (**17**) and $[\{Ru_2(CO)_4(PPh_3)_2\}_2(O_2CC_{44}H_{26}N_4ZnCO_2)_2]$ (**18**) have been prepared (Fig. 37).

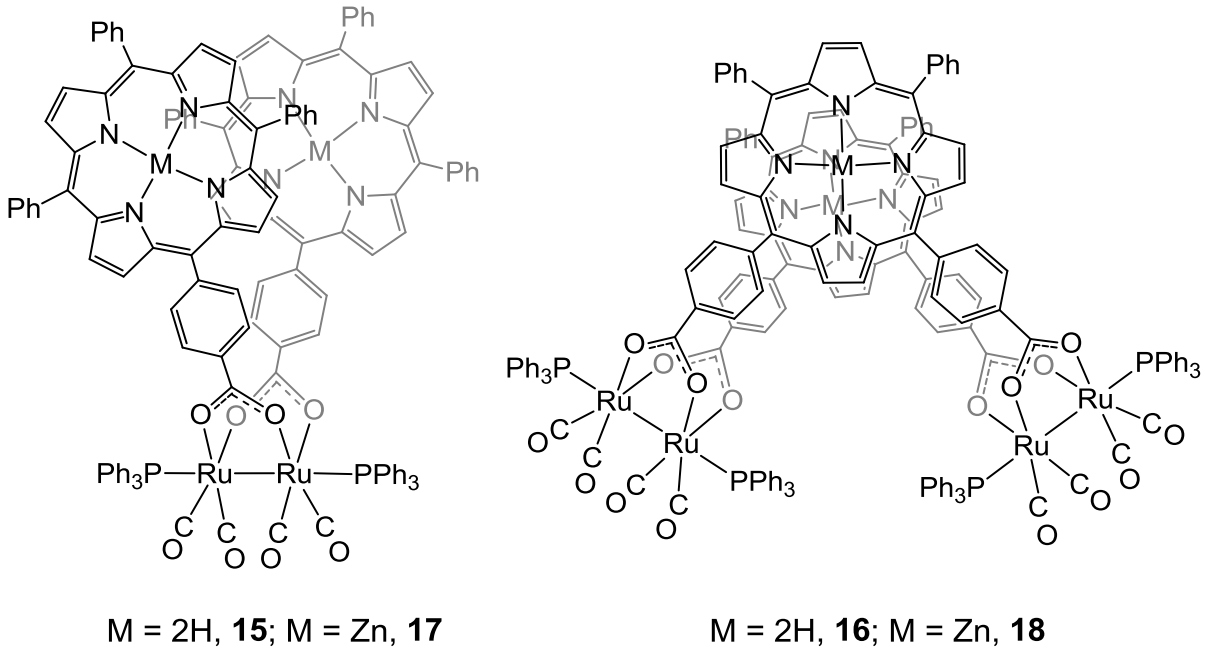

Fig. 37. *Molecular structures of sawhorse-type diruthenium tetracarbonyl tweezers incorporating porphyrin moieties.*

All complexes possess two porphyrin moieties perfectly positioned to potentially act as molecular tweezers for guest molecules. The efficacy for molecular recognition of these organometallic tweezers have been studied with fullerene (C_{60}), pyridine (pyr), 4,4'-bipyridine (bipy), 1,2-bis(4-pyridyl)ethylene (bpe), and photoactive guests such as 5,10-di-(4-pyridyl)-15,20-diphenyl-21H,23H-porphyrin (5,10-dpp) and 5,15-di-(4-pyridyl)-10,20-diphenyl-21H,23H-porphyrin (5,15-dpp) using optical spectroscopic methods (Fig. 38).

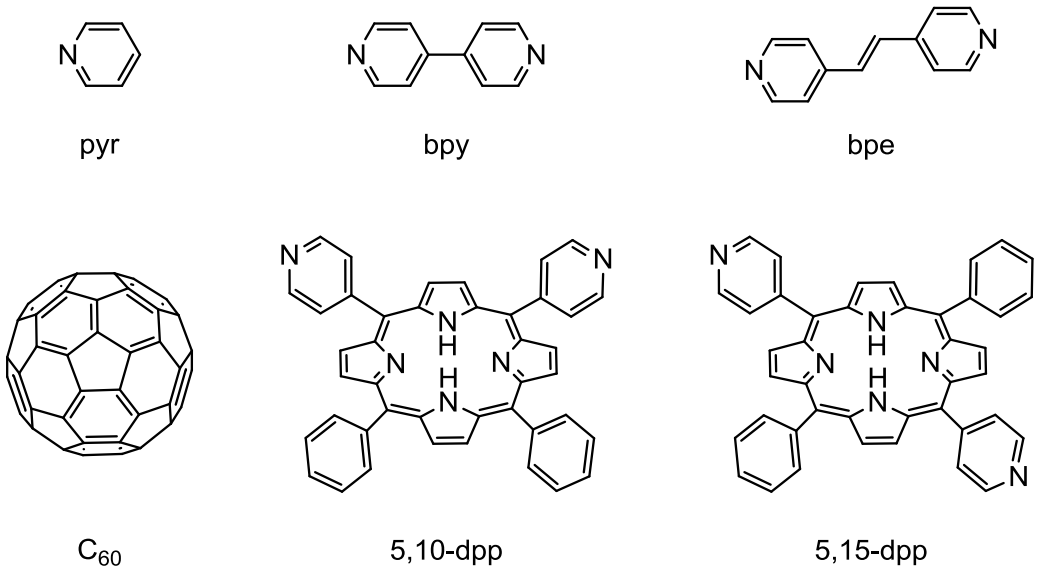

Fig. 38. *Molecular structure of the guest molecules*

3.4.1. Synthesis of molecular tweezers

The thermal reaction of $Ru_3(CO)_{12}$ with excesses of 5-(4-carboxyphenyl)-10,15-20-triphenyl-21H,23H-porphyrin ($HO_2CC_{44}H_{29}N_4$), the corresponding zinc(II)-porphyrin complex ($HO_2CC_{44}H_{27}N_4Zn$), 5,10-di(4-carboxyphenyl)-15,20-diphenyl-21H,23H-porphyrin ($HO_2CC_{44}H_{28}N_4CO_2H$) or the corresponding zinc(II)-porphyrin ($HO_2CC_{44}H_{26}N_4ZnCO_2H$) in refluxing thf yields a solution containing the thf complexes $[Ru_2(CO)_4(O_2CC_{44}H_{29}N_4)_2(thf)_2]$, $[Ru_2(CO)_4(O_2CC_{44}H_{27}N_4Zn)_2(thf)_2]$, $[\{Ru_2(CO)_4(thf)_2\}_2(O_2CC_{44}H_{28}N_4CO_2)_2]$ or $[\{Ru_2(CO)_4(thf)_2\}_2(O_2CC_{44}H_{26}N_4ZnCO_2)_2]$, respectively. These labile thf intermediates react easily with triphenylphosphine to afford, after precipitation and column chromatography, the neutral complexes $[Ru_2(CO)_4(O_2CC_{44}H_{29}N_4)_2(PPh_3)_2]$ (**15**), $[\{Ru_2(CO)_4(PPh_3)_2\}_2(O_2CC_{44}H_{28}N_4CO_2)_2]$ (**16**), $[Ru_2(CO)_4(O_2CC_{44}H_{27}N_4Zn)_2(PPh_3)_2]$ (**17**) and $[\{Ru_2(CO)_4(PPh_3)_2\}_2(O_2CC_{44}H_{26}N_4ZnCO_2)_2]$ (**18**) in moderate yields. These four bis-porphyrin molecular tweezers built from sawhorse diruthenium units are depicted in (Fig. 37).

All compounds are air-stable, dark-purple solids, which are sparingly soluble in polar organic solvents and they were characterized by IR (KBr pellet), NMR, UV-Vis and fluorescence spectroscopic techniques as well as by combustion analysis. In the $\nu_{(CO)}$ region of the infrared spectrum (2100-1900 cm^{-1}), the characteristic three-band pattern of the $Ru_2(CO)_4$ sawhorse moiety, which is observed in all complexes of this type.[7] Moreover, due

to the presence of the porphyrin groups, a strong absorption centered at 1587 cm^{-1} that corresponding to $\nu_{(NCN)}$ is observed, and a medium absorption at 3054 cm^{-1} is associated to the C-H stretching vibration.[85]

The ^{1}H NMR spectra of **15-18** in $CDCl_3$ at room temperature display a similar signal pattern for the protons of the coordinated porphyrin(carboxyphenyl) derivatives as well as for the triphenylphosphine axial ligands. In **15** and **16** an additional signal attributed to the N-H protons is observed at δ = -2.8 ppm, while in all complexes multiplets at δ = 7.43, 7.77, 7.82 and 8.22 ppm are found in the aromatic region, which corresponding to the protons of the phenyl rings of both the porphyrin and the triphenylphosphine ligands. Moreover, in the $^{31}P\{^{1}H\}$ NMR spectra, a sharp singlet at ≈ 17 ppm corresponding to the PPh_3 axial ligands is observed. All NMR data were consistent with the proposed structures.

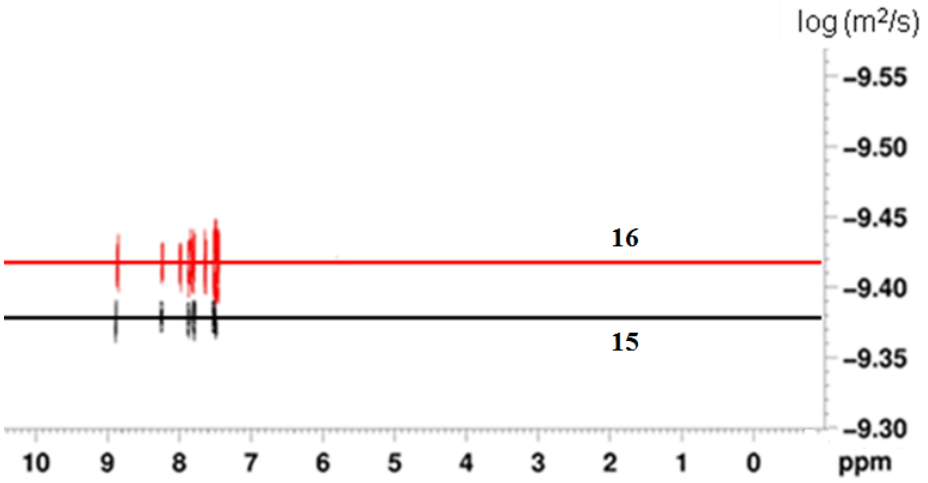

Fig. 39. *DOSY NMR spectra of **15** (black line) and **16** (red line) in $CDCl_3$ at room temperature.*

Unable to grow crystals suitable for X-ray structure analysis, the size and shape of the complexes were estimated using diffusion-ordered NMR spectroscopy (DOSY) and molecular modeling. The radii of the complexes were derived from the diffusion coefficients (*D*) by using the Stokes-Einstein equation.[86] The radii of complexes **15** and **17** are equivalent at 9.7 Å, whereas the radii of complexes **16** and **18** are slightly longer at 10.5 Å. These values determined from DOSY experiments (Fig. 39) are in agreement with the structural data obtained from molecular modeling (Fig. 40), for which the volume of the dinuclear complex

15 is only slightly smaller than the volume of the tetranuclear derivative **16**. In addition, it is worth mentioning that these models show median porphyrin-porphyrin cavity sizes of ca. 16 Å for all complexes.

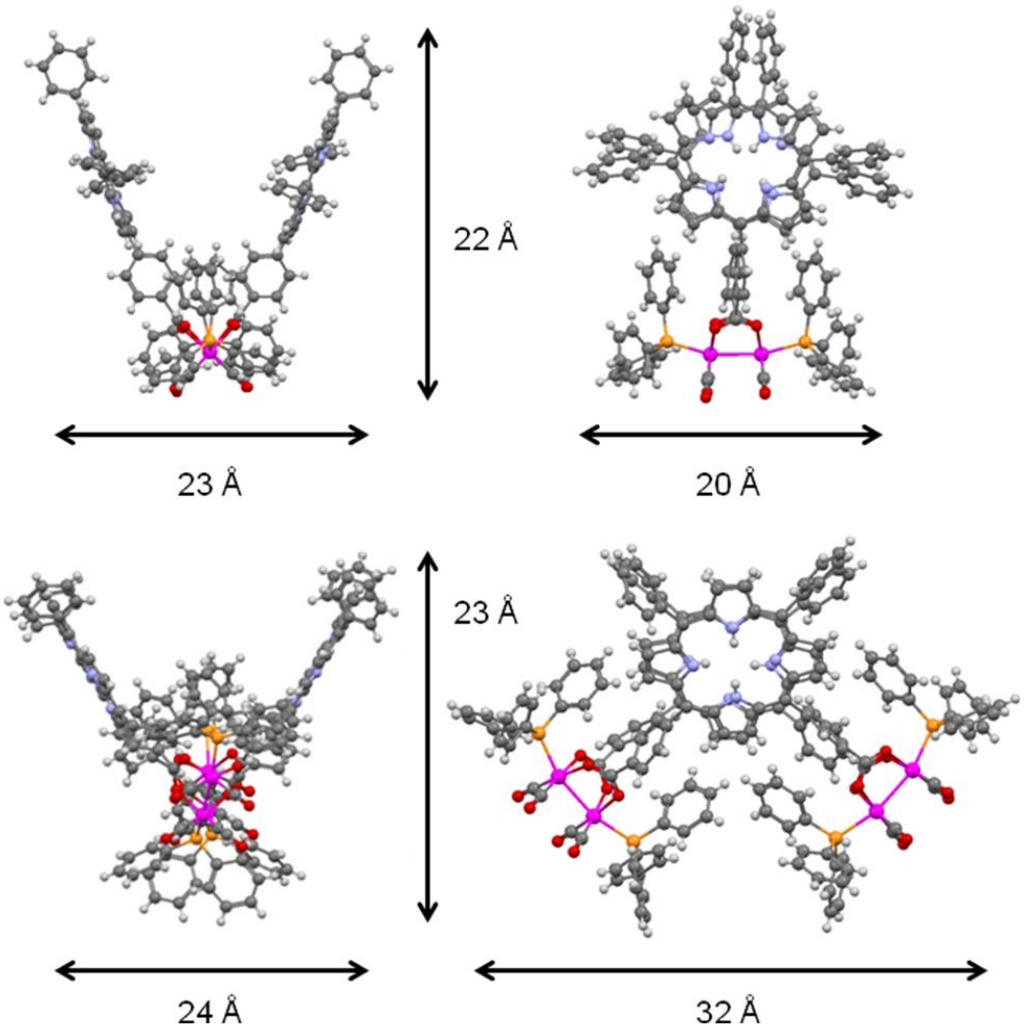

Fig. 40. *Molecular modeling of complexes **15** (top) and **16** (bottom)*

The absorption spectra of bis-porphyrin complexes **15**-**18** and of the reference sawhorse complex containing no porphyrin units, $[Ru_2(CO)_4(O_2CC_8H_{17})_2(PPh_3)_2]$ (**3b**),[53a] are shown in Fig. 41. The limited solubility of **15** in CCl_4 forced us to use cyclohexane for this compound. All four bis-porphyrin derivatives absorb throughout the visible region, showing the characteristic Soret and Q bands; the absorption features of **16** are slightly red-shifted

compared to **15**, as a consequence of the different solvents. The reference sawhorse-type complex **3b** shows a weak absorption maximum at 382 nm, which scarcely contributes to the spectra of multi-chromophoric systems **15**-**18**. Notably, the molar extinction coefficients of all complexes match those of similar bis-porphyrin systems, suggesting the absence of sizeable ground state inter-porphyrin electronic interactions.[87]

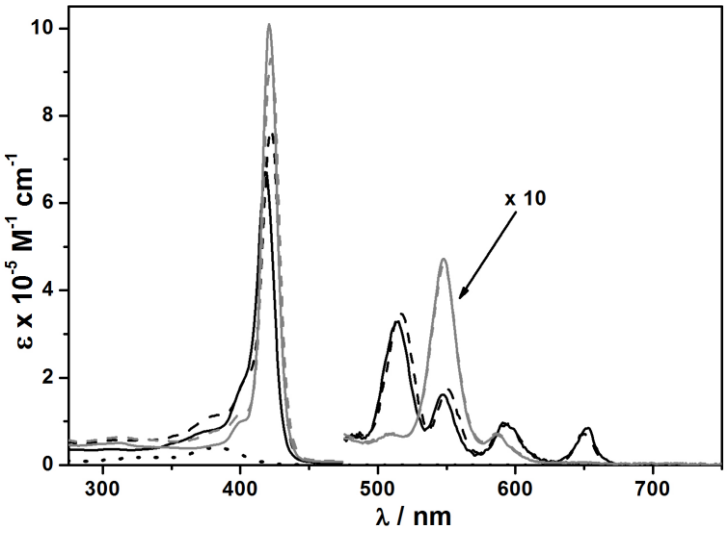

Fig. 41. *The electronic absorption spectra of **15** in cyclohexane (black line), **16**–**18** and **3b** in CCl_4 (black dashed, grey, grey dashed and black dotted lines, respectively).*

The fluorescence spectra of **15** and **16** are almost identical in shape and position to the non-coordinated porphyrin ligands (not shown), and the similar singlet lifetime (τ) values (9.3 and 8.1 ns respectively) indicate negligible intramolecular porphyrin interactions in the excited state. The same is observed for the Zn-porphyrin derivatives (τ = 2.3 ns and 2.2 ns for **17** and **18** respectively), and this confirms that the presence of diruthenium sawhorse moieties does not perturb the electronic properties of the porphyrin moieties. Also, the luminescence of the reference complex **3b** is rather weak and it cannot significantly contribute to the emission spectra of bis-porphyrin complexes **15**-**18**.

By taking advantage of the strong affinity of porphyrin units for fullerene (C_{60}) in apolar solvents,[77h,84a,87b,88] the bis-porphyrin hosts **15** and **16** were titrated with increasing amounts of C_{60} in cyclohexane and CCl_4, respectively. The process was monitored by UV-

Vis absorption spectroscopy. The spectra of the titrated solutions containing **15** or **16** and C_{60} (5 equiv.) are shown in Fig. 42 and Fig. 43. Unlike other bis-porphyrin host platforms,[87b,88] no significant changes are observed in the absorption features of **15** and **16** indicating the absence of sizeable interaction between the two components. The large cavity size (Fig. 40) and the rigid bis-porphyrin framework of **15** and **16** could be the reasons for the lack of formation of supramolecular adducts. In fact, molecular modeling suggests that allowing porphyrins to move freely around C_{60} would facilitate the supramolecular complexation (Fig. 44). Hence, the experimental results suggest that the porphyrin units anchored to the sawhorse backbone in **15** and **16** apparently cannot provide the structural conditions for the formation of stable adducts with C_{60}.

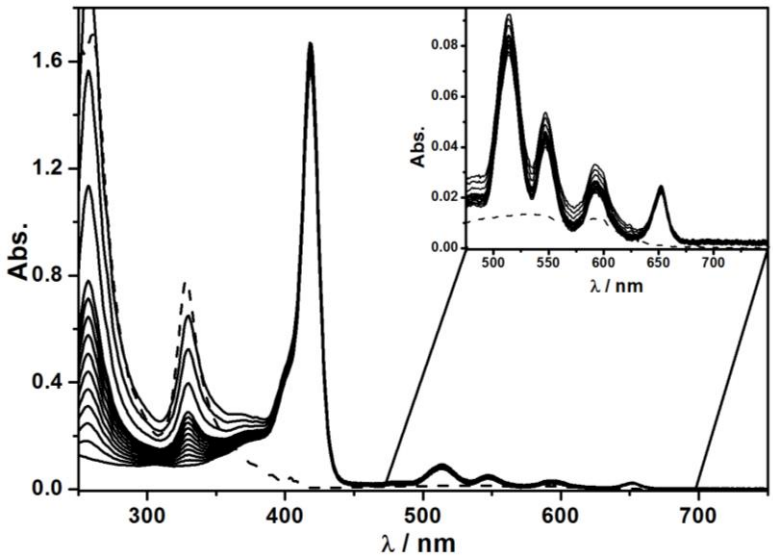

Fig. 42. *Change in the absorption spectra of* ***15*** *(2.3 × 10^{-6} M) upon addition of increasing amounts of C_{60} (up to 5 equiv.) in cyclohexane. Inset: The corresponding changes in the Q bands spectral region. All the observed spectral variations are solely attributable to the added fullerene chromophore.*

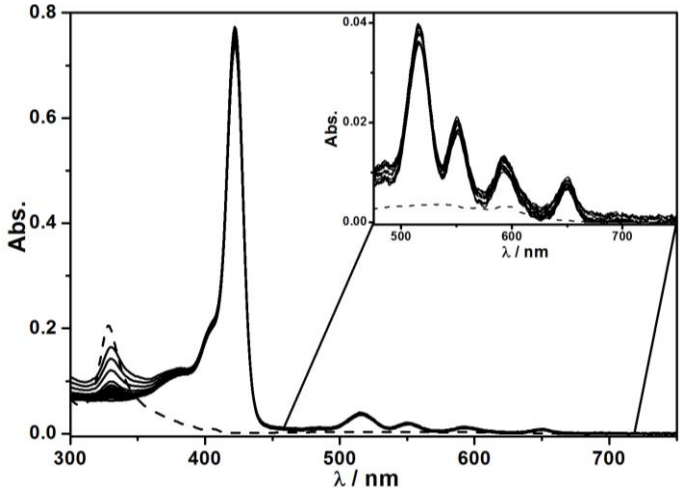

Fig. 43. *Change in the absorption spectra of* ***16*** *(5.8 × 10^{-7} M) upon addition of increasing amounts of C_{60} (up to 5 equiv.) in CCl_4. Inset: The corresponding changes in the Q bands spectral region. All the observed spectral variations are solely attributable to the added fullerene chromophore.*

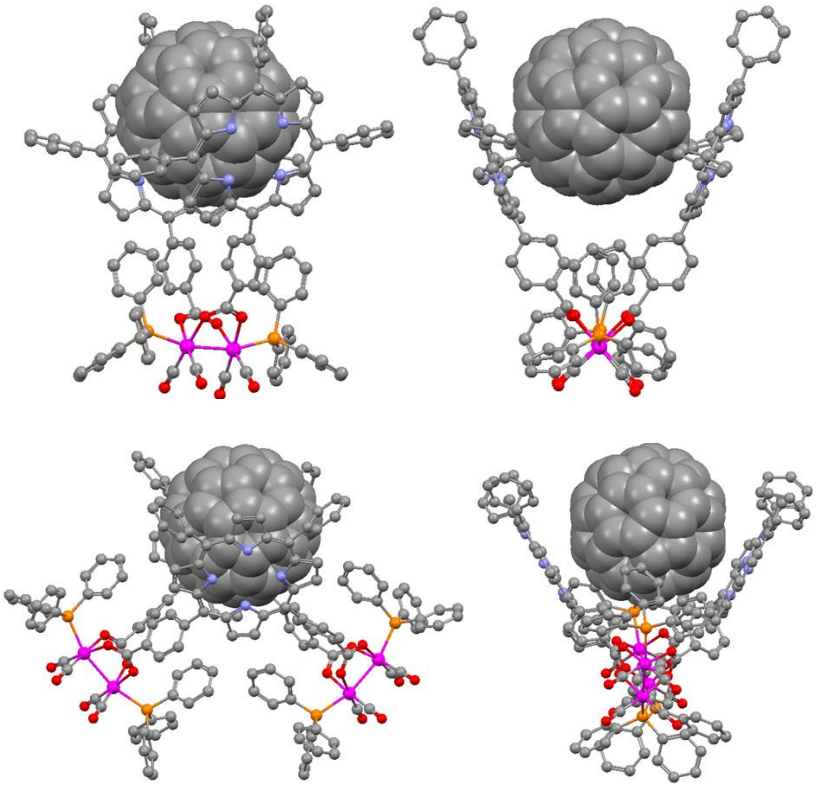

Fig. 44. *Molecular modeling of C_{60}⊂**15** (top) and C_{60}⊂**16** (bottom) adducts.*

Zinc-porphyrin hosts are expected to have a structural rigidity similar to their free-base analogues, with no tendency to give adducts with C_{60}. Therefore, **17** and **18** were titrated with molecules bearing two pyridine units,[87a,89] namely 4,4'-bipyridine (bpy), 1,2-bis(4-pyridyl)ethylene (bpe), 5,10-di-(4-pyridyl)-15,20-diphenyl-21,23H-porphyrin (5,10-dpp) and 5,15-di-(4-pyridyl)-10,20-diphenyl-21,23H-porphyrin (5,15-dpp) (Fig. 38), which can afford a bridging bidentate coordination to the Zn(II) ions of the bis-porphyrin tweezers **17** and **18**. It has to be emphasized that external coordination of Zn-porphyrin by the pyridine (pyr), bpy and bpe moieties are in principle possible, but monodentate coordination exhibits a much lower association constant (ca. 10^4 M^{-1})[87a] compared to bidentate (ca. 10^7 M^{-1})[90] complexation. To discern the two different coordination modes, titrations of **17** and **18** were first carried out with pristine pyridine (Fig. 45). The absorption spectral changes of the host molecules upon addition of increasing amounts of pyridine (up to 8000 equiv.) in CCl_4; a significant red shift in the Soret ($\Delta\lambda$ = 10 nm) and Q bands ($\Delta\lambda$ = 15 nm) of the bis-porphyrin hosts were observed. Similar results can be found in the literature with Zn-porphyrin systems.[87a,89a] Therefore, the observed absorption changes are attributed to the pyridine coordination to the Zn-porphyrin moieties of **17** and **18**. The related association constants were derived from Benesi-Hildebrand equations[91] and, as expected, are in the order of 10^3 M^{-1} (Table 5). The fitted absorption spectral points are shown in Fig. 46.

Table 5. Association constants of **17** and **18** with different pyridyl containing guests in CCl_4 at room temperature.

Compound	Association constant K_a [M^{-1}]			
	pyr	Bpy	bpe	5,10-dpp[a]
17	6.4×10^3	9.9×10^4	8.8×10^4	4.5×10^4
18	6.7×10^3	1.5×10^5	3.5×10^5	4.0×10^7

[a] Titrations carried out in toluene

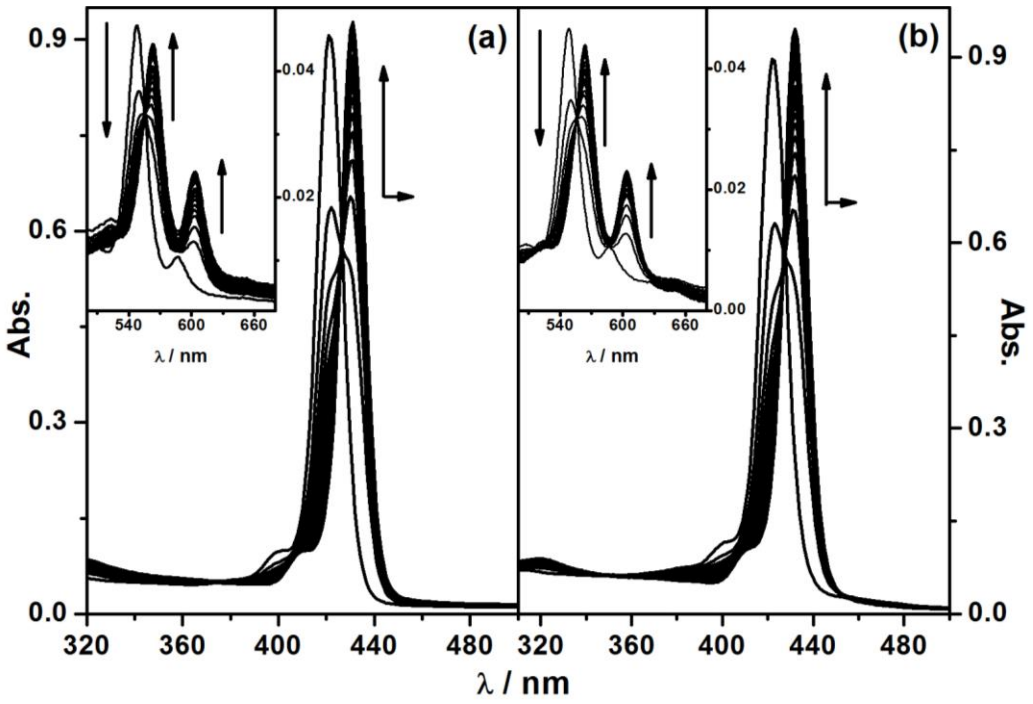

Fig. 45. *Change in the absorption spectra of* ***17*** *{9.9×10^{-7} M, (a)} and* ***18*** *{9.9 × 10^{-7} M, (b)} upon addition of increasing amounts of pyridine (up to 8000 eq.) in CCl_4. Insets: The corresponding changes in the Q bands spectral region.*

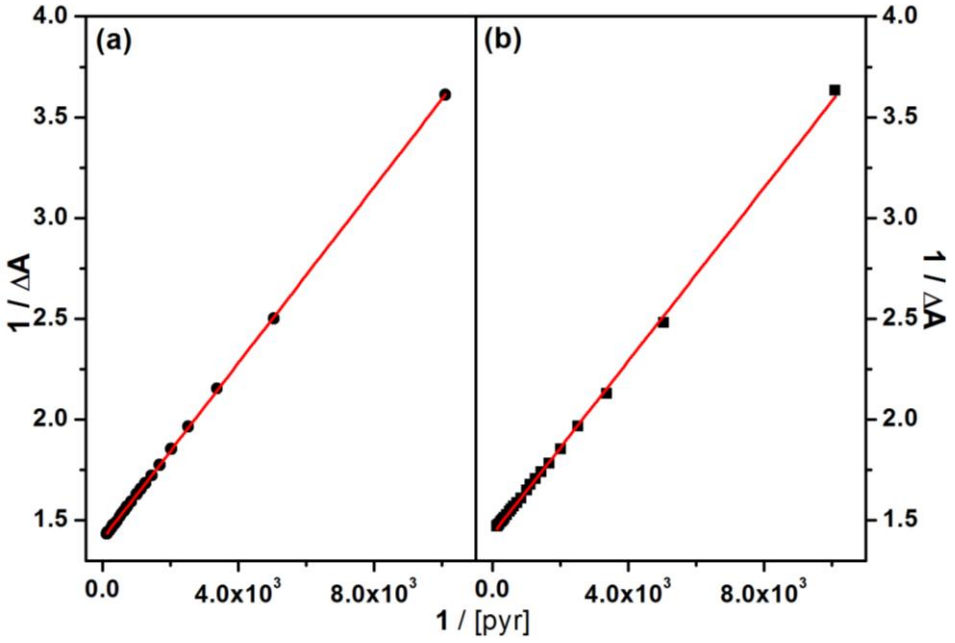

Fig. 46. *The Benesi-Hildebrand linear fitting of absorption data points collected from the titration curves of* ***17*** *(at 421 nm) and* ***18*** *(at 422 nm) against increasing amounts of pyridine in CCl_4.*

Taking these values as benchmark for monodentate coordination, **17** and **18** were then titrated with bpy and bpe in CCl_4. The absorption spectra of the Zn-porphyrin derivatives upon continuous addition of aliquot amounts of bpy (up to 10 equiv.) display a moderate intensity decrease of the Soret and Q bands together with a slight red-shift (Fig. 47). On the other hand, the titration with bpe, which exhibits longer interpyridyl distance, leads to sharp changes in the absorption spectra of the hosts (Fig. 48). Particularly in the case of **18**, an optimized fitting of the interpyridyl distance of bpe with the size of the cavity the between Zn-porphyrin moieties could enable a strong interaction. Fluorescence measurements support this hypothesis, because the emission features of the Zn-porphyrin are significantly red-shifted in bpe⊂**18** (bpe-in-**18**), corroborating the occurrence of a stronger host-guest complexation,[87a,89b] whereas bpe⊂**17** shows fluorescence attributable to the free porphyrin units (Fig. 49).

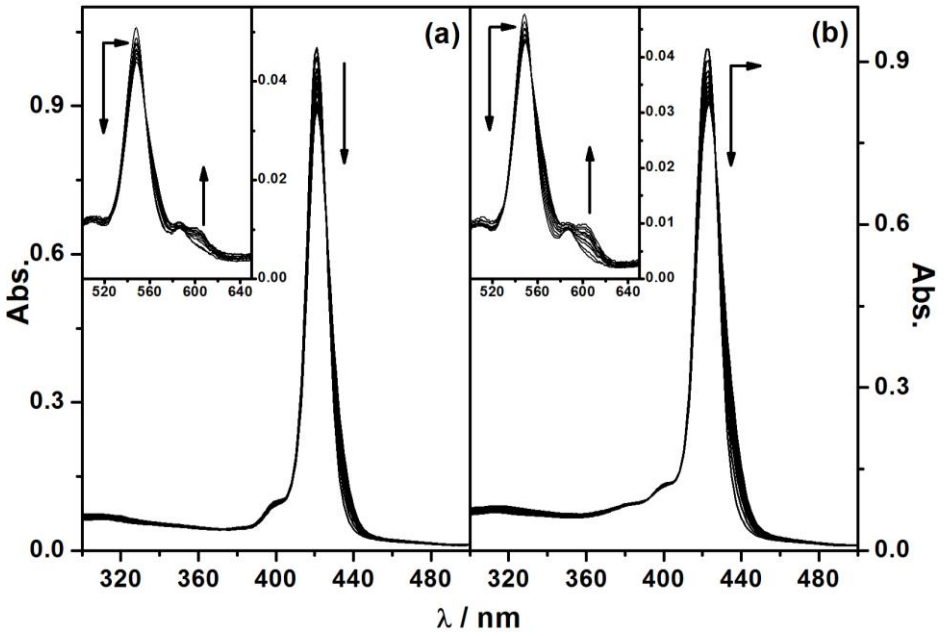

Fig. 47. *Change in the absorption spectra of* ***17*** *{1.0 × 10^{-6} M, (a)} and* ***18*** *{1.0 × 10^{-6} M, (b)} upon addition of increasing amounts of bpy (up to 10 equiv.) in CCl_4. Insets: The corresponding changes in the Q bands spectral region.*

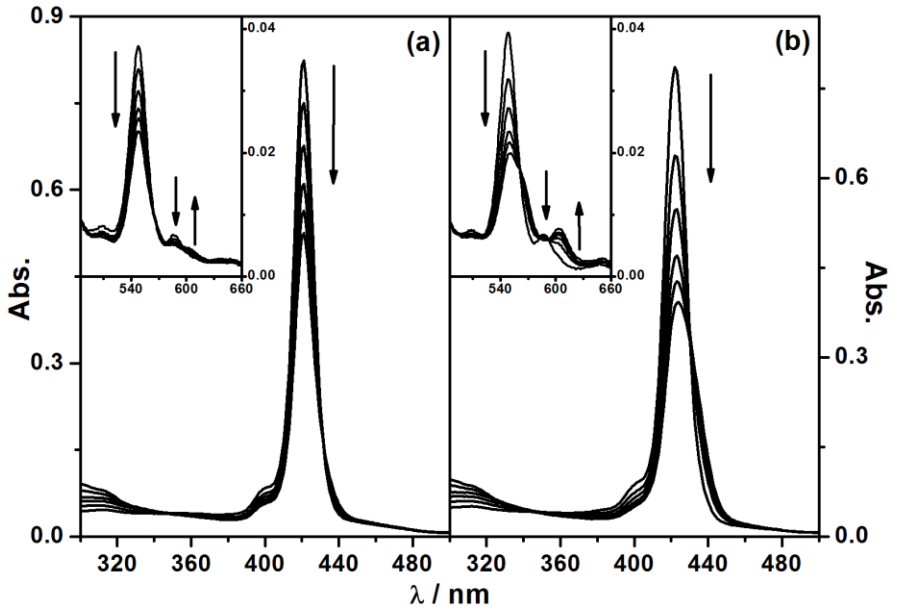

Fig. 48. *Changes in the absorption spectra of **17** {1.0 × 10-6 M, (a)} and **18** {1.0 × 10-6 M, (b)} upon addition of increasing amounts of bpe (up to 5 equiv.) in CCl4. Insets: The corresponding changes in the Q bands spectral region.*

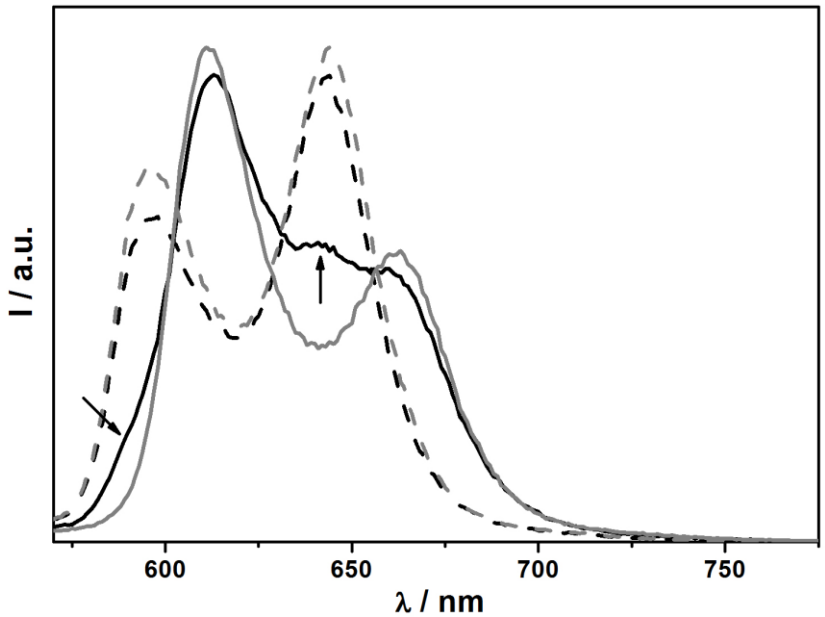

Fig. 49. *Fluorescence spectra of 1.0 × 10^{-6} M solutions of **17** (black dashed line) and **18** (grey dashed line), and supramolecular adducts bpe⊂**17** (**17** = 1.0 × 10^{-6} M, [bpe] = 5.0 × 10^{-6} M, black line) and bpe⊂**18** (**18** = 1.0 × 10^{-6} M, [bpe] = 5.0 × 10^{-6} M, grey line), excited at 545 nm in CCl_4. The emission of **17** and **18** are normalized at the corresponding maxima of the supramolecular complexes. The arrows in the spectrum of **17** indicate a feature attributable to the emission from free porphyrin units.*

The weak interaction between **17** and bpe is attributed to the comparatively larger bis-porphyrin cavity size (*vide supra*). The host-guest binding efficiency was determined quantitatively by plotting the absorption changes of the Soret band of **17** and **18** against the concentration of guest moieties. The resulting curves were fitted with a nonlinear equation (Fig. 50),[87a,92] and the corresponding association constant values are collected in Table 5. The stronger affinity of **17** and **18** to bpy and bpe guest molecules compared (one and two orders of magnitude, respectively) to pyridine suggests bidentate complexation of bpe and bpy within the cavity. On the other hand, analogous bis-porphyrin based host systems[87a,89b,c] display a 2-3 times higher association constants compared to the present case, indicating a non-optimal match between the host cavity of **17** and **18** and the length of these bis-pyridyl guests.

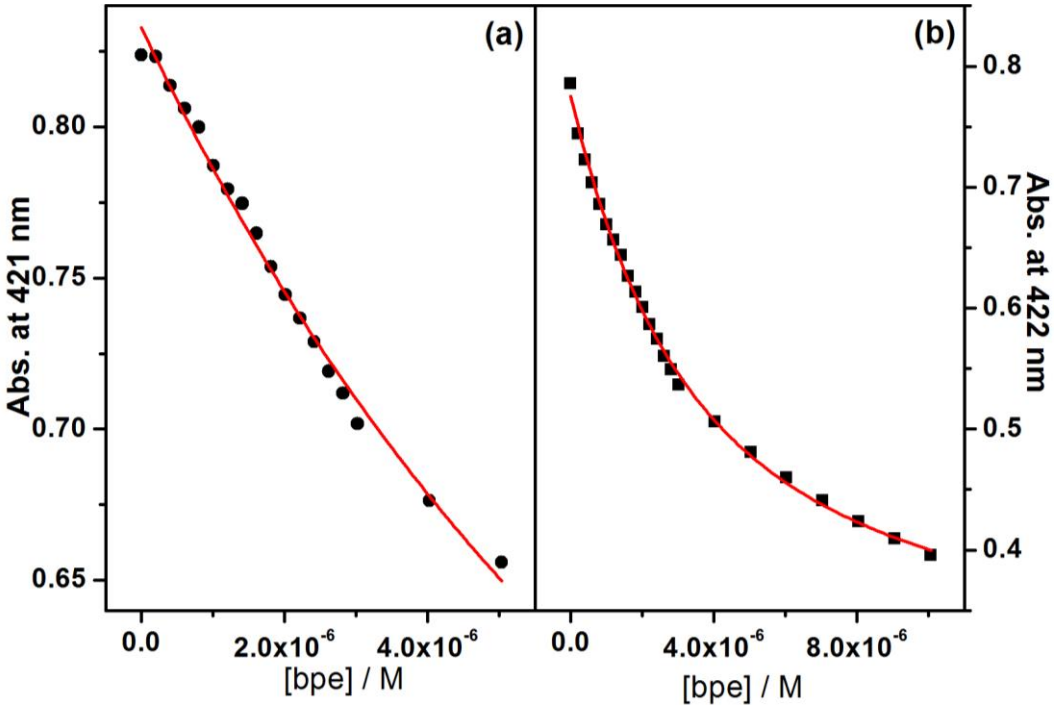

Fig. 50. *Non-linear fitting of the absorption data points collected from the titration curves of **17** (at 421 nm) and **18** (at 422 nm) against increasing amounts of bpe (up to 5 equiv.) in CCl_4.*

Subsequently, we have investigated the interaction of **17** and **18** with 5,10-dpp and 5,15-dpp, which are strong chromophoric guests having a free base porphyrin core and two coordinating pyridine units; toluene was used as solvent for solubility reasons. The absorption changes during the titration of **17** and **18** with 5,10-dpp and 5,15-dpp are

monitored by "differential" measurements, i.e. the absorption contribution of the added guest being subtracted from that of the host.[87a] The differential absorption spectral traces of **17** upon adding increasing amounts of 5,10-dpp in toluene are shown in Fig. 51a. Similar to the cases described above, the addition of 10 equiv. of 5,10-dpp to **17** results in a continuous bathochromic shift of the Soret and Q bands. Surprisingly, the absorption changes in the differential spectra of **18** reach a plateau after the addition of less than 2 equiv. of 5,10-dpp (Fig. 51b). It is worth emphasizing that the concentrations of **17** and **18** are of the order of 10^{-7} M, and additionally both the host and the guest show excellent solubility in toluene. Therefore, the formation of aggregates can be ruled out, and the changes observed in the titration curves are solely the consequence of host-guest complexation. The association constants are calculated in a similar way as mentioned above and the values are in the order of 10^4 M^{-1} and 10^7 M^{-1} for 5,10-dpp⊂**17** and 5,10-dpp⊂**18**, respectively (Table 4). The significantly higher binding constant value of 5,10-dpp⊂**18** reflects the higher affinity of **18** for 5,10-dpp and can be attributed to two factors: (i) the inter-pyridyl distance in 5,10-dpp summed with the length of two coordination bonds $N_{pyridyl}$-Zn (2.2 Å each) perfectly matches the cavity size of **18**; (ii) the pyridine units in 5,10-dpp show an appropriate orientation to coordinate with the Zn-porphyrin units in **18**, where a coordination angle of approximately 45° from the porphyrin molecular plane is required to facilitate coordination. In other words, 5,10-dpp can approach **18** with an optimal angle, thus, the combined spatial and structural effects favor a strong host-guest interaction, which is corroborated by molecular modeling (Fig. 52).

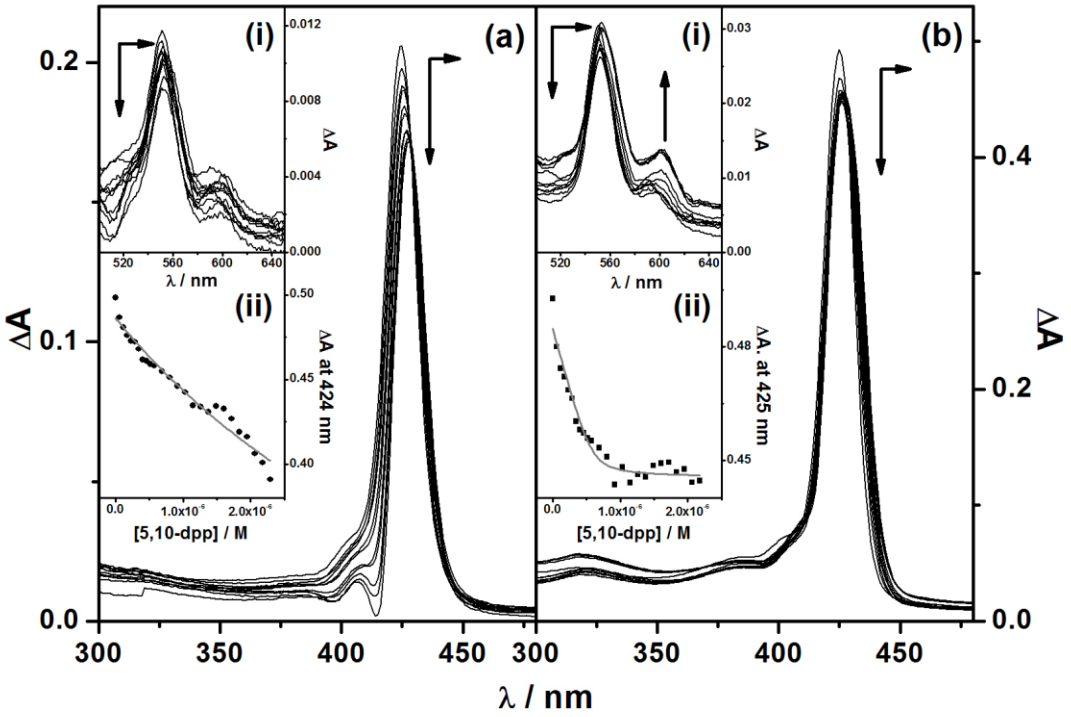

Fig. 51. *Differential absorption spectral traces of* ***17*** *(2.4 × 10^{-7} M, (a)) and* ***18*** *(5.8×10^{-7} M, (b)) upon addition of increasing amounts of 5,10-dpp (up to 10 and 4 equiv. respectively) in toluene. Inset (i): The corresponding changes in the Q bands spectral region; inset (ii): The fitted data points collected at 424 and 425 nm from* ***17*** *and* ***18****, respectively.*

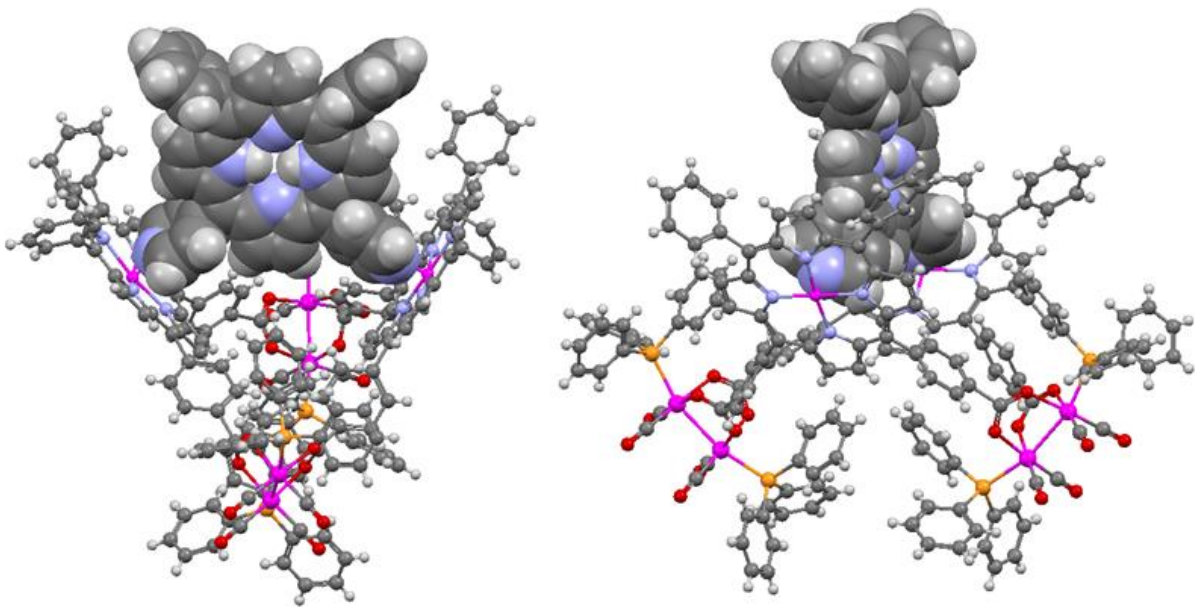

Fig. 52. *Molecular modeling of the 5,10-dpp⊂****18*** *adduct (5,10-dpp represented as space-filling model).*

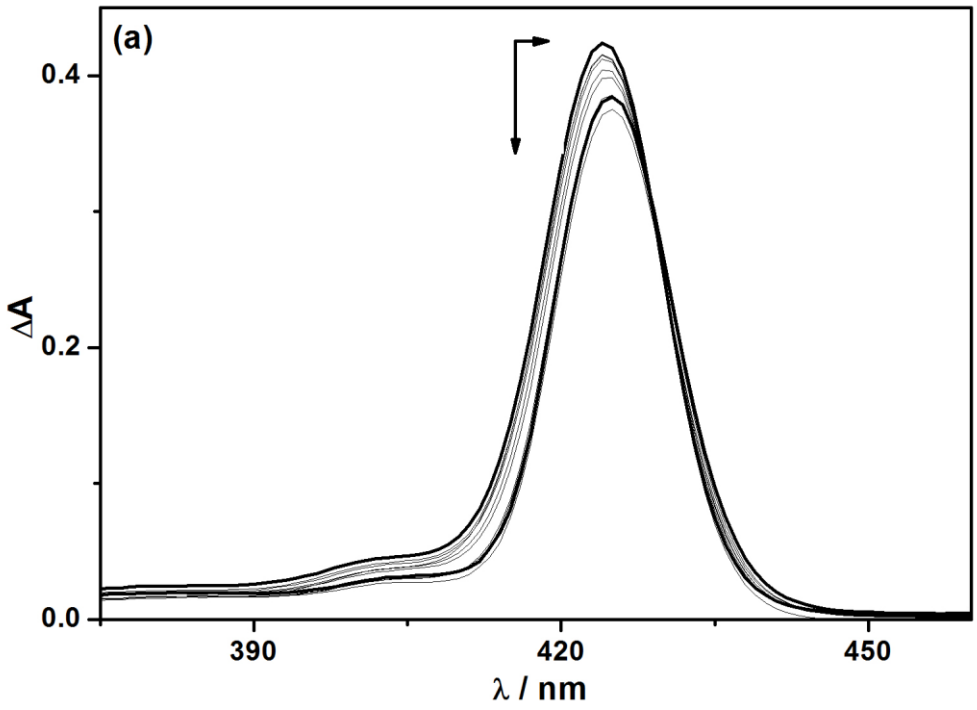

Fig. 53. *Differential absorption spectral traces of* ***17*** *(5.1×10^{-7} M, (a)) upon addition of increasing amounts of 5,15-dpp (up to 3.5 equiv.) in toluene.*

Similarly, **17** and **18** were titrated in toluene with 5,15-dpp, the bidentate guest with the longest interpyridyl distance (ca. 16 Å)[87a] among those investigated here. Because of the linear arrangement of the two pyridine units, 5,15-dpp clearly prefers axial coordination with Zn-porphyrin moieties in **17** and **18**. Fig. 53 and Fig. 54 show the differential spectral traces of hosts **17** and **18** upon addition of increasing amounts of 5,15-dpp. The absorption changes observed therein are significantly weaker than those observed with 5,10-dpp. In the case of **17**, some changes are observed, which is likely due to the increased inter-pyridine distance of 5,15-dpp (ca. 16 Å) compared to 5,10-dpp (ca. 11 Å).[87a] However, in **18**, structural and spatial mismatching between the host and the guest resulted in negligible interactions. As a result of the minimal changes in the absorption spectra of the hosts, the binding affinity constants could not be appraised quantitatively.

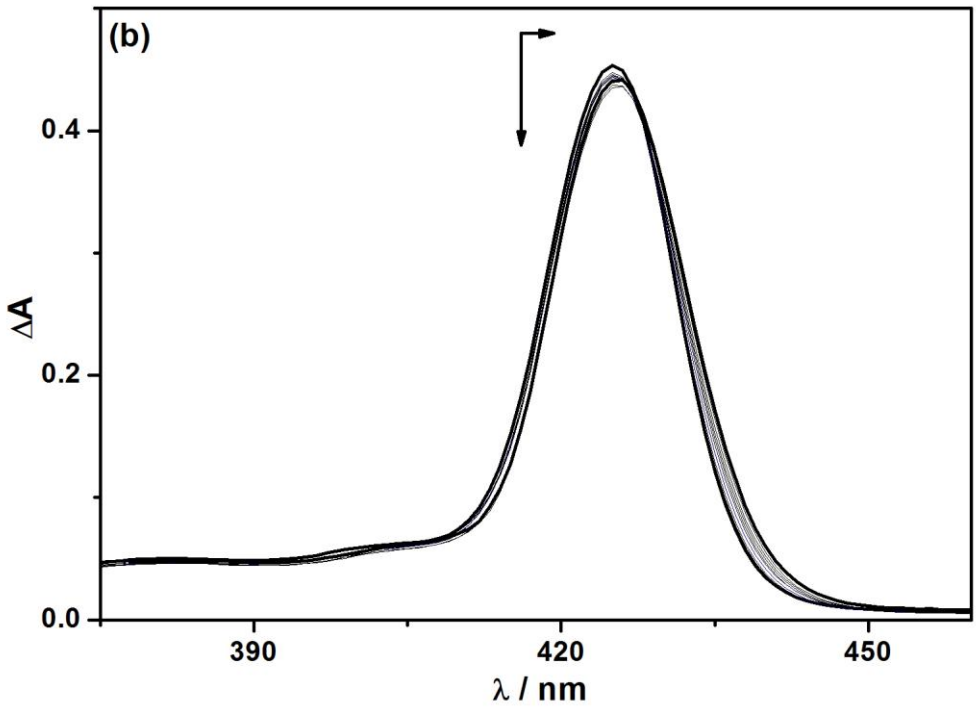

Fig. 54. *Differential absorption spectral traces of* ***18*** *(5.2×10^{-7} M, (b)) upon addition of increasing amounts of 5,15-dpp (up to 3.5 equiv.) in toluene.*

In conclusion, we have synthesized and photophysically characterized a series of sawhorse-type diruthenium tetracarbonyl tweezers derived from either pyrenyl or porphyrin carboxylic bridging units. The molecular modeling of **14**, **15** and **16** suggests that the pyrenyl and porphyrin moieties are adequately positioned to allow these complexes to act as molecular tweezers with fullerene. However, these systems have showed no interaction with fullerene in solution, despite possessing appropriate structural features, as predicted by modeling for compounds **14**, **15** and **16**. On the other hand, with the Zn(II)-porphyrin derivatives, **17** and **18** interaction with bis-pyridyl ligands were observed. In particular, a relatively high association constant between 5,10-di-(4-pyridyl)-15,20-diphenyl-21,23H-porphyrin and **18** was found, thus indicating size specific tweezing properties, and overall showing a new application for an old class of compounds, the sawhorse-type diruthenium tetracarbonyl complexes.

Chapter 4: Biological application of dinuclear (Ru, Rh and Ir) complexes

4. Biologically application of dinuclear (Ru, Rh and Ir) complexes

4.1. Transition metal complexes in cancer treatment

Cancer results from the uncontrolled growth of cells; unless the growth is controlled the disease could be lethal. According to a recent survey, cancer is the second leading cause of death in developed countries and third leading cause of death in developing countries.[93] One in four deaths in the USA and one in eight deaths worldwide are due to cancer. Cancer can be treated by surgery, radiotherapy and/or chemotherapy. Among the treatment methods, chemotherapy has been widely accepted and used all around the world.[94]

Though organic molecules have been used as an active ingredient in most of the anticancer drugs, the development of metal based therapeutic agents for cancer treatments is gaining momentum in recent years.[95] The square planar cisplatin or *cis*-dichlorodiamineplatinum(II) (Fig. 55) was the first metal based drug approved for clinical use.[96] Cisplatin is being used as an effective drug to treat human malignancies such as lung, head-and-neck, ovarian, bladder and testicular cancers by itself or in combination with other drugs.[97] Although cisplatin is an effective drug for cancer treatment, it also has limitations. Particularly, the non-selective cytotoxicity towards healthy cells, which leads to undesirable side-effects and intrudes into drug resistance mechanisms.[98] Thus, it is necessary and challenging to develop alternate drugs based on platinum with superior activity and minimal side effects compared to cisplatin. Over the last three decades there were more than 4000 platinum derived compounds investigated for chemotherapy. Among them only ten reached clinical trials. The food and drug administration (FDA) has approved only carboplatin and oxaliplatin for clinical use (Fig. 55).[96a,99] Even though some of the problems encountered with cisplatin were diminished by carboplatin and oxaliplatin, they still showed high level of non-selective cytotoxicity which hampered their extensive use as an anticancer drugs.[100]

Many organometallic compounds of titanium,[101] ruthenium,[102] rhodium,[103] palladium,[104] copper[105] and gold[106] have been studied for cancer treatment because of their cytotoxicities on cancer cells. Among these metal derivatives ruthenium has been considered as an interesting alternative to the platinum counterparts. Most of the ruthenium anticancer drugs directly attack and kill primary tumors while others prevent the tumor growth from spreading to rest of the healthy tissues.

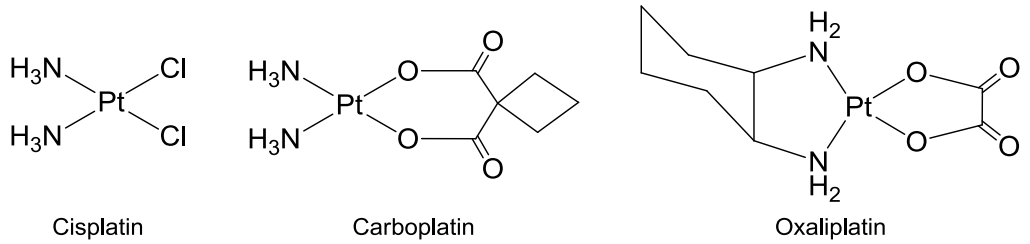

Fig. 55. *Structures of platinum based cancer drugs.*

Ruthenium, with the atomic number of 44, is located just below iron (Fe) in the periodic table. Among its numerous oxidation states, Ru(II) and Ru(III) have been shown to be effective in anticancer treatments. Most Ru(II) ($S = {}^{1}/_{2}$) and Ru(III) ($S = 0$) complexes have low-spin and the first-order water exchange rate constants (k), for aquated Ru(II) is about one order of magnitude faster than that of Pt(II), suggesting that complexes of Ru(II) suit better to react with biological system. The high exchange rate of aquated Ru(II) is an added advantage towards the elimination of metal ruthenium from biological systems. Consequently, the accumulation effect of platinum drug in the biological system could be overcome by ruthenium drugs. Also, it has been shown that due to the redox behavior of ruthenium inside the biological system, Ru(III) is being reduced to Ru(II) and subsequently eliminated, which could give a better explanation for the elimination of Ru(III) drugs, suggesting that Ru(II) is the active species.[107]

Imidazolium *trans*-[imidazoledimethylsulfoxide-tetrachlororuthenate(III)] (NAMI-A) (Fig. 56) and indazolium-*trans*-[tetrachlorobis(1H-indazole)ruthenate(III)] (KP1019) (Fig. 56) are the two ruthenium(III) complexes that have successfully completed phase-I clinical trial.[102] Preclinical studies show that NAMI-A has a remarkable effect against the formation of cancer metastases in a variety of tumor models, but appears to be poorly active against primary tumors.[108] NAMI-A weakly binds with DNA which is in contrast to cisplatin, suggesting that its mode of action is different from that of other platinum(II) compounds.[109] On the other hand, KP1019 was found to be more stable and has a high anti-tumor activity. More interestingly, KP1019 showed higher anti-tumor activity towards primary cisplatin-resistant colorectal tumors but it did not show any anti-metastatic activities.[110]

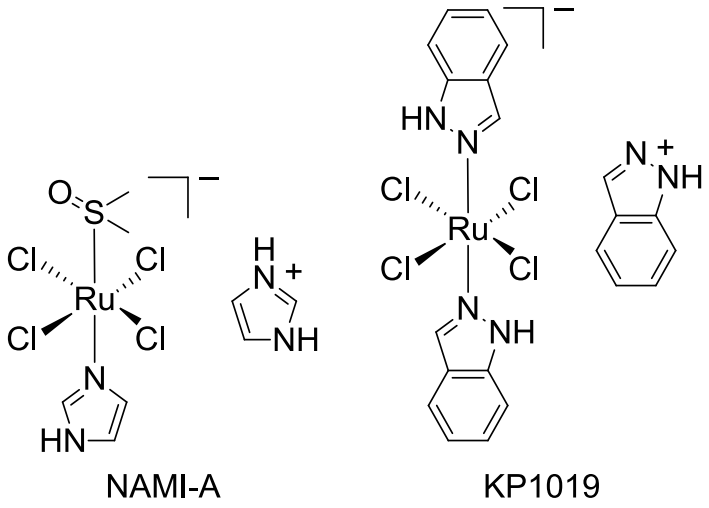

Fig. 56. *Structure of NAMI-A and KP1019*

In contrast to NAMI-A and KP1019, arene-ruthenium complexes are more cytotoxic in their ruthenium (II) oxidation state. Dyson's RAPTA-C {[(η^6-*p*-$MeC_6H_4Pr^i$)Ru(PTA)Cl_2]; PTA = 1,3,5-triaza-7-phosphatricyclo[3.3.1.1]decane} (Fig. 57)[96a,98,111] as well as Sadler's derivative {[(C_6H_5Ph)Ru(en)Cl][PF_6]} (RM175, en = ethane-1,2-diamine) (Fig. 57)[112] are the two promising drugs having anticancer activities *in vitro* and *in vivo*.[113] Though RAPTA-C exhibits very low activity *in vitro*, it is very active *in vivo* (with lung metastases in CBA mice); RAPTA-C is also an anti-metastatic agent like NAMI-A.[114]

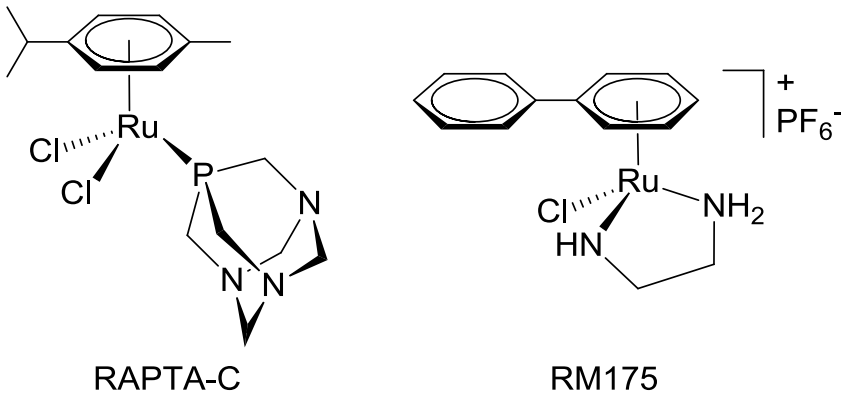

Fig. 57. *Structure of anticancer ruthenium complexes RAPTA-C and RM175*

Unlike the mononuclear complexes, dinuclear or multinuclear ruthenium complexes have recently been reported for their anticancer activities:[114-115] Hartinger *et al*. synthesized the dinuclear arene ruthenium complexes of pyridinone derivatives (η^6-*p*-$MeC_6H_4Pr^i$)Ru-(O,O-$C_6H_5O_2N(CH_2)_nNC_6H_5O_2$-O,O)Ru($\eta^6$-*p*-$MeC_6H_4Pr^i$) (n = 3, 6 and 12) (Fig. 58). *In vitro* studies of the complex (η^6-*p*-$MeC_6H_4Pr^i$)Ru(O,O-$C_6H_5O_2N(CH_2)_{12}NC_6H_5O_2$-O,O)Ru($\eta^6$-*p*-$MeC_6H_4Pr^i$) showed very high cytotoxic effect against ovarian (A2780; IC_{50} = 1.5 μM) and colon (SW480; IC_{50} = 0.29 μM) cancer cell lines.[116] Sadler *et al*. studied the photodynamic therapy effects of this type $[\{(arene)RuCl\}_2(N,N:N,N\text{-dpp})\}]^{2+}$ of dinuclear arene ruthenium complexes {arene = C_6H_6, C_6Me_6, C_9H_{10}, *p*-$MeC_6H_4Pr^i$; dpp = 2,3-bis(2-pyridyl)pyrazine}. The indane derivative $[\{(\eta^6\text{-}C_9H_{10})RuCl\}_2(N,N:N,N\text{-dpp})]^{2+}$ (Fig. 58) gives dinuclear reactive species upon UV irradiation in the presence of water in the dark and this dinuclear active species strongly interact with DNA to give diruthenium DNA adducts.[117] Notably, these types of dinuclear arene-ruthenium complexes have interesting advantages of photo-induced cell death and fluorescence image traceability of localizations inside biological systems.[114,117]

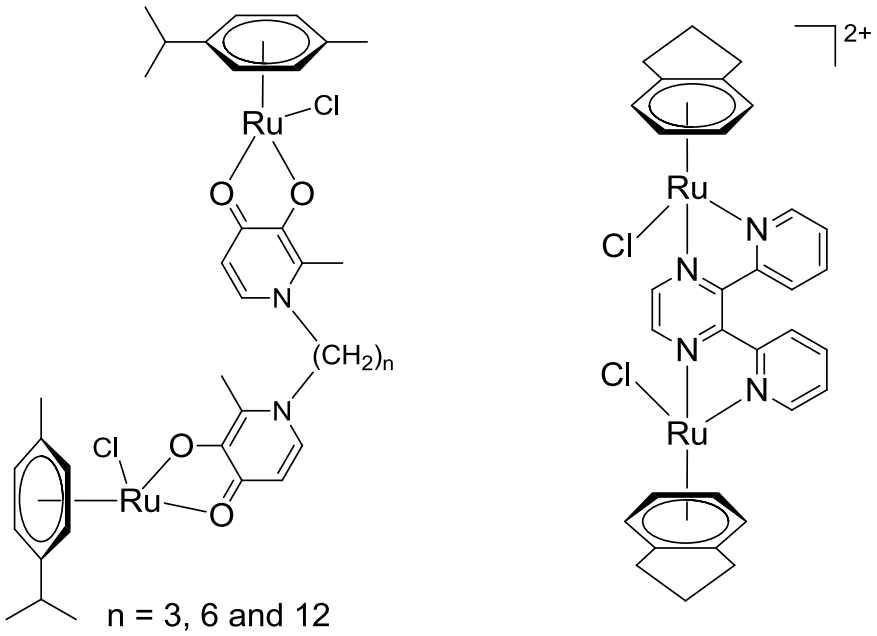

Fig. 58. *Structure of [(η^6-p-$MeC_6H_4Pr^i$)Ru(O,O-$C_6H_5O_2N(CH_2)_nNC_6H_5O_2$-O,O)Ru($\eta^6$-p-$MeC_6H_4Pr^i$)] (Left) and $[\{(C_9H_{10})RuCl\}_2(N,N:N,N\text{-dpp})]^{2+}$ (Right).*

Among the dinuclear complexes, thiolato bridged arene ruthenium complexes are well known for their biological applications.[38a,118] Giannini *et al.*[118] reported a series of water soluble and air-stable arene ruthenium cationic complexes of the type $[(\eta^6\text{-arene})_2Ru_2(SR)_3]^+$ (Fig. 59) which were tested for anticancer activity. From the *in vitro* studies it was shown that the thiolato bridged arene ruthenium complex $[(\eta^6\text{-}p\text{-}MeC_6H_4Pr^i)_2Ru_2(\mu\text{-}SC_6H_4\text{-}p\text{-}Bu^t)_3]^+$ (Fig. 59) displayed a very high cytotoxicity (IC_{50} value of 0.03 μM on both A2780 and A2780cisR cancer cell lines) even at very low concentration.

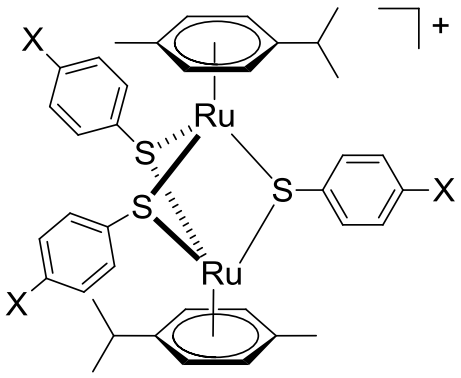

X = H, Me, Ph, Br, OH, NO_2, OMe, CF_3, Bu^t

Fig. 59. *Highly cytotoxic thiolato bridged arene ruthenium complexes.*

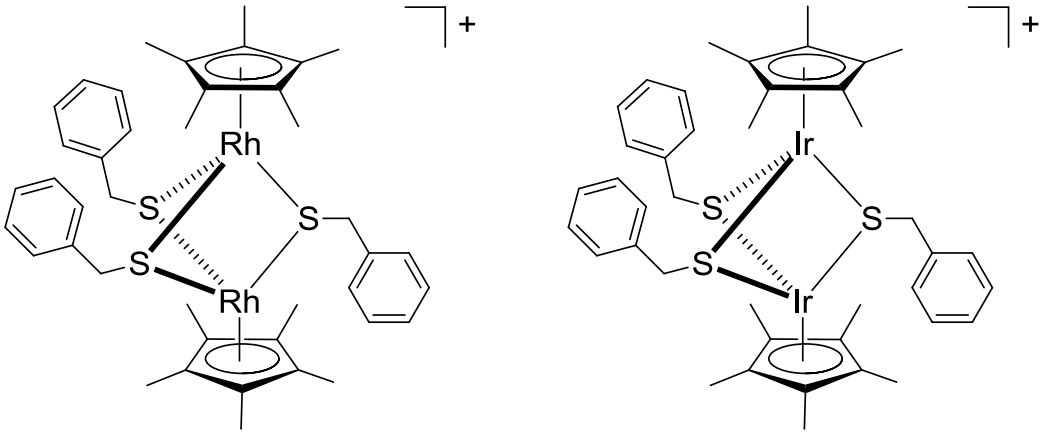

Fig. 60. *Structures of $[(\eta^5\text{-}C_5Me_5)_2Rh_2(\mu\text{-}SCH_2Ph)_3]^+$ (left) and $[(\eta^5\text{-}C_5Me_5)_2Ir_2(\mu\text{-}SCH_2Ph)_3]^+$ (right).*

The chemistry of cyclopentadienyl rhodium(III) and iridium(III) is similar to that of the arene ruthenium(II) analogues.[119] Like arene ruthenium derivatives, cyclopentadienyl rhodium or iridium derivatives react with thiolato ligands to give thiolato-bridged cyclopentadienyl rhodium or iridium complexes under similar reaction conditions. Recently, we have shown that dinuclear thiolato-bridged pentamethylcyclopentadienyl rhodium and iridium complexes possess surprising cytotoxicities. These rhodium(III) and iridium(III) metal complexes had very high cytotoxicity, which were similar to arene ruthenium(II) complexes. For example, the complex $[(\eta^5\text{-}C_5Me_5)_2Rh_2(\mu\text{-}SCH_2Ph)_3]$ (Fig. 60) showed IC_{50} values of 0.14 μM on A2780 and 0.09 μM on A2780cisR cancer cell lines. The complex $[(\eta^5\text{-}C_5Me_5)_2Ir_2(\mu\text{-}SCH_2Ph)_3]$ (Fig. 60) showed IC_{50} values of 0.09 μM on A2780 and 0.06 μM on A2780cisR cancer cell lines.[119]

4.2. Cytotoxic chalcogenolato-bridged dinuclear half-sandwich complexes

4.2.1. Introduction

In biology, selenium is essential to life and it plays an important role in redox enzymatic processes.[120] At low concentrations, selenium stimulates cell growth and exhibits anticancer properties, while at higher concentrations it can induce cell death.[121] In addition, studies have shown that in combination with cisplatin, the most successful metal-based drug,[122] selenium reduces the nephrotoxicity associated with cisplatin treatment.[123] On the other hand, the biological relevance of tellurium remains uncertain, but the potential of using tellurium derivatives as therapeutic agents has been already recognized.[124]

Recently, we have shown that the thiolato-bridged dinuclear arene ruthenium complexes of the type $[(\eta^6\text{-}p\text{-}MeC_6H_4Pr^i)_2Ru_2(\mu\text{-}SR)_3]^+$,[38a,43,118,125] as well as the rhodium and iridium pentamethylcyclopentadienyl analogues $[(\eta^5\text{-}C_5Me_5)_2M_2(\mu\text{-}SR)_3]^+$ (M = Rh, Ir),[119] possess excellent cytotoxicity on the ovarian cancer cell lines A2780 and A2780cisR. The most active compounds show cytotoxicity against both cell lines in the sub-micromolar range with IC_{50} values below 0.1 μM. The high antiproliferative effect was tentatively ascribed to the presence of the thiolato-bridging groups and the catalytic activity of the complexes.[38a,43,118-119,125] These dinuclear arene ruthenium complexes are among the most active arene ruthenium complexes evaluated so far *in vitro*.[38a,43,118,125]

Therefore, due to the high activity of the dinuclear thiolato-bridged half-sandwich complexes and the biological relevance of selenium and tellurium, we have prepared a series of selenolato and tellurolato *p*-cymene ruthenium derivatives $[(\eta^6\text{-}p\text{-}MeC_6H_4Pr^i)_2Ru_2(\mu\text{-}EC_6H_5)_3]^+$ (E = S, **19**; E = Se, **20**; E = Te, **21**), as well as the pentamethylcyclopentadienyl (C_5Me_5) rhodium and iridium analogues $[(\eta^5\text{-}C_5Me_5)_2M_2(\mu\text{-}EC_6H_5)_3]^+$ (M = Rh, E = S, **22**; E = Se, **23**; E = Te, **24**; M = Ir, E = S, **25**; E = Se, **26**; E = Te, **27**). In addition, a series of mixed thiolato-selenolato and thiolato-tellurolato bridged complexes have also been synthesized, $[(\eta^6\text{-}p\text{-}MeC_6H_4Pr^i)_2Ru_2(\mu\text{-}EC_6H_5)(\mu\text{-}SCH_2C_6H_4\text{-}p\text{-}Bu^t)_2]^+$ (E = Se, **28**; E = Te, **29**) and $[(\eta^5\text{-}C_5Me_5)_2M_2(\mu\text{-}EC_6H_5)(\mu\text{-}SCH_2C_6H_5)_2]^+$ (M = Rh, E = Se, **30**; E = Te, **31**; M = Ir, E = Se, **32**; E = Te, **33**). The cytotoxicity of all complexes was evaluated on human ovarian cancer cells, and comparison with the parent thiolato-derivatives is discussed.

4.2.2. Synthesis of chalcogenolato-bridged dinuclear half-sandwich complexes

Despite numerous papers dealing with thiolato-bridged dinuclear arene ruthenium complexes,[42a,126] the only investigation of a dinuclear selenolato complex, $[(\eta^6\text{-}p\text{-}MeC_6H_4Pr^i)_2Ru_2(\mu\text{-}SeC_6H_5)_3]PF_6$, was reported 15 years ago by Mashima.[127] Low yield (19 %) and difficulties with reproducibility of the method prompted us to prepare the desired cationic complex under new conditions (Scheme 2). Our synthetic strategy is based on the synthesis of the thiolato-bridged analogues[38a,43,118,125] and affords $[(\eta^6\text{-}p\text{-}MeC_6H_4Pr^i)_2Ru_2(\mu\text{-}SeC_6H_5)_3]Cl$ in 66 % yield after column chromatography. The rhodium and iridium analogues are obtained in comparable yields following the same strategy (Scheme 2). The known thiolato-bridged *p*-cymene ruthenium complex, $[(\eta^6\text{-}p\text{-}MeC_6H_4Pr^i)_2Ru_2(\mu\text{-}SC_6H_5)_3]^+$, was also synthesized for comparison.[40,43]

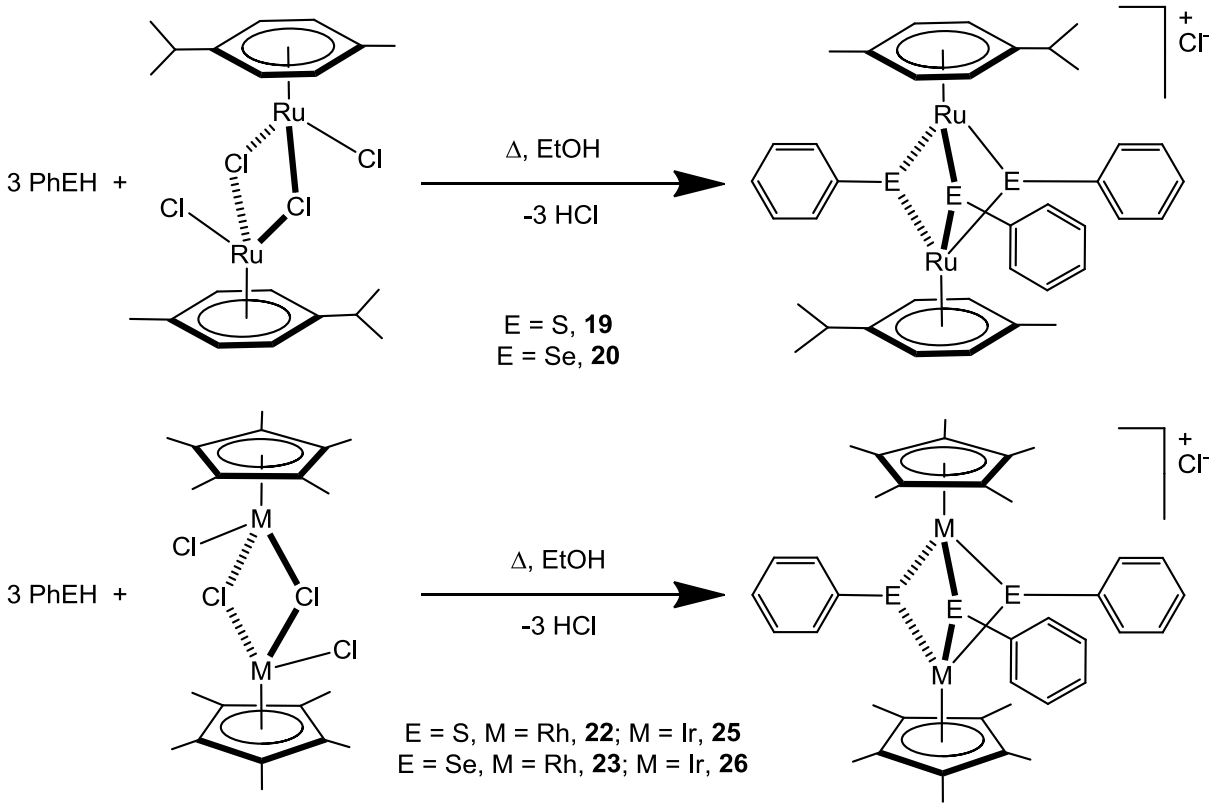

Scheme 2. *Synthesis of thiolato- and selenolato-bridged complexes* ***19***, ***20***, ***22***, ***23***, ***25*** *and* ***26***

The tellurolato derivatives **21**, **24** and **27** are prepared following an established procedure.[127] They are synthesized in ethanol from the reaction of $(\eta^6\text{-}p\text{-}MeC_6H_4Pr^i)_2Ru_2(\mu\text{-}Cl)_2Cl_2$ or $(\eta^5\text{-}C_5Me_5)_2M_2(\mu\text{-}Cl)_2Cl_2$ (M = Rh, Ir) with sodium tellurophenolate (Scheme 3): Sodium tellurophenolate being prepared in situ by treating diphenyl ditelluride with sodium borohydride. These complexes are all isolated as their hexafluorophosphate salts, which are obtained upon addition of 1 eq. of KPF_6 to the crude ethanolic solution, just before purification of the corresponding salts by column chromatography. The analytical data of the salt, $[(\eta^6\text{-}p\text{-}MeC_6H_4Pr^i)_2Ru_2(\mu\text{-}TeC_6H_5)_3]PF_6$, are in agreement with those reported by Mashima.[127]

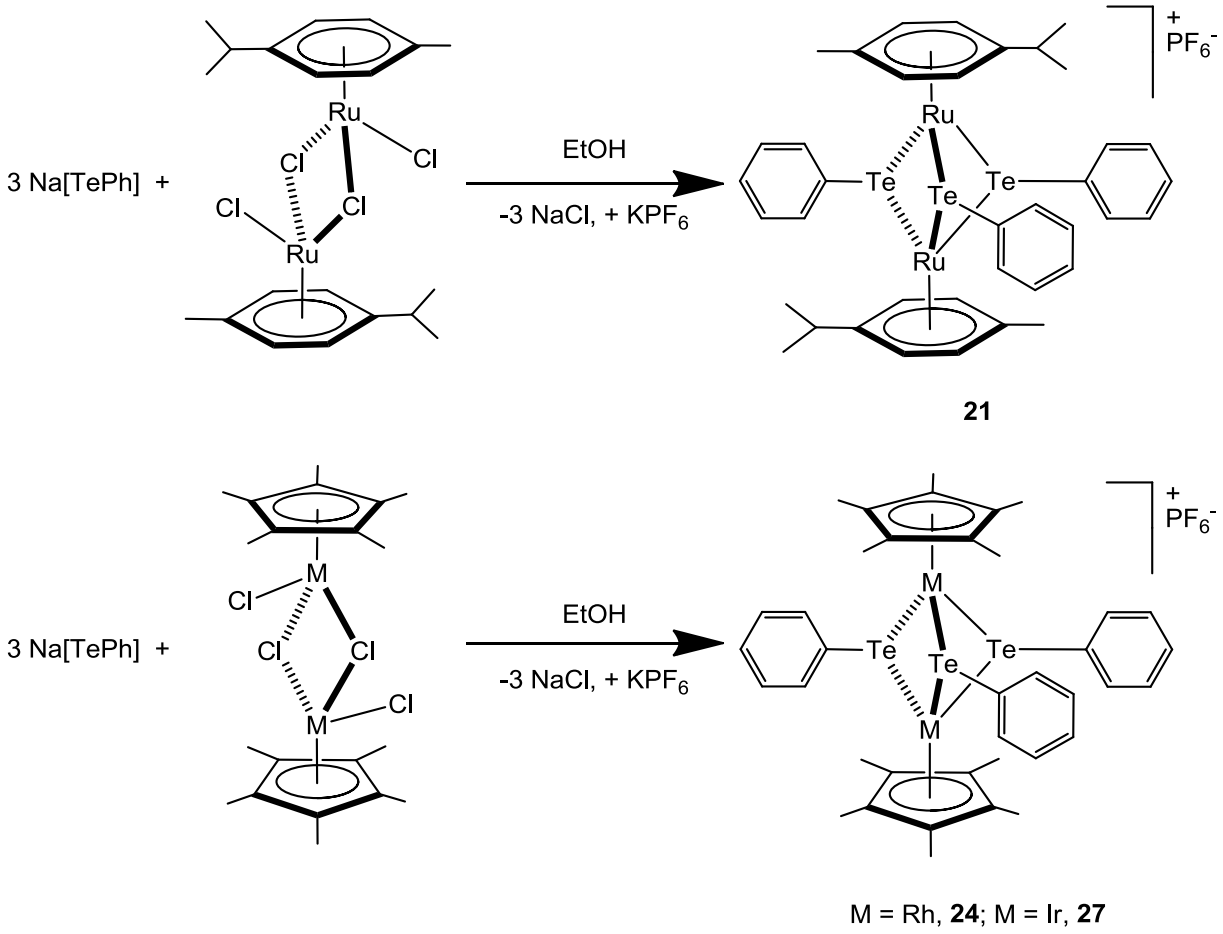

Scheme 3. *Synthesis of tellurolato-bridged complexes **21**, **24** and **27**.*

As previously reported for analogous *p*-cymene ruthenium complexes,[42,126] all ^{1}H NMR spectra show diastereotopic protons for the dinuclear complexes **19**-**21**, two doublets and a multiplet for the isopropyl group, a singlet for the methyl, four doublets for the aromatic protons of the *p*-cymene and two broad multiplets for the protons of the chalcogen-phenyl groups. The ESI mass spectrum in positive mode gives the expected cationic parent peak of $[(\eta^6\text{-}p\text{-}MeC_6H_4Pr^i)_2Ru_2(\mu\text{-}EC_6H_5)_3]^+$ at *m/z* = 799.1, 939.1 and 1084.3, respectively. The ^{1}H NMR spectra of the pentamethylcyclopentadienyl derivatives are much simpler, showing only an intense singlet between 1.3 and 1.8 ppm for the C_5Me_5 groups and multiplets in the aromatic region for the bridging chalcogen-phenyl groups. The ESI MS spectra show as well the cationic peaks corresponding to the intact complexes **22**-**27**.

The neutral dichloro dithiolato complexes $(\eta^6\text{-}p\text{-}MeC_6H_4Pr^i)_2Ru_2Cl_2(\mu\text{-}SCH_2C_6H_4\text{-}p\text{-}Bu^t)_2$ [38a] and $(\eta^5\text{-}C_5Me_5)_2M_2Cl_2(\mu\text{-}SCH_2C_6H_5)_2$ [41,119] react with benzeneselenol and sodium tellurophenolate in ethanol to give the mixed dithiolato-selenolato and dithiolato-tellurolato cationic dinuclear complexes $[(\eta^6\text{-}p\text{-}MeC_6H_4Pr^i)_2Ru_2(\mu\text{-}EC_6H_5)(\mu\text{-}SCH_2C_6H_4\text{-}p\text{-}Bu^t)_2]^+$ (E = Se, **28**; E = Te, **29**) and $[(\eta^5\text{-}C_5Me_5)_2M_2(\mu\text{-}EC_6H_5)(\mu\text{-}SCH_2C_6H_5)_2]^+$ (M = Rh, E = Se, **30**; E = Te, **31**; M = Ir, E = Se, **32**; E = Te, **33**) (Scheme 4 and Scheme 5).

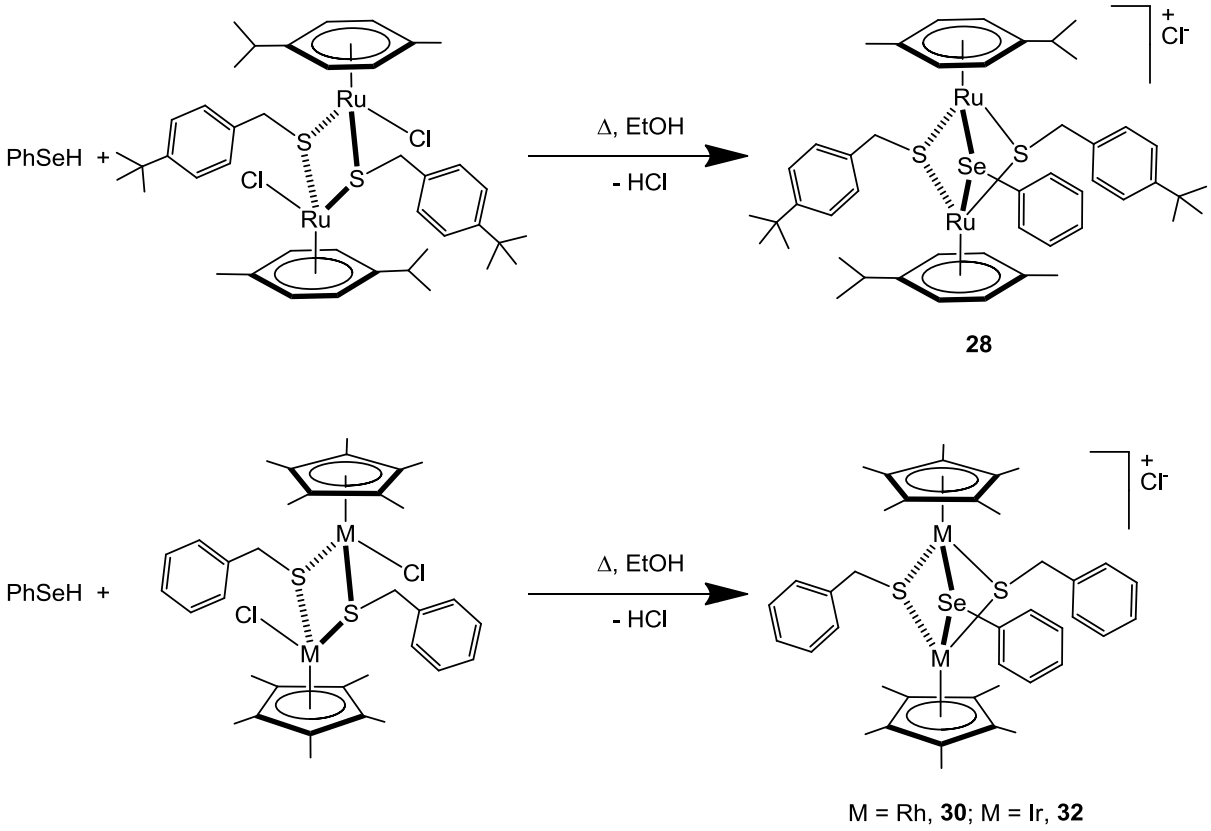

Scheme 4. *Synthesis of the mixed dithiolato-selenoato-bridged complexes **28**, **30** and **32**.*

The dithiolato-selenolato derivatives (**28**, **30**, **32**) are synthesized in ethanol at reflux from the neutral dichloro dithiolato intermediates and benzeneselenol (Scheme 4), while the dithiolato-tellurolato analogues are obtained at room temperature by adding sodium tellurophenolate to the same neutral intermediates (Scheme 5). The selenolato derivatives are obtained as chloride salts, while the tellurolato complexes (**29**, **31, 33**) are isolated as hexafluorophosphate salts, after addition of KPF_6 to the reaction mixture.

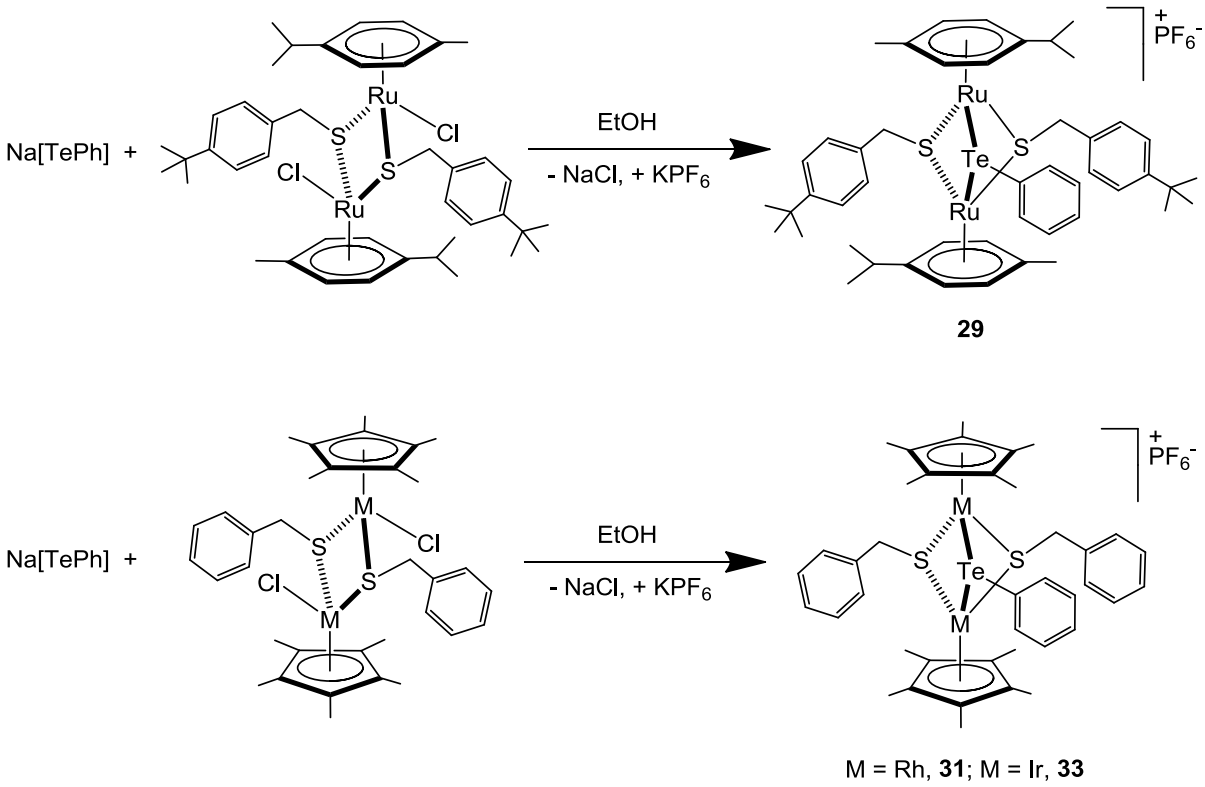

Scheme 5. *Synthesis of the mixed dithiolato-tellurolato-bridged complexes **29**, **31** and **33**.*

These mixed dithiolato-selenolato and dithiolato-tellurolato complexes are extremely stable under the harsh conditions of electro-spray ionization mass spectrometry, showing peaks corresponding to the intact cations; $[M - Cl]^+$ for complexes **28**, **30** and **32** and $[M - PF_6]^+$ for complexes **29**, **31** and **33** (see Experimental section). These peaks are unambiguously assigned on the basis of their respective isotope patterns.

4.2.3. Biological studies of chalcogenolato-bridged dinuclear half-sandwich complexes

In order to evaluate the biological potential of these chalcogenolato-bridged dinuclear half-sandwich complexes *in vitro*, cell biology and biophysical experiments have been carried out. Effect of these complexes on normal (CRL-2115, CRL-2120) and human cancer (A549, B16F10 and MCF-7) cell lines was studied using MTT assays (MTT = 3-(4,5-dimethyl-2-thiazoyl)-2,5-diphenyltetrazolium bromide) and cell count assays. Among the

organometallic complexes evaluated in the present study, the most active derivatives were selected and further analysed using flow cytometry, confocal microscopy and DNA cleavage experiments. In order to better understand their unique intracellular activity, interaction with DNA for the selected candidates was also studied.

4.2.3.1. MTT assays

MTT assay is a simple, accurate and reliable test to estimate the activity of living cells before and after addition of a biological agent.[128] Therefore, this assay was used with complexes **19-33** on normal (CRL-2115 and CRL-2120 fibroblasts) and human cancer (A549 lung, B16F10 melanoma and MCF-7 breast cancers) cell lines. The assay was performed at different concentrations of complexes (10 nM, 50 nM, 100 nM, 300 nM, 500 nM, 1 μM and 2 μM) and the absorbance obtained at 570 nm was plotted against the concentration of the complex to determine the half maximal inhibitory concentration (IC_{50} value). The IC_{50} values of the complexes and the T_m (T_m = melting temperature) values obtained in the presence of CT-DNA (calf thymus DNA) are presented in Table 6, together with the corresponding standard deviations. Among the normal and cancer cell lines studied, the cytotoxic effect is higher in the B16F10 cell line and among all complexes, compounds **19**, **22** and **25** appear to be the most active derivatives. Indeed, the IC_{50} of **19** on the B16F10 cell line is approximately 300 nM, closely followed by complexes **22** (≈ 315 nM) and **25** (≈ 320 nM). Complexes **19**, **22** and **25** are those with thiolato bridges, thus suggesting that the nature of the metal plays only a minor role, while the nature of the chalcogenolato bridges is somehow important. These trends are clearly seen on the B16F10 cell line.

Accordingly, complex **19** shows the strongest affinity with CT-DNA with a T_m of ≈ 75 °C, which is closely followed by complexes **22** (≈ 70 °C) and **25** (≈ 69 °C). Overall, all complexes interact with CT-DNA, showing T_m values higher than 62 °C. In addition, the complexes show some selectivity towards the cancerous cell lines, being less active by half on the CRL-2115 and CRL-2120 normal fibroblast cells.

Table 6. Cytotoxicity of complexes **19**-**33** after 24 h exposure to various cell lines and Tm values of the complexes with CT-DNA.

complex	IC_{50} (nM)					T_m (^oC)
	CRL-2115	CRL-2120	MCF-7	B16F10	A549	
19	935 ±4	1078 ± 5	543 ± 5	306 ± 3	424 ± 4	75
20	965 ± 6	1082 ± 7	574 ± 6	352 ± 5	440 ± 5	66
21	950 ± 5	1074 ± 6	562 ± 4	346 ± 4	432 ± 3	68
22	965 ± 3	1172 ± 4	567 ±6	314 ± 2	437 ± 5	70
23	987 ± 7	1354 ± 6	553 ± 4	357 ± 5	457 ± 4	64
24	976 ± 6	1287 ± 7	561 ± 5	332 ± 4	442 ± 5	66
25	1024 ± 5	1136 ± 4	582 ± 6	319 ± 5	442 ± 6	69
26	1037 ± 7	1232 ± 6	597 ± 7	358 ± 6	472 ± 5	64
27	1025 ± 8	1187 ± 8	587 ± 4	341 ± 5	456 ± 4	67
28	967 ± 7	1087 ± 7	592 ± 5	342 ± 4	445 ± 7	68
29	953 ± 5	1079 ± 8	583 ± 6	331 ± 5	432 ± 5	65
30	986 ± 7	1089 ± 7	557 ± 4	345 ± 6	446 ± 4	62
31	972 ± 5	1076 ± 8	543 ±7	328 ± 5	439 ± 7	64
32	1028 ± 7	1254 ± 7	568 ± 6	354 ± 7	453 ± 5	63
33	1017 ± 8	1215 ± 6	552 ± 5	346 ± 5	446 ± 6	66

4.2.3.2. Cell viability assays

Cell viability assays were performed to corroborate the results obtained from the MTT assays, to find the extent of cytotoxicity induced in these cell lines and to study the selectivity of the complexes between normal and cancerous cells. Both normal and cancer cells were treated with the compounds at a 300 nM concentration. After 24 h of incubation, the number of viable cells was counted in normal as well as in cancer cells using

a hemocytometer. From these results, it is clear that among the complexes studied, complexes **19**, **22** and **25** exhibit a higher cytotoxicity in cancer cells as compared to normal cells. The elevated cytotoxicity in cancer cells can be due to a higher uptake of the cationic complexes into cancer cells.[129] Among the cell lines tested, the melanoma B16F10 cells are the most affected by the presence of the complexes. Bar graphs indicating the number of viable cells in normal as well as in cancer cells after treatment with complexes **19**, **22** and **25** are shown in Fig. 61. The bar graphs which are statistically significant with p values ≤ 0.05 are marked with an asterisk (*).

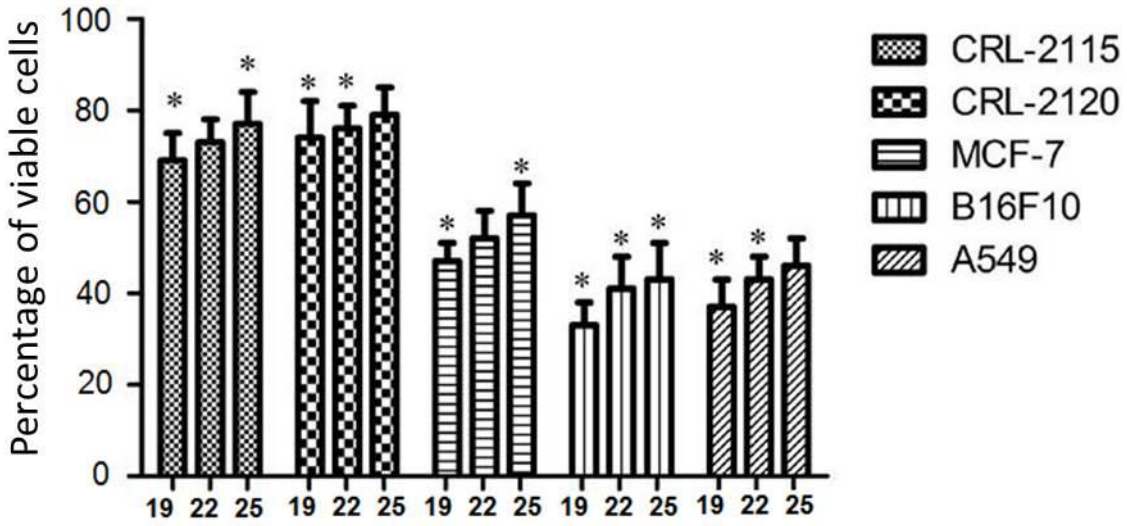

Fig. 61. *Cell viability assays with normal and cancer cells after 24 h of treatment with complexes* ***19****,* ***22*** *and* ***25*** *at 300 nM concentrations.*

4.2.3.3. Flow cytometry experiments

The results obtained from cell viability and MTT assays indicate that among the complexes studied, complexes **19**, **22** and **25** exhibited the highest cytotoxicity in these cancer cell lines. Therefore, to better understand the role of these complexes in cells and to find a plausible cause for the higher cytotoxicity and efficacy of complexes **19**, **22** and **25** in cells, cell cycle assays and apoptotic assays were performed using flow cytometry in the presence and absence of the complexes at their respective IC_{50} values. These tests suggest that complexes **19**, **22** and **25** inhibit the cell cycle at the G2 stage (Fig. 62). It has been previously reported that G2 arrest can enhance cytotoxicity and induce

apoptosis in cells.[130] Among the complexes studied, the G2 phase inhibition is maximum in the B16F10 cells with complex **19** (24.82 %) followed by complex **22** (23.05 %) and complex **25** (21.37 %), while the untreated B16F10 cells show a G2 phase inhibition of only 14.71 % (Table 7). Similarly, inhibition of cell cycle at sub-G1 phase with complexes **19** (6.79 %), **22** (5.59 %) and **25** (4.80 %) also occurs in the same order as compared to untreated cells (4.58 %). These results confirm that all the complexes induce cytotoxicity followed by apoptosis induction in the cancer cell lines through G2 phase inhibition. G2 phase inhibition prevents the cells to proceed further to the mitotic phase. The details of the cell cycle assays are presented in Fig. 62.

Table 7. Distribution of cells in various phases of the cell cycle in untreated (control) and treated B16F10 cells with complexes **19**, **22** and **25**.

complex	sub-G1 (%)	G0/G1 (%)	S (%)	G2/M (%)
control	4.58	57.40	9.80	14.71
19	6.79	44.79	9.60	24.82
22	5.59	46.17	9.09	23.05
25	4.80	52.20	8.47	21.37

Table 8. Percentage of alive, early apoptotic, late apoptotic and necrotic cells in untreated (control) and treated B16F10 cells with complexes **19**, **22** and **25**.

complex	alive cells (%)	early apoptotic (%)	late apoptotic (%)	necrotic cells (%)	total apoptotic cells (%)
unstained control	99.66	0.02	0.01	0.05	low
stained control	69.54	0.02	0.10	29.33	low
19	9.16	55.82	33.15	0.78	88.97
22	20.18	68.79	10.03	0.31	78.82
25	29.30	54.50	15.31	0.41	69.81

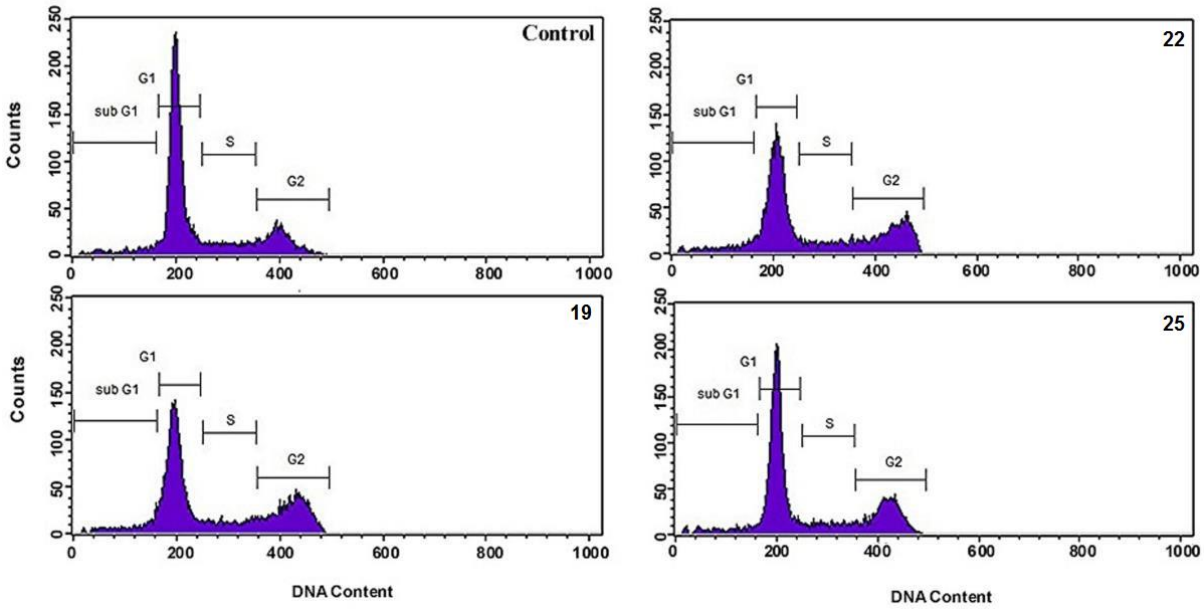

Fig. 62. *Untreated (control) and treated B16F10 cells with complexes* ***19****,* ***22*** *and* ***25****, the cells were stained with propedium iodide (PI). The cellular DNA content frequency histogram and scatter plots are shown.*

From apoptotic assays it is clear that complex **19** possesses a higher potential to induce apoptosis (88.97 %) in B16F10 cells than complexes **22** (78.82 %) and **25** (69.81 %) (Table 8). From the results, it is evident that **19** is effective in inducing higher proportion of apoptotic cells: more late apoptotic cells (Annexin-V+/PI+) than early apoptotic cells Annexin-V+/PI-) in B16F10 cells. Whereas on treatment with complex **22** a higher percentage of early apoptotic cells are observed (Annexin-V+/PI-) over treated cells with complexes **19** and **25**. On the other hand, when the B16F10 cells are treated with complexes **19** and **25**, more late apoptotic cells (Annexin-V+/PI+) are observed as compared to complex **22**, emphasizing the higher potential of complex **19** in inducing both early and late apoptosis in human cancer cells. The results obtained with apoptotic assays support the findings of the MTT and cell viability assays. The percentages of cell population which are in viable, necrotic, early or late apoptotic phase and in various stages of the cell cycle are shown in Table 8. The results obtained in the apoptotic assays with stained and unstained controls as well as in cells treated with complexes **19**, **22** and **25** are presented in Fig. 63.

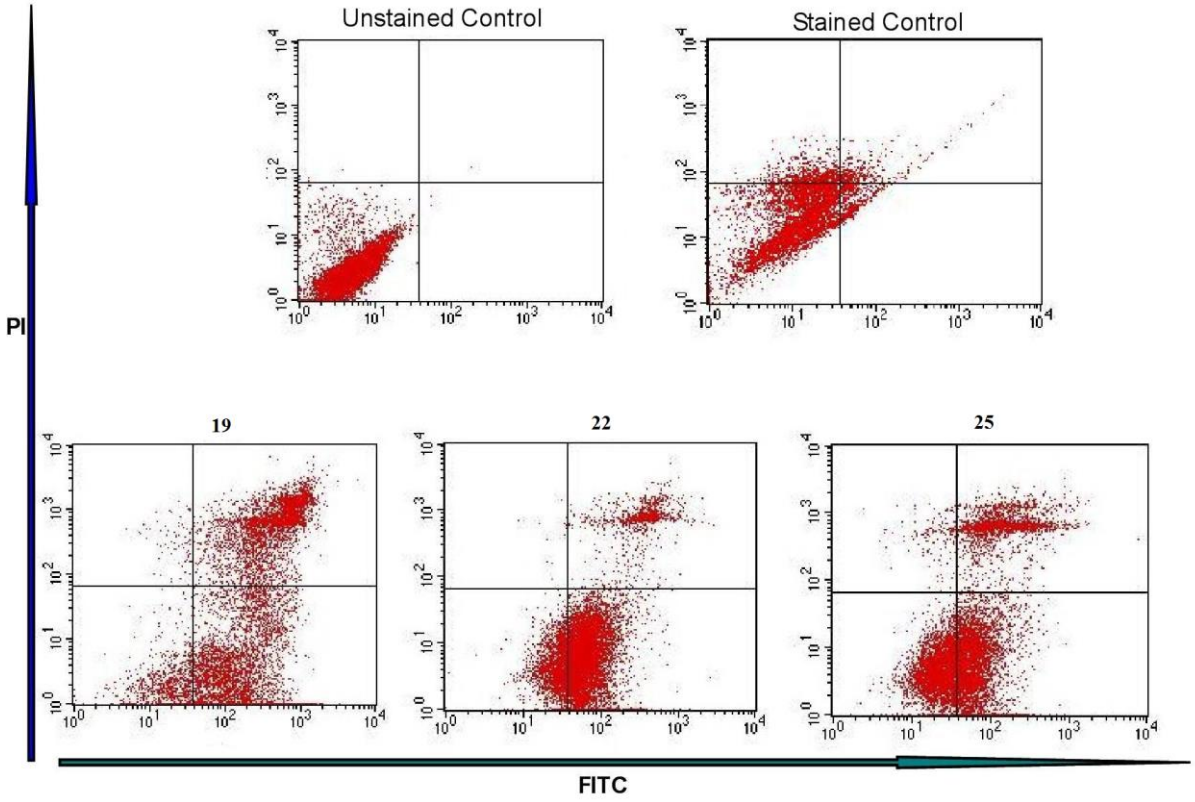

Fig. 63*. Untreated and treated B16F10 cells with complexes* ***19****,* ***22*** *and* ***25****. The cells were stained with Annexin-V and propedium iodide and analysed for various types of cells like: viable (lower left), early apoptotic (lower right), late apoptotic (upper right) and necrotic cells (upper left).*

4.2.3.4. Confocal studies

In order to corroborate the results obtained by flow cytometry and to understand the interaction of the complexes with cellular DNA in cells, the B16F10 melanoma cells were treated with complexes **19**, **22** and **25** for 48 hours and the state of DNA in cells after treatment was examined by staining of the DNA with 300 nM DAPI (4',6-diamidino-2-phenylindole). On careful examination under a microscope of the cellular DNA of both, treated and untreated B16F10 cells, it appears that complex **19** creates maximum DNA fragmentations, followed by **22** and **25**, respectively. We can speculate that the higher cytotoxicity observed with **19** is due to its greater DNA fragmentation activity. The results indicate that complexes **19**, **22** and **25** are capable of crossing the cell membrane barrier and to interact with the cellular DNA. The data obtained from the confocal studies are shown in Fig. 64. It is evident from Fig. 64 that several B16F10 cells have lost

their usual shape and have wrinkled upon treatment with complex **19**. The number of cells with altered shapes is comparatively less with complexes **22** and **25**. The presence of wrinkled and shrunken cells indicates that the cells are entering into the apoptosis phase.[131] These results also indicate that complex **19** has higher potential to fragment cellular DNA and to induce apoptosis, which overall supports the results obtained by MTT cell viability and flow cytometry assays.

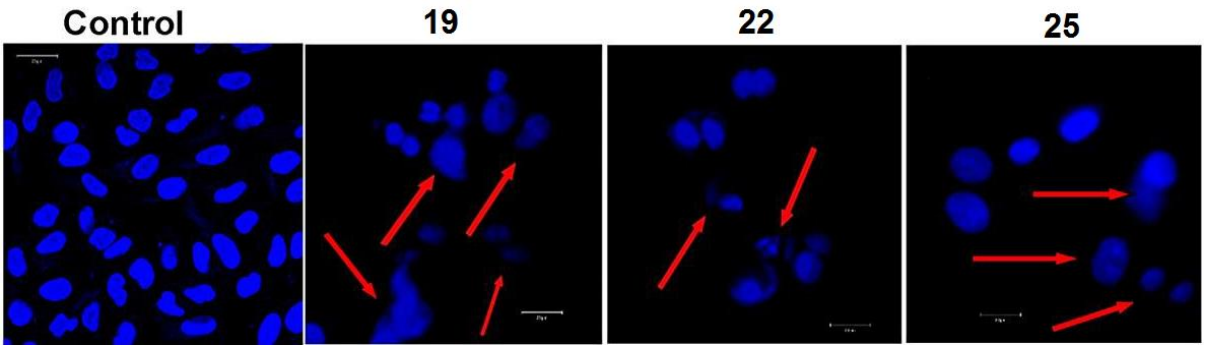

Fig. 64. *Confocal microscopic pictures of B16F10 cells stained with 300 nM DAPI. B16F10 cells were treated with 300 nM of complexes* ***19****,* ***22*** *and* ***25*** *for 24 h. Untreated cells are considered as control.*

4.2.3.5. DNA cleavage experiments

Confocal experiments clearly suggest that DNA in cell is getting fragmented on treatment with complexes **19**, **22** and **25**. It also confirms that complex **19** yields maximum DNA cleavage at its IC_{50} concentration (i.e at around 300 nM) which is closely followed by **22** and **25**. To verify these results, DNA cleavage experiments were carried out by incubating B16F10 cells with each complex and the results confirm that all compounds enter the cells by crossing the cell membrane barrier and are able to interact with DNA. B16F10 cells were treated with 300 nM of complexes **19**, **22** and **25**. DNA cleavage assay also indicates that fragmentation of DNA is prominently observed in cells treated with complex **19** followed by complexes **22** and **25**. The picture of the agarose gel after electrophoresis is shown in Fig. 65.

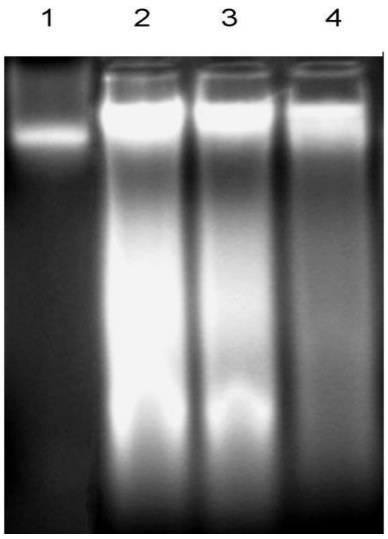

Fig. 65. *Agarose gel showing the fragmentation of DNA in B16F10 cells after treatment with complexes **19**, **22** and **25** for 48 h. Lane 1, B16F10 cells without any treatment. lanes 2, 3 and 4, B16F10 cells after treatment with 300 nM concentration of complexes **19**, **22** and **25**, respectively.*

4.2.3.6. DNA binding studies

The previous experiments such as flow cytometry, confocal and DNA cleavage assays suggest that complexes **19**, **22** and **25** are efficient in inducing apoptosis in various cancer cells. It is understood that the interaction with DNA is playing a major role for the development of various biological activities in cells. Interaction of these complexes with CT-DNA under *in vitro* conditions can therefore provide insight to better understand the role of these complexes in inducing apoptosis.

CT-DNA interactions with the selected complexes were studied by spectroscopic methods, circular dichroism (CD) and UV-Vis spectroscopy. CD spectra of CT-DNA were recorded with complexes **19**, **22** and **25**. The CD spectrum of CT-DNA alone exhibit a positive band at 275 nm and a negative band at around 245 nm, which is a characteristic CD signature of the right handed B form of DNA.[132] Among the studied complexes, **19** exhibits hyperchromicity of the positive CD band at 275 nm, indicating its potential to stabilize DNA upon interaction. On the other hand, with complexes **22** and **25**, the intensity of the CD bands at 275 nm exhibits a hypochromic effect indicating its role in unwinding CT-DNA. The CD spectra obtained on interaction with complexes **19**, **22** and **25** with CT-DNA at higher stoichiometry (1:1) are shown in Fig. 66.

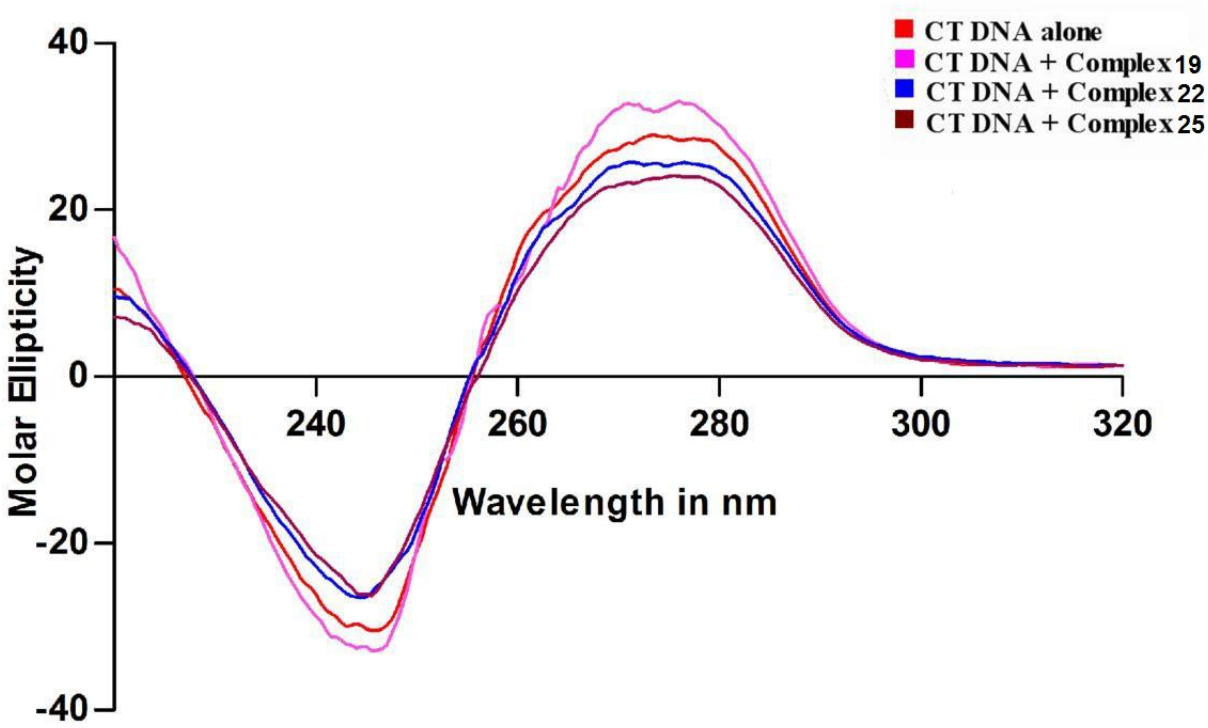

Fig. 66. *CD spectra obtained when complexes* ***19***, ***22*** *and* ***25*** *interact with CT-DNA. The spectra were labeled accordingly and the corresponding sample names are shown as an inset in the Figure. CD spectra were recorded twice and averaged to limit experimental errors.*

The UV-Vis spectrum of complex **19** shows an absorption peak at 230 nm. On addition of CT-DNA, the soret band at 230 nm exhibits hypochromicity (about 10-15 %) and shifts to 263 nm (about 33 nm bathochromic shift). Hypochromicity of the soret band occurs due to interaction between the electronic states of the cationic complex and those of the DNA bases,[133] whereas a bathochromic shift is associated with the decrease in the energy gap between the highest occupied molecular orbital (HOMO) and the lowest unoccupied molecular orbital (LUMO).[134] In general, hypochromicity and bathochromic shifts indicate that molecules bind to the DNA-helix by intercalative mode through π-staking interactions of the aromatic chromophore of the complex between DNA bases.[135] An isobestic point is also observed around 240 nm and it is not a single sharp point suggesting that the interaction between complex **19** and CT-DNA takes place in multiple steps and at a given time more than one species exist at equilibrium (Fig. 67A). The UV-Vis spectra of complexes **22** and **25** show two absorption bands at 230 nm -263 nm, and 230 nm - 325 nm, respectively. On addition of CT-DNA, the soret bands exhibit

hypochromicity. The extent of hypochromicity of the soret band is an indication of strength of ligand intercalation to DNA.[136] From Fig. 67B and 67C, it is also clear that the soret band of **25** at 230 nm shows higher hypochromicity as compared to complex **22**. This suggests that complex **25** has a better interaction with DNA and unwinds the double helical structure more effectively than **22**.[137] The UV-Vis absorption spectra of CT-DNA obtained in the presence of complexes **19**, **22** and **25** are shown in Fig. 67(A, B, C).

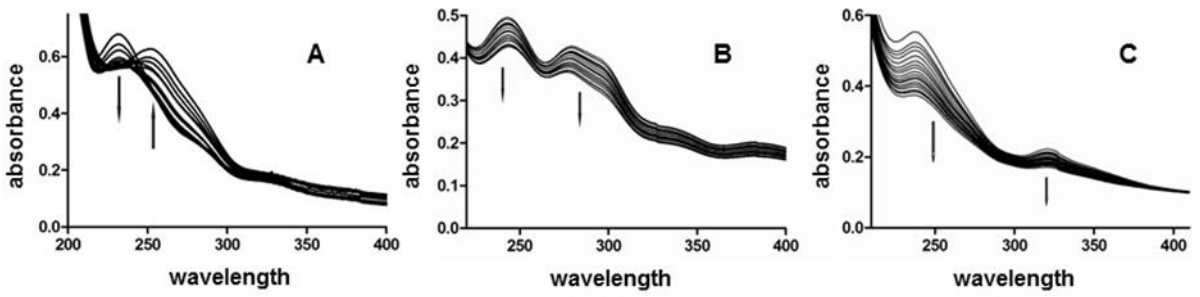

Fig. 67. *UV-Vis spectra obtained on titrating CT-DNA with complexes **19** (A), **22** (B) and **25** (C). UV-Vis spectra were recorded twice and averaged to limit experimental errors.*

In conclusion, fifteen chalcogenolato-bridged diruthenium, dirhodium and diiridium complexes have been prepared and characterized. The biological activity of the complexes has been evaluated *in vitro* on normal (CRL-2115, CRL-2120) and human cancer (A549, B16F10, MCF-7) cell lines. All complexes are highly cytotoxic showing activity in the sub-micromolar range with even some selectivity for cancer cells over normal fibroblast cells. Interestingly, the nature of the chalcogenolato bridges seems to have an impact on the activity: The complexes with the thiolato bridges being slightly more cytotoxic than the selenolato and tellurolato analogues. Additionally, the nature of the metal centers appears to have a modest impact on the activity: The ruthenium derivatives being more active by a few nM on all cell lines tested. The best candidates were further studied by flow cytometry, showing that the complexes can induce early and late apoptosis in B16F10 cells. In addition, all complexes show strong interaction with DNA, a potential target for these complexes.

4.3. Sawhorse-type diruthenium tetracarbonyl complexes containing biologically relevant acids

Carbon monoxide and nitric oxide have now been recognized as two essential signaling agents in the body.[138] Despite the CO ability to bind to hemoglobin and inhibit the respiratory cycle, evidence has been found that CO possesses valuable anti-inflammatory, vasodilatory and anti-apoptotic therapeutic effects.[139] In that respect, complexes able to release CO in biological media have been studied by Mann and his co-workers. For example, the ruthenium complexes $\{Ru(\mu\text{-}Cl)Cl(CO)_3\}_2$ (tricarbonyldichlororuthenium(II) dimer) and $Ru(CO)_3Cl(glycinate)$ {tricarbonylchloro(glycinato)ruthenium(II)} (Fig. 68), two known CO-releasing molecules (CORMs), have shown anti-microbial activity on several types of bacteria,[140] as well as interesting *in vivo* activity in human.[141]

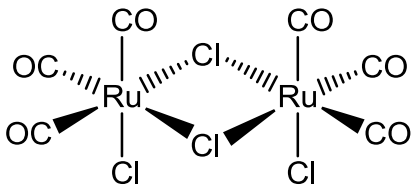

tricarbonyldichloro ruthenium(II) dimer
(CORM-2)

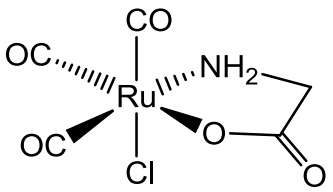

tricarbonylchloro(glycinato)ruthenium(II)
(CORM-3)

Fig. 68. *Examples of CO-releasing ruthenium complexes*[139]

In these CO-releasing complexes, the choice of exploiting ruthenium centers was not accidental. Ruthenium complexes are showing great promises as chemotherapeutic agents,[114-115,142] and the ability of ruthenium to mimic iron in biological environments gives to ruthenium complexes several interesting properties in designing metal-based drugs.[114-115,142] In addition, the chemistry of ruthenium carbonyl complexes is well developed and known for many years.[143] Among ruthenium carbonyl complexes, sawhorse-type diruthenium tetracarbonyl complexes are well known for their interesting biological applications.[7,144] Recently, we have shown that porphyrin-derived diruthenium tetracarbonyl complexes possess interesting phototoxicity towards female reproductive cancer cells[12b,145] while sawhorse-type diruthenium complexes derived from biological active acids such as aspirin, ibuprofen, ethacrynic acid and chlorambucil were not cytotoxic due to their low solubility in

water[12a,54] (Fig. 69). Consequently, a new series of sawhorse-type diruthenium tetracarbonyl complexes incorporating other biologically relevant carboxylic acids has been synthesized. Three commercially available carboxylic acids were selected for their therapeutic properties (Fig. 69): Probenecid (uricosuric drug);[146] indomethacin and sulindac, two anti-inflammatory agents.[146b,147] All $Ru_2(CO)_4(\mu_2\text{-}\eta^2\text{-}OOCR)_2L_2$ complexes were fully characterized with L being pyridine (NC_5H_5), triphenylphosphine (PPh_3) or 5-(4-pyridyl)-10,15,20-triphenylporphyrin ($C_{43}H_{29}N_5$).

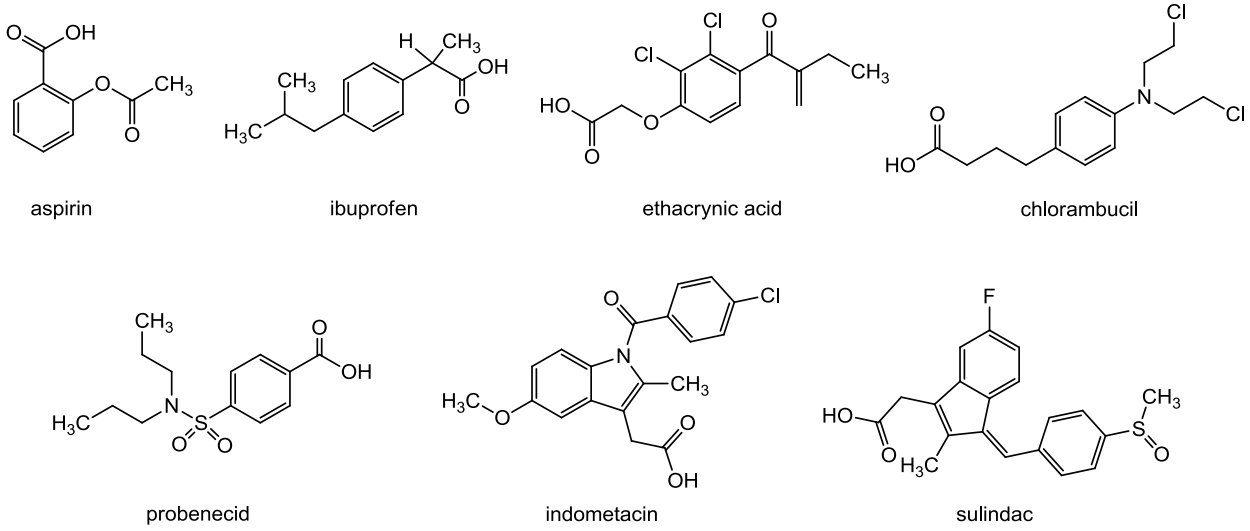

***Fig. 69**. Biologically active carboxylic acids incorporated within sawhorse-type diruthenium tetracarbonyl complexes.*

4.3.1. Synthesis of sawhorse-type diruthenium tetracarbonyl complexes

Dodecacarbonyltriruthenium reacts with an excess of the biologically relevant carboxylic acids, probenecid ($C_{13}H_{19}NO_4S$), indomethacin ($C_{19}H_{16}ClNO_4$), and sulindac ($C_{20}H_{17}FO_3S$) in refluxing tetrahydrofuran (thf) to yield a solution containing the thf intermediates $Ru_2(CO)_4(\mu_2\text{-}\eta^2\text{-}O_2CC_{12}H_{18}NO_2S)_2(thf)_2$, $Ru_2(CO)_4(\mu_2\text{-}\eta^2\text{-}O_2CC_{18}H_{15}ClNO_2)$-$(thf)_2$ and $Ru_2(CO)_4(\mu_2\text{-}\eta^2\text{-}O_2CC_{19}H_{16}FOS)(thf)_2$, respectively. These labile dinuclear thf intermediates further react with two electron donor ligands (L), such as pyridine (NC_5H_5) (**a**), triphenylphosphine (PPh_3) (**b**) or 5-(4-pyridyl)-10,15,20-triphenylporphyrin ($C_{43}H_{29}N_5$) (**c**), to generate in moderate yields the stable dinuclear complexes $Ru_2(CO)_4(\mu_2\text{-}\eta^2\text{-}$

$O_2CC_{12}H_{18}NO_2S)_2L_2$ (L = NC_5H_5, **34a**; PPh_3, **34b**; $C_{43}H_{29}N_5$, **34c**), $Ru_2(CO)_4(\mu_2\text{-}\eta^2\text{-}O_2CC_{18}H_{15}ClNO_2)L_2$ (L = NC_5H_5, **35a**; PPh_3, **35b**; $C_{43}H_{29}N_5$, **35c**), and $Ru_2(CO)_4(\mu_2\text{-}\eta^2\text{-}O_2CC_{19}H_{16}FOS)L_2$ (L = PPh_3, **36b**) (Fig 70). Within the sulindac series, only the complex containing axial triphenylphosphine ligands was isolated in sufficient yield.

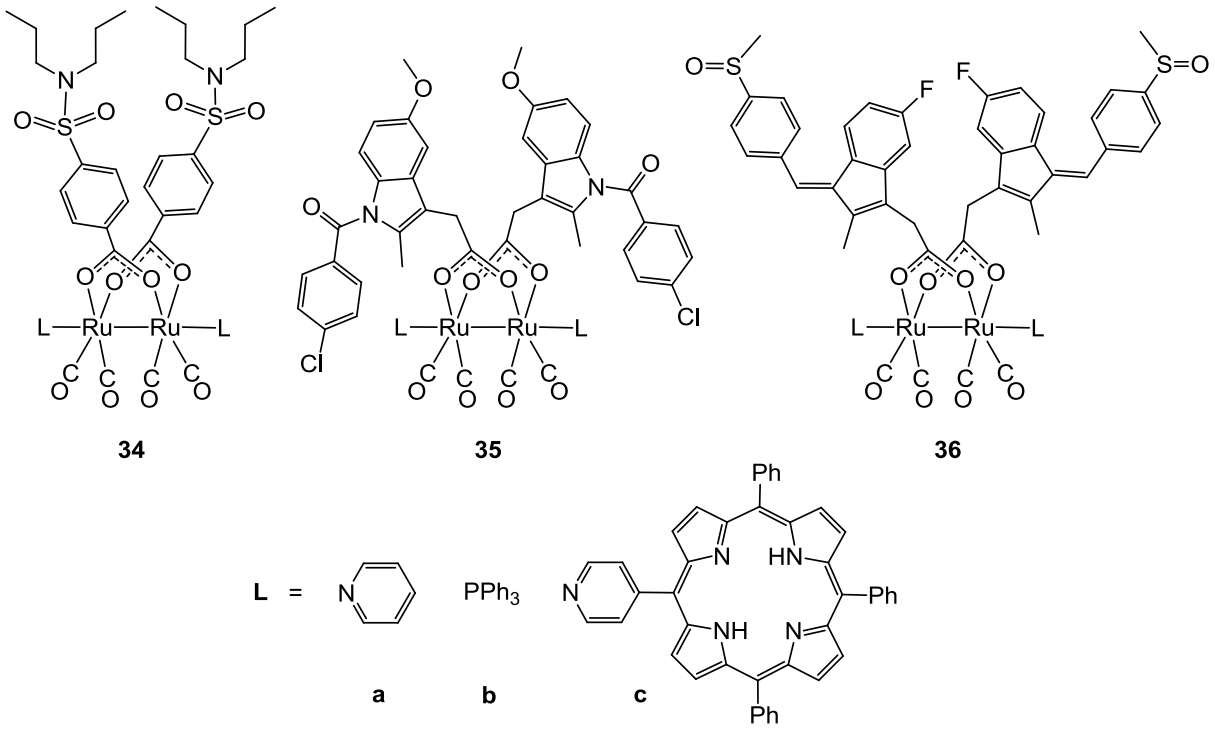

Fig 70. *Sawhorse-type diruthenium tetracarbonyl complexes **34**–**36** containing biologically relevant acids, probenecid (**34**), indomethacin (**35**) and sulindac (**36**).*

All complexes are air stable, and compounds **34a**, **34b**, **35a**, **35b**, **36b** are yellow crystalline powders, while **34c** and **35c** are purple in color due to the presence of the porphyrin ligands. All complexes have been characterized by IR, NMR, MS, UV-Vis spectroscopy (**34c** and **35c**) as well as by elemental analysis. In the infrared spectra, the $Ru_2(CO)_4$ sawhorse unit exhibits the characteristic three-band pattern for the $\nu_{(CO)}$ absorption at 1950, 1975 and 2020 cm^{-1}.[7] In addition, the two carboxylato bridges show absorption for the $\nu_{(OCO)}$ stretching frequencies around 1550 cm^{-1}, whilst for complexes **34c** and **35c**, a strong absorption centered at 1580 cm^{-1} corresponding to $\nu_{(NCN)}$, along with a strong

absorption at 1224 cm^{-1} for N-H deformation and a medium absorption at 3055 cm^{-1} attributed to the $\nu_{(CH)}$ of the porphyrinic axial ligands can be observed. The UV-visible spectra of complexes **34c** and **35c** display an intense Soret band around 418 nm, and four Q bands between 515 and 645 nm (Table 9). As previously observed with analogous sawhorse-type complexes with porphyrinic ligands,[12b,145] the absorption bands of the uncoordinated porphyrinic ligand and those observed after coordination to the diruthenium backbone remain identical, suggesting no perturbation of the porphyrin π-orbitals upon coordination.

Table 9. The electronic absorption spectra of complexes **34c**, **35c** and the porphyrinic ligand (**c**) (10^{-6} M concentration) in CH_2Cl_2 at room temperature.

Compound	Soret band	Q band IV	Q band III	Q band II	Q band I
34c	418	515	551	590	646
35c	418	515	551	590	645
c	415	514	548	589	645

The NMR spectrum of all complexes was carried out in $CDCl_3$ at room temperature. All spectra show the signals corresponding to the bridging and axial ligands. For example, the ^1H NMR spectra of **34c** and **35c** display similar pattern for the protons of the coordinated 5-(4-pyridyl)-10,15,20-triphenylporphyrin units. The N-H protons are observed at δ = -2.7 ppm, while two multiplets at 7.8 and 8.2 ppm are found in the aromatic region corresponding to the protons of the phenyl rings of the porphyrin ligands, whereas the pyrrolic protons are found between 8.9 and 9.0 ppm. The $^{13}C\{^1H\}$ NMR spectrum of this type of complexes shows signals for the terminal carbonyl groups (CO) and the carboxylato bridges (μ_2-η^2-O_2CR) at 205 and 176 ppm, respectively. In addition, for complexes **34b**, **35b** and **36b**, in the $^{31}P\{^1H\}$ NMR spectra, a sharp singlet is observed at ≈ 15 ppm which corresponds to the PPh_3 axial ligands. Overall, these data are consistent with the proposed structures.

The molecular structure of **34a** was further confirmed by single-crystal structure analysis. Crystals were obtained by the slow diffusion of benzene in a $CDCl_3$ solution of **34a**,

thus giving rise to a crystalline benzene solvate adduct (**34a** · 0.5 C_6H_6). As expected, the molecular structure shows a normal diruthenium tetracarbonyl core being completed with two pyridine axial ligands and two carboxylato-probenecid ligands in the equatorial positions (Fig. 71). At 2.6701(7) Å, the Ru-Ru distance is in the range of a single metal-metal bond, while the N-Ru-Ru-N torsion angle is almost linear at 2.8(7)º. These data are comparable to those observed in analogous C_5H_5N-Ru-Ru-NC_5H_5 sawhorse-type diruthenium tetracarbonyl complexes.[53a] Similarly, the alike OCO bond angles of the carboxylato bridges in **34a**, both being 125.4(5)°, differ only slightly from those observed in other $Ru_2(CO)_4(\mu_2\text{-}\eta^2\text{-}OOCR)_2L_2$ complexes (Table 10).[53a]

Table 10. Selected bond lengths (Å) and angles (°)

34a · 0.5 C_6H_6			
Selected bond lengths (Å) and angles (°)			
Ru1-Ru2	2.6701(7)	Ru2-O6	2.123(4)
Ru1-N3	2.213(5)	O1-C1-O2	125.4(5)
Ru2-N4	2.216(5)	O5-C14-O6	125.4(5)
Ru1-O1	2.120(4)	O1-Ru1-O5	83.15(16)
Ru1-O5	2.126(4)	O2-Ru2-O6	83.55(16)
Ru2-O2	2.143(4)	N1-Ru1-Ru2-N2	2.8(7)

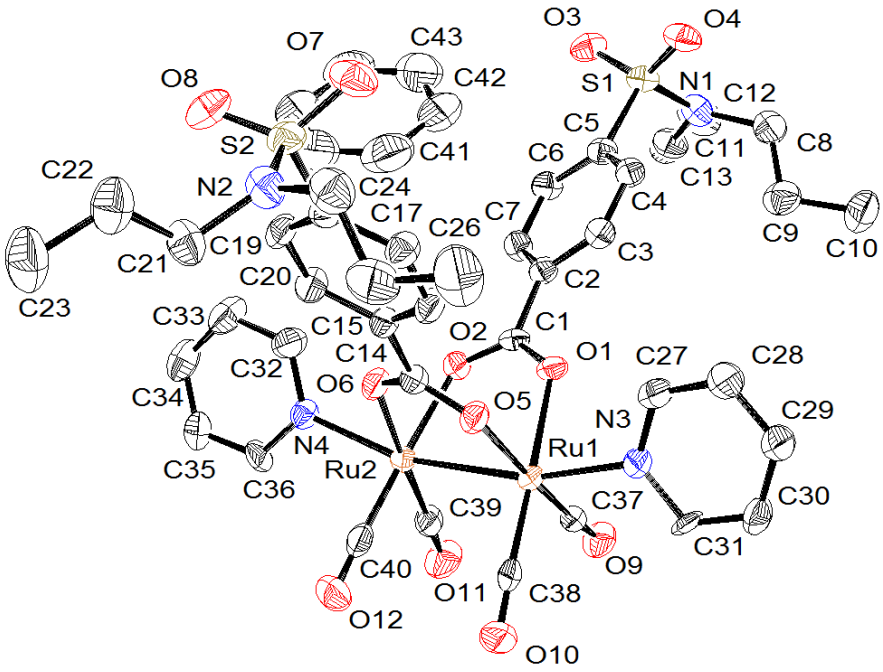

Fig. 71. *ORTEP drawing of* ***34a*** *· 0.5 C_6H_6 at 35 % probability level ellipsoids (hydrogen atoms and C_6H_6 solvent molecule omitted for clarity).*

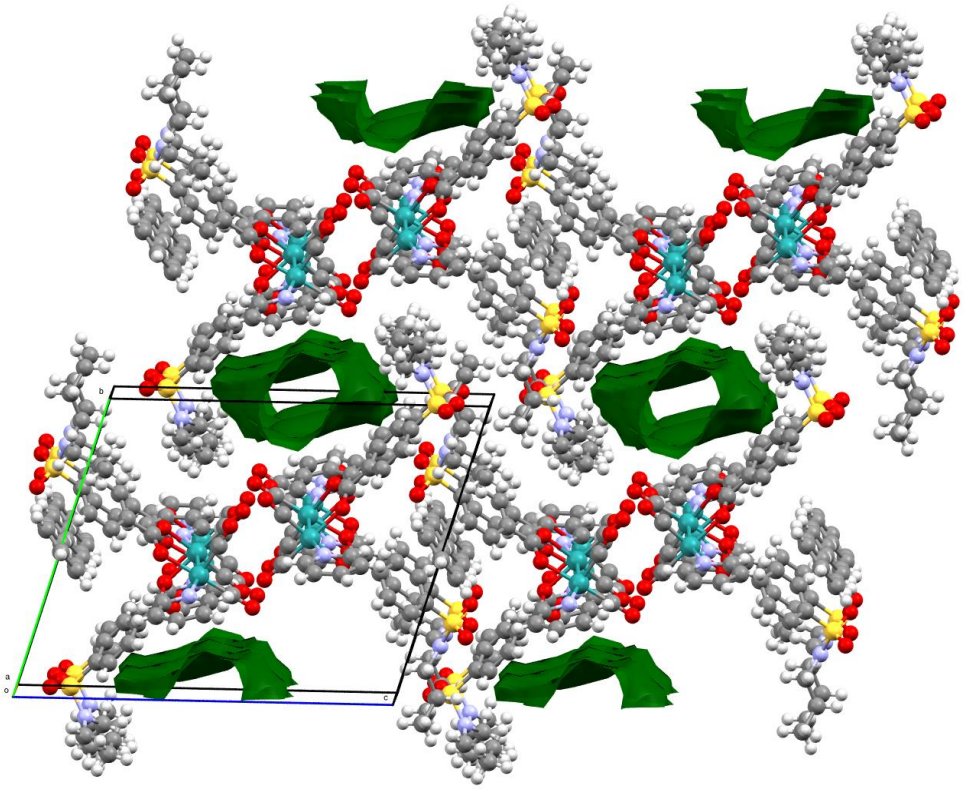

Fig. 72. *Crystal packing of* ***34a*** *· 0.5 C_6H_6 showing the empty voids of 185 $Å^3$ along the a axis.*

The unit cell of **34a** contains a molecule of benzene, which is located between the two probenecid units of **34a**, thus filling some of the voids observed in the crystals. These benzene molecules form weak slipped-parallel and T-shaped π-stacking interactions with the neighboring phenyl ring of the probenecid moieties. However, more voids remain in the crystal packing, which seem to be empty despite being of approximately 185 $Å^3$: No significant residual densities being observed in that empty space. Empty channels are observed along the *a* axis and represent almost 7 % of the total volume within the unit cell (Fig. 72).

The effects of the organometallic complexes **34-36** were investigated *in vitro* on human ovarian cancer cells (A2780). The complexes were first dissolved in dimethyl sulfoxide (DMSO) and then diluted in complete medium (RPMI 1640 medium) to the desired concentration, the DMSO concentration remaining below 5 % v/v. In all cases, after cell exposure at 37 ºC to increasing concentration of complexes, precipitation of the complexes in the culture medium occurred and accordingly no cytotoxicity was observed.

In conclusion, we have synthesized and characterized seven new sawhorse-type diruthenium tetracarbonyl complexes with pyridine, triphenylphosphine, 5-(4-pyridyl)-10,15,20-triphenylporphyrin as axial ligands and containing biologically relevant acids as carboxylato bridging ligands. However, the limited solubility of these complexes in aqueous medium resulted in no cytotoxicity for these systems against human cancer cells.

4.4. Anticancer activities of sawhorse-type diruthenium tetracarbonyl complexes derived from fluorinated fatty acids

On the other hand, sawhorse-type diruthenium tetracarbonyl complexes **8a, 8b** and **8c** derived from fluorinated fatty acids showed moderate cytotoxicity on human cancer cell lines. The synthesis of sawhorse-type complexes derived from fluorinated fatty acid **8** and **9** were detailed in chapter 2. Cytotoxicity of complexes **8a**, **8b** and **8c** were evaluated with HeLa cervix, A549 pulmonary, Me300 melanoma and A2780 ovarian cancer cell lines. Unfortunately, the poor solubility of fluorinated complexes **9a**, **9b** and **9c** did not allow their assessment. Cells were exposed for 72 h to increasing concentrations of compounds **8a-8c**, and their survival was determined using the MTT assay. In all cell lines, the complexes show similar cytotoxicity with an IC_{50} ranging from 60 to 200 μM depending on the cell line tested

(Table 11). These results suggest that the nature of the axial ligands plays only a minor role on the overall cytotoxicity. Interestingly, among the cell lines tested, it appears that the Me300 melanoma cells were the most sensitive cells to all complexes. This point is important since melanoma tumours are aggressive and resistant to common chemotherapeutic treatments.[148]

Table 11. Cytotoxicity of complexes **8a-8c** after 72 h exposure of human cancer cells.

	IC_{50} [μM]		
cell lines	**8a**	**8b**	**8c**
HeLa	199 ± 9	179 ± 1	178 ± 2
A549	190 ± 9	184 ± 5	190 ± 2
Me300	73 ± 1	61 ± 8	63 ± 1
A2780	124 ± 1	111 ± 1	129 ± 1

In conclusion, the *in vitro* studies showed that, the complexes $Ru_2(CO)_4(\mu_2\text{-}\eta^2\text{-}O_2CC_3F_7)_2(L)_2$ (**8a-8c**) exhibit moderate cytotoxicity with cancer cell lines such as HeLa, A549, Me300 and A2780. Observed cytotoxicity on Me300 melanoma cells is encouraging for further investigations.

4.5. Photoactive sawhorse-type diruthenium tetracarbonyl complexes

Photodynamic therapy (PDT) is a treatment which can be used to cure cancer and other diseases.[149] During PDT treatment, a photosensitizing agent (photosensitizer) is activated by light of specific wavelength. This results in the production of reactive oxygen species (ROS) such as singlet oxygen ($^1O_2$) and oxygen radicals. These oxygen species oxidize cell components leading to cell death either by apoptosis or necrosis.[150] The light needed to activate the photosensitizer is often a drawback of PDT as most photosensitizer's efficacy is limited by the penetration of light across biological tissues, which are in the order

of several mm for wavelengths shorter than 640 nm. For this reason, PDT is mostly used to treat retinal, skin, mucosal or endothelial lesions.[151] To overcome this limitation, it is necessary to use photosensitizers that can be excited by light at longer wavelengths, as the optimal window for light tissue penetration in PDT is between 650-850 nm.[152]

Most of the photosensitizers used in PDT are porphyrin-like compounds. Initially proposed by Figge *et al.*[153] different classes of porphyrins are now available. Hematoporphyrin and its derivatives were the first porphyrin-like compounds clinically used in PDT.[154] Isolated from blood, hematoporphyrin is a mixture of compounds which was commercialized as Photofrin®, also called porfimer sodium (Fig 73). This mixture is effective but patients remain subject to skin photosensitization several weeks after treatment.[155] Furthermore, the short excitation wavelength (630 nm) is another limitation of the treatment. Preparation of chlorin, the reduced form of porphyrin, can potentially overcome this wavelength limitation. Foscan®, meta-tetrahydroxyphenylchlorin (Fig 73), which strongly absorbs light at 652 nm has been approved and commercialized. However, the phototoxicity of the product is highly variable in human cancer and its long-term skin photosensitization is also problematic,[155-156] thus limiting its application in the clinic. Nowadays, photosensitizers are tethered to biomolecules[157] in view to enhance their cellular uptake, solubility, selectivity, and ultimately to increase PDT efficiency. However, the ideal photosensitizer has still to be found.[158]

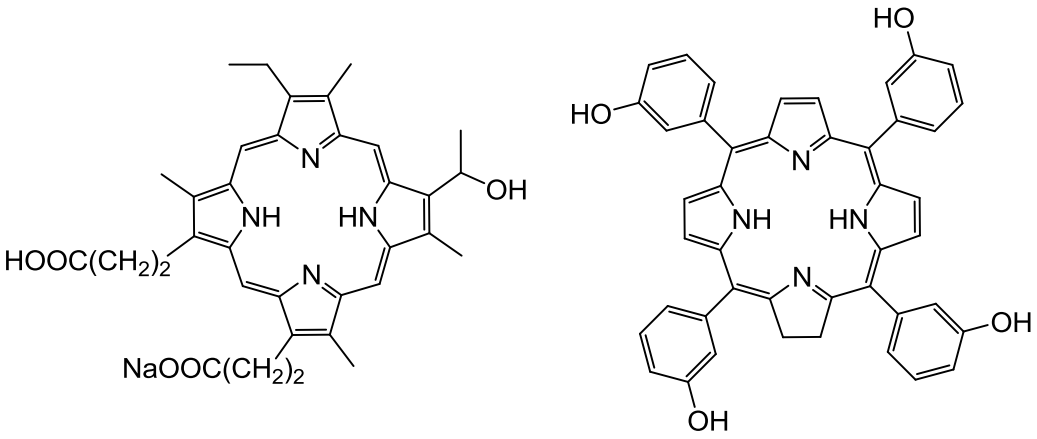

Fig 73. *Structures of photofrin and foscan.*

In chemotherapy, metal-based drugs are widely used since the introduction of cisplatin on the market in the 1970s.[159] In analogy to the functionalization of photosensitizers

with biomolecules to increase efficiency or overcome limitations, cisplatin has been coupled to several functional groups.[160] Among these combinations, Brunner and his co-workers have coordinated $\{Pt(NH_3)_2\}^{2+}$ units to porphyrin ligands.[161] Several platinum-porphyrin derivatives were synthesized and some of them were evaluated *in vitro.*[162] For example, the diammine {7,12-bis[1-(poly(ethylenglycol)-750-monomethylether-1-yl)ethyl]-3,8,13,17-tetra-methylporphyrin-2,18-dipropionato}platinum(II) complex (Fig 74, left) has shown low selectivity and high toxicity in both healthy and cancer cells, thus hampering its biological potential. Therefore, replacing platinum by a less toxic metal, such as ruthenium,[114-115,142c,163] is offering interesting perspectives for the development of chemotherapeutics. A few years ago, we,[164] Swavey,[165] and soon after Alessio[166] have described ruthenium-porphyrin systems potentially able to combine PDT and chemotherapy. Among those, the sawhorse-type diruthenium tetracarbonyl porphyrin system, $[Ru_2(CO)_4(\mu_2\text{-}\eta^2\text{-}OOCCH_3)_2(L)_2]$ (L = 5-(4-pyridyl)-10,15,20-triphenyl-21,23H-porphyrin) (Fig 74, right), has demonstrated an interesting selectivity for female reproductive cancer cells.[12b] These results encouraged us to study further this family of ruthenium-porphyrin complexes.

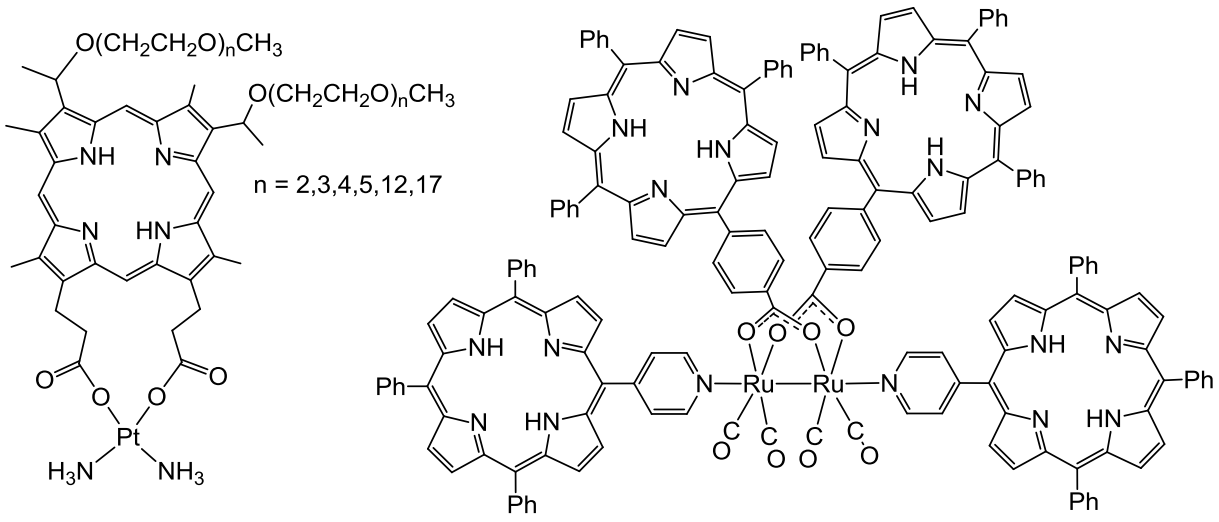

Fig 74. *Structures of metal-based porphyrin derivatives*

Herein, we describe the synthesis, characterization and *in vitro* activity in the dark and after light irradiation of a new series of sawhorse-type diruthenium tetracarbonyl complexes

incorporating carboxyphenyl porphyrin moieties and pyridine axial ligands, the photosensitizers being anchored to the diruthenium backbone by the carboxylato binding sites of the sawhorse diruthenium unit.

4.5.1. Synthesis of photoactive sawhorse-type diruthenium tetracarbonyl complexes

The thermal reaction of $Ru_3(CO)_{12}$ with an excess of the mono-carboxylic porphyrin derivatives 5-(4-carboxyphenyl)-10,15,20-triphenyl-21,23H-porphyrin ($HO_2CC_{44}H_{29}N_4$) and the corresponding zinc(II) metallo-porphyrin ($HO_2CC_{44}H_{27}N_4Zn$), the di-carboxylic porphyrin derivatives 5,10-di(4-carboxyphenyl)-15,20-diphenyl-21,23H-porphyrin ($HO_2CC_{44}H_{28}N_4CO_2H$) and the corresponding zinc(II) metallo-porphyrin ($HO_2CC_{44}H_{26}N_4ZnCO_2H$) in refluxing tetrahydrofuran (thf) yields a solution containing the thf complexes $[Ru_2(CO)_4(\mu_2\text{-}\eta^2\text{-}O_2CC_{44}H_{29}N_4)_2(thf)_2]$, $[Ru_2(CO)_4(\mu_2\text{-}\eta^2\text{-}O_2CC_{44}H_{27}N_4Zn)_2\text{-}(thf)_2]$, $[\{Ru_2(CO)_4(thf)_2\}_2(\mu_2\text{-}\eta^2\text{-}O_2CC_{44}H_{28}N_4CO_2\text{-}\eta^2\text{-}\mu_2)_2]$, and $[\{Ru_2(CO)_4(thf)_2\}_2(\mu_2\text{-}\eta^2\text{-}O_2CC_{44}H_{26}N_4ZnCO_2\text{-}\eta^2\text{-}\mu_2)_2]$, respectively. These labile thf intermediates react easily with pyridine to afford, after precipitation and/or column chromatography the neutral complexes $[Ru_2(CO)_4(\mu_2\text{-}\eta^2\text{-}OOCC_{44}H_{29}N_4)_2(NC_5H_5)_2]$ (**37**), $[Ru_2(CO)_4(\mu_2\text{-}\eta^2\text{-}O_2CC_{44}H_{27}N_4Zn)_2\text{-}(NC_5H_5)_2]$ (**38**), $[\{Ru_2(CO)_4(NC_5H_5)_2\}_2(\mu_2\text{-}\eta^2\text{-}O_2CC_{44}H_{28}N_4CO_2\text{-}\eta^2\text{-}\mu_2)_2]$ (**39**) and $[\{Ru_2(CO)_4(NC_5H_5)_2\}_2(\mu_2\text{-}\eta^2\text{-}O_2CC_{44}H_{26}N_4ZnCO_2\text{-}\eta^2\text{-}\mu_2)_2]$ (**40**) in moderate yields (Fig. 75).

The air-stable dark purple solids **37**−**40** are sparingly soluble in polar organic solvents, and they have been characterized by IR, MS, NMR, UV-Vis and by micro-analytical data. In the infrared spectra, complexes **37**−**40** exhibit the characteristic three-band pattern of the $Ru_2(CO)_4$ sawhorse moiety at 1950, 1975 and 2020 cm^{-1}, which is observed in all complexes of this type.[7] In addition, due to the presence of the porphyrin groups, a strong absorption centered at 1587 cm^{-1} associated to $\nu_{(NCN)}$ and a medium absorption at 3054 cm^{-1} corresponding to the C-H stretching vibration are observed. The ^1H NMR spectra of **37**−**40** at room temperature show a similar signal pattern for the protons of the coordinated carboxyphenyl porphyrin moieties and for the axial pyridine ligands. All complexes exhibit in the aromatic region multiplets at 7.6, 7.8, 8.0 and 8.2 ppm, corresponding to the phenyl protons of both the porphyrin and pyridine ligands, while the pyrrolic protons are observed at 8.8 and 8.9 ppm. Complexes **37** and **40** display an additional signal at δ = -2.8 ppm for the N-H protons of the porphyrin core.

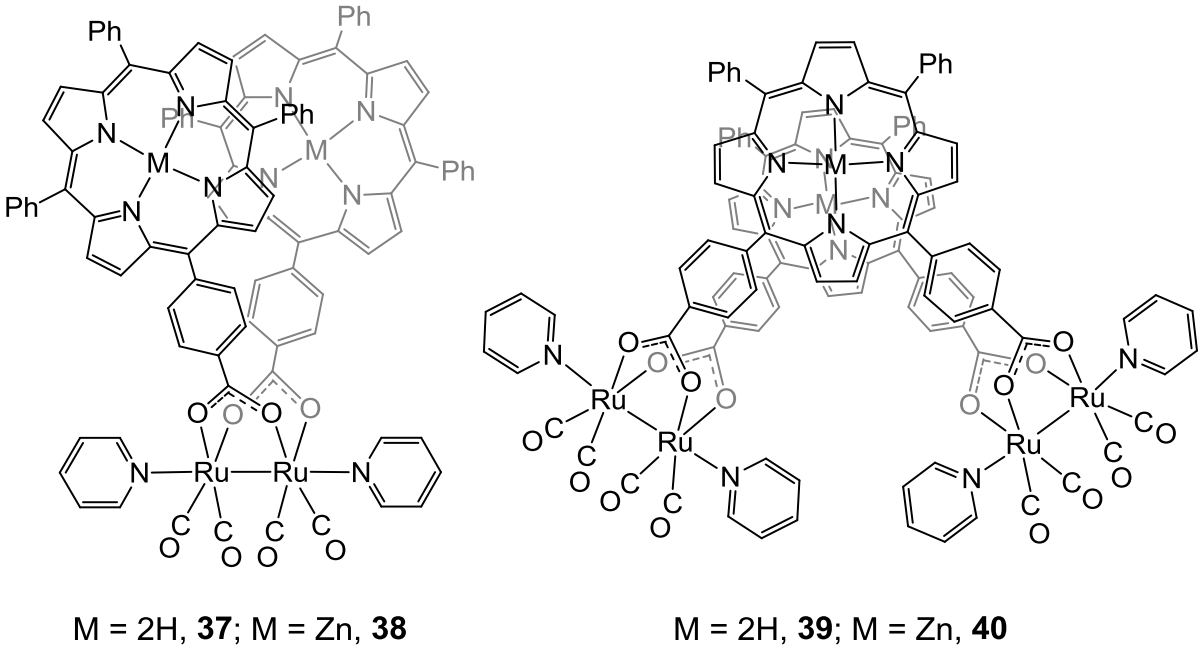

Fig. 75. *Molecular structure of complexes **37**−**40**.*

The electronic absorption spectra of the sawhorse-type diruthenium tetracarbonyl complexes **37**−**40** and the non-coordinated carboxyphenyl porphyrin derivatives ($HO_2CC_{44}H_{29}N_4$, $HO_2CC_{44}H_{27}N_4Zn$, $HO_2CC_{44}H_{28}N_4CO_2H$ and $HO_2CC_{44}H_{26}N_4ZnCO_2H$) display the typical Soret band at 420 nm, and the Q bands between 500 and 700 nm. The metal-free porphyrin derivatives possess four Q bands, while all Zn(II) metallo-porphyrin compounds show no Q bands I and IV in their absorption spectra. The absorption bands of the uncoordinated carboxyphenyl porphyrin unit and those of complexes **37**−**40** remain unchanged after complexation, suggesting no perturbation of the porphyrin π-orbitals upon coordination (Table 12).

Table 12. UV-Vis maximum absorption wavelength (nm) of complexes **37**−**40, 15** and **17** and the porphyrinic ligands in CH_2Cl_2 at 10^{-6} M concentration.

Compound	Soret band	Q band IV	Q band III	Q band II	Q band I
37	414	515	550	590	647
38	418	-	550	592	-
39	415	515	548	589	645
40	423	-	551	591	-
15	418	515	549	590	647
17	418	-	550	592	-
$HO_2CC_{44}H_{29}N_4$	415	515	549	590	646
$HO_2CC_{44}H_{27}N_4Zn$	420	-	551	592	-
$HO_2CC_{44}H_{28}N_4CO_2H$	418	515	549	589	645
$HO_2CC_{44}H_{26}N_4ZnCO_2H$	423	-	552	593	-

The organometallic porphyrin complexes were investigated *in vitro* as potential drug candidates for cancer therapy by evaluating the growth inhibition of human A549 lung cancer, HeLa cervix cancer, A2780 ovarian cancer and Me300 melanoma cells. For comparison, the known triphenylphosphine derivative, $[Ru_2(CO)_4(OOCC_{44}H_{27}N_4Zn)_2(PPh_3)_2]$ (**17**),[167] was also evaluated. And for discussion, the previously tested metal-free porphyrin derivative with triphenylphosphine axial ligands, $[Ru_2(CO)_4(OOCC_{44}H_{29}N_4)_2(PPh_3)_2]$ (**15**),[12b] was used. The molecular structures of these two analogues of complexes **15** and **17** are presented in Fig. 37 (chapter 3).

Cells were exposed for 72 h to increasing concentrations of compounds **37**-**40** and **17**, their survival was determined using the MTT assay in the absence of laser exposure (dark toxicity). In all cell lines, complex **38** presented the highest cytotoxicity with an IC_{50} ranging from 22 to 52 µM depending on the cell line tested, while complex **37**, its metal-free related compound, induced the lowest cytotoxicity. Therefore, the presence of the Zn(II) ion in the

porphyrin tetrapyrrolic ring increased significantly the cytotoxicity. In comparison, the other Zn(II) metallo-derivatives **40** and **17** are moderately cytotoxic in the dark. Among the cell lines tested, it appears that the Me300 melanoma cells were the most sensitive cells to all complexes (Table 13). This point is important since melanoma tumors are aggressive and resistant to common chemotherapeutic treatments,[148a,b,168] whilst easily accessible by PDT protocols.

Table 13. Cytotoxicity in the dark of complexes **37**−**40** and **17** after 72 h exposure of human cancer cells.

	IC_{50} [μM]				
cell lines	**37**	**38**	**39**	**40**	**17**
HeLa	191 ± 9	42 ± 2	193 ± 7	196 ± 4	155 ± 22
A549	173 ± 3	52 ± 7	118 ± 6	137 ± 12	131 ± 5
Me300	58 ± 13	22 ± 3	49 ± 2	37 ± 12	41 ± 6
A2780	174 ± 15	32 ± 3	198 ± 11	191 ± 8	76 ± 14

The phototoxicities of the different complexes were also evaluated using a red laser irradiating at 652 nm. The cells were exposed for 24 h to 5 μM concentration of the complexes, since all complexes were not cytotoxic in the dark at this concentration and exposure time. Then, cell cultures were irradiated with an irradiance of 30 mW/cm^2 and light doses ranging between 2 and 20 J/cm^2. Cell toxicity was determined using the MTT assay 24 h after the completion of the irradiation. Untreated cells were not photosensitive in the absence of complexes. Cells exposed to the complexes under identical conditions but not irradiated were used as controls for phototoxicity. The viability of the HeLa cervix and A2780 ovarian cells exposed to complexes **37**−**40**, **17** and light-irradiated at increasing doses is shown in Fig. 76. Complex **37** induced good phototoxicity in both cancer cells with corresponding LD_{50} values (light dose necessary to inhibit 50 % cell survival) of 4.5 and 7.5

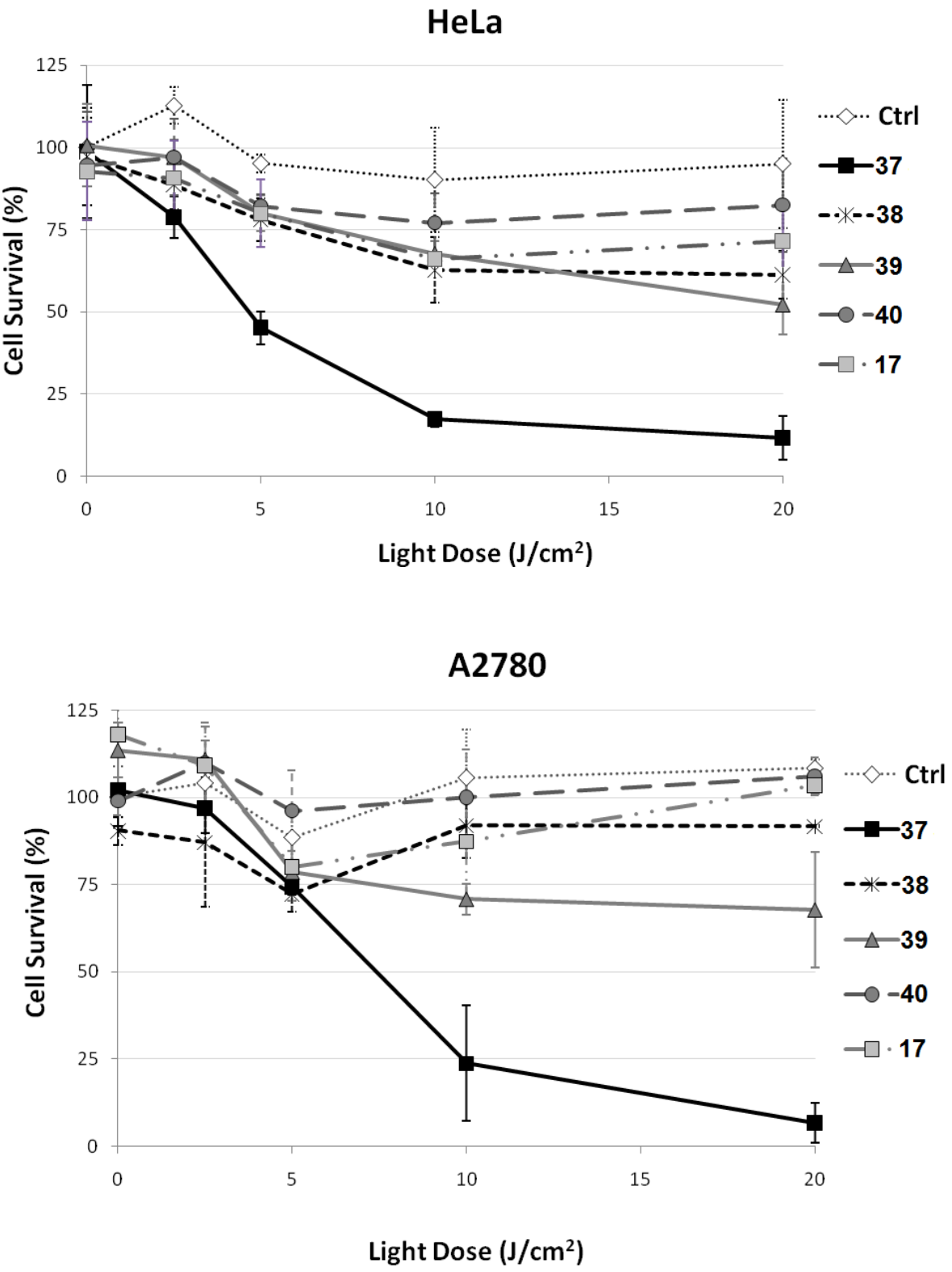

Fig. 76. *PDT effect in HeLa cervix and A2780 ovarian cancer cells, 5 μM concentration of* ***37***−***40***, ***17*** *and irradiation at 652 nm (irradiance = 30 mW/cm^2; Ctrl = cells exposed to the complexes under identical conditions but not irradiated).*

J/cm^2, respectively. Good phototoxicity was also observed on HeLa cervix and A2780ovarian cells when exposed to the triphenylphosphine derivative **15,**[12b] thus suggesting that the nature of the axial ligands is not crucial. Complex **39** was slightly phototoxic with LD_{50} values higher than 20 J/cm^2, while complexes **38**, **40** and **17**, the Zn(II) metallo-porphyrin derivatives, were not phototoxic in our experimental conditions. Thus, these results revealed that only zinc-free porphyrin-ruthenium complexes present good phototoxic activity. This is in agreement with the spectroscopic data which indicate that for the Zn(II) metallo-porphyrin compounds the Q band I is not observed around 650 nm (Table 13), thus explaining the absence of PDT effect for complexes **38**, **40** and **17**.

In conclusion, a series of sawhorse-type diruthenium tetracarbonyl complexes appended with two porphyrin units positioned at 90° from each other has been synthesized and characterized. The presence of Zn(II) ions within the porphyrin cores increases the cytotoxicity and reduced the photocytotoxicity. On the other hand, the non-metallated porphyrin derivatives are poorly cytotoxic, and interestingly in the case of $[Ru_2(CO)_4(\mu_2\text{-}\eta^2\text{-}O_2CC_{44}H_{29}N_4)_2(NC_5H_5)_2]$ (**37**), highly phototoxic.

Chapter 5:

General conclusion

5. General conclusion

The present work deals with the synthesis and characterization of dinuclear Ru(II), Rh(III) and Ir(III) complexes. These dinuclear complexes have been studied for their catalytic, supramolecular and biological applications. In the first part, we have shown the synthesis and characterization of a series of sawhorse-type complexes derived from saturated (fluorinated and non-fluorinated) fatty acids. The single-crystal X-ray structure analyses of **2a**, **3a**, **4a** and **5a** revealed that for $n \geq 8$, the packing of the non-fluorinated alkyl chains and the π-π interactions between pyridyl groups dominated, while for $n \leq 7$, only the arrangement of the axial pyridyl ligands played a significant role in the crystalline packing of these sawhorse-type complexes. Complexes **8**, **9**, **10** and **11** were evaluated as catalyst for the hydrogenation of styrene under $scCO_2$. All the catalysts gave a very poor conversion.

In the second part, we have synthesized and photophysically characterized a series of sawhorse-type molecular tweezers derived from either pyrenyl or porphyrin carboxylic bridging units. The molecular modeling of **14**, **15** and **16** suggests that the pyrenyl and porphyrin moieties are adequately positioned to allow these complexes to act as molecular tweezers with fullerene. However, these systems have showed no interaction with fullerene in solution, despite possessing appropriate structural features, as predicted by modeling for compounds **14**, **15** and **16**. On the other hand, with the Zn(II)-porphyrin derivatives, **17** and **18**, interaction with bis-pyridyl ligands were observed. In particular, a relatively high association constant between 5,10-di-(4-pyridyl)-15,20-diphenyl-21,23H-porphyrin and **18** was found, thus indicating size specific tweezing properties, and overall showing a new application for an old class of compounds, the sawhorse-type diruthenium tetracarbonyl complexes.

In the final part, we have investigated the anti-cancer ability of different dinuclear (Ru, Rh and Ir) complexes. Fifteen chalcogenolato-bridged diruthenium, dirhodium and diiridium complexes (**19**-**33**) have been synthesized and the biological activity of these complexes has been studied *in vitro* on normal (CRL-2115, CRL-2120) and human cancer (A549, B16F10 and MCF-7) cell lines. All complexes are highly cytotoxic even in the sub-micromolar range. Interestingly, the nature of the chalcogenolato bridges seems to have an impact on the activity: The complexes with the thiolato bridges (**19**, **22** and **25**) being slightly more cytotoxic than the selenolato and tellurolato analogues. In addition, all complexes show

strong interaction with DNA, a potential target for these complexes. Overall, these results confirm that the thiolato-bridged dinuclear half-sandwich complexes are very promising anticancer agents and deserve more biological studies.

Similarly, a series of sawhorse-type diruthenium tetracarbonyl complexes (**8**, **17**, **34-36**, and **37-40**) have been synthesized and evaluated for biological studies. The complexes **34-36** were synthesized from biological active acids such as probenecid, indomethacin and sulindac. However, the limited solubility of the complexes **34-36** in aqueous medium resulted in no cytotoxicity against human cancer cells. On the other hand, complexes of sawhorse-type diruthenium complexes derived from fluorinated carboxylic acid $Ru_2(CO)_4(\mu_2\text{-}\eta^2\text{-}O_2C(CF_2)_2CF_3)_2(L)_2$ (**8a**, L = C_5H_5N; **8b**, L = PPh_3; **8c**, L = PTA) showed moderated cytotoxicity on HeLA, A549, Me300 and A2780.

In a similar fashion, photoactive sawhorse-type diruthenium tetracarbonyl complexes were synthesized from porphyrin carboxylic units **17** and **37-40**. These complexes were evaluated *in vitro* as anticancer drugs on HeLA, A549, Me300 and A2780 cancer cells. The presence of Zn(II) ions within the porphyrin cores $[Ru_2(CO)_4(O_2CC_{44}H_{27}N_4Zn)_2(NC_5H_5)_2]$ (**38**) increases the cytotoxicity and reduced the photocytotoxicity. While, the non-metallated porphyrin derivative $[Ru_2(CO)_4(O_2CC_{44}H_{29}N_4)_2(NC_5H_5)_2]$ (**37**) were poorly cytotoxic and interestingly phototoxic. Complex **37** possesses an excellent ratio of cytotoxicity versus phototoxicity, and optimization of the system is currently under investigation in our laboratory. Replacement of the porphyrin units with chlorins or phthalocyanines is envisaged with the goal to induce a bathochromic shift of the absorption bands and consequently to potentially further increase the gap between cytotoxicity versus phototoxicity.

Chapter 6:

Experimental Section

6. Experimental section

6.1. General Remarks

Unless otherwise stated, all manipulations were carried out under nitrogen atmosphere by conventional Schlenk techniques. Organic solvents were degassed and saturated with nitrogen prior to use, except ethanol. 5-(4-Carboxyphenyl)-10,15,20-triphenyl-21,23H-porphyrin, 5-(4-carboxyphenyl)-10,15,20-triphenylporphyrin-Zn, 5,10-di(4-carboxyphenyl)-15,20-diphenyl-21,23H-porphyrin, 5,10-di(4-carboxyphenyl)-15,20-diphenylporphyrin-Zn, 5-(4-Pyridyl)-10,15,20-triphenyl-21,23H-porphyrin, 5,10-di-(4-pyridyl)-15,20-diphenyl-21,23H-porphyrin and 5,15-di-(4-pyridyl)-10,20-diphenyl-21,23H-porphyrin were purchased from TriPorTech GmbH, fullerene was purchased from SES RESEARCH (Houston, Texas). 1-Pyrenecarboxylic acid, 1-pyreneacetic acid, 1-pyrenebutyric acid, pyridine, 4,4'-bipyridine, 1,2-bis(4-pyridyl)ethylene, 1,3,5-triaza-7-phosphatricyclo[3.3.1.1]decane and triphenyl-phosphine were commercially available from Sigma-Aldrich and used as received. The starting materials $Ru_3(CO)_{12}$,[3] $(\eta^6\text{-}p\text{-}MeC_6H_4Pr^i)_2Ru_2(\mu\text{-}Cl)_2Cl_2$,[33] $(\eta^5\text{-}C_5Me_5)_2Rh_2(\mu\text{-}Cl)_2Cl_2$,[36-37] $(\eta^5\text{-}C_5Me_5)_2Ir_2(\mu\text{-}Cl)_2Cl_2$,[36-37] $(\eta^6\text{-}p\text{-}MeC_6H_4Pr^i)_2Ru_2Cl_2(\mu\text{-}SCH_2C_6H_4\text{-}p\text{-}Bu^t)_2$[38a], $(\eta^5\text{-}C_5Me_5)_2Rh_2Cl_2(\mu\text{-}SCH_2C_6H_5)_2$ [119] and $(\eta^5\text{-}C_5Me_5)_2Ir_2Cl_2(\mu\text{-}SCH_2C_6H_5)_2$[41] were prepared according to published methods. Column chromatography was performed using silica gel 60 (63-200, 60 Å, Brunschwig).

6.1.1. Infrared spectroscopy

IR spectra were recorded on a Perkin-Elmer 1720x FT-IR spectrometer (4000 - 400 cm^{-1}). Samples were analysed in solution (CaF_2 plates) or as solids (KBr pellet).

6.1.2. Mass spectroscopy

Mass spectra were performed by the analytical service faculty of university of Neuchâtel or the University of Fribourg.

6.1.3. NMR spectroscopy

The ^1H, ^{13}C, ^{19}F, ^{31}P, 2D and DOSY NMR spectra were recorded on a Bruker 400 MHz spectrometer and operated with Mestre-C and Mnova. All the deuterated solvents were purchased from Cambridge Isotope Laboratories, Inc. the chemical shifts δ are given in ppm

and coupling constants J are given in Hz spectra were calibrated to the residual signal of the non-deuterated solvent. For all DOSY experiments, the temperature was regulated at 298 K, the airflow was increased to 670 $Lmin^{-1}$, and the NMR tube was spun. The diffusion NMR experiments were performed using a standard pulsed-gradient stimulated echo (LED-PFGSTE) sequence, using bipolar gradient.[169] DOSY spectra were generated by using the TopSpin 2.0 software package (Bruker). Experimental parameters were Δ = 50.0 ms (diffusion delay), τ_{DOSY} = 1.0 ms (gradient recovery delay), and *Te* = 5.0 ms (eddy current recovery delay). For each data set, 4096 complex points were collected, and the gradient dimension was sampled using 16 experiments in which the gradient strength was exponentially incremented from 1.0 to 50.8 Gcm^{-1}. The gradient duration $\delta/2$ was adjusted to observe a near complete signal loss at 50.8 Gcm^{-1}. Typically, the $\delta/2$ delay was chosen in the 1.2-2.0 ms range. A 1.0 s recycle delay was used between scans for data shown. For each data set, the spectral axis was processed with an exponential function (3-5 Hz line broadening), and Fourier transform was applied in order to obtain 4096 real points. The DOSY reconstruction was realized with 256 points in the diffusion dimension. The number of scans ranged from 8 to 64 and was adapted to each sample. The experimental time ranged from 4 to 30 min.

6.1.4. UV-Vis and fluorescence spectroscopy

For porphyrin complexes (**14-18**), the spectroscopic investigations were carried out in cyclohexane, carbon tetrachloride and toluene (Carlo Erba spectroscopic grade) in fluorimetric cuvettes with an optical path of 1 cm. Absorption spectra were recorded with a Perkin-Elmer λ950 spectrophotometer. Steady-state photoluminescence spectra were measured in right angle mode with an Edinburgh FLS920 spectrometer (continuous 450 W Xe lamp), equipped with a Peltier-cooled Hamamatsu R928 photomultiplier tube (185-850 nm) at room temperature. The excitation and emission monochromators slit widths were manually adjusted to have a peak resolution of ± 3 nm for the emission measurements. Fluorescence lifetimes were measured with an IBH 5000F time-correlated single-photon counting device, by using pulsed NanoLED excitation sources at 331, 373, 465 and 560 nm. Analysis of the luminescence decay profiles against time was accomplished with the Decay Analysis Software DAS6 provided by the manufacturer. For pyrene complexes (**12-14**), UV-Vis absorption spectra were recorded on an Uvikon 930 spectrophotometer using precision

quartz cells (1 cm). Fluorescence titrations were performed on a Varian Cary Eclipse spectrophotometer using Sarstedt acrylic cuvettes (10 x 10 x 45 mm).

6.1.5. Elemental analyses

Elemental analyses were performed by the Mikroelementarisches Laboratorium, ETH Zürich (Switzerland) or the laboratory of pharmaceutical chemistry, university of Geneva (Switzerland).

6.2. Catalytic experiments (complexes 8-11)

General procedure for hydrogenation of styrene in supercritical carbon dioxide: The reaction was carried out in a 125 mL stainless steel reactor equipped with a magnetic stirrer. The reactor was purged with argon prior to the introduction of adequate amounts of Ru-catalyst and styrene (amount of catalyst = 0.02 mmol, substrate/catalyst ratio = 1/500) via a cannula transfer. When methanol was used as co-solvent, catalysts were prior dissolved in 1 mL of degassed methanol. After introduction of H_2 (10 bar), CO_2 was admitted, leading to a total reaction pressure of 120 bar. The reaction temperature was controlled by an internal thermocouple. After a reaction time of 16 h the reactor was cooled down to 0 °C, the pressure was gently released and the liquid phase was transferred to a Schlenk tube. Trap-to-trap distillation under vacuum at ambient temperature allowed separation of volatile compounds that were quantitatively analysed by GC (Thermo Scientific FOCUS GC, TR-Wax 30 m capillary column, FID detector).

Safety Warning: Experiments involving pressurized gases can be hazardous and must only be conducted with suitable equipment and following appropriate safety conditions.[170]

6.3. Biological studies (complexes 19-33)

6.3.1. MTT assay

In order to find the half maximal inhibitory concentration (IC_{50}) of each potential complex with normal human cell lines (CRL-2115, CRL-2120) and human cancer cell lines

(MCF-7, B16F10 and A549) were cultured according to the supplier's recommendations. To study the cytotoxicity of the ligands, after 80 % confluence, cells were trypsinized with 0.1 % trypsin-EDTA and harvested by centrifugation at 500 x g. Serial dilutions of cells were made from 1 x 10^6 to 1 x 10^3 cells per ml. The cells were seeded in triplicate in a 96 well plate. The suspended cells were treated for 24 h with 10 nM, 50 nM, 100 nM, 300 nM, 500 nM, 1 µM and 2 µM of each complex. Normal as well as cancer cells to which no ligand added, served as control. After incubation, MTT (100 µl, 5 mg/ml) solution was added to each well and the cell viability was determined by measuring the ability of cells to transform MTT to a purple coloured formazan dye. The absorbance of samples at 570 nm was measured using a UV-Vis spectrophotometer. Percentage of viable cells was calculated using the formula given below. Where the OD_{570} (sample) corresponds to absorbance obtained from the wells treated with ligands and the OD_{570} (control) represents the absorbance from the wells in which no ligand was added.

$$\text{Percentage of cell viability} = \frac{OD_{570}\ \text{sample}}{OD_{570}\ \text{control}} \times 100$$

The melting experiments were carried out using UV-Vis spectrophotometer (Lambda 35, ABI, USA) with a water bath attached to control the temperature. CT-DNA and each complex concentration were maintained at 25 µM in the cuvette. The variation of the CT-DNA absorbance at 260 nm was recorded plotted verses the temperature.

6.3.2. Cell viability assays

Normal and cancer cell lines were seeded at 20000-40000 cells/cm^2 with 0.2 ml/cm^2 media and incubated for 48 h at 37 ºC, 6 % CO2, 95 % relative humidity. All cells were treated with complexes at 300 nM concentrations. After 24 h of incubation, cells were washed with 300 µl PBS or 0.02 % EDTA, trypsinized, followed by harvesting at 37 ºC. A 200 µl cell suspension was transferred into a 1.5 ml micro-centrifuge tube. To the cell suspension, 300 µl PBS followed by 500 µl of 0.4 % trypan blue solutions were added. To get

a homogenized solution, the micro-centrifuge tube was gently tapped for 5 min, 20 µl of cell suspension was loaded into a chamber of the hemocytometer for measurements.

6.3.3. Flow cytometry and confocal microscopy studies

Since MTT and cell culture assays yielded encouraging results with B16F10 cells, hence they were considered for confocal and flow cytometry experiments. Cell cycle assay was performed by following the protocol reported by Angelis *et al.*.[171] After 70 % confluence, the cells were treated with 300 nM concentration of each complexes, for 3 h (1 x 10^6) cells were washed with 2x binding buffer and re-suspended in 100 µl binding buffer and Annexin-V-FITC from Abcam (USA) (1.0 µg). The cells were then incubated at room temperature for 10 min, followed by the addition of 400 µl of binding buffer containing 1 µl of propidium iodide (PI) from Sigma-Aldrich. Stained cells were analysed using FACS Calibur Flow Cytometer from B.D. Biosceinces (USA). Annexin-V-FITC and PI labeled cells were excited using a 488 nm solid-state laser and fluorescence emission intensity of FITC and PI was captured using 530/30 and 585/42 band pass filters, respectively.

For confocal microscopic studies, B16F10 cells were rinsed with 1X PBS and incubated with 2.5 % formaldehyde in PBS for 10 min at room temperature, followed by permeabilization with 0.5 % Triton X-100 for 5 min. The fixed cells were incubated with 10 % FCS in PBS for 1 h at room temperature. The culture plate was then washed with 1X PBS and placed in mounting medium (Vectashield), containing anti-fade reagent with 300 nM DAPI and incubated for 1-5 min. The cells were rinsed with PBS several times and observed using a fluorescent microscope.

6.3.4. DNA fragmentation assays

B16F10 cells were seeded (1 x 10^6) in six-well plates. After 24 h of incubation, cells were treated with 300 nM of complexes **19**, **22** and **25** (at half maximal inhibitory concentration). After 24 h of treatment, cells were collected and centrifuged at 2500 rpm for 5 min at 4 ºC. Pellet was collected and washed with phosphate buffered saline (PBS). Then 100 µl of lysis buffer was added and centrifuged at 3000 rpm for 5 min at 4 ºC and the supernatant was collected. To the mixture, 10 µl of 10 % SDS and 10 µl of (50 mg/ml) RNaseA were added and incubated for 2 h at 56 ºC. After incubation, Proteinase K (25 mg/ml) was added and the cells were incubated at 37 ºC for an additional 2 h. Further 65 µl

of 10 M ammonium acetate and 500 µl of ice cold ethanol was added and mixed well. Then these samples were incubated at 80 ºC for 1 h. The incubated samples were centrifuged at 12000 rpm for 20 min at 4 ºC, washed with 80 % ethanol and air dried for 10 min at room temperature. The pellets were dissolved in 50 µl of TE buffer and electrophoresis was carried out using 2 % agarose gel in a TE buffer.

6.3.5. DNA-complex interaction studies

UV-Visible titrations were performed using a Lambda 35 spectrophotometer (ABI, USA). The stock solutions of CT-DNA (obtained from Sigma-Aldrich, USA) and of the complexes were prepared in the BPES buffer. Equal aliquots of CT-DNA (50 µM) solution were added to 25 µM solution of the complex in a quartz cuvette. Absorbance spectra were collected from 200 nm to 400 nm after each addition of CT-DNA into the **19**, **22** and **25** solutions of the complexes. Titration was performed until the absorption bands of the complex remained intact. Each titration was repeated twice to minimize errors.

CD analyses were performed using a JASCO 815 CD Spectrometer (Jasco, Tokyo, Japan) equipped with a 1 cm path length quartz cuvette. All CD measurements and titrations were performed at 25 ºC in 100 mM KBPES buffer (pH 7.0) with spectra collected over a wavelength range of 200-400 nm. The CT-DNA concentration was maintained at 50 µM and titrated by adding fixed aliquots of the complexes **1**, **4** and **7** (100 µM stock solutions) to the CT-DNA solution. CD spectra were collected at stoichiometry values (DNA: complex) 1:0, 1:1 and 1:2 for each complex.

6.3.6. Statistical analyses

The results obtained from cell viability and MTT assays were subjected to a statistical analysis. The SPSS statistic software (Version 18.0, Chicago, IL) was used for all statistical analyses. The statistical parameters like mean value and standard deviation were calculated using descriptive statistics. Data were considered significant with p value ≤ 0.05.

6.4. Biological studies (complexes 8, 17, 37-40)

6.4.1. Cell culture

Lung A549 and cervix (HeLa) cancer cells were obtained from the American Tissue Type Culture Collection (Manassas, VA, USA). A2780 ovarian cancer cells were obtained from the ECACC (Salisbury, UK). Human Me300 melanoma cells were kindly provided by D. Rimoldi, Ludwig Institute of Cancer Research, Lausanne. A549 and HeLa cervix cells were routinely grown in Dulbecco's modified Eagle's medium containing 4.5 g/L glucose, while A2780 and Me300 cells were grown in RPMI 1640 medium. All were supplemented with 10 % heat-inactivated fetal calf serum and with antibiotics (all from Gibco, Basel, Switzerland). The organometallic complexes were dissolved in dimethyl sulfoxide and then diluted in complete medium to the required concentration. The dimethyl sulfoxide concentration did not exceed 1 % v/v and this concentration did not show any effects on cells.

6.4.2. Determination of cytotoxicity

Cells in 96-well plates (Costar) were exposed at 37 °C to increasing concentrations of complexes in complete culture medium for 72 h. Cell survival was measured using the MTT test. MTT (Merck) was added at 250 µg/ml and incubation was continued for 2 h, as previously described.[12b] Then the cell culture supernatants were removed, the cell layer was dissolved in isopropanol/0.04 N HCl, and the absorbance at 540 nm was measured in a 96-well multiwell-plate reader (iEMS Reader MF, Labsystems, Bioconcept, Switzerland) and compared with the values of control cells incubated without complexes. Experiments were conducted in triplicate wells and repeated three times.

6.4.3. Determination of phototoxicity

Cells were grown in 96-well cell culture plates (Costar) until 20 % confluence. The culture medium was replaced with complete medium containing ruthenium complexes **17**, **37-40** at 5 µM concentration (1 mM stock solution in DMSO), and the cells were exposed to the complexes for 24 h. Thereafter, Culture medium was replaced by fresh medium free of photosensitizer and the cells were irradiated at 652 nm using a diode laser (Ceralas PDT 652, Bonn, Germany) coupled to a frontal diffuser (Type FD1, Medlight SA, Ecublens, Switzerland), at an irradiance of 30 mW/cm^2 and light doses ranging from 2 to 20 J/cm^2 as

previously described.[12b] Experiments were conducted in triplicate. Analysis of cell viability using the MTT assay as described above was performed 24 h after irradiation and the obtained values were compared with the values of control cells irradiated without the complexes.

6.5. Sawhorse-type complexes containing μ^2-η^2 carboxylato ligands derived from saturated fatty acids and fluorinated fatty acid (Chapter-2)

*6.5.1. General method for the preparation of complexes **1-7, 10** and **11***

A solution of $Ru_3(CO)_{12}$ (100 mg, 0.16 mmol) and the appropriate carboxylic acid (0.47 mmol) in dry tetrahydrofuran (25 ml) was heated at 120 °C in a pressure Schlenk tube for 22 hours. Then the appropriate axial ligand L (0.47 mmol) was added (L = pyridine **1a-7a**, L = triphenylphosphine **1b-7b, 10** and **11**). The solution was stirred at room temperature for 3 hours, evaporated and the product isolated from the residue by crystallization from a tetrahydrofuran/hexane or dichloromethane/pentane mixture. In order to improve the purity, the raw product was subjected to thin-layer chromatography on silica gel using dichloromethane/pentane as eluents and obtained as yellow products.

$Ru_2(CO)_4\{\mu_2$-η^2-$O_2C(CH_2)_5CH_3\}_2(C_5H_5N)_2$ (**1a**)

Yield: 50 mg (44 %). ^{1}H NMR (400 MHz, $CDCl_3$): δ = 0.85 (t, 6 H, ^3J = 6.8 Hz, CH_3), 1.22-1.24 (m, 12 H, CH_2), 1.48-1.53 (m, 4 H, CH_2), 2.27 (t, 4 H, ^3J = 7.3 Hz, CH_2COO), 7.44-7.48 (m, 4 H, C_5H_5N), 7.81-7.85 (tt, 2 H, C_5H_5N, ^3J = 7.6 Hz, ^4J = 1.6 Hz), 8.73-8.75 (m, 4 H, C_5H_5N). IR (KBr): $\nu_{(OCO)}$ 1568 s, $\nu_{(CO)}$ 1945 vs, 1966 m, 2021 vs cm^{-1}. ESI-MS: *m/z* = 704.3 $[M - CO]^+$. Anal. Calc. for $C_{28}H_{36}N_2O_8Ru_2$: C 46.02, H 4.97. Found C 45.95, H 4.87 %.

$Ru_2(CO)_4\{\mu_2$-η^2-$O_2C(CH_2)_5CH_3\}_2(PPh_3)_2$ (**1b**)

Yield: 161 mg (94 %). ^{1}H NMR (400 MHz, $CDCl_3$): δ = 0.84 (t, 6 H, ^3J = 7.2 Hz, CH_3), 0.91-1.40 (m, 16 H, CH_2), 1.94 (t, 4 H, ^3J = 7.3 Hz, CH_2COO), 7.39-7.55 (m, 30 H, CH_{ph}). $^{31}P\{^1H\}$ NMR (161 MHz, ($CDCl_3$): δ = 14.21 ppm. IR (KBr): $\nu_{(OCO)}$ 1565 s $\nu_{(CO)}$ 1951 vs, 1977 m, 2024 vs cm^{-1}. ESI-MS: *m/z* = 1015.72 $[M - 3CO]^+$. Anal. Calc. for $C_{54}H_{56}O_8P_2Ru_2$: C 59.12, H 5.14. Found C 59.02, H 4.97 %.

$Ru_2(CO)_4\{\mu_2\text{-}\eta^2\text{-}O_2C(CH_2)_7CH_3\}_2(C_5H_5N)_2$ (**2a**)

Yield: 80 mg (65 %). ^{1}H NMR (400 MHz, $CDCl_3$): δ = 0.87 (t, 6 H, ^3J = 6.9 Hz, CH_3), 1.22-1.28 (m, 20 H, CH_2), 1.48-1.53 (m, 4 H, CH_2), 2.27 (t, 4 H, ^3J = 7.3 Hz, CH_2COO), 7.40-7.43 (m, 4 H, C_5H_5N), 7.81-7.85 (tt, 2 H, ^3J = 7.6 Hz, ^4J = 1.6 Hz, C_5H_5N), 8.73-8.75 (m, 4 H, C_5H_5N). IR (KBr): $\nu_{(OCO)}$ 1567 s, $\nu_{(CO)}$ 1945 vs, 1968 m, 2021 vs cm^{-1}. ESI-MS: *m/z* = 758.76 $[M\text{-}CO+H]^+$. Anal. Calc. for $C_{32}H_{44}N_2O_8Ru_2$: C 48.89, H 5.64, N 3.56. Found C 48.76, H 5.60, N 3.50 %.

$Ru_2(CO)_4\{\mu_2\text{-}\eta^2\text{-}O_2C(CH_2)_7CH_3\}_2(PPh_3)_2$ (**2b**)

Yield: 50 mg (27 %). ^{1}H NMR (400 MHz, $CDCl_3$): δ = 0.87 (t, 6 H, ^3J = 7.1 Hz, CH_3), 0.90-1.44 (m, 24 H, CH_2), 1.94 (t, 4 H, CH_2COO, ^3J = 7.3 Hz), 7.39-7.55 (m, 30 H, CH_{ph}). $^{31}P\{^1H\}$ NMR (161 MHz, $CDCl_3$): δ = 14.22 ppm. IR (KBr): $\nu_{(OCO)}$ 1559 s, $\nu_{(CO)}$ 1942 vs, 1974 m, 2019 vs, cm^{-1}. ESI-MS: *m/z* = 1070.23 $[M\text{-}3CO]^+$. Anal. Calc. for $C_{58}H_{64}O_8P_2Ru_2$: C 60.55, H 5.66. Found C 60.41, H 5.59 %.

$Ru_2(CO)_4\{\mu_2\text{-}\eta^2\text{-}O_2C(CH_2)_8CH_3\}_2(C_5H_5N)_2$ (**3a**)

Yield: 80 mg (32 %). ^{1}H NMR (400 MHz, $CDCl_3$): δ = 0.88 (t, 6 H, CH_3, ^{3}J = 6.9 Hz), 1.22-1.28 (m, 22 H, CH_2), 1.50-1.53 (m, 6 H, CH_2), 2.27 (t, 4 H, CH_2COO,^{3}J = 7.1Hz), 7.40-7.43 (m, 4 H, C_5H_5N), 7.81-7.85 (m, 2 H, C_5H_5N), 8.73-8.75 (m, 4 H, C_5H_5N). IR (KBr): $\nu_{(OCO)}$ 1568 s, 1945 vs, 1966 m, $\nu_{(CO)}$ 2021 vs cm^{-1}. ESI-MS: *m/z* = 759.10 $[M - 2CO]^+$. Anal. Calc. for $C_{34}H_{48}N_2O_8Ru_2$: C 50.11, H 5.94, N 3.44. Found C 49.12, H 5.82, N 3.29 %.

$Ru_2(CO)_4\{\mu_2\text{-}\eta^2\text{-}O_2C(CH_2)_8CH_3\}_2(PPh_3)_2$ (**3b**)

Yield: 127 mg (69 %). ^{1}H NMR (400 MHz, $CDCl_3$): δ = 0.88 (t, 6 H, CH_3, ^3J = 7 Hz), 1.09-1.18 (m, 16 H, CH_2), 1.23-1.35 (m, 12 H, CH_2), 1.97 (t, 4 H, CH_2COO, ^3J = 7.2 Hz), 7.26-7.55 (m, 30 H, CH_{ph}). $^{31}P\{^1H\}$ NMR (161 MHz, ($CDCl_3$): δ = 14.01 ppm. IR (KBr): $\nu_{(OCO)}$ 1557 s, $\nu_{(CO)}$ 1942 m, 1976 m, 2018 vs cm^{-1}. ESI-MS: *m/z* = 1182.25 $[M + H]^+$. Anal. Calc. for $C_{60}H_{68}O_8P_2Ru_2$: C 61.01, H 5.80. Found C 61.00, H 5.83 %.

$Ru_2(CO)_4\{\mu_2\text{-}\eta^2\text{-}O_2C(CH_2)_{11}CH_3\}_2(C_5H_5N)_2$ (**4a**)

Yield: 85 mg (55 %). ^{1}H NMR (400 MHz, $CDCl_3$): δ = 0.88 (t, 6 H, ^3J = 7.2 Hz, CH_3), 1.22-1.25 (m, 36 H, CH_2), 1.51-1.53 (m, 4 H, CH_2), 2.26 (t, 4 H, ^3J = 7.1Hz, CH_2COO), 7.40-7.43

(m, 4 H, C_5H_5N), 7.81-7.85 (m, 2 H, C_5H_5N), 8.73-8.75 (m, 4 H, C_5H_5N). IR (KBr): $\nu_{(OCO)}$ 1569 s, $\nu_{(CO)}$ 1945 m, 1968 m, 2022 vs cm^{-1}. ESI-MS: *m/z* = 843.19 $[M - 2CO]^+$. Anal. Calc. for $C_{40}H_{60}N_2O_8Ru_2$: C 53.44, H 6.72, N 3.11. Found C 53.17, H 6.53, N 2.99 %.

$Ru_2(CO)_4\{\mu_2\text{-}\eta^2\text{-}O_2C(CH_2)_{11}CH_3\}_2(PPh_3)_2$ (**4b**)

Yield: 85 mg (42 %). ^1H NMR (400 MHz, $CDCl_3$): δ = 0.90 (t, 6 H, ^3J = 6.8 Hz, CH_3), 1.01-1.15 (m, 16 H, CH_2), 1.20-1.34 (m, 24 H, CH_2), 1.94 (t, 4 H, ^3J = 7.2 Hz, CH_2COO), 7.26-7.58 (m, 30 H, CH_{ph}). $^{31}P\{^1H\}$ NMR: (161 MHz, ($CDCl_3$): δ = 14.23 ppm. IR (KBr): $\nu_{(OCO)}$ 1558 s, $\nu_{(CO)}$ 1943 m, 1974 m, 2021 vs cm^{-1}. ESI-MS: *m/z* = 1266.35 $[M + H]^+$. Anal. Calc. for $C_{66}H_{80}O_8P_2Ru_2$: C 62.64, H 6.37. Found C 62.68, H 6.45 %.

$Ru_2(CO)_4\{\mu_2\text{-}\eta^2\text{-}O_2C(CH_2)_{12}CH_3\}_2(C_5H_5N)_2$ (**5a**)

Yield: 50 mg (34 %). ^1H NMR (400 MHz, $CDCl_3$): δ = 0.88 (t, 6 H, CH_3, ^3J = 6.8 Hz), 1.22-1.32 (m, 40 H, CH_2), 1.48-1.53 (m, 4 H, CH_2), 2.28 (t, 4 H, CH_2COO, ^3J = 7.2 Hz), 7.40-7.43 (m, 4 H, C_5H_5N), 7.80-7.84 (m, 2 H, C_5H_5N), 8.73-8.75 (m, 4 H, C_5H_5N). IR (KBr): $\nu_{(OCO)}$ 1568 s, $\nu_{(CO)}$ 1944 m, 1969 m, 2022 vs cm^{-1}. ESI-MS: *m/z* = 872.22 $[M - 2CO]^+$. Anal. Calc. for $C_{42}H_{64}N_2O_8Ru_2$: C 54.41, H 6.99, N 3.02. Found C 54.03, H 6.92, N 2.91 %.

$Ru_2(CO)_4\{\mu_2\text{-}\eta^2\text{-}O_2C(CH_2)_{12}CH_3\}_2(PPh_3)_2$ (**5b**)

Yield: 60 mg (30 %). ^1H NMR (400 MHz, $CDCl_3$): δ = 0.88 (t, 6 H, ^3J = 6.8 Hz, CH_3), 1.22-1.65 (m, 44 H, CH_2), 1.91 (t, 4 H, ^3J = 7.2 Hz, CH_2COO), 7.35-7.52 (m, 30 H, CH_{ph}). $^{31}P\{^1H\}$ NMR (161 MHz, ($CDCl_3$): δ =14.21 ppm. IR (KBr): $\nu_{(OCO)}$ 1559 s, $\nu_{(CO)}$ 1952 vs, 1981 m, 2031 vs cm^{-1}. ESI-MS: *m/z* = 1266.40 $[M - CO]^+$. Anal. Calc. for $C_{68}H_{84}O_8P_2Ru_2$: C 63.14, H 6.55. Found C 63.16, H 6.53 %.

$Ru_2(CO)_4\{\mu_2\text{-}\eta^2\text{-}O_2C(CH_2)_{15}CH_3\}_2(C_5H_5N)_2$ (**6a**)

Yield: 50 mg (43 %). ^1H NMR (400 MHz, $CDCl_3$): δ = 0.88 (t, 6 H, ^3J = 6.8 Hz, CH_3), 1.22-1.29 (m, 52 H, CH_2), 1.48-1.53 (m, 4 H, CH_2), 2.26 (t, 4 H, ^3J = 7.2 Hz, CH_2COO), 7.40-7.43 (ddd, 4 H, ^3J = 7.6 Hz, ^3J = 4.9 Hz, ^4J = 1.4 Hz, C_5H_5N), 7.80-7.84 (tt, 2 H, ^3J = 7.6Hz, ^4J = 1.6 Hz, C_5H_5N), 8.73-8.75 (m, 4 H, C_5H_5N). IR (KBr): $\nu_{(OCO)}$ 1567 s, $\nu_{(CO)}$ 1946 vs, 1969 m, 2022 vs cm^{-1}. ESI-MS: *m/z* = 955.33 $[M - 2CO]^+$. Anal. Calc. for $C_{48}H_{76}N_2O_8Ru_2$: C 57.01, H 7.58, N 2.77. Found C 57.03, H 7.58, N 2.72 %.

$Ru_2(CO)_4\{\mu_2\text{-}\eta^2\text{-}O_2C(CH_2)_{15}CH_3\}_2(PPh_3)_2$ (**6b**)

Yield: 170 mg (78 %). ^{1}H NMR (400 MHz, $CDCl_3$): δ = 0.86 (t, 6 H, ^3J = 6.76 Hz, CH_3), 0.90-1.11 (m, 16 H, CH_2), 1.20-1.32 (m, 40 H, CH_2), 1.92 (t, 4 H, CH_2COO, ^3J = 7.26 Hz), 7.35-7.57 (m, 30 H, CH_{ph}). $^{31}P\{^1H\}$ NMR (161 MHz, ($CDCl_3$): δ =14.21 ppm. IR (KBr): $\nu_{(OCO)}$ 1567 s, $\nu_{(CO)}$ 1952 vs, 1978 m, 2022 vs cm^{-1}. ESI-MS: *m/z* = 1347.93 $[M - CO]^+$. Anal. Calc. for $C_{74}H_{96}O_8P_2Ru_2$: C 64.52, H 7.02. Found C 64.59, H 7.13 %.

$Ru_2(CO)_4\{\mu_2\text{-}\eta^2\text{-}O_2C(CH_2)_{16}CH_3\}_2(C_5H_5N)_2$ (**7a**)

Yield: 50 mg (30 %). ^{1}H NMR (400 MHz, $CDCl_3$): δ = 0.88 (t, 6 H, CH_3 ,^3J = 6.8 Hz), 1.22-1.26 (m, 56 H, CH_2), 1.47-1.49 (m, 4 H, CH_2), 2.26 (t, 4 H, CH_2COO, ^3J = 7.2 Hz), 7.43-7.40 (m, 4 H, C_5H_5N), 7.80-7.84 (m, 2 H, C_5H_5N), 8.73-8.75 (m, 4 H, C_5H_5N). IR (KBr): $\nu_{(OCO)}$ 1568 s, $\nu_{(CO)}$ 1945 vs, 1969 m, 2022 vs cm^{-1}. ESI-MS: *m/z* = 1012.6 $[M - CO]^+$. Anal. Calc. for $C_{50}H_{80}N_2O_8Ru_2$: C 57.78, H 7.76, N 2.70. Found C 57.89, H 7.82, N 2.58 %.

$Ru_2(CO)_4\{\mu_2\text{-}\eta^2\text{-}O_2C(CH_2)_{16}CH_3\}_2(PPh_3)_2$ (**7b**)

Yield: 113 mg (34 %). ^{1}H NMR (400 MHz, $CDCl_3$): δ = 0.88 (t, 6 H, CH_3, ^3J = 6.8 Hz), 0.90-1.13 (m, 16 H, CH_2), 1.20-1.32 (m, 44 H, CH_2), 1.92 (t, 4 H, CH_2COO, ^3J = 7.3 Hz), 7.37-7.52 (t, 18 H, CH_{ph}), 7.54-7.56 (m, 12 H, CH_{ph}). $^{31}P\{^1H\}$ NMR (161 MHz, $CDCl_3$): δ = 14.21 ppm. IR (KBr): $\nu_{(OCO)}$ 1567 s, $\nu_{(CO)}$ 1950 vs, 1982 m, 2033 vs cm^{-1}. ESI-MS: *m/z* = 1348.88 $[M\text{-}2CO]^+$. Anal. Calc. for $C_{76}H_{100}O_8P_2Ru_2$: C 65.00, H 7.27. Found C 64.94, H 7.17 %.

6.5.2. *General method for the preparation of complexes **8-9***. (Chapters 2 and 4)

A solution of $Ru_3(CO)_{12}$ and three equivalent of the appropriate fluorinated fatty acids in dry tetrahydrofuran (20 mL), was heated at 110 ˚C in a pressure Schlenk tube for 15 h. Then, addition of three equivalent of the axial ligand [(L = NC_5H_5); (L = PTA); (L = PPh_3)] under stirring at room temperature for 2 h, afforded the final products. The complexes were isolated from the residue by precipitation from dichloromethane/pentane. In order to improve the purity, the crude products were subjected to chromatography on silica gel using a dichloromethane/pentane mixture as eluent (for **8c** and **9c** a dichloromethane/ethanol mixture was used), and the solid obtained was dried under vacuum.

$Ru_2(CO)_4(\mu_2\text{-}\eta^2\text{-}O_2C(CF_2)_2CF_3)_2(NC_5H_5)_2$ (**8a**)

Yield: 200 mg (71 %). ^{1}H NMR (400 MHz, $CDCl_3$): δ = 7.46-7.50 (m, 4 H, H_{C5H5N}), 7.90 (m, 2 H, ^3J = 8 Hz, ^3J = 8 Hz, ^4J = 2 Hz, H_{C5H5N}), 8.63 (m, ^3J = 8 Hz, ^4J = 2 Hz, 4 H, H_{C5H5N}). ^{19}F{^{1}H} NMR (376 MHz, $CDCl_3$) δ = -81.7 (6 F), -118.8 (4 F), -128.1 (4 F). IR (KBr, cm^{-1}) $\nu_{(OCO)}$ 1650.9 vs, $\nu_{(CO)}$ 1967.4 vs, (ν_{CO}) 1992.7 m, (ν_{CO}) 2041.6 vs. ESI-MS (positive mode): *m/z* = 935.58 $[M + 2\ H_2O + H]^+$. Anal. Calc. for $C_{22}H_{10}F_{14}N_2O_8Ru_2 \cdot C_5H_{12}$ (970.59) C 33.41, H 2.28, N 2.89; Found: C 33.69, H 1.88, N 3.06 %.

$Ru_2(CO)_4(\mu_2\text{-}\eta^2\text{-}O_2C(CF_2)_2CF_3)_2(PPh_3)_2$ (**8b**)

Yield: 150 mg (76 %) ^{1}H NMR (400 MHz, $CDCl_3$): δ = 7.39-7.45 (m, 18 H, H_{PPh3}), 7.48-7.55 (m, 12 H, H_{PPh3}). ^{31}P{^{1}H} NMR (162 MHz, $CDCl_3$) δ = 15.23 ppm. ^{19}F{^{1}H} NMR (376 MHz, $CDCl_3$) δ = -82.0 (6 F), -118.6 (4 F), -128.3 (4 F). IR (KBr, cm^{-1}) $\nu_{(OCO)}$ 1658.9 vs, $\nu_{(CO)}$ 1966.4 vs, (ν_{CO}) 1991.1 m, (ν_{CO}) 2030.9 vs. ESI-MS (positive mode): *m/z* = 1183.96 [M - 3 CO + H]$^+$. Anal. Calc. for $C_{48}H_{30}F_{14}O_8P_2Ru_2$ (1264.81) C 45.58, H 2.39; Found: C 45.84, H 2.56 %.

$Ru_2(CO)_4(\mu_2\text{-}\eta^2\text{-}O_2C(CF_2)_2CF_3)_2(PTA)_2$ (**8c**)

Yield: 97 mg (59 %) ^{1}H NMR (400 MHz, $CDCl_3$): δ = 4.25 (br-m, 12 H, H_{PTA}), 4.62 (m, 12 H, H_{PTA}). ^{31}P{^{1}H} NMR (162 MHz, $CDCl_3$) δ = -54.68 ppm. ^{19}F{^{1}H} NMR (376 MHz, $CDCl_3$) δ = -81.7 (6 F), -118.6 (4 F), -128.4 (4 F). IR (KBr, cm^{-1}) $\nu_{(OCO)}$ 1663.0 vs, $\nu_{(CO)}$ 1967.8 vs, (ν_{CO}) 1991.6 m, (ν_{CO}) 2037.4 vs. ESI-MS (positive mode): *m/z* = 1055.90 [M + H]$^+$. Anal. Calc. for $C_{24}H_{24}F_{14}N_6O_8P_2Ru_2 \cdot C_2H_5OH \cdot CH_2Cl_2$ (1365.45) C 27.35, H 2.72, N 7.09; Found: C 27.62, H 2.66, N 6.63 %.

$Ru_2(CO)_4(\mu_2\text{-}\eta^2\text{-}O_2C(CF_2)_{10}CF_3)_2(NC_5H_5)_2$ (**9b**)

Yield: 153 mg (67 %) ^{1}H NMR (400 MHz, $CDCl_3$): δ = 7.45-7.49 (m, 4 H, H_{C5H5N}), 7.90 (m, 2 H, ^3J = 8 Hz, ^3J = 8 Hz, ^4J = 2 Hz, H_{C5H5N}), 8.62-8.64 (m, 4 H, H_{C5H5N}). ^{19}F{^{1}H} NMR (376 MHz, $CDCl_3$) δ = -81.8 (6 F), -117.8 (4 F), -122.5 (4 F), -122.9 (20 F), -123.8 (8 F), -127.2 (4 F). IR (KBr, cm^{-1}) $\nu_{(OCO)}$ 1667.4 vs, $\nu_{(CO)}$ 1964.0 vs, (ν_{CO}) 1984.2 m, (ν_{CO}) 2046.5 vs. ESI-MS (positive mode): *m/z* = 980.97 [M - $C_{12}F_{23}O_2$ - C_5H_5N - CO + H]$^+$. Anal. Calc. for $C_{38}H_{10}F_{46}N_2O_8Ru_2$ (1698.56) C 26.87, H 0.59, N 1.65; Found: C 26.58, H 0.72, N 2.04 %.

$Ru_2(CO)_4(\mu_2\text{-}\eta^2\text{-}O_2C(CF_2)_{10}CF_3)_2(PPh_3)_2$ (**9b**)

Yield: 60 mg (54 %) ^{1}H NMR (400 MHz, $CDCl_3$): δ = 7.36-7.44 (m, 18 H, H_{PPh3}), 7.46-7.50 (m, 12 H, H_{PPh3}). $^{31}P\{^1H\}$ NMR (162 MHz, $CDCl_3$) δ = 15.24 ppm. $^{19}F\{^1H\}$ NMR (376 MHz, $CDCl_3$) δ = -81.8 (6 F), -117.57 (4 F), -122.9 (24 F), -123.8 (8 F), -127.2 (4 F). IR (KBr, cm^{-1}) $\nu_{(OCO)}$ 1658.9 vs, $\nu_{(CO)}$ 1966.8 vs, (ν_{CO}) 1991.3 m, (ν_{CO}) 2031.9 vs. ESI-MS (positive mode): *m/z* = 1692.86 $[M - PPh_3 - 4\ CO + H]^+$. Anal. Calc. for $C_{64}H_{30}F_{46}O_8P_2Ru_2$ (2064.93) C 37.23, H 1.46; Found: C 37.19, H 1.55 %.

$Ru_2(CO)_4(\mu_2\text{-}\eta^2\text{-}O_2C(CF_2)_{10}CF_3)_2(PTA)_2$ (**9c**)

Yield: 56 mg (26 %) ^{1}H NMR (400 MHz, $CDCl_3$): δ = 4.25 (br-s, 12 H, H_{PTA}), 4.62 (m, 12 H, H_{PTA}). $^{31}P\{^1H\}$ NMR (162 MHz, $CDCl_3$) δ = -54.70 ppm. $^{19}F\{^1H\}$ NMR (376 MHz, $CDCl_3$) δ = -81.8 (6 F), -117.6 (4 F), -122.6 (4 F), -122.8 (16 F), -123.0 (4 F), -123.8 (4 F), -124.0 (4 F), -127.2 (4 F). IR (KBr, cm^{-1}) $\nu_{(OCO)}$ 1662.3 vs, $\nu_{(CO)}$ 1960.6 vs, (ν_{CO}) 1982.5 m, (ν_{CO}) 2038.0 vs. ESI-MS (positive mode): *m/z* = 1856.77 $[M + H]^+$. Anal. Calc. for $C_{40}H_{24}F_{46}N_6O_8P_2Ru_2 \cdot C_2H_5OH$ (1900.74) C 26.54, H 1.59, N 4.42; Found: C 26.59, H 1.57, N 4.31 %.

$Ru_2(CO)_4(\mu_2\text{-}\eta^2\text{-}O_2C(CH_2)_2CH_3)_2(PPh_3)_2$ (**10**)

Yield: 80 mg (52 %). ^{1}H NMR (400 MHz, $CDCl_3$): δ = 0.60 (t, 6 H, ^3J = 7 Hz, CH_3), 1.10-1.17 (m, 4 H, CH_2), 1.92 (t, 4 H, ^3J = 7 Hz, CH_2), 7.36-7.41 (m, 18 H, H_{PPh3}), 7.54-7.57 (m, 12 H, H_{PPh3}). $^{31}P\{^1H\}$ NMR (162 MHz, $CDCl_3$) δ = 14.11 ppm. IR (KBr, cm^{-1}) $\nu_{(OCO)}$ 1564.1 vs, $\nu_{(CO)}$ 1941.1 vs, (ν_{CO}) 1975.9 m, (ν_{CO}) 2018.4 vs. ESI-MS (positive mode): *m/z* = 987.04 $[M - CO + H]^+$. Anal. Calc. for $C_{48}H_{44}O_8P_2Ru_2$ (1012.95) C 56.91, H 4.38; Found: C 56.41, H 4.40 %.

$Ru_2(CO)_4(\mu_2\text{-}\eta^2\text{-}O_2C(CH_2)_{10}CH_3)_2(PPh_3)_2$ (**11**)

Yield: 108 mg (56 %). ^{1}H NMR (400 MHz, $CDCl_3$): δ = 0.89 (t, 6 H, ^3J= 7 Hz, CH_3), 1.00-1.11 (m, 16 H, CH_2), 1.22-1.29 (m, 20 H, CH_2), 1.92 (t, 4 H, ^3J= 7 Hz, CH_2) 7.36-7.40 (m, 18 H, H_{PPh3}), 7.54-7.55 (m, 12 H, H_{PPh3}). $^{31}P\{^1H\}$ NMR (162 MHz, $CDCl_3$) δ = 14.21 ppm. IR (KBr, cm^{-1}) $\nu_{(OCO)}$ 1567.6 vs, $\nu_{(CO)}$ 1952.4 vs, (ν_{CO}) 1981.5 m, (ν_{CO}) 2031.1 vs. ESI-MS (positive mode): *m/z* = 1238.33 $[M]^+$. Anal. Calc. for $C_{64}H_{76}O_8P_2Ru_2$ (1237.37) C 62.12, H 6.19; Found: C 62.00, H 6.12 %.

6.6. Sawhorse-type diruthenium tetracarbonyl complexes derived from pyrenyl-carboxylic acids (Chapter-3)

6.6.1. Preparation of sawhorse-type diruthenium tetracarbonyl complexes (***12*** *-* ***14***)

A solution of $Ru_3(CO)_{12}$ (100mg, 0.156 mmol) and three equivalents of the appropriate pyrene appended carboxylic acid (0.469 mmol) in dry tetrahydrofuran (20 mL), was heated at 110˚C in a pressure Schlenk tube for 15 h. Then, addition of three equivalents of the axial ligand [**12a**, **13a**, **14a** (L = NC_5H_5); **12b**, **13b**, **14b** (L = PPh_3)] under stirring at room temperature for 3 h, affords the final products. The complexes were isolated from the residue by precipitation from dichloromethane/hexane. In order to improve the purity, the crude products were subjected to chromatography on silica gel using a dichloromethane/pentane mixture (1:1) as eluent and the solid obtained thus were dried under vacuum.

$Ru_2(CO)_4(\mu_2\text{-}\eta^2\text{-}O_2CC_{16}H_9)_2(C_5H_5N)_2$ (**12a**)

Yield: 102 mg (68 %). ^{1}H NMR (400 MHz, CD_2Cl_2): δ = 7.57-7.61 (m, 4 H, H_{ar}), 7.77 (d, 2 H, ^3J = 9 Hz, H_{ar}), 7.98-8.03 (m, 6 H, H_{ar}), 8.07-8.14 (m, 6 H, H_{ar}), 8.19 (d, 2 H, ^3J = 8 Hz , H_{ar}), 8.52 (d, 2 H, ^3J = 8 Hz, H_{ar}), 8.88 (d, 2 H, ^3J = 9 Hz, H_{ar}), 9.14-9.15 (m, 4 H, H_{ar}) ppm. IR (CaF_2, thf, cm^{-1}) $\nu_{(OCO)}$ 1567.55, $\nu_{(CO)}$ 1944.03 vs, (ν_{CO}) 1974.57 m, (ν_{CO}) 2024.86 vs. UV-Vis (1.0×10^{-5} M, CH_2Cl_2): λ_{max} = 283, 355 nm. ESI-MS (positive mode): *m/z* = 935.58 [M - CO + H]$^+$. Anal. Calc. for $C_{48}H_{28}N_2O_8Ru_2$ (962.88) C 59.87, H 2.93, N 2.91; Found: C 59.77, H 3.18, N 2.80 %.

$Ru_2(CO)_4(\mu_2\text{-}\eta^2\text{-}O_2CC_{16}H_9)_2(PPh_3)_2$ (**12b**)

Yield: 170 mg (82 %). ^{1}H NMR (400 MHz, CD_2Cl_2): δ = 7.27-7.31 (m, 12 H, H_{ar}), 7.33-7.37 (m, 8 H, H_{ar}), 7.69-7.76 (m, 14 H, H_{ar}), 7.83 (d, 2 H, ^3J = 8 Hz, H_{ar}), 7.93-8.05 (m, 6 H, H_{ar}), 8.04 (d, 2 H, ^3J = 8 Hz, H_{ar}), 8.10 (d, 2 H, ^3J = 8, H_{ar}), 8.65 (d, 2 H, ^3J = 8 Hz, H_{ar}) ppm. ^{31}P{^{1}H} NMR (162 MHz, CD_2Cl_2) δ = 13.53 ppm. IR (CaF_2, thf, cm^{-1}) $\nu_{(OCO)}$ 1580.64, $\nu_{(CO)}$ 1952.68 vs, (ν_{CO}) 1980.64 m, (ν_{CO}) 2023.78 vs. UV-Vis (1.0×10^{-5} M, CH_2Cl_2): λ_{max} = 282, 352, 383 nm. ESI-MS (positive mode): *m/z* = 1330.07 [M + H]$^+$. Anal. Calc. for $C_{74}H_{48}O_8P_2Ru_2$ (1329.28) C 66.86, H 3.64; Found: C 66.82, H 3.68 %.

$Ru_2(CO)_4(\mu_2\text{-}\eta^2\text{-}O_2CCH_2C_{16}H_9)_2(C_5H_5N)_2$ (**13a**)

Yield: 98 mg (63 %). ^{1}H NMR (400 MHz, CD_2Cl_2): δ = 4.17 (s, 4 H, H_{CH2}), 6.56 (t, 4 H, ^3J = 8 Hz, H_{ar}), 7.27 (t, 2 H, ^3J = 8 Hz, H_{ar}), 7.60 (d, 2 H, ^3J = 8 Hz, H_{ar}), 7.70 (d, 2 H, ^3J = 9 Hz, H_{ar}), 7.90-7.96 (m, 4 H, H_{ar}), 8.00-8.11 (m, 12 H, H_{ar}), 8.22 (d, 2 H, ^3J = 7 Hz, H_{ar}) ppm. IR (CaF_2, thf, cm^{-1}) $\nu_{(OCO)}$ 1584.91, $\nu_{(CO)}$ 1941.33 vs, (ν_{CO}) 1972.55 m, (ν_{CO}) 2023.47 vs. UV/Vis (1.0×10^{-5} M, CH_2Cl_2): λ_{max} = 278, 330, 347 nm. ESI-MS (positive mode): *m/z* = 935.59 [M - 2 CO]$^+$. Anal. Calc. for $C_{50}H_{32}N_2O_8Ru_2$ (990.94) C 60.60, H 3.25, N 2.83; Found: C 60.33, H 3.48, N 2.88 %.

$Ru_2(CO)_4(\mu_2\text{-}\eta^2\text{-}O_2CCH_2C_{16}H_9)_2(PPh_3)_2$ (**13b**)

Yield: 150 mg (71 %). ^{1}HNMR (400 MHz, CD_2Cl_2): δ = 3.68 (s, 4 H, H_{CH2}), 7.06-7.10 (m, 12 H, H_{ar}), 7.20-7.27 (m, 20 H, H_{ar}), 7.60 (d, 2 H, ^3J = 9 Hz, H_{ar}), 7.76-7.80 (m, 4 H, H_{ar}), 7.97-8.08 (m, 6 H, H_{ar}), 8.15 (d, 2 H, ^3J = 7.4 Hz, H_{ar}), 8.21 (m, 2 H, H_{ar}) ppm. ^{31}P{^{1}H} NMR (162 MHz, CD_2Cl_2) δ = 15.18 ppm. IR (CaF_2, thf, cm^{-1}) $\nu_{(OCO)}$ 1579.49, $\nu_{(CO)}$ 1952.58 vs, (ν_{CO}) 1979.58 m, (ν_{CO}) 2023.47 vs. UV-Vis (1.0×10^{-5} M, CH_2Cl_2): λ_{max} = 278, 329, 346, 382 nm. ESI-MS (positive mode): *m/z* = 1358.13 [M + H]$^+$. Anal. Calc. for $C_{76}H_{52}O_8P_2Ru_2 \cdot 1.5C_5H_{12}$ (1465.53) C 68.43, H 4.81; Found: C 68.85, H 4.42 %.

$Ru_2(CO)_4\{\mu_2\text{-}\eta^2\text{-}O_2C(CH_2)_3C_{16}H_9\}_2(C_5H_5N)_2$ (**14a**)

Yield: 110 mg (67 %). ^{1}H NMR (400 MHz, CD_2Cl_2): δ = 2.03-2.09 (p, 4 H, ^3J = 7 Hz, H_{ar}), 2.47 (t, 4 H, ^3J = 7 Hz, H_{CH2}), 3.19 (t, 4 H, ^3J = 8 Hz, H_{ar}), 7.36-7.39 (m, 4 H, H_{ar}), 7.60 (d, 2 H, ^3J = 8 Hz, H_{ar}), 7.79-7.82 (m, 4 H, H_{ar}), 7.88-7.99 (m, 8 H, H_{ar}), 8.03-8.06 (m, 4 H, H_{ar}), 8.13 (d, 2 H, ^3J = 8 Hz, H_{ar}), 8.83-8.85 (m, 4 H, H_{ar}) ppm. IR (CaF_2, thf, cm^{-1}) $\nu_{(OCO)}$ 1576.28, $\nu_{(CO)}$ 1941.01 vs, (ν_{CO}) 1972.01 m, (ν_{CO}) 2023.21 vs. UV-Vis (1.0×10^{-5} M, CH_2Cl_2): λ_{max} = 278, 329, 345 nm. ESI-MS (positive mode): *m/z* = 1048.09 [M + H]$^+$. Anal. Calc. for $C_{54}H_{40}N_2O_8Ru_2$ (1047.04) C 61.94, H 3.85, N 2.68; Found: C 62.04, H 4.13, N 2.53 %.

$Ru_2(CO)_4\{\mu_2\text{-}\eta^2\text{-}O_2C(CH_2)_3C_{16}H_9\}_2(PPh_3)_2$ (**14b**)

Yield: 139 mg (63 %).NMR (400 MHz, $CDCl_3$): δ = 1.68 (p, 4 H, ^3J = 8 Hz, CH_2), 2.14 (t, 4 H, ^3J = 7, H_{CH2}), 2.93 (t, 4 H, ^3J = 8, H_{CH2}), 7.24-7.27 (m, 18 H, H_{ar}), 7.48 (d, 2 H, ^3J = 8, H_{ar}), 7.51-7.56 (m, 12 H, H_{ar}), 7.84 (d, 2 H, ^3J = 8, H_{ar}), 7.89 (d, 2 H, ^3J = 8, H_{ar}), 7.98-8.03 (m, 8 H, H_{ar}), 8.08 (d, 2 H, ^3J = 7, 2 H, H_{ar}), 8.15 (m, 2 H, H_{ar}) ppm. ^{31}P{^{1}H} NMR (162

MHz, CD_2Cl_2) δ = 14.09 ppm. IR (CaF_2, thf, cm^{-1}) $\nu_{(OCO)}$ 1567.46, $\nu_{(CO)}$1951.78 vs, (ν_{CO}) 1978.90 m, (ν_{CO}) 2022.89 vs. UV-Vis (1.0×10^{-5} M, CH_2Cl_2): λ_{max} = 277, 329, 345, 383 nm. ESI-MS (positive mode): *m/z* = 1414.19 $[M]^+$. Anal. Calc. for $C_{80}H_{60}O_8P_2Ru_2$ (1413.44) C 67.98, H 4.28; Found: C 67.95, H 4.34 %.

6.7. **Porphyrin derived sawhorse-type diruthenium tetracarbonyl complexes** (chapter-3)

6.7.1. Preparation of sawhorse-type diruthenium tetracarbonyl complexes (***15*** **-** ***18***)

$Ru_2(CO)_4(\mu_2\text{-}\eta^2\text{-}O_2CC_{44}H_{29}N_4)_2(PPh_3)_2$ (**15**)

A solution of $Ru_3(CO)_{12}$ (16 mg, 0.026 mmol) and 5-(4-carboxyphenyl)-10,15,20-triphenyl-21,23H-porphyrin (60 mg, 0.091 mmol) in dry thf (30 mL) were heated at 120 °C in a high pressure Schlenk tube for 18 h. After cooling to room temperature, PPh_3 (20 mg, 0.078 mmol) was added. The solution was stirred for 2 h and the product was isolated by precipitation from a dichloromethane/pentane mixture and dried under vacuum. The product was obtained as air-stable purple crystalline powder.

Yield: 98 mg (59 %). ^{1}H NMR (400 MHz, $CDCl_3$) δ = -2.75 (s, 4 H, NH), 7.46-7.55 (m, 18 H, H_{PPh3}), 7.60 (d, 4 H, ^3J = 8 Hz, C_6H_4COO), 7.77-7.84 (m, 18 H, H_{porph}), 7.86-7.90 (m, 12 H, H_{PPh3}), 8.01 (d, 4 H, ^3J = 8 Hz, C_6H_4COO), 8.24-8.26 (m, 12 H, H_{porph}), 8.86-8.91 (m, 16 H, H_{porph}) ppm. $^{31}P\{^1H\}$ NMR (162 MHz, $CDCl_3$) δ = 15.99 ppm. IR (KBr, cm^{-1}) $\nu_{(NCN)}$ 1587.90, $\nu_{(OCO)}$ 1545.04 s, $\nu_{(CO)}$ 1952.73 vs, 1980.21 m, 2024.90 vs. Anal. Calc. for $C_{130}H_{88}N_4O_8P_2Ru_2 \cdot 5\ H_2O$ (2244.33): C 69.57, H 4.40, N 4.99; found: C 69.24, H 4.55, N 4.87. ESI-MS (positive mode): *m/z* = 2154.45 $[M + H]^+$.

$\{Ru_2(CO)_4(PPh_3)_2\}_2(\mu_2\text{-}\eta^2\text{-}O_2CC_{44}H_{28}N_4CO_2\text{-}\eta^2\text{-}\mu_2)_2$ (**16**)

The same procedure was used for the preparation of **16** using $Ru_3(CO)_{12}$ (50 mg, 0.08 mmol), 5,10-di-(4-carboxyphenyl)-15,20-diphenyl-21,23*H*-porphyrin (95 mg, 0.14 mmol) and PPh_3 (13 mg, 0.23 mmol). In order to improve the purity, the raw product was subjected to chromatography on silica gel using a dichloromethane/pentane mixture as eluent and air-stable purple crystalline powder was obtained.

Yield: 120 mg (50 %). ^{1}H NMR (400 MHz, $CDCl_3$) δ = -2.80 (s, 4 H, NH), 7.42-7.51 (m, 36 H, H_{PPh3}), 7.62 (d, 8 H, ^{3}J = 7 Hz, C_6H_4COO), 7.77 (m, 12 H, H_{porph}), 7.82-7.85 (m, 24 H, H_{PPh3}), 7.97 (d, 8 H, ^{3}J = 7 Hz, C_6H_4COO), 8.22 (d, 8 H, ^{3}J = 7 Hz, H_{porph}), 8.80-8.89 (m, 16 H, H_{porph}) ppm. $^{31}P\{^{1}H\}$ NMR (162 MHz, $CDCl_3$) δ = 17.42 ppm. IR (KBr, cm^{-1}) $\nu_{(NCN)}$ 1588.01, $\nu_{(OCO)}$ 1545.93 s, $\nu_{(CO)}$ 1950.99 vs, 1983.21 m, 2024.56 vs. Anal. Calc. for $C_{172}H_{120}N_8O_{16}P_4Ru_4$ (3078.98): C 67.01, H 3.92, N 3.63; found: C 67.18, H 4.22, N 3.48. ESI-MS (positive mode): *m*/*z* = 1278.61 $[M/2 - PPh_3 + 2\ H]^{2+}$.

$Ru_2(CO)_4(\mu_2\text{-}\eta^2\text{-}O_2CC_{44}H_{27}N_4Zn)_2(PPh_3)_2$ (**17**)

The same procedure was used for the preparation of **17** using $Ru_3(CO)_{12}$ (19 mg, 0.03 mmol), 5-(4-carboxyphenyl)-10,15,20-triphenylporphyrin-Zn (65 mg, 0.09 mmol) and PPh_3 (24 mg, 0.09 mmol). The product was isolated by precipitation from a dichloro-methane/pentane mixture and dried under vacuum. The product was obtained as air-stable purple crystalline powder.

Yield: 38 mg (56 %). ^{1}H NMR (400 MHz, $CDCl_3$) δ = 7.43-7.52 (m, 18 H, H_{PPh3}), 7.56 (d, 4 H, ^{3}J = 8 Hz, C_6H_4COO), 7.77-7.84 (m, 18 H, H_{porph}), 7.86-7.90 (m, 12 H, H_{PPh3}), 8.00 (d, 4 H, ^{3}J = 8 Hz, C_6H_4COO), 8.24 (d, 12 H, ^{3}J = 7 Hz, H_{porph}), 8.93-8.98 (m, 16 H, H_{porph}) ppm. $^{31}P\{^{1}H\}$ NMR (162 MHz, $CDCl_3$) δ = 17.87 ppm. IR (KBr, cm^{-1}) $\nu_{(OCO)}$ 1613.98 s, $\nu_{(CO)}$ 1950.00 vs, 1974.82 m, 2022.72 vs. Anal. Calc. for $C_{135}H_{94}N_8O_8P_2Ru_2Zn_2 \cdot 5\ CH_2Cl_2$ (2705.66): C 59.93, H 3.50, N 4.14; found: C 59.60, H 3.60, N 4.08. ESI-MS (positive mode): *m*/*z* = 1555.14 $[M - porph + H]^{+}$.

$\{Ru_2(CO)_4(PPh_3)_2\}_2(\ \mu_2\text{-}\eta^2\text{-}O_2CC_{44}H_{26}N_4ZnCO_2\text{-}\eta^2\text{-}\mu_2)_2$ (**18**)

The same procedure was used for the preparation of **18** using $Ru_3(CO)_{12}$ (25 mg, 0.04 mmol), 5,10-di(4-carboxyphenyl)-15,20-diphenyl-porphyrin-Zn (45 mg, 0.06 mmol) and PPh_3 (30 mg, 0.12 mmol). In order to improve the purity, the raw product was subjected to chromatography on silica gel using dichloromethane/pentane mixture as eluent and air-stable purple crystalline powder was obtained.

Yield: 35 mg (28 %). ^{1}H NMR (400 MHz, $CDCl_3$) δ = 7.41-7.51 (m, 36 H, H_{PPh3}), 7.62 (d, 8 H, ^{3}J = 8 Hz, C_6H_4COO), 7.77 (m, 12 H, H_{porph}), 7.82-7.87 (m, 24 H, H_{PPh3}), 7.98 (d, 8 H, ^{3}J = 8 Hz, C_6H_4COO), 8.22 (d, 8 H, ^{3}J = 7 Hz, H_{porph}), 8.90-8.99 (m, 16 H, H_{porph}) ppm. $^{31}P\{^{1}H\}$

NMR (162 MHz, $CDCl_3$) δ = 17.50 ppm. IR (KBr, cm^{-1}) $\nu_{(NCN)}$ 1587.01, $\nu_{(OCO)}$ 1545.54 s, $\nu_{(CO)}$ 1950.69 vs, 1983.10 m, 2025.00 vs. Anal. Calc. for $C_{172}H_{120}N_8O_{18}P_4Ru_4Zn_2 \cdot 2\ CH_2Cl_2 \cdot 2\ H_2O$ (3411.64) C 61.26, H 3.55, N 3.28; found: C 61.01, H 3.83, N, 3.28. ESI-MS (positive mode): *m*/*z* = 1389.32 $[M/2 - PPh_3 + 2\ Na + 2\ H]^{2+}$.

6.8. Cytotoxic chalcogenolato-bridged dinuclear (Ru, Rh, Ir) half-sandwich complexes (chapter-4)

6.8.1. *Preparation of chalcogenolato-bridged dinuclear complexes (19-27)*

Synthesis of $[(\eta^6\text{-}p\text{-}MeC_6H_4Pr^i)_2Ru_2(\mu\text{-}SC_6H_5)_3]Cl$ (**19**), $[(\eta^6\text{-}p\text{-}MeC_6H_4Pr^i)_2Ru_2(\mu\text{-}SeC_6H_5)_3]Cl$ (**20**), $[(\eta^5\text{-}C_5Me_5)_2Rh_2(\mu\text{-}SC_6H_5)_3]Cl$ (**22**), $[(\eta^5\text{-}C_5Me_5)_2Rh_2(\mu\text{-}SeC_6H_5)_3]Cl$ (**23**), $[(\eta^5\text{-}C_5Me_5)_2Ir_2(\mu\text{-}SC_6H_5)_3]Cl$ (**25**) and $[(\eta^5\text{-}C_5Me_5)_2Ir_2(\mu\text{-}SeC_6H_5)_3]Cl$ (**26**).

The dinuclear dichloro complexes $(\eta^6\text{-}p\text{-}MeC_6H_4Pr^i)_2Ru_2(\mu\text{-}Cl)_2Cl_2$ (0.16 mmol, 100 mg for **19** and **20**), $(\eta^5\text{-}C_5Me_5)_2Rh_2(\mu\text{-}Cl)_2Cl_2$ (0.16 mmol, 100 mg for **22** and **23**) or $(\eta^5\text{-}C_5Me_5)_2Ir_2(\mu\text{-}Cl)_2Cl_2$ (0.13 mmol, 100 mg for **25** and **26**) were dissolved in technical-grade ethanol (20 mL). An ethanolic solution (2.5 mL) of benzenethiol (0.50 mmol, 50 µl for **19**; 0.48 mmol, 49 µl for **22**; 0.38 mmol, 38 µl for **25**) or an ethanolic solution (2.5 mL) of benzeneselenol (0.49 mmol, 52 µl for **20**; 0.48 mmol, 52 µl for **23**; 0.38 mmol, 40 µl for **26**) were added drop wise to the reaction mixture. Then the reaction was carried out at reflux for 15 h. Then, ethanol was evaporated and the final dinuclear complexes (**19**, **20**, **22**, **23**, **25** and **26**) were isolated from the residue by precipitation from a dichloromethane/diethyl ether mixture. In order to improve the purity, the crude products were subjected to column chromatography on silica gel using a 95:5 dichloromethane:ethanol mixture as eluent. The second fraction was collected, evaporated and the solid dried under vacuum.

Synthesis of $[(\eta^6\text{-}p\text{-}MeC_6H_4Pr^i)_2Ru_2(\mu\text{-}TeC_6H_5)_3]PF_6$ (**21**), $[(\eta^5\text{-}C_5Me_5)_2Rh_2(\mu\text{-}TeC_6H_5)_3]PF_6$ (**24**) and $[(\eta^5\text{-}C_5Me_5)_2Ir_2(\mu\text{-}TeC_6H_5)_3]PF_6$ (**27**).

The dinuclear dichloro complexes $(\eta^6\text{-}p\text{-}MeC_6H_4Pr^i)_2Ru_2(\mu\text{-}Cl)_2Cl_2$ (0.13 mmol, 79 mg for **21**), $(\eta^5\text{-}C_5Me_5)_2Rh_2(\mu\text{-}Cl)_2Cl_2$ (0.16 mmol, 100 mg for **24**) or $(\eta^5\text{-}C_5Me_5)_2Ir_2(\mu\text{-}Cl)_2Cl_2$ (0.07 mmol, 58 mg for **27**) were dissolved in technical-grade ethanol (25 ml) and added to an ethanolic solution of sodium tellurophenolate, which was prepared by the

treatment of diphenyl ditelluride (0.32 mmol, 132 mg for **21**; 0.48 mmol, 197 mg for **24**; 0.22 mmol, 89 mg for **27**) with sodium borohydride (0.37 mmol, 14 mg for **21**; 0.48 mmol, 18 mg for **24**; 0.22 mmol, 8 mg for **27**).[127] After being stirred for 15 h at room temperature, 1 eq. of potassium hexafluorophosphate was added to the reaction mixture and then the solution was stirred for another 2 h. The reaction mixture was filtered off to remove impurities and then evaporated. The products were isolated from the residue by precipitation from a dichloromethane/diethylether mixture. To improve the purity, the raw products were subjected to chromatography on silica gel using a 9:1 dichloromethane:ethanol mixture. The second fraction was collected, evaporated and the solid dried under vacuum.

$[(\eta^6\text{-}p\text{-}MeC_6H_4Pr^i)_2Ru_2(\mu\text{-}SC_6H_5)_3]Cl$ (**19**)

Yield: 155 mg (93 %). ^{1}H NMR (400 MHz, $CDCl_3$): δ = 0.77 (d, 6 H, ^3J = 7 Hz, $H_{CH(C\mathbf{H}3)2}$), 0.88 (d, 6 H, ^3J = 7 Hz, $H_{CH(C\mathbf{H}3)2}$), 1.61 (s, 6 H, H_{CH3}), 1.92 (m, 2 H, $H_{C\mathbf{H}(CH3)2}$), 5.10 (d, 2 H, ^3J = 6 Hz, $H_{p\text{-cymene}}$), 5.13 (d, 2 H, ^3J = 6 Hz, $H_{p\text{-cymene}}$), 5.23 (d, 2 H, ^3J = 6 Hz, $H_{p\text{-cymene}}$), 5.52 (m, 2 H, $H_{p\text{-cymene}}$), 7.36-7.41 (m, 9 H, H_{ar}), 7.89 (d, 6 H, ^3J = 7 Hz, H_{ar}) ppm. ^{13}C{^{1}H} NMR (100 MHz, $CDCl_3$): δ = 17.71 (C_{CH3}), 21.95 ($C_{CH(CH3)2}$), 22.53 ($C_{CH(CH3)2}$), 30.58 ($C_{CH(CH3)2}$), 83.65 (Ru-C_{ar}), 84.76 (Ru-C_{ar}), 85.03 (Ru-C_{ar}), 85.37 (Ru-C_{ar}), 99.97 (Ru-C_{ar}), 107.39 (Ru-C_{ar}), 128.45 (C_{ar}), 129.19 (C_{ar}), 132.57 (C_{ar}), 137.81 (C_{ar}) ppm. MS (positive mode): *m/z* = 799.1 $[M - Cl]^+$. Anal. Calc. for $C_{38}H_{43}ClRu_2S_3$ (833.54): C 54.76, H 5.20; Found: C 54.69, H 5.32%. These data are in agreement with those reported by Mashima for $[(\eta^6\text{-}p\text{-}MeC_6H_4Pr^i)_2Ru_2(\mu\text{-}SC_6H_5)_3]PF_6$.[40]

$[(\eta^6\text{-}p\text{-}MeC_6H_4Pr^i)_2Ru_2(\mu\text{-}SeC_6H_5)_3]Cl$ (**20**)

Yield: 105 mg (66 %). ^{1}H NMR (400 MHz, $CDCl_3$): δ = 0.74 (d, 6 H, ^3J = 7 Hz, $H_{CH(C\mathbf{H}3)2}$), 0.87 (d, 6 H, ^3J = 7 Hz, $H_{CH(C\mathbf{H}3)2}$), 1.72 (s, 6 H, H_{CH3}), 2.08 (m, 2 H, $H_{C\mathbf{H}(CH3)2}$), 5.19 (d, 2 H, ^3J = 6 Hz, $H_{p\text{-cymene}}$), 5.25 (d, 2 H, ^3J = 6 Hz, $H_{p\text{-cymene}}$), 5.31 (d, 2 H, ^3J = 6 Hz, $H_{p\text{-cymene}}$), 5.51 (d, 2 H, ^3J = 6 Hz, $H_{p\text{-cymene}}$), 7.31-7.36 (m, 9 H, H_{ar}), 7.75-7.79 (m, 6 H, H_{ar}) ppm. ^{13}C{^{1}H} NMR (100 MHz, $CDCl_3$): δ = 18.21 (C_{CH3}), 21.83 ($C_{CH(CH3)2}$), 22.84 ($C_{CH(CH3)2}$), 30.90 ($C_{CH(CH3)2}$), 82.41 (Ru-C_{ar}), 83.43 (Ru-C_{ar}), 83.65 (Ru-C_{ar}), 84.32(Ru-C_{ar}), 99.15 (Ru-C_{ar}), 107.27 (Ru-C_{ar}), 128.51 (C_{ar}), 129.33 (C_{ar}), 130.34 (C_{ar}), 133.24 (C_{ar}) ppm. MS (positive mode): *m/z* = 939.1 $[M - Cl]^+$. These data are in agreement with those reported by Mashima for $[(\eta^6\text{-}p\text{-}MeC_6H_4Pr^i)_2Ru_2(\mu\text{-}SeC_6H_5)_3]PF_6$.[127]

$[(\eta^6\text{-}p\text{-}MeC_6H_4Pr^i)_2Ru_2(\mu\text{-}TeC_6H_5)_3]PF_6$ (**21**)

Yield: 74 mg (47 %). ^{1}H NMR (400 MHz, $CDCl_3$): δ = 0.77 (d, 6 H, ^3J = 7 Hz, H $H_{CH(CH3)2}$), 0.90 (d, 6 H, ^3J = 7 Hz, H $H_{CH(CH3)2}$), 1.96 (s, 6 H, H_{CH3}), 2.32-2.35 (m, 2 H, H $H_{CH(CH3)2}$), 5.41 (d, 2 H, ^3J = 6 Hz, $H_{p\text{-cymene}}$), 5.48-5.51 (m, 4 H, $H_{p\text{-cymene}}$), 5.63-5.64 (m, 2 H, $H_{p\text{-cymene}}$), 7.27-7.39 (m, 9 H, H_{ar}), 7.62-7.64 (m, 6 H, H_{ar}) ppm. ^{31}P{^{1}H} NMR (162 MHz, CD_2Cl_2) δ = -144.46 (m) ppm. ^{13}C{^{1}H} NMR (100 MHz, $CDCl_3$): δ = 19.32 (C_{CH3}), 22.04 ($C_{CH(CH3)2}$), 23.34 ($C_{CH(CH3)2}$), 31.71 ($C_{CH(CH3)2}$), 82.10 (Ru-C_{ar}), 82.70 (Ru-C_{ar}), 83.40 (Ru-C_{ar}), 84.20 (Ru-C_{ar}), 99.81 (Ru-C_{ar}), 109.22 (Ru-C_{ar}), 128.92 (C_{ar}), 129.20 (C_{ar}), 136.70 (C_{ar}) ppm. ESI-MS (positive mode): *m/z* = 1084.3 $[M - PF_6]^+$. Anal. Calc. for $C_{38}H_{43}F_6PRu_2Te_3 \cdot 2\ CH_2Cl_2$ (1399.52): C 34.33, H 3.38; Found: C 34.72, H 3.74%. These data are in agreement with those reported by Mashima for $[(\eta^6\text{-}p\text{-}MeC_6H_4Pr^i)_2Ru_2(\mu\text{-}TeC_6H_5)_3]PF_6$.[127]

$[(\eta^5\text{-}C_5Me_5)_2Rh_2(\mu\text{-}SC_6H_5)_3]Cl$ (**22**)

Yield: 105 mg (77 %). ^{1}H NMR (400 MHz, $CDCl_3$): δ = 1.34 (s, 30 H, C_5Me_5), 7.33-7.37 (m, 9 H, H_{ar}), 7.80-7.81 (m, 6 H, H_{ar}) ppm. ^{13}C{^{1}H} NMR (100 MHz, CH_2Cl_2): δ = 8.78 (C_{CH3}), 97.87 (Rh-C_{ar}), 128.83 (C_{ar}), 128.92 (C_{ar}), 132.49 (C_{ar}), 133.24 (C_{ar}) ppm. ESI MS (positive mode): m/z = 803.1 $[M - Cl]^+$. Anal. Calc. for $C_{38}H_{45}ClRh_2S_3 \cdot 2\ H_2O$ (875.25): C 52.15, H 5.64; Found C 51.87, H 5.69 %.

$[(\eta^5\text{-}C_5Me_5)_2Rh_2(\mu\text{-}SeC_6H_5)_3]Cl$ (**23**)

Yield: 90 mg (57 %). ^{1}H NMR (400 MHz, $CDCl_3$): δ = 1.49 (S, 30 H, H_{C5Me5}), 7.31-7.34 (m, 6 H, H_{ar}), 7.38-7.42 (m, 3 H, H_{ar}), 7.65-7.67 (m, 6 H, H_{ar}) ppm. ^{13}C{^{1}H} NMR (100 MHz, $CDCl_3$): δ = 9.35 (C_{CH3}), 97.77 (Rh-C_{ar}), 125.15 (C_{ar}), 128.98 (C_{ar}), 129.04 (C_{ar}), 134.03 (C_{ar}) ppm. ESI-MS (positive mode): *m/z* = 943.9 $[M - Cl]^+$. Anal. Calc. for $C_{38}H_{45}ClRh_2Se_3 \cdot 2\ H_2O$ (1015.94): C 44.92, H 4.86; Found C 45.03, H 4.83 %.

$[(\eta^5\text{-}C_5Me_5)_2Rh_2(\mu\text{-}TeC_6H_5)_3]PF_6$ (**24**)

Yield: 102 mg (51 %). ^{1}H NMR (400 MHz, CD_2Cl_2): δ = 1.79 (s, 30 H, H_{C5Me5}), 7.27-7.31 (m, 6 H, H_{ar}), 7.42-7.47 (m, 3 H, H_{ar}), 7.57-7.59 (m, 6 H, H_{ar}) ppm. ^{31}P{^{1}H} NMR (162 MHz, CD_2Cl_2) δ = -144.54 (m) ppm. ^{13}C{^{1}H} NMR (100 MHz, $CDCl_3$): δ = 10.30 (C_{CH3}), 99.38 (Rh-C_{ar}), 128.97 (C_{ar}), 129.02 (C_{ar}), 129.23 (C_{ar}), 137.77 (C_{ar}) ppm. ESI-MS (positive

mode): *m/z* = 1091.6 [M - PF_6]$^+$. Anal. Calc. for $C_{38}H_{45}F_6PRh_2Te_3$ (1235.34): C 36.95, H 3.67; Found C 36.87, H 3.81 %.

[(η^5-C_5Me_5)$_2$$Ir_2$($\mu$-$SC_6H_5$)$_3$]Cl (**25**)

Yield: 100 mg (78 %). ^{1}H NMR (400 MHz, $CDCl_3$): δ =1.38 (s, 30 H, H_{C5Me5}), 7.36-7.38 (m, 9 H, H_{ar}), 7.75-7.78 (m, 6 H, H_{ar}) ppm. ^{13}C{^{1}H} NMR (100 MHz, CH_2Cl_2): δ = 8.50 (C_{CH3}), 91.52 (Rh-C_{ar}), 128.75 (C_{ar}), 129.35 (C_{ar}), 130.56 (C_{ar}), 132.99 (C_{ar}) ppm. ESI MS (positive mode): m/z = 982.2 [M - Cl]$^+$. Anal. Calc. for $C_{38}H_{45}ClIr_2S_3 \cdot 2\ H_2O$ (1053.88): C 43.31, H 4.69; Found C 43.31, H 4.58 %.

[(η^5-C_5Me_5)$_2$$Ir_2$($\mu$-$SeC_6H_5$)$_3$]Cl (**26**)

Yield: 91 mg (63 %). ^{1}H NMR (400 MHz, CD_2Cl_2): δ = 1.52 (s, 30 H, H_{C5Me5}), 7.33-7.42 (m, 9 H, H_{ar}), 7.66-7.68 (m, 6 H, H_{ar}) ppm. ^{13}C{^{1}H} NMR (100 MHz, CD_2Cl_2): δ = 8.67 (C_{CH3}), 91.36 (Ir-C_{ar}), 124.65 (C_{ar}), 128.80 (C_{ar}), 128.96 (C_{ar}), 133.84 (C_{ar}) ppm. ESI-MS (positive mode): *m/z* = 1123.8 [M - Cl]$^+$. Anal. Calc. for $C_{38}H_{45}ClIr_2Se_3 \cdot 2\ H_2O$ (1194.56): C 38.21, H 4.13; Found C 38.60, H 4.21 %.

[(η^5-C_5Me_5)$_2$$Ir_2$($\mu$-$TeC_6H_5$)$_3$]$PF_6$ (**27**)

Yield: 45 mg (43 %). ^{1}H NMR (400 MHz, CD_2Cl_2): δ = 1.82 (s, 30 H, H_{C5Me5}), 7.28-7.32 (m, 6 H, H_{ar}), 7.38-7.43 (m, 3 H, H_{ar}), 7.57-7.59 (m, 6 H, H_{ar}) ppm. ^{31}P{^{1}H} NMR (162 MHz, CD2Cl2) δ = -144.55 (m) ppm. ^{13}C{^{1}H} NMR (100 MHz, CD_2Cl_2): δ = 9.69 (C_{CH3}), 93.16 (Ir-C_{ar}), 129.07 (C_{ar}), 129.30 (C_{ar}), 137.34 (C_{ar}), 137.45 (C_{ar}) ppm. ESI-MS (positive mode): *m/z* = 1269.6 [M - PF_6] $^+$. Anal. Calc. for $C_{38}H_{45}F_6Ir_2PTe_3$ (1413.96): C 32.28, H 3.21; Found C, 32.34; H, 3.48 %.

6.8.2. *Preparation of mixed chalcogenolato-bridged dinuclear complexes (**28**-**33**).*

Synthesis of [(η^6-*p*-$MeC_6H_4Pr^i$)$_2$$Ru_2$($\mu$-$SeC_6H_5$)($\mu$-$SCH_2C_6H_4$-*p*-$Bu^t$)$_2$]Cl (**28**), [($\eta^5$-$C_5Me_5$)$_2$$Rh_2$($\mu$-$SeC_6H_5$)($\mu$-$SCH_2C_6H_5$)$_2$]Cl (**30**) and [($\eta^5$-$C_5Me_5$)$_2$$Ir_2$($\mu$-$SeC_6H_5$)($\mu$-$SCH_2C_6H_5$)$_2$]Cl (**32**).

The neutral dinuclear dichloro complexes (η^6-*p*-$MeC_6H_4Pr^i$)$_2$$Ru_2Cl_2$($\mu$-$SCH_2C_6H_4$-*p*-$Bu^t$)$_2$ (0.07 mmol, 60 mg for **28**), (η^5-C_5Me_5)$_2$$Rh_2Cl_2$($\mu$-$SCH_2C_6H_5$)$_2$ (0.13 mmol, 100 mg for **30**) or (η^5-C_5Me_5)$_2$$Ir_2Cl_2$($\mu$-$SCH_2C_6H_5$)$_2$ (0.09 mmol, 88 mg for **32**) were dissolved in technical-

grade ethanol (20 mL). Then, an ethanolic solution (2.5 mL) of benzeneselenol (0.13 mmol, 14 µl for **28**; 0.25 mmol, 27 µl for **30**; 0.18 mmol, 19 µl for **32**) was added drop wise to the reaction mixture. The reaction was carried out at reflux for 18 h. After this period, ethanol was evaporated and the salts were isolated from the residue by precipitation from a dichloromethane/hexane solution. After filtration, the residue was washed several time with diethyl ether and hexane and dried under vacuum.

Synthesis of $[(\eta^6\text{-}p\text{-}MeC_6H_4Pr^i)_2Ru_2(\mu\text{-}TeC_6H_5)(\mu\text{-}SCH_2C_6H_4\text{-}p\text{-}Bu^t)_2]PF_6$ (**29**), $[(\eta^5\text{-}C_5Me_5)_2Rh_2(\mu\text{-}TeC_6H_5)(\mu\text{-}SCH_2C_6H_5)_2]PF_6$ (**31**) and $[(\eta^5\text{-}C_5Me_5)_2Ir_2(\mu\text{-}TeC_6H_5)(\mu\text{-}SCH_2C_6H_5)_2]PF_6$ (**33**).

The dinuclear dichloro complexes $(\eta^6\text{-}p\text{-}MeC_6H_4Pr^i)_2Ru_2Cl_2(\mu\text{-}SCH_2C_6H_4\text{-}p\text{-}Bu^t)_2$ (0.11 mmol, 100 mg for **29**), $(\eta^5\text{-}C_5Me_5)_2Rh_2Cl_2(\mu\text{-}SCH_2C_6H_5)_2$ (0.13 mmol, 100 mg for **31**) or $(\eta^5\text{-}C_5Me_5)_2Ir_2Cl_2(\mu\text{-}SCH_2C_6H_5)_2$ (0.13 mmol, 125 mg for **33**) were dissolved in technical-grade ethanol (25 mL) and added to an ethanolic solution of sodium tellurophenolate, which was prepared by the treatment of diphenyl ditelluride (0.11 mmol, 45 mg for **29**; 0.13 mmol, 52 mg for **31**; 0.13 mmol, 52 mg for **33**) with sodium borohydride (0.22 mmol, 8 mg for **29**; 0.25 mmol, 38 mg for **31**; 0.26 mmol, 10 mg for **33**).[127] After being stirred for 15 h, 1 eq. of potassium hexafluorophosphate was added to the solution and the solution was stirred for another 2 h. The reaction mixture was filtered off to remove impurities and the solvent evaporated. The products were isolated from the residue by precipitation from a dichloromethane/diethyl ether mixture. To improve the purity, the raw products were subjected to chromatography on silica gel using a 9:1 dichloromethane:ethanol mixture. The second fraction was collected, evaporated and the solid dried under vacuum.

$[(\eta^6\text{-}p\text{-}MeC_6H_4Pr^i)_2Ru_2(\mu\text{-}SeC_6H_5)(\mu\text{-}SCH_2C_6H_4\text{-}p\text{-}Bu^t)_2]Cl$ (**28**)

Yield: 40 mg (59 %). ^{1}H NMR (400 MHz, CD_2Cl_2): δ = 0.87 (d, 6 H, ^3J = 7 Hz, $H_{CH(C\mathbf{H}3)2}$), 0.96 (d, 6 H, ^3J = 7 Hz, $H_{CH(C\mathbf{H}3)2}$), 1.36 (d, 18 H, ^3J = 7 Hz, $H_{(CH3)3}$), 1.82 (s, 6 H, H_{CH3}), 1.91-2.00 (m, 2 H, $H_{C\mathbf{H}(CH3)2}$), 3.49 (s, 2 H, H_{CH2}), 3.52 (s, 2 H, H_{CH2}), 4.58 (d, 2 H, ^3J = 6 Hz, $H_{p\text{-cymene}}$), 4.85 (d, 2 H, ^3J = 6 Hz, $H_{p\text{-cymene}}$), 5.06 (d, 2 H, ^3J = 6 Hz, $H_{p\text{-cymene}}$), 5.20 (d, 2 H, ^3J = 6 Hz, $H_{p\text{-cymene}}$), 7.29-7.52 (m, 11 H, H_{ar}), 7.79 (d, 2 H, ^3J = 7 Hz, H_{ar}) ppm. $^{13}C\{^1H\}$ NMR (100 MHz, $CDCl_3$): δ = 18.02 (C_{CH3}), 22.23 ($C_{CH(CH3)2}$), 22.84 ($C_{CH(CH3)2}$), 31.06 ($C_{(CH3)3}$), 34.58 ($C_{CH(CH3)2}$), 40.20 (C_{CH2}), 41.49 (C_{CH2}), 82.10 (Ru-C_{ar}), 82.88 (Ru-C_{ar}), 83.01 (Ru-C_{ar}),

83.52 (Ru-C_{ar}), 100.23 (Ru-C_{ar}), 106.76 (Ru-C_{ar}), 125.47 (C_{ar}), 128.52 (C_{ar}), 128.91 (C_{ar}), 129.23 (C_{ar}), 133.44 (C_{ar}), 136.57 (C_{ar}), 136.92 (C_{ar}), 151.62 (C_{ar}) ppm. ESI-MS (positive mode): *m/z* = 986.4 $[M - Cl]^+$. Anal. Calc. for $C_{48}H_{63}ClRu_2S_2Se \cdot CH_2Cl_2$ (1105.09): C 53.23, H 5.93; Found C 53.62, H 6.20 %.

$[(\eta^6\text{-}p\text{-}MeC_6H_4Pr^i)_2Ru_2(\mu\text{-}TeC_6H_5)(\mu\text{-}SCH_2C_6H_4\text{-}p\text{-}Bu^t)_2]PF_6$ (**29**)

Yield: 86 mg (66 %). ^{1}H NMR (400 MHz, $CDCl_3$): δ = 0.80 (d, 6 H, ^3J = 7 Hz, $H_{CH(CH3)2}$), 0.96 (d, 6 H, ^3J = 7 Hz, $H_{CH(CH3)2}$), 1.34 (d, 18 H, ^3J = 7 Hz, $H_{(CH3)3}$), 1.89 (s, 6 H, H_{CH3}), 2.00-2.08 (m, 2 H, $H_{CH(CH3)2}$), 3.14 (s, 2 H, H_{CH2}), 3.60 (s, 2 H, H_{CH2}), 4.45 (d, 2 H, ^3J = 6 Hz, $H_{p\text{-cymene}}$), 4.77 (d, 2 H, ^3J = 6 Hz, $H_{p\text{-cymene}}$), 5.18 (d, 2 H, ^3J = 6 Hz, $H_{p\text{-cymene}}$), 5.33 (d, 2 H, ^3J = 6 Hz, $H_{p\text{-cymene}}$), 7.20-7.24 (m, 2 H, H_{ar}), 7.33-7.39 (d, 4 H, H_{ar}), 7.41-7.47 (m, 5 H, H_{ar}), 7.72 (d, 2 H, ^3J = 8 Hz, H_{ar}) ppm. ^{31}P{^{1}H} NMR (162 MHz, CD_2Cl_2) δ = -144.48 (m) ppm. ^{13}C{^{1}H} NMR (100 MHz, $CDCl_3$): δ = 18.45 (C_{CH3}), 22.14 ($C_{CH(CH3)2}$), 22.94 ($C_{CH(CH3)2}$), 31.06 ($C_{(CH3)3}$), 34.60 ($C_{CH(CH3)2}$), 43.45 (C_{CH2}), 44.24 (C_{CH2}), 82.04 (Ru-C_{ar}), 82.33 (Ru-C_{ar}), 83.31 (Ru-C_{ar}), 100.46 (Ru-C_{ar}), 107.12 (Ru-C_{ar}), 107.72 (Ru-C_{ar}), 125.53 (C_{ar}), 128.90 (C_{ar}), 129.18 (C_{ar}), 129.89 (C_{ar}), 136.12 (C_{ar}), 136.98 (C_{ar}), 137.16 (C_{ar}), 151.84 (C_{ar}) ppm. ESI-MS (positive mode): *m/z* = 1034.6 $[M - PF_6]^+$. Anal. Calc. for $C_{48}H_{63}F_6PRu_2S_2Te \cdot 2\ CH_2Cl_2$ (1348.71): C 44.53, H 5.01; Found: C 44.83, H 4.80 %.

$[(\eta^5\text{-}C_5Me_5)_2Rh_2(\mu\text{-}SeC_6H_5)(\mu\text{-}SCH_2C_6H_5)_2]Cl$ (**30**)

Yield: 67 mg (58 %). ^{1}H NMR (400 MHz, CD_2Cl_2): δ = 1.48 (s, 30 H, H_{CH3}), 3.65 (s, 2 H, H_{CH2}), 3.80 (s, 2 H, H_{CH2}), 7.32-7.37 (m, 4 H, H_{ar}), 7.43-7.47 (m, 5 H, H_{ar}), 7.61 (t, 4 H, ^3J = 8 Hz, H_{ar}), 7.70-7.72 (m, 2 H, H_{ar}) ppm. ^{13}C{^{1}H} NMR (100 MHz, CD_2Cl_2): δ = 9.12 (CH_3), 35.93 (CH_2), 36.45(CH_2), 98.11 (Rh-C_{ar}), 125.59 (C_{ar}), 127.47 (C_{ar}), 127.69 (C_{ar}), 128.62 (C_{ar}), 128.90 (C_{ar}), 133.79 (C_{ar}), 139.56 (C_{ar}), 139.64 (C_{ar}) ppm. ESI-MS (positive mode): *m/z* = 879.7 $[M - Cl]^+$. Anal. Calc. for $C_{40}H_{49}ClRh_2S_2Se \cdot 2\ H_2O$ (950.20): C 50.56, H 5.62; Found: C 50.29, H 5.81 %.

$[(\eta^5\text{-}C_5Me_5)_2Rh_2(\mu\text{-}TeC_6H_5)(\mu\text{-}SCH_2C_6H_5)_2]PF_6$ (**31**)

Yield: 107 mg (79 %). ^{1}H NMR (400 MHz, CD_2Cl_2): δ = 1.57 (s, 30 H, H_{CH3}), 3.39 (s, 2 H, H_{CH2}), 3.91 (s, 2 H, H_{CH2}), 7.28-7.31 (m, 2 H, H_{ar}), 7.34-7.38 (m, 2 H, H_{ar}), 7.42-7.46 (m, 5 H, H_{ar}), 7.53 (d, 2 H, ^3J = 8 Hz, H_{ar}), 7.62 (d, 2 H, ^3J = 8 Hz, H_{ar}), 7.72-7.75 (m, 2 H, H_{ar})

ppm. $^{31}P\{^{1}H\}$ NMR (162 MHz, CD_2Cl_2) δ = -144.56 (m) ppm. $^{13}C\{^{1}H\}$ NMR (100 MHz, CD_2Cl_2): δ = 9.59 (C_{CH3}), 37.82 (C_{CH2}), 39.19 (C_{CH2}), 98.59 (Rh-C_{ar}), 127.39 (C_{ar}), 127.77 (C_{ar}), 128.65 (C_{ar}), 129.01 (C_{ar}), 129.45 (C_{ar}), 137.32 (C_{ar}), 139.39 (C_{ar}), 139.82 (C_{ar}) ppm. ESI-MS (positive mode): *m/z* = 928.1 $[M - PF_6]^+$. Anal. Calc. for $C_{40}H_{49}F_6PRh_2S_2Te$ (1072.32): C 44.80, H 4.61; Found C 44.76, H 4.73 %.

$[(\eta^5\text{-}C_5Me_5)_2Ir_2(\mu\text{-}SeC_6H_5)(\mu\text{-}SCH_2C_6H_5)_2]Cl$ (**32**)

Yield: 65 mg (66 %). ^{1}H NMR (400 MHz, CD_2Cl_2): δ = 1.49 (s, 30 H, H_{CH3}), 3.86 (s, 2 H, H_{CH2}), 4.03 (s, 2 H, H_{CH2}), 7.32-7.39 (m, 4 H, H_{ar}), 7.43-7.47 (m, 5 H, H_{ar}), 7.58 (t, 4 H, ^{3}J = 8 Hz, H_{ar}), 7.67-7.69 (m, 2 H, H_{ar}) ppm. $^{13}C\{^{1}H\}$ NMR (100 MHz, CD_2Cl_2): δ = 8.86 (C_{CH3}), 35.85 (C_{CH2}), 37.26 (C_{CH2}), 91.86 (Ir-C_{ar}), 123.28 (C_{ar}), 127.65 (C_{ar}), 127.85 (C_{ar}), 128.72 (C_{ar}), 128.94 (C_{ar}), 129.16 (C_{ar}), 133.32 (C_{ar}), 138.98 (C_{ar}) ppm. ESI-MS (positive mode): *m/z* = 1057.9 $[M - Cl]^+$. Anal. Calc. for $C_{40}H_{49}ClIr_2S_2Se$ (1093.14): C 43.96, H 4.52; Found C 43.32, H 4.93 %.

$[(\eta^5\text{-}C_5Me_5)_2Ir_2(\mu\text{-}TeC_6H_5)(\mu\text{-}SCH_2C_6H_5)_2]PF_6$ (**33**)

Yield: 132 mg (82 %). ^{1}H NMR (400 MHz, CD_2Cl_2): δ = 1.59 (s, 30 H, H_{CH3}), 3.65 (s, 2 H, H_{CH2}), 4.12 (s, 2 H, H_{CH2}), 7.27-7.31 (m, 2 H, H_{ar}), 7.35-7.39 (m, 2 H, H_{ar}), 7.41-7.46 (m, 5 H, H_{ar}), 7.50-7.52 (m, 2 H, H_{ar}), 7.58-7.60 (d, 2 H, H_{ar}), 7.70-7.72 (m, 2 H, H_{ar}) ppm. $^{31}P\{^{1}H\}$ NMR (162 MHz, CD_2Cl_2) δ = -144.55 (m) ppm. $^{13}C\{^{1}H\}$ NMR (100 MHz, CD_2Cl_2): δ = 9.24 (C_{CH3}), 39.76 (C_{CH2}), 40.84 (C_{CH2}), 92.47 (Ir-C_{ar}), 127.59 (C_{ar}), 127.97 (C_{ar}), 128.59 (C_{ar}), 128.80 (C_{ar}), 129.50 (C_{ar}), 137.08 (C_{ar}), 138.93 (C_{ar}), 139.07 (C_{ar}) ppm. ESI-MS (positive mode): *m/z* = 1106.1 $[M - PF_6]^+$. Anal. Calc. for $C_{40}H_{49}F_6Ir_2PS_2Te$ (1250.95): C 38.41, H 3.95; Found C 38.40, H 4.02 %.

6.9. Sawhorse-type complexes containing biologically relevant acids (chapter-4)

*6.9.1. Preparation of sawhorse-type diruthenium tetracarbonyl complexes **34-36***

A solution of $Ru_3(CO)_{12}$ (100 mg, 0.156 mmol) and the carboxylic acid (0.470 mmol) in dry tetrahydrofuran (25 mL), was heated at 120 ˚C in a pressure Schlenk tube for 18 h. Then, addition of three equivalent of the axial ligand [**34a**, **35a** (L = NC_5H_5); **34b**, **35b**, **36b**

(L = PPh_3); **34c**, **35c** (L = $C_{43}H_{29}N_5$)] followed by stirring at room temperature for 3 h, affords the final products. The complexes are isolated from the residue by precipitation from dichlormethane/pentane. In order to improve the purity, the raw products were subjected to chromatography on silica gel using a dichloromethane/pentane mixture as eluent and the solid obtained was dried under vacuum.

$Ru_2(CO)_4(\mu_2\text{-}\eta^2\text{-}O_2CC_{12}H_{18}NO_2S)_2(NC_5H_5)_2$ (**34a**)

Yield: 130 mg (79 %). ^{1}H NMR (400 MHz, $CDCl_3$): δ = 0.83 (t, 12 H, ^3J = 7 Hz, H_{CH3}), 1.46-1.53 (m, 8 H, H_{CH2}), 3.01 (t, 8 H, ^3J = 8 Hz, H_{CH2}), 7.56-7.60 (m, 4 H, H_{ar}), 7.72 (d, 4 H, ^3J = 8 Hz, H_{ar}), 7.96-7.98 (m, 6 H, H_{ar}), 8.90-8.92 (m, 4 H, H_{ar}). $^{13}C\{^1H\}$ NMR (100 MHz, $CDCl_3$): δ = 11.12 (4 C, CH_3), 21.95 (4 C, CH_2), 50.00 (4 C, CH_2), 125.12 (4 C, C_{ar}), 126.56 (4 C, C_{ar}), 130.19 (4 C, C_{ar}), 136.42 (2 C, C_{ar}), 137.72 (2 C, C_{ar}), 142.44 (4 C, C_{ar}), 151.81 (2 C, C_{ar}), 177.36 (2 C, C_{COO}), 203.74 (4 C, C_{CO}). IR (KBr, cm^{-1}) $\nu_{(OCO)}$ 1558.17, $\nu_{(CO)}$ 1946.64 vs, (ν_{CO}) 1976.27 m, (ν_{CO}) 2026.98 vs. ESI-MS (positive mode): *m/z* = 935.58 [M - NC_5H_5 - CO + H]$^+$. Anal. Calc. for $C_{40}H_{46}N_4O_{12}Ru_2S_2$ (1041.08) C 46.15, H 4.45, N 5.38. Found: C 46.27, H 4.42, N 5.31 %.

$Ru_2(CO)_4(\mu_2\text{-}\eta^2\text{-}O_2CC_{12}H_{18}NO_2S)_2(PPh_3)_2$ (**34b**)

Yield: 159 mg (72 %). ^{1}H NMR (400 MHz, $CDCl_3$): δ = 0.86 (t, 12 H, ^3J = 7 Hz, H_{CH3}), 1.46-1.52 (m, 8 H, H_{CH2}), 3.01 (t, 8 H, ^3J = 7 Hz, H_{CH2}), 7.10 (d, 4 H, ^3J = 8 Hz, H_{ar}), 7.39-7.49 (m, 22 H, H_{ar}), 7.60-7.65 (m, 12 H, H_{ar}). $^{13}C\{^1H\}$ NMR (100 MHz, $CDCl_3$): δ = 11.14 (4 C, C_{CH3}), 21.92 (4 C, C_{CH2}), 49.89 (4 C, C_{CH2}), 126.20 (4 C, C_{ar}), 128.57 (12 C, C_{ar}), 129.90 (6 C, C_{ar}), 130.44 (4 C, C_{ar}), 133.13 (12 C, C_{ar}), , 133.71 (6 C, C_{ar}), 136.41 (2 C, C_{ar}), 142.46 (2 C, C_{ar}), 179.16 (2 C, C_{COO}), 205.08 (4 C, C_{CO}). $^{31}P\{^1H\}$ NMR (162 MHz, $CDCl_3$) δ = 18.20 ppm. IR (KBr, cm^{-1}) $\nu_{(OCO)}$ 1558.06, $\nu_{(CO)}$ 1957.11 vs, (ν_{CO}) 1983.87 m, (ν_{CO}) 2026.80 vs. ESI-MS (positive mode): *m/z* = 1431.13 [M+Na]$^+$. Anal. Calc. for $C_{66}H_{66}N_2O_{12}P_2Ru_2S_2$ (1407.45) C 56.32, H 4.73, N 1.99. Found: C 56.60, H, 4.90, N 2.00 %.

$Ru_2(CO)_4(\mu_2\text{-}\eta^2\text{-}O_2CC_{12}H_{18}NO_2S)_2(C_{43}H_{29}N_5)_2$ (**34c**)

Yield: 40 mg (57 %) ^{1}H NMR (400 MHz, $CDCl_3$): δ = -2.72 (s, 4 H, NH), 0.80 (t, 12 H, ^3J = 7 Hz, H_{CH3}), 1.47-1.54 (m, 8 H, H_{CH2}), 3.02 (t, 8 H, ^3J = 8 Hz, H_{CH2}), 7.78-7.86 (m, 22 H, H_{porph} and H_{ar}), 8.23-8.25 (m, 12 H, ^3J = 8 Hz, H_{porph}), 8.31 (d, 4 H, ^3J = 8 Hz, H_{ar}), 8.51 (d, 4

H, ^{3}J = 6 Hz, H_{ar}), 8.90 (s, 8 H, H_{porph}), 9.02 (s, 8 H, H_{porph}), 9.40 (d, 4 H, ^{3}J = 6 Hz, H_{porph}). $^{13}C\{^{1}H\}$ NMR (100 MHz, $CDCl_3$): δ = 11.10 (4 C, C_{CH3}), 21.95 (4 C, C_{CH2}), 50.02 (4 C, C_{CH2}), 114.67 (8 C, C_{ar}), 120.92 (6 C, C_{ar}),126.74 (4 C, C_{ar}), 126.83 (4 C, C_{ar}), 127.90 (12 C, C_{ar}), 127.98 (16 C, C_{ar}), 130.43 (4 C, C_{ar}), 130.83 (12 C, C_{ar}), 130.94 (12 C, C_{ar}), 134.52 (6 C, C_{ar}), 136.62 (2 C, C_{ar}), 141.76 (4 C, C_{ar}), 150.00 (2 C, C_{ar}), 177.96 (2 C, C_{COO}), 204.01 (4 C, C_{CO}). UV-Vis [1.0×10^{-6} M, CH_2Cl_2] λ_{max}/nm ($\varepsilon \times 10^{6}$ M^{-1} cm^{-1}) = 418 (3.251), 515 (0.230), 551 (0.121), 590 (0.074), 646 (0.055). IR (KBr, cm^{-1}): $\nu_{(porph\ N\text{-}H)}$ 1214.92, $\nu_{(OCO)}$ 1557.00, (ν_{CO}) 1979.01 vs, (ν_{CO}) 1976.27 m, (ν_{CO}) 2028.45 vs, ($\nu_{C\text{-}H\ aro}$) 3056.83 m. ESI-MS (positive mode): *m/z* = 1501.23 $[M - C_{43}H_{29}N_5 + H]^{+}$. Anal. Calc. for $C_{116}H_{94}N_{12}O_{12}Ru_2S_2 \cdot 2\ H_2O$ (2150.36) C 64.79, H 4.59, N 7.82, Found: C 64.70, H 4.64, N 7.65 %.

$Ru_2(CO)_4(\mu_2\text{-}\eta^2\text{-}O_2CC_{18}H_{15}ClNO_2)(NC_5H_5)_2$ (**35a**)

Yield: 60 mg (32 %) ^{1}H NMR (400 MHz, $CDCl_3$): δ = 2.12 (s, 6 H, H_{CH3}), 3.47 (s, 4 H, H_{CH2}), 3.67 (s, 6 H, H_{CH3}), 6.64 (dd, 2 H, ^{3}J = 9 Hz, ^{4}J = 2 Hz, H_{ar}), 6.83 (d, 2 H, ^{4}J = 2 Hz, H_{ar}), 6.93 (d, 2 H, ^{3}J = 9 Hz, H_{ar}), 7.19 (dd, 4 H, ^{3}J = 7 Hz, ^{4}J = 2 Hz H_{ar}), 7.43 (d, 4 H, ^{3}J = 8 Hz, H_{ar}), 7.57 (d, 4 H, ^{3}J = 8 Hz, H_{ar}), 7.73 (t, 2 H, ^{3}J = 8 Hz, H_{ar}), 8.42 (d, 4 H, ^{3}J = 5 Hz, H_{ar}). $^{13}C\{^{1}H\}$ NMR (100 MHz, $CDCl_3$): δ = 13.21 (2 C, C_{CH3}), 32.25 (2 C, C_{CH2}), 55.44 (2 C, C_{CH3}), 101.95 (2 C, C_{ar}), 111.14 (2 C, C_{ar}), 114.66 (2 C, C_{ar}), 115.13 (2 C, C_{ar}), 124.57 (4 C, C_{ar}), 129.01 (2 C, C_{ar}), 130.77 (4 C, C_{ar}), 131.03 (4 C, C_{ar}), 131.16 (2 C, C_{ar}), 134.00 (2 C, C_{ar}), 134.79 (2 C, C_{ar}), 137.11 (2 C, C_{ar}), 139.06 (2 C, C_{ar}), 151.63 (4 C, C_{ar}), 155.84 (2 C, C_{ar}), 168.23 (2 C, C_{CON}), 183.66 (2 C, C_{COO}), 203.93 (4 C, C_{CO}). IR (KBr, cm^{-1}): $\nu_{(OCO)}$ 1581.79, (ν_{CO}) 1936.73 vs, (ν_{CO}) 1970.86 m, (ν_{CO}) 2022.40 vs. ESI-MS (positive mode): *m/z* = 1187.02 $[M + H]^{+}$. Anal. Calc. for $C_{52}H_{40}Cl_2N_4O_{12}Ru_2$ (1185.94) C 52.66, H 3.40, N 4.72. Found: C 52.39, H 3.59, N 4.60 %.

$Ru_2(CO)_4(\mu_2\text{-}\eta^2\text{-}O_2CC_{18}H_{15}ClNO_2)(PPh_3)_2$ (**35b**)

Yield: 277 mg (83 %) ^{1}H NMR (400 MHz, $CDCl_3$): δ = 1.76 (s, 6 H, H_{CH3}), 3.31 (s, 4 H, H_{CH2}), 3.63 (s, 6 H, H_{CH3}), 6.68- (br-s, 2 H, ^{3}J = 9 Hz, H_{ar}), 6.9 (d, 2 H, ^{4}J = 2 Hz, H_{ar}), 7.01 (d, 2 H, ^{3}J = 9 Hz H_{ar}), 7.14-7.19 (m, 18 H, H_{ar}), 7.21 (d, 2 H, ^{3}J = 7 Hz, H_{ar}), 7.32 (t, 6 H, ^{3}J = 7 Hz, H_{ar}), 7.38-7.42 (m, 12 H, H_{ar}). $^{13}C\{^{1}H\}$ NMR (100 MHz, $CDCl_3$): δ = 12.95 (2 C, C_{CH3}), 32.32 (2 C, C_{CH2}), 55.48 (2 C, C_{CH3}), 101.19 (2 C, C_{ar}), 111.35 (2 C, C_{ar}), 114.54 (2 C, C_{ar}), 114.92 (2 C, C_{ar}), 128.19 (18 C, C_{ar}), 128.78 (4 C, C_{ar}) 129.65 (2 C, C_{ar}), 130.89 (12 C,

C_{ar}), 133.34 (4 C, C_{ar}), 133.49 (6 C, C_{ar}), , 133.66 (2 C, C_{ar}), 133.84 (2 C, C_{ar}), 134.86 (2 C, C_{ar}), 138.68 (2 C, C_{ar}), 156.06 (2 C, C_{ar}), 167.98 (2 C, C_{CON}), 185.77 (2 C, C_{COO}), 204.95 (4 C, C_{CO}). $^{31}P\{^{1}H\}$ NMR (162 MHz, $CDCl_3$) δ = 12.99 ppm. IR (KBr, cm^{-1}): $\nu_{(OCO)}$ 1578.77, (ν_{CO}) 1950.87 vs, (ν_{CO}) 1980.63 m, (ν_{CO}) 2023.55 vs. ESI-MS (positive mode): *m*/*z* = 1575.12 $[M + Na]^+$. Anal. Calc. for $C_{78}H_{60}Cl_2N_2O_{12}P_2Ru_2$ (1552.31) C 60.35, H 3.90, N 1.80, Found: C 60.08, H 4.08, N 1.81 %.

$Ru_2(CO)_4(\mu_2\text{-}\eta^2\text{-}O_2CC_{18}H_{15}ClNO_2)(C_{43}H_{29}N_5)_2$ (**35c**)

Yield: 107 mg (86 %) ^{1}H NMR (400 MHz, $CDCl_3$): δ = -2.74 (s, 4 H, H_{NH}), 2.41 (s, 6 H, H_{CH3}), 3.67 (s, 6 H, H_{CH2}), 3.84 (s, 4 H, H_{CH3}), 6.64 (dd, 2 H, ^{3}J = 9 Hz, ^{4}J = 2 Hz, H_{ar}), 6.71 (d, 2 H, ^{3}J = 9 Hz, H_{ar}), 6.98 (d, 4 H, ^{3}J = 8 Hz, H_{ar}), 7.15 (d, 2 H, ^{4}J = 2 Hz, H_{ar}), 7.35 (d, 4 H, ^{3}J = 8 Hz, H_{ar}), 7.79-7.85 (m, 18 H, H_{porph}), 8.11 (d, 4 H, ^{3}J = 6 Hz, H_{porph}), 8.25-8.27 (m, 12 H, H_{porph}), 8.84-8.90 (m, 16 H, H_{porph}), 8.96 (d, 4 H, ^{3}J = 5 Hz, H_{porph}). $^{13}C\{^{1}H\}$ NMR (100 MHz, $CDCl_3$): δ = 13.47 (2 C,C_{CH3}), 32.53 (2 C, C_{CH2}), 55.56 (2 C, C_{CH3}), 102.56 (2 C, C_{ar}), 110.79 (2 C, C_{ar}), 110.82 (2 C, C_{ar}), 114.67 (2 C, C_{ar}), 120.77 (8 C, C_{ar}), 126.72 (12 C, C_{ar}), 126.79 (4 C, C_{ar}), 128.73 (2 C, C_{ar}), 130.41 (4 C, C_{ar}), 130.87 (4 C, C_{ar}), 131.40 (2 C, C_{ar}), 133.70 (16 C, C_{ar}), 134.54 (2 C, C_{ar}), 135.29 (2 C, C_{ar}), 141.84 (2 C, C_{ar}), 149.90 (4 C, C_{ar}), 152.00 (16 C, C_{ar}), 155.88 (2 C, C_{ar}), 168.12 (2 C, C_{CON}), 184.43 (2 C, C_{COO}), 204.25 (4 C, C_{CO}). UV-Vis [1.0×10^{-6} M, CH_2Cl_2] λ_{max}/nm ($\varepsilon \times 10^6\ M^{-1}\ cm^{-1}$) = 418 (3.343), 515 (0.355), 551 (0.171), 590 (0.109), 645 (0.083). IR (KBr, cm^{-1}): $\nu_{(porph\ N\text{-}H)}$ 1224.17, $\nu_{(OCO)}$ 1580.28, (ν_{CO}) 1942.78 vs, (ν_{CO}) 1975.35 m, (ν_{CO}) 2025.14 vs, ($\nu_{C\text{-}H\ aro}$) 3056.41 m. ESI-MS (positive mode): *m*/*z* = 616.25 $[C_{43}H_{29}N_5 + H]^+$. Anal. Calc. for $C_{128}H_{88}Cl_2N_{12}O_{12}Ru_2 \cdot 3\ H_2O$ (2313.23) C 66.46, H 4.10, N 7.27, Found: C 66.55, H 4.03, N 7.19 %.

$Ru_2(CO)_4(\mu_2\text{-}\eta^2\text{-}O_2CC_{19}H_{16}FOS)(PPh_3)_2$ (**36b**)

Yield 54 mg (23 %) ^{1}H NMR (400 MHz, DMSO): δ = 1.68 (s, 6 H, H_{CH3}), 2.80 (s, 6 H, H_{CH3}), 3.18 (s, 4 H, H_{CH2}), 6.35 (dd, 2 H, ^{3}J = 9 Hz, ^{4}J = 2 Hz, H_{CH2}), 6.65-6.70 (m, 2 H, H_{ar}), 7.10-7.14 (m, 2 H, H_{ar}), 7.15 (s, 2 H, H_{ar}), 7.35-7.36 (m, 22 H, H_{ar}), 7.41-7.45 (m, 8 H, H_{ar}), 7.61 (d, 4 H, ^{3}J = 8 Hz, H_{ar}), 7.77 (d, 4 H, ^{3}J = 8 Hz, H_{ar}). $^{13}C\{^{1}H\}$ NMR (100 MHz, $CDCl_3$): δ = 9.87 (2 C, C_{CH3}), 32.32 (2 C, C_{CH2}), 43.86 (2 C,C_{CH3}), 105.95 (2 C, C_{ar}), 110.41 (2 C, C_{ar}), 123.28 (2 C, C_{ar}) 123.74 (4 C, C_{ar}), 127.01 (4 C, C_{ar}), 128.13 (18 C, C_{ar}), , 129.57 (2 C, C_{ar}), 130.14 (2 C, C_{ar}), 133.09 (12 C, C_{ar}), 133.65 (6 C, C_{ar}), 133.77 (2 C, C_{ar}), 137.05 (2 C, C_{ar}),

139.87 (2 C, C_{ar}), 141.87 (2 C, C_{ar}), 145.22 (2 C, C_{ar}), 147.33 (2 C, C_{ar}), 164.39 (2 C, C_{ar})184.93 (2 C, C_{COO}), 205.05 (4 C,C_{CO}). $^{31}P\{^{1}H\}$ NMR (162 MHz, $CDCl_3$) δ = 14.57 ppm. IR (KBr, cm^{-1}): $\nu_{(OCO)}$ 1580.41, (ν_{CO}) 1954.58 vs, (ν_{CO}) 1980.41 m, (ν_{CO}) 2025.10 vs. ESI-MS (positive mode): *m*/*z* = 997.56 $[M - 2\ PPh_3 - CO + H]^+$. Anal. Calc. for $C_{80}H_{62}F_2O_{10}P_2Ru_2S_2$ (1549.56) C 62.01, H 4.03, Found: C 61.60, H 4.15 %.

6.10. Photoactive sawhorse-type diruthenium tetracarbonyl complexes (chapter-4)

6.10.1. Preparation of sawhorse-type diruthenium tetracarbonyl complexes (37-40)

$[Ru_2(CO)_4(\mu_2\text{-}\eta^2\text{-}O_2CC_{44}H_{29}N_4)_2(NC_5H_5)_2]$ (**37**)

A solution of $Ru_3(CO)_{12}$ (19 mg, 0.03 mmol) and 5-(4-carboxyphenyl)-10,15,20-triphenyl-21,23H-porphyrin (65 mg, 0.09 mmol) in dry thf (25 mL) were heated at 120 ºC in a high pressure schlenk tube for 18 h. After cooling to room temperature, pyridine (7.4 µL, 0.09 mmol) was added and the solution was stirred for 2 h. The product was isolated by precipitation from dichloromethane/pentane mixture and dried under vacuum. The product was obtained as air-stable purple crystalline powder.

Yield: 35 mg (65 %). ^{1}H NMR (400 MHz, $CDCl_3$) δ = -2.76 (s, 4 H, NH), 7.65 (t, 4 H, ^{3}J = 7 Hz, H_{py}), 7.74-7.81 (m, 18 H, H_{porph}), 7.96 (t, 2 H, ^{3}J = 8 Hz, H_{py}), 8.21-8.25 (m, 16 H, H_{porph}), 8.40 (d, 4 H, ^{3}J = 8 Hz, H_{porph}), 8.85 (s, 8 H, H_{porph}), 8.86 (s, 8 H, H_{porph}), 9.23 (d, 4 H, ^{3}J = 4 Hz, H_{py}) ppm. IR (KBr, cm^{-1}) $\nu_{(OCO)}$ 1545.04 s, $\nu_{(NCN)}$ 1587.90 s, $\nu_{(CO)}$ 1942.72 vs, 1976.26 m, 2026.28 vs, $\nu_{(C\text{-}H\ aro)}$ 3054.66 m. Anal. Calc. for $C_{104}H_{68}N_{10}O_8Ru_2 \cdot 3\ H_2O$ (1841.88) C 67.82, H 4.05, N 7.60; found: C 67.60, H 3.88, N 7.47 %. ESI-MS (positive mode): *m*/*z* = 816.13 $[M - 2\ C_5H_5N + 2\ H]^{2+}$.

$[Ru_2(CO)_4(\mu_2\text{-}\eta^2\text{-}O_2CC_{44}H_{27}N_4Zn)_2(NC_5H_5)_2]$ (**38**)

The same procedure as for 1 was used: $Ru_3(CO)_{12}$ (19 mg, 0.03 mmol), 5-(4-carboxyphenyl)-10,15,20-triphenyl-porphyrin-Zn(II) (68 mg, 0.09 mmol), and pyridine (7.4 µL, 0.09 mmol). The product was isolated by precipitation from a dichloromethane/pentane mixture and dried under vacuum. The product was obtained as air-stable purple crystalline powder.

Yield: 35 mg (61 %). ^{1}H NMR (400 MHz, $CDCl_3$) δ = 7.65 (t, 4 H, ^3J = 7 Hz H_{py}), 7.72-7.80 (m, 18 H, H_{porph}), 7.96 (t, 2 H, ^3J = 7 Hz, H_{py}), 8.20-8.24 (m, 16 H, H_{porph}), 8.39 (d, 4 H, ^3J = 8 Hz, H_{porph}), 8.92 (s, 8 H, H_{porph}), 8.93 (s, 8 H, H_{porph}), 9.23 (d, 4 H, ^3J = 4 Hz, H_{py}) ppm. IR (KBr, cm^{-1}) $\nu_{(OCO)}$ 1560.83 s, $\nu_{(NCN)}$ 1597.11 s, $\nu_{(CO)}$ 1940.96 vs, 1973.77 m, 2024.02 vs, $\nu_{(C\text{-}H\ aro)}$ 3056.63 m. Anal. Calc. for $C_{104}H_{64}N_{10}O_8Ru_2Zn_2 \cdot 3CH_2Cl_2 \cdot H_2O$ (2187.46) C 58.75, H 3.32, N 6.40; found: C 58.51, H 3.48, N 6.42 %. ESI-MS (positive mode): *m*/*z* = 877.54 [M - 2 C_5H_5N + 2 H]$^{2+}$.

[{$Ru_2(CO)_4(NC_5H_5)_2$}$_2$(μ_2-η^2-$O_2CC_{44}H_{28}N_4CO_2$-η^2-μ_2)$_2$] (**39**)

The same procedure as used for the preparation of 1 was followed using $Ru_3(CO)_{12}$ (48 mg, 0.075 mmol), 5,10-di-(4-carboxyphenyl)-15,20-diphenyl-21,23H-porphyrin (80 mg, 0.114 mmol) and pyridine (18 µL, 0.23 mmol). In order to improve the purity, the raw product was subjected to chromatography on silica gel using dichloromethane/pentane mixture as eluent. The complex was obtained as an air-stable purple crystalline powder.

Yield: 36 mg (20 %). ^{1}H NMR (400 MHz, $CDCl_3$) δ = -2.81 (s, 4 H, NH), 7.61 (t, 8 H, ^3J = 7 Hz, H_{py}), 7.76-7.80 (m, 12 H, H_{porph}), 7.91-7.95 (m, 4 H, H_{py}), 8.18-8.22 (m, 18 H, H_{porph}), 8.38 (d, 8 H, ^3J = 8 Hz, H_{porph}), 8.76-8.87 (m, 16 H, H_{porph}), 9.20 (d, 8 H, ^3J = 4 Hz, H_{py}) ppm. IR (KBr, cm^{-1}) $\nu_{(OCO)}$ 1546.98 s, $\nu_{(NCN)}$ 1591.63 s, $\nu_{(CO)}$ 1940.75 vs, 1974.49 m, 2024.96 vs, $\nu_{(C\text{-}H\ aro)}$ 3047.61 m. Anal. Calc. for $C_{120}H_{76}N_{12}O_{16}Ru_4 \cdot C_5H_{12} \cdot H_2O$ (2436.40) C 61.62, H 3.72, N 6.90; found: C 61.60, H 3.82, N 6.37 %. ESI-MS (positive mode): *m*/*z* = 1095.12 [M - 2 C_5H_5N + 2 H]$^{2+}$.

[{$Ru_2(CO)_4(NC_5H_5)_2$}$_2$(μ_2-η^2-$O_2CC_{44}H_{26}N_4ZnCO_2$-$\eta^2$-$\mu_2$)$_2$] (**40**)

The same procedure as for 1 was used: $Ru_3(CO)_{12}$ (25 mg, 0.04 mmol), 5,10-di-(4-carboxyphenyl)-15,20-diphenyl-porphyrin-Zn(II) (29 mg, 0.06 mmol) and pyridine (10 µL, 0.12 mmol). In order to improve the purity, the raw product was subjected to chromatography on silica gel using dichloromethane/pentane mixture as eluent. Air-stable purple crystalline powder was isolated after evaporation of the solvent.

Yield: 20 mg (21 %). ^{1}H NMR (400 MHz, DMSO) δ = 7.35-7.38 (m, 8 H, H_{py}), 7.74-7.77 (m, 4 H, H_{py}), 7.78-7.84 (m, 12 H, H_{porph}), 8.17-8.19 (m, 8 H, H_{porph}), 8.30 (d, 8 H, ^3J = 8 Hz, H_{porph}), 8.46 (d, 8 H, ^3J = 8 Hz, H_{porph}), 8.54-8.56 (m, 8 H, $H_{py)}$, 8.74-8.86 (m, 16 H, H_{py})

ppm. IR (KBr, cm^{-1}) $\nu_{(OCO)}$ 1543.98 s, $\nu_{(NCN)}$ 1591.28 s, $\nu_{(CO)}$ 1942.46 vs, 1974.82 m, 2026.10 vs, $\nu_{(C\text{-}H\ aro)}$ 3065.70 m. Anal. Calc. for $C_{120}H_{72}N_{12}O_{16}Ru_4Zn_2$ (2473.03) C 58.28, H 2.93, N 6.80; Found: C 58.22, H 3.10, N 6.55 %. ESI-MS (positive mode): *m*/*z* = 1157.96 [M - 2 C_5H_5N + 2 H]$^{2+}$.

6.11. Single-crystal X-ray structure analyses

All the crystals were mounted on a Stoe Image Plate Diffraction system equipped with a ϕ circle goniometer, using Mo-Kα graphite monochromated radiation (λ = 0.71073 Å) with ϕ range 0-200º. The structures were solved by direct methods using the program SHELXS-97, while the refinement and all further calculations were carried out using SHELXL-97.[172] The H-atoms were included in calculated positions and treated as riding atoms using the SHELXL default parameters. The non-H atoms were refined anisotropically, using weighted full-matrix least-square on F^2. Crystallographic details are summarized in Table 14 - Table 23. ORTEP were used to draw the single crystal structures.[173]

Table 14. Crystallographic and structure refinement parameters for complex **1b**.

1b	
Chemical formula	$C_{54}H_{56}O_8P_2Ru_2$
Formula weight	1097.07
Crystal system	Triclinic
Space group	*P*-1 (No. 2)
Crystal colour and shape	Yellow block
Crystal size	0.23×0.19×0.16
a (Å)	13.2493(13)
b (Å)	14.4189(14)
c (Å)	15.0855(15)
α (°)	106.912(11)
β (°)	93.503(12)
γ (°)	109.986(11)
V (Å^3)	2549.6(4)
Z	2
T (K)	173(2)
D_c (g·cm^{-3})	1.429
μ (mm^{-1})	0.707
Scan range (°)	$2.17 < \theta < 26.18$
Unique reflections	9374
Reflections used [I>2σ(I)]	6441
R_{int}	0.0433
Final *R* indices [I>2σ(I)]*	0.0370, wR_2 0.0879
R indices (all data)	0.0658, wR_2 0.1115
Goodness-of-fit	1.010
Max, Min Δρ/e (Å^{-3})	0.836, -1.314

* Structure was refined on F_0^2: $wR_2 = [\Sigma [w (F_0^2 - F_c^2)^2]/ \Sigma w(F_0^2)^2]^{1/2}$, where $w^{-1} = [\Sigma(F_0^2) + (aP)^2 + bP]$ and $P = [\max(F_0^2, 0) + 2F_c^2]/3$.

Table 15. Crystallographic and structure refinement parameters for complex **2a**.

2a	
Chemical formula	$C_{32}H_{44}N_2O_8Ru_2$
Formula weight	786.83
Crystal system	Triclinic
Space group	*P*-1 (No. 2)
Crystal colour and shape	Yellow block
Crystal size	0.25×0.22×0.18
a (Å)	10.6836(8)
b (Å)	11.2916(9)
c (Å)	15.8511(13)
α (°)	69.609(6)
β (°)	82.296(6)
γ (°)	109.986(11)
V (Å^3)	1746.0(2)
Z	2
T (K)	173(2)
D_c (g·cm^{-3})	1.497
μ (mm^{-1})	0.913
Scan range (°)	$1.96 < \theta < 29.19$
Unique reflections	9140
Reflections used [I>2σ(I)]	4338
R_{int}	0.1547
Final *R* indices [I>2σ(I)]*	0.0795, wR_2 0.1691
R indices (all data)	0.1783, wR_2 0.1388
Goodness-of-fit	0.929
Max, Min Δρ/e (Å^{-3})	0.930, -0.839

* Structure was refined on F_0^2: $wR_2 = [\Sigma [w (F_0^2 - F_c^2)^2]/ \Sigma w(F_0^2)^2]^{1/2}$, where $w^{-1} = [\Sigma(F_0^2) + (aP)^2 + bP]$ and $P = [\max(F_0^2, 0) + 2F_c^2]/3.s$

Table 16. Crystallographic and structure refinement parameters for complex **3a**.

	3a
Chemical formula	$C_{32}H_{48}N_2O_8Ru_2$
Formula weight	814.88
Crystal system	Triclinic
Space group	*P*-1 (No. 2)
Crystal colour and shape	Yellow block
Crystal size	0.22×0.18×0.15
a (Å)	10.6712(6)
b (Å)	11.3078(7)
c (Å)	16.3035(11)
α (°)	78.011(5)
β (°)	84.539(5)
γ (°)	76.100(4)
V (Å^3)	1865.9(2)
Z	2
T (K)	173(2)
D_c (g·cm^{-3})	1.450
μ (mm^{-1})	0.858
Scan range (°)	$1.86 < \theta < 29.19$
Unique reflections	10080
Reflections used [I>2σ(I)]	6410
R_{int}	0.1053
Final *R* indices [I>2σ(I)]*	0.0529, wR_2 0.0837
R indices (all data)	0.1041, wR_2 0.0943
Goodness-of-fit	0.928
Max, Min Δρ/e (Å^{-3})	0.947, -0.857

* Structure was refined on F_0^2: $wR_2 = [\Sigma [w (F_0^2 - F_c^2)^2]/ \Sigma w(F_0^2)^2]^{1/2}$, where $w^{-1} = [\Sigma(F_0^2) + (aP)^2 + bP]$ and $P = [\max(F_0^2, 0) + 2F_c^2]/3$.

Table 17. Crystallographic and structure refinement parameters for complex **4a**.

	4a
Chemical formula	$C_{40}H_{60}N_2O_8Ru_2$
Formula weight	899.04
Crystal system	Triclinic
Space group	*P*-1 (No. 2)
Crystal colour and shape	Yellow block
Crystal size	0.16×0.13×0.11
a (Å)	10.6008(14)
b (Å)	10.9131(17)
c (Å)	18.886(3)
α (°)	94.899(13)
β (°)	96.721(12)
γ (°)	101.726(12)
V (Å^3)	2111.1(5)
Z	2
T (K)	173(2)
D_c (g·cm^{-3})	1.414
μ (mm^{-1})	0.765
Scan range (°)	$1.92 < \theta < 29.37$
Unique reflections	11378
Reflections used [I>2σ(I)]	3606
R_{int}	0.2887
Final *R* indices [I>2σ(I)]*	0.1064, wR_2 0.2178
R indices (all data)	0.2762, wR_2 0.2874
Goodness-of-fit	0.862
Max, Min Δρ/e (Å^{-3})	1.722, -1.187

* Structure was refined on F_0^2: $wR_2 = [\Sigma [w (F_0^2 - F_c^2)^2]/ \Sigma w(F_0^2)^2]^{1/2}$, where $w^{-1} = [\Sigma(F_0^2) + (aP)^2 + bP]$ and $P = [\max(F_0^2, 0) + 2F_c^2]/3$.

Table 18. Crystallographic and structure refinement parameters for complex **5a**.

	5a
Chemical formula	$C_{42}H_{64}N_2O_8Ru_2$
Formula weight	927.09
Crystal system	Triclinic
Space group	*P*-1 (No. 2)
Crystal colour and shape	Yellow block
Crystal size	0.24×0.21×0.16
a (Å)	10.6356(7)
b (Å)	11.1666(8)
c (Å)	19.3877(15)
α (°)	88.198(6)
β (°)	89.544(6)
γ (°)	76.654(6)
V (Å^3)	2239.3(3)
Z	2
T (K)	173(2)
D_c (g·cm^{-3})	1.414
μ (mm^{-1})	0.724
Scan range (°)	$1.88 < \theta < 29.19$
Unique reflections	12099
Reflections used [I>2σ(I)]	7893
R_{int}	0.1744
Final *R* indices [I>2σ(I)]*	0.0680, wR_2 0.1419
R indices (all data)	0.1120, wR_2 0.1574
Goodness-of-fit	0.967
Max, Min Δρ/e (Å^{-3})	0.687, -1.219

* Structure was refined on F_0^2: $wR_2 = [\Sigma [w (F_0^2 - F_c^2)^2]/ \Sigma w(F_0^2)^2]^{1/2}$, where $w^{-1} = [\Sigma(F_0^2) + (aP)^2 + bP]$ and $P = [\max(F_0^2, 0) + 2F_c^2]/3$.

Table 19. Crystallographic and structure refinement parameters for complexes **8a**.

	8a
Chemical formula	$C_{22}H_{10}F_{14}N_2O_8Ru_2$
Formula weight	898.46
Crystal system	Monoclinic
Space group	*C* 2/*c* (no. 15)
Crystal colour and shape	Yellow block
Crystal size	0.24 x 0.20 x 0.17
a (Å)	15.630(3)
b (Å)	17.900(4)
c (Å)	10.860(2)
β (°)	106.41(3)
V (Å^3)	2914.6(10)
Z	4
T (K)	293(2)
D_c (g·cm^{-3})	2.048
μ (mm^{-1})	1.175
Scan range (°)	2.28 < θ < 26.10
Unique reflections	2797
Observed refls [I>2σ(I)]	1918
R_{int}	0.0441
Final *R* indices [I>2σ(I)]*	0.0440, wR_2 0.1231
R indices (all data)	0.0616, wR_2 0.1304
Goodness-of-fit	0.998
Max, Min Δρ/e (Å^{-3})	1.053, -0.531

* Structure was refined on F_0^2: $wR_2 = [\Sigma [w (F_0^2 - F_c^2)^2]/ \Sigma w(F_0^2)^2]^{1/2}$, where $w^{-1} = [\Sigma(F_0^2) + (aP)^2 + bP]$ and $P = [\max(F_0^2, 0) + 2F_c^2]/3$.

Table 20. Crystallographic and structure refinement parameters for complexes **10**.

	10
Chemical formula	$C_{48}H_{44}O_8P_2Ru_2$
Formula weight	1012.91
Crystal system	Monoclinic
Space group	*C* 2/*c* (no. 15)
Crystal colour and shape	Yellow block
Crystal size	0.25 x 0.23 x 0.18
a (Å)	24.7037(11)
b (Å)	9.5100(3)
c (Å)	18.9324(9)
β (°)	102.530(4)
V (Å^3)	4341.9(3)
Z	4
T (K)	173(2)
D_c (g·cm^{-3})	1.550
μ (mm^{-1})	0.824
Scan range (°)	1.69 < θ < 29.22
Unique reflections	5854
Observed refls [I>2σ(I)]	4532
R_{int}	0.0842
Final *R* indices [I>2σ(I)]*	0.0491, wR_2 0.0876
R indices (all data)	0.0734, wR_2 0.0944
Goodness-of-fit	1.044
Max, Min Δρ/e (Å^{-3})	0.896, -0.799

* Structures were refined on F_0^2: $wR_2 = [\Sigma[w (F_0^2 - F_c^2)^2] / \Sigma w (F_0^2)^2]^{1/2}$, where $w^{-1} = [\Sigma(F_0^2) + (aP)^2 + bP]$ and $P = [\max(F_0^2, 0) + 2F_c^2]/3$.

Table 21. Crystallographic and structure refinement parameters for complexes **13b**.

	13b
Chemical formula	$C_{76}H_{52}O_8P_2Ru_2$
Formula weight	1357.26
Crystal system	Triclinic
Space group	*P* -1 (no. 2)
Crystal colour and shape	Yellow block
Crystal size	0.17 x 0.16 x 0.12
a (Å)	9.9733(4)
b (Å)	10.8151(5)
c (Å)	28.7024(13)
α (°)	89.544(3)
β (°)	87.422(4)
γ (°)	78.134(3)
V (Å^3)	3026.7(2)
Z	2
T (K)	173(2)
D_c (g·cm^{-3})	1.489
μ (mm^{-1})	0.612
Scan range (°)	1.92 < θ< 29.21
Unique reflections	16278
Observed refls [I>2σ(I)]	12255
R_{int}	0.0687
Final *R* indices [I>2σ(I)]*	0.0444, *wR*2 0.0755
R indices (all data)	0.0721, *wR*2 0.0817
Goodness-of-fit	1.025
Max, Min Δρ/e (Å^{-3})	0.565, - 0.657

* Structures were refined on F_0^2: $wR_2 = [\Sigma[w (F_0^2 - F_c^2)^2] / \Sigma w (F_0^2)^2]^{1/2}$, where $w^{-1} = [\Sigma(F_0^2) + (aP)^2 + bP]$ and $P = [\max(F_0^2, 0) + 2F_c^2]/3$

Table 22. Crystallographic and structure refinement parameters for complexes **14b**.

14b · $2C_6H_5Me$	
Chemical formula	$C_{94}H_{76}O_8P_2Ru_2$
Formula weight	1597.63
Crystal system	Monoclinic
Space group	*C* 2/*c* (no. 15)
Crystal colour and shape	Yellow block
Crystal size	0.24 x 0.20 x 0.19
a (Å)	36.0388(15)
b (Å)	9.1563(3)
c (Å)	28.5506(9)
α (°)	90
β (°)	126.953(2)
γ (°)	90
V (Å^3)	7528.7(5)
Z	4
T (K)	173(2)
D_c (g·cm^{-3})	1.409
μ (mm^{-1})	0.504
Scan range (°)	$1.79 < \theta < 29.19$
Unique reflections	10175
Observed refls [I>2σ(I)]	7424
R_{int}	0.1236
Final *R* indices [I>2σ(I)]*	0.0558, wR_2 0.0752
R indices (all data)	0.0911, wR_2 0.0816
Goodness-of-fit	1.055
Max, Min Δρ/e (Å^{-3})	0.546, -1.274

* Structures were refined on F_0^2: $wR_2 = [\Sigma[w (F_0^2 - F_c^2)^2] / \Sigma w (F_0^2)^2]^{1/2}$, where $w^{-1} = [\Sigma(F_0^2) + (aP)^2 + bP]$ and $P = [\max(F_0^2, 0) + 2F_c^2]/3$

Table 23. Crystallographic and structure refinement parameters for complex **34a** · 0.5 C_6H_6.

34a · 0.5 C_6H_6	
Chemical formula	$C_{43}H_{49}N_4O_{12}Ru_2S_2$
Formula weight	1080.12
Crystal system	Triclinic
Space group	*P* -1 (no. 2)
Crystal colour and shape	Yellow block
Crystal size	0.23 x 0.19 x 0.16
a (Å)	10.4848(6)
b (Å)	15.3189(11)
c (Å)	18.2466(12)
α (°)	72.648(5)
β (°)	84.706(5)
γ (°)	73.398(5)
V (Å^3)	2680.6(3)
Z	2
T (K)	173(2)
D_c (g·cm^{-3})	1.338
μ (mm^{-1})	0.697
Scan range (°)	1.58 < θ < 29.26
Unique reflections	14483
Observed refls [I>2σ(I)]	9716
R_{int}	0.1231
Final *R* indices [I>2σ(I)]*	0.0910, wR_2 0.1523
R indices (all data)	0.1472, wR_2 0.1734
Goodness-of-fit	1.131
Max, Min Δρ/e (Å^{-3})	0.847, - 1.939

* Structure was refined on F_0^2: $wR_2 = [\Sigma[w\ (F_0^2 - F_c^2)^2] / \Sigma w\ (F_0^2)^2]^{1/2}$, where $w^{-1} = [\Sigma(F_0^2) + (aP)^2 + bP]$ and $P = [\max(F_0^2, 0) + 2F_c^2]/3$.

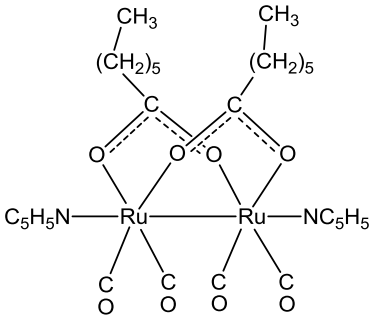

1a

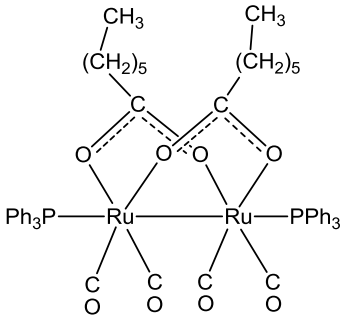

1b

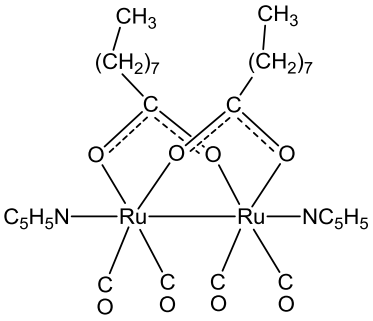

2a

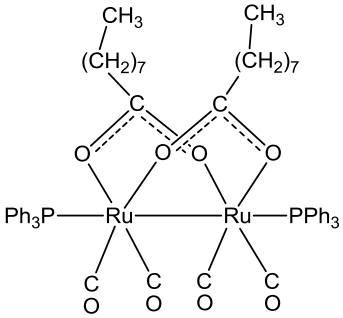

2b

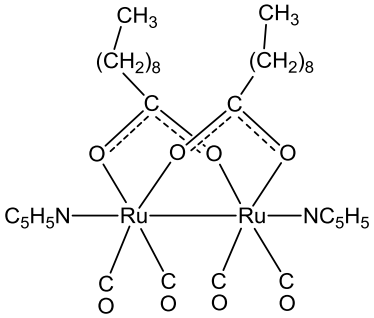

3a

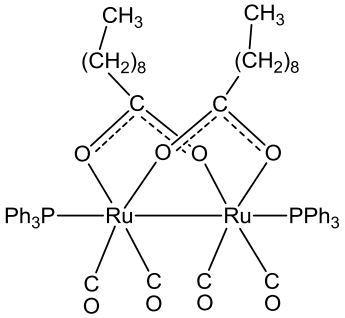

3b

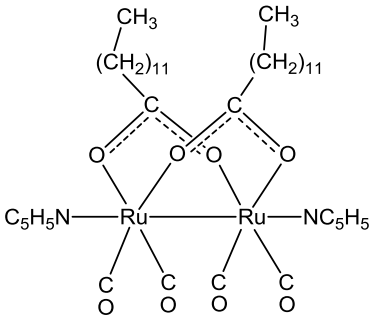

4a

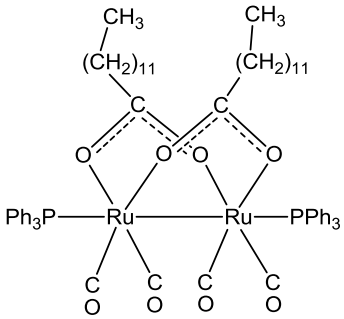

4b

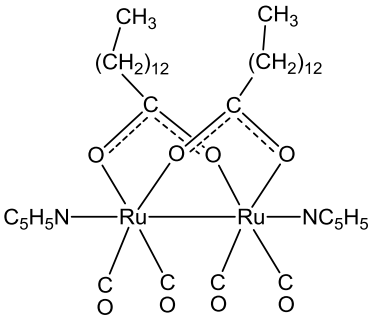

5a

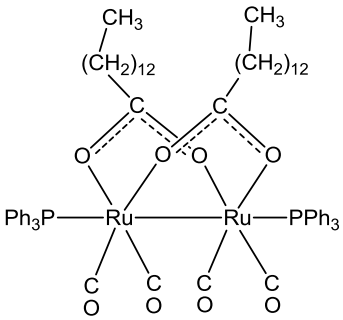

5b

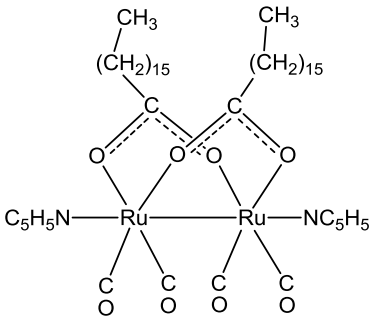

6a

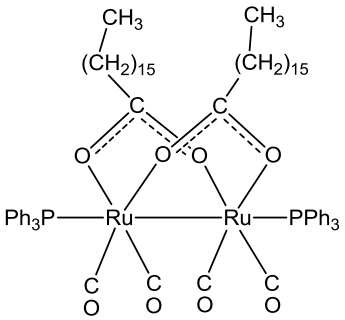

6b

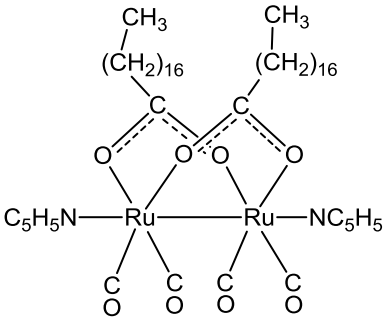

7a

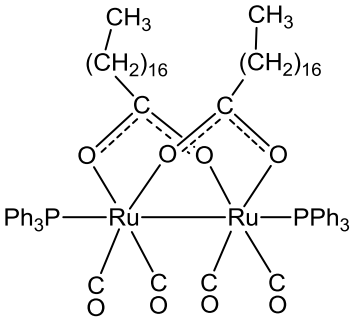

7b

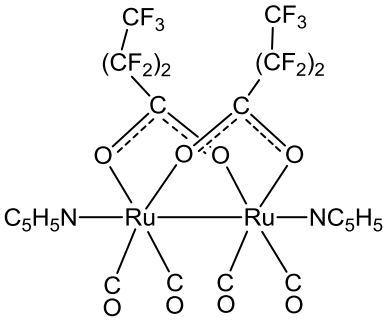

8a

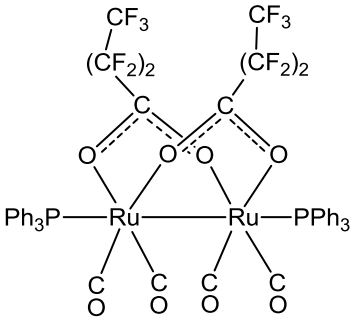

8b

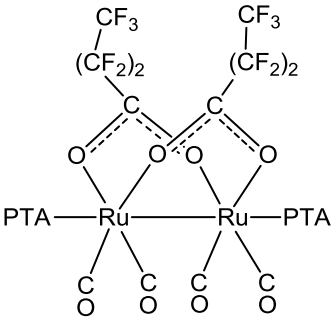

8c

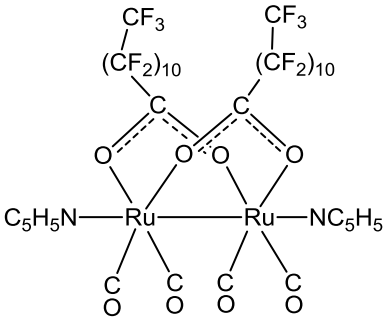

9a

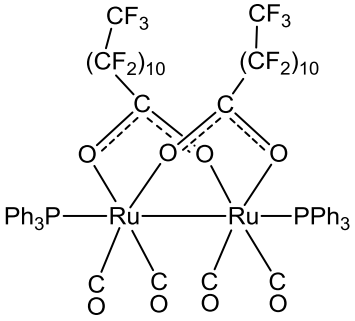

9b

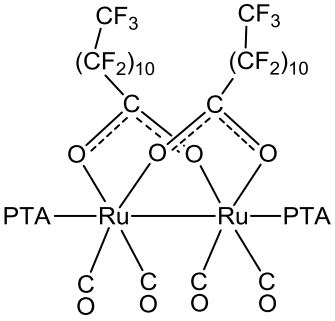

9c

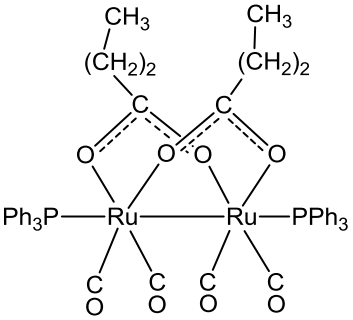

10

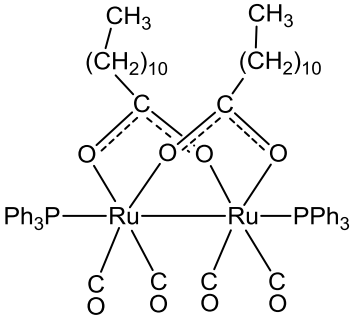

11

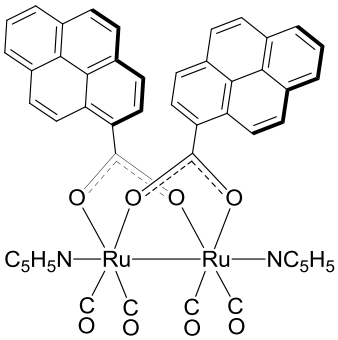

12a

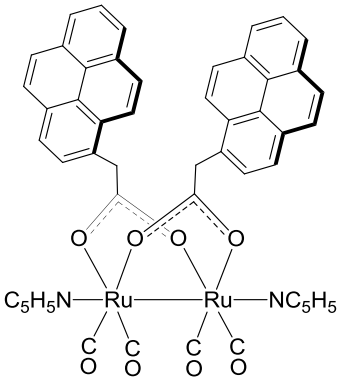

13a

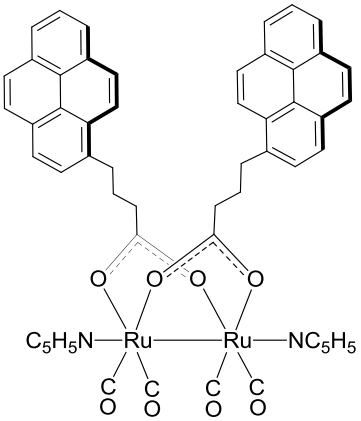

14a

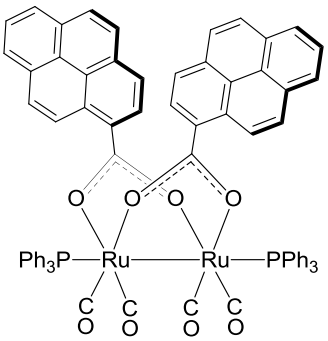

12b

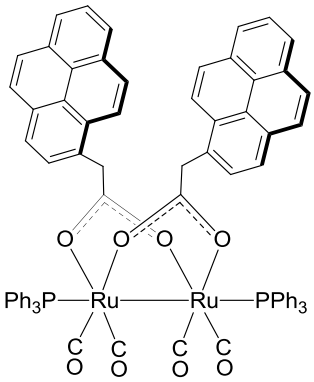

13b

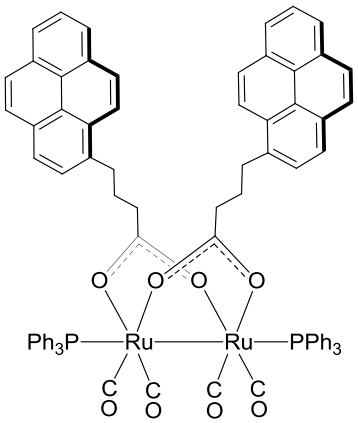

14b

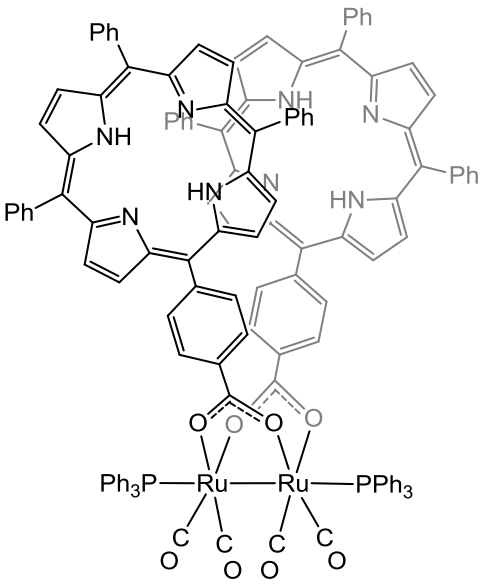

15

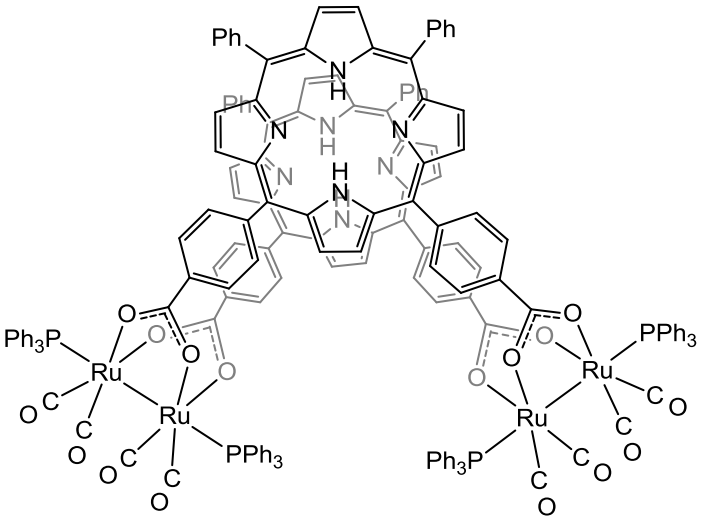

16

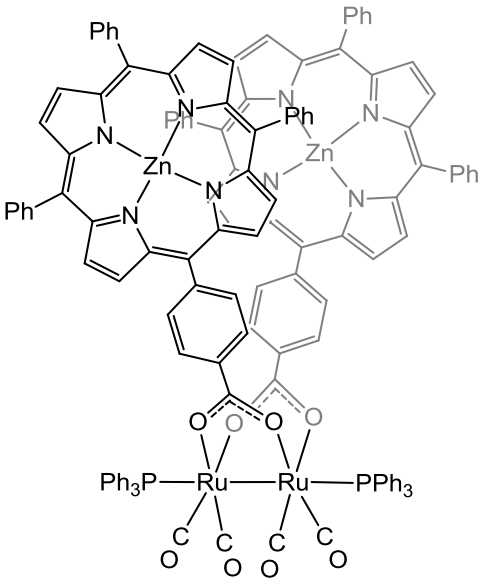

17

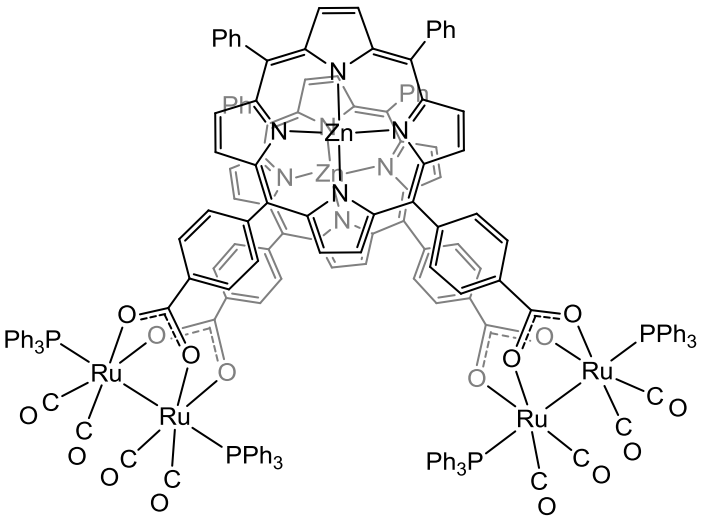

18

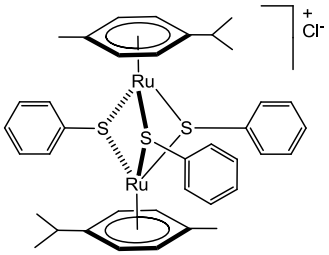

19

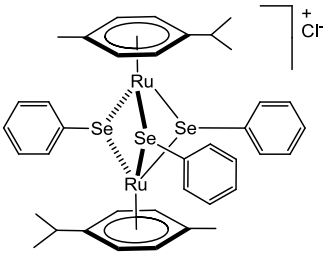

20

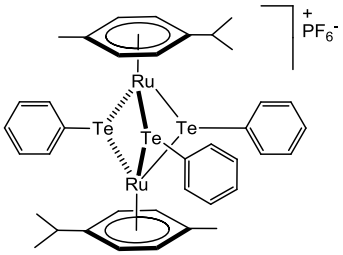

21

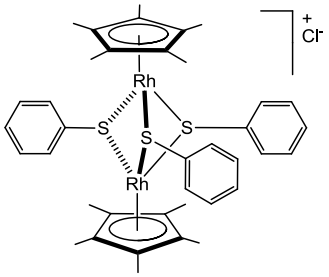

22

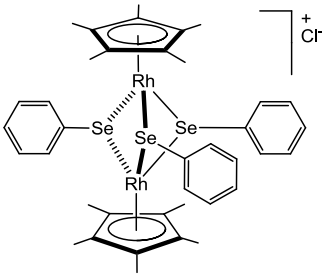

23

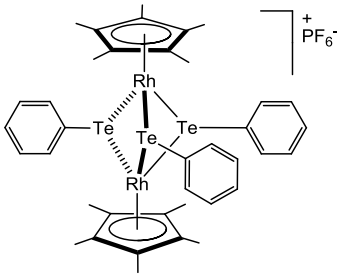

24

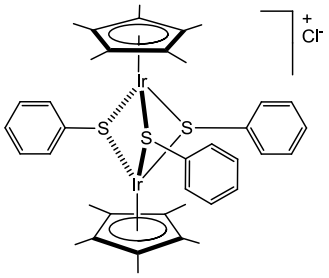

25

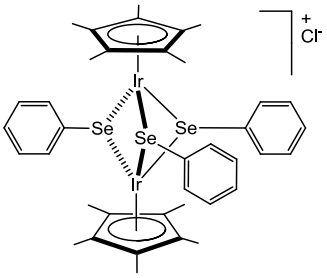

26

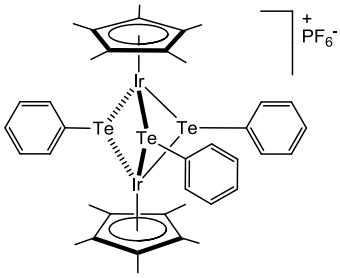

27

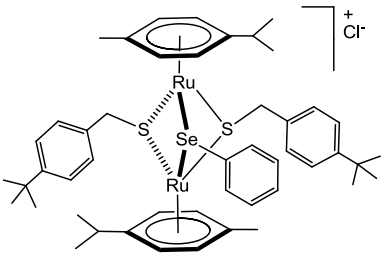

28

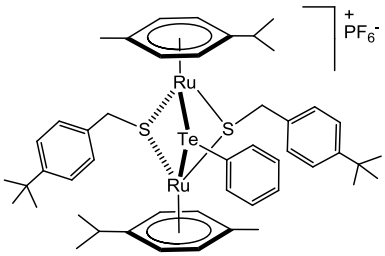

29

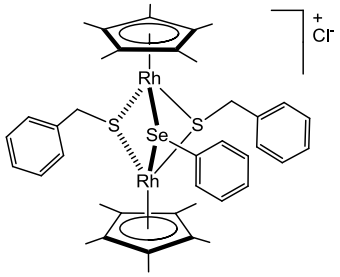

30

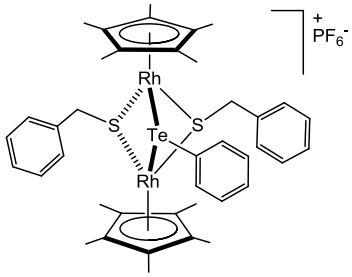

31

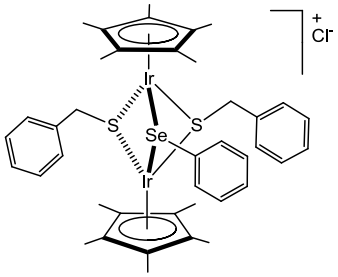

32

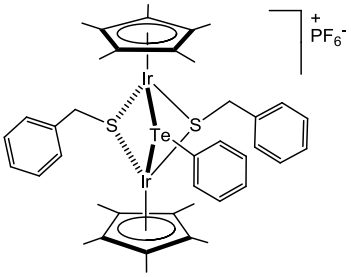

33

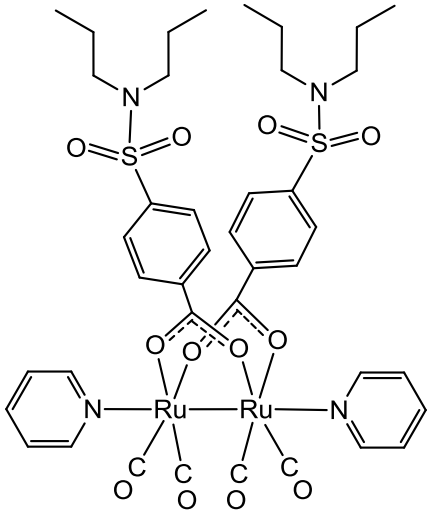

34a

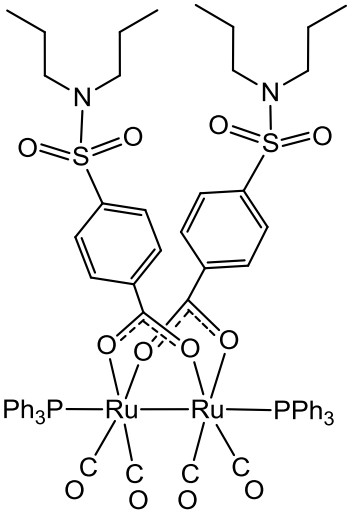

34b

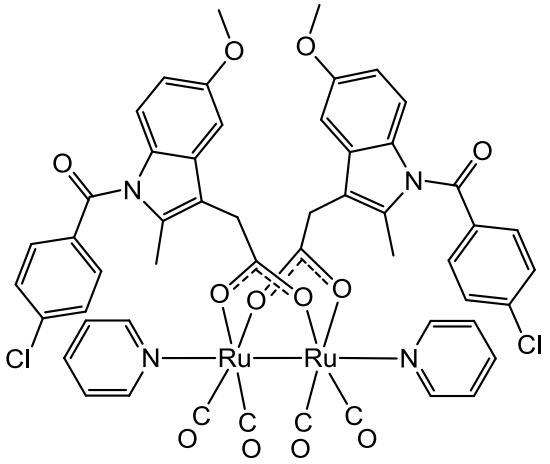

35a

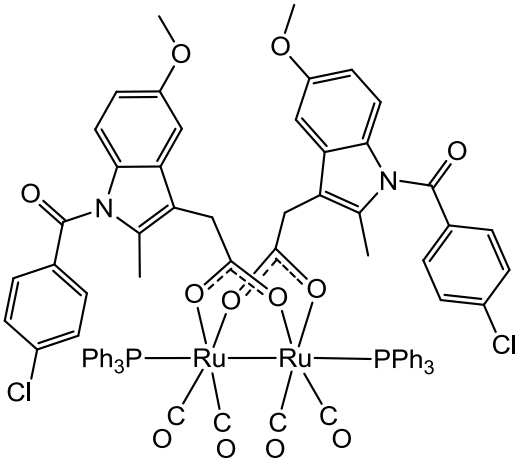

35b

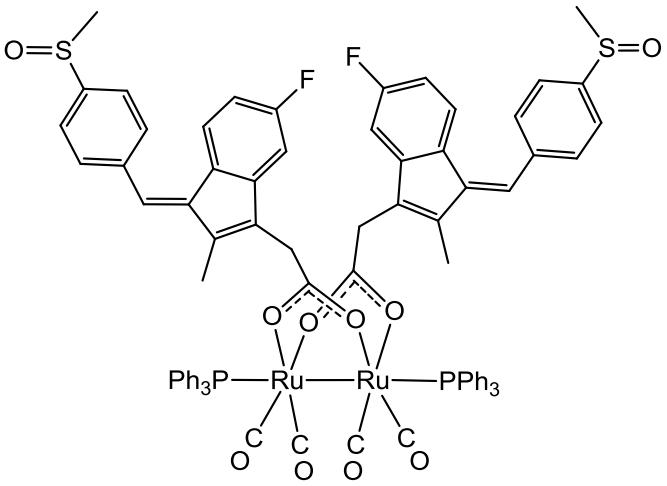

36

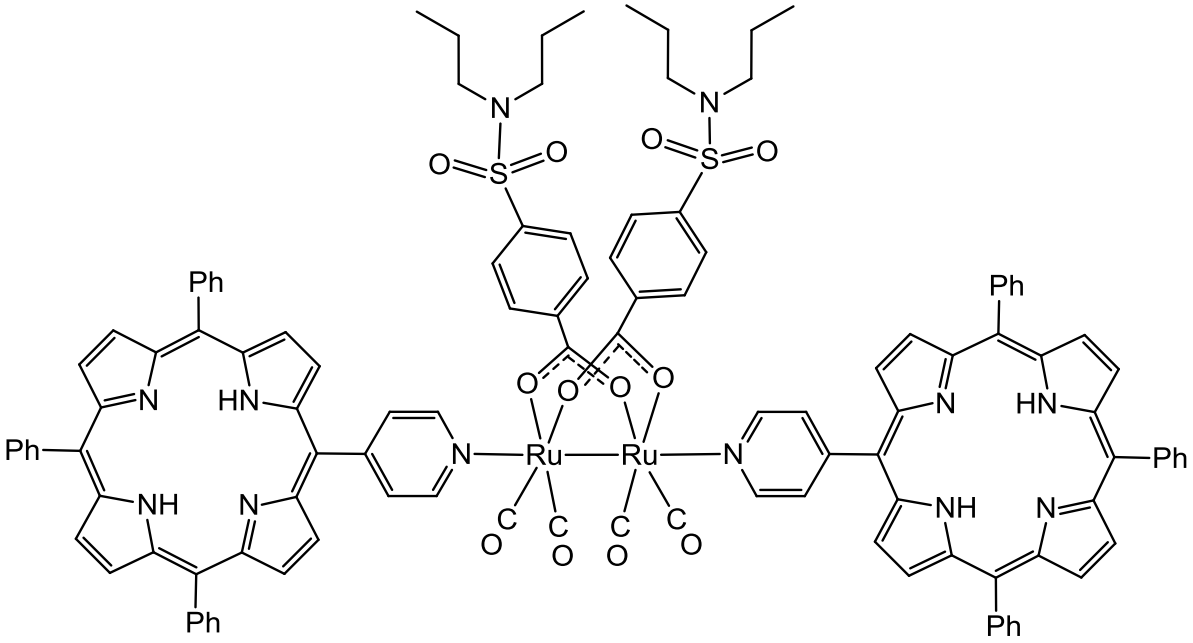

34c

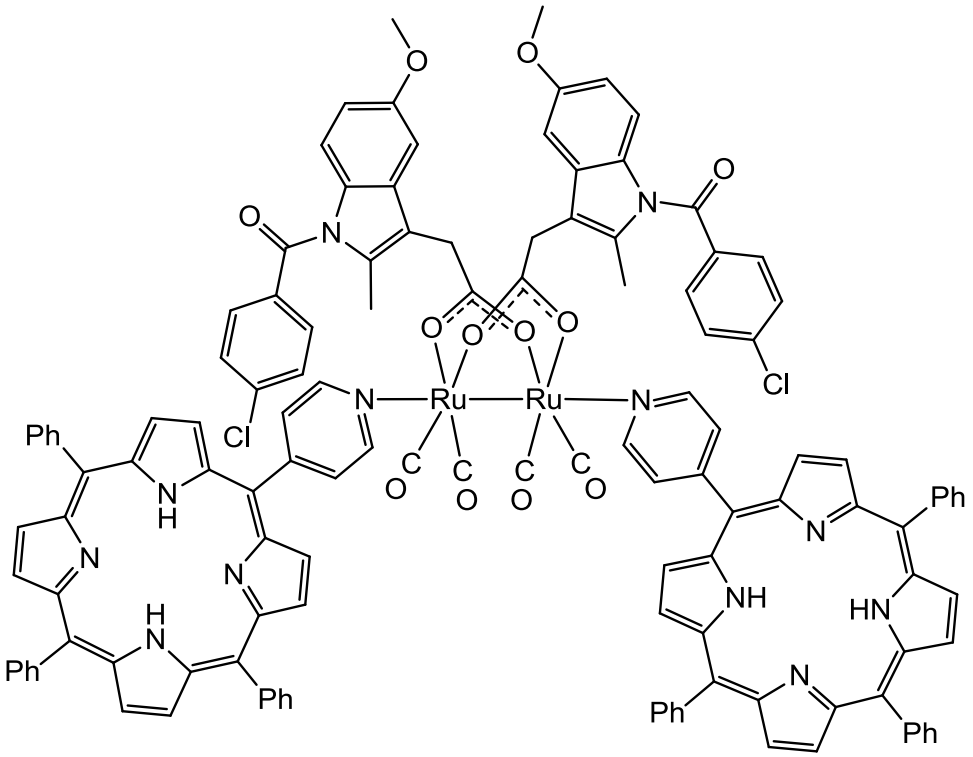

35c

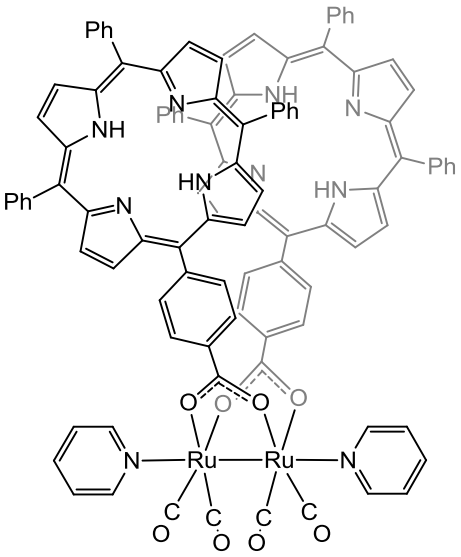

37

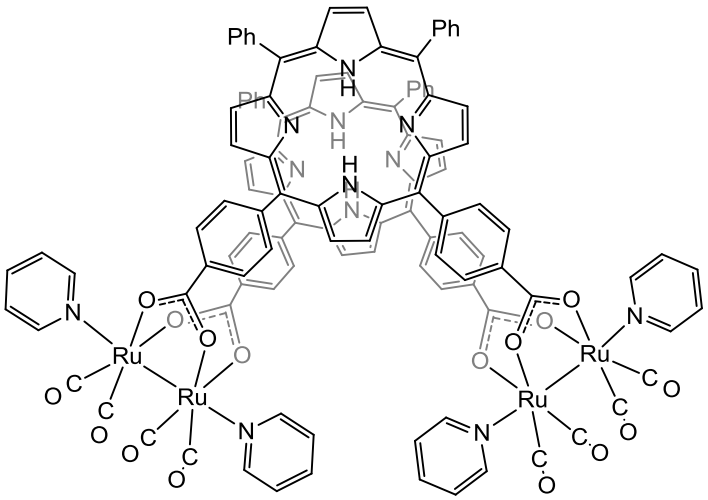

39

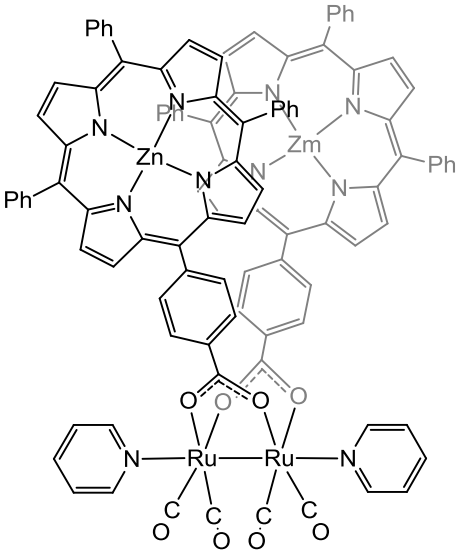

38

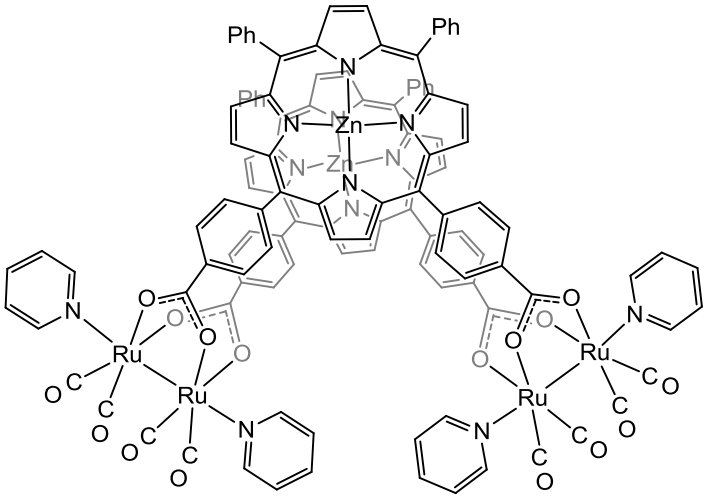

40

(1) Li, H.; Feng, H.; Sun, W.; King, R. K.; Schaefer, H. F. *Inorg. Chem.*, **2013**, *52*, 6893.

(2) Bruce, M. I.; Jensen, C. M.; Jones, N. L. *Inorg. Synth.*, **1989**, *26*, 259.

(3) Fauré, M.; Saccavini, C.; lavigne, G. *Inorg. Synth.*, **2004**, *34*, 110.

(4) (a) James, B. R.; Rempel, G. L.; Teo, W. K. *Inorg. Synth.*, **1975**, *16*, 45; (b) Mantovani, A.; Cenini, S. *Inorg. Synth.*, **1975**, *16*, 47.

(5) Leadbeater, N. E.; Shoemaker, K. A. *Organometallics*, **2008**, *27*, 1254.

(6) Mason, R.; Rae, A. I. M. *J. Chem. Soc. A.*, **1968**, 778.

(7) Therrien, B.; Süss-Fink, G. *Coord. Chem. Rev.*, **2009**, *253*, 2639.

(8) Crooks, G. R.; Johnson, B. F. G.; Lewis, J.; Williams, I. G.; Gamlen, G. *J. Chem. Soc. A.*, **1969**, 2761.

(9) Schumann, H.; Opitz, J.; Pickardt, J. *J. Organomet. Chem.*, **1977**, *128*, 253.

(10) Bright, T. A.; Jones, R. A.; Nunn, C. M. *J. Coord. Chem.*, **1988**, *18*, 361.

(11) Süssfink, G.; Herrmann, G.; Morys, P.; Ellermann, J.; Veit, A. *J. Organomet. Chem.*, **1985**, *284*, 263.

(12) (a) Auzias, M.; Mattsson, J.; Therrien, B.; Süss-Fink, G. *Z. Anorg. Allg. Chem.*, **2009**, *635*, 115; (b) Schmitt, F.; Auzias, M.; Štěpnička, P.; Sei, Y.; Yamaguchi, K.; Süss-Fink, G.; Therrien, B.; Juillerat-Jeanneret, L. *J. Biol. Inorg. Chem.*, **2009**, *14*, 693; (c) Frein, S.; Auzias, M.; Sondenecker, A.; Vieille-Petit, L.; Guintchin, B.; Maringa, N.; Süss-Fink, G.; Barbera, J.; Deschenaux, R. *Chem. Mater.*, **2008**, *20*, 1340; (d) Auzias, M.; Therrien, B.; Labat, G.; Stoeckli-Evans, H.; Süss-Fink, G. *Inorg. Chim. Acta.*, **2006**, *359*, 1012; (e) Auzias, M.; Therrien, B.; Süss-Fink, G.; Stepnicka, P.; Ludvik, J. *J. Organomet. Chem.*, **2007**, *692*, 755; (f) Auzias, M.; Therrien, B.; Süss-Fink, G. *Inorg. Chem. Commun.*, **2007**, *10*, 1420.

(13) (a) Neumann, F.; Stoeckli-Evans, H.; Süss-Fink, G. *J. Organomet. Chem.*, **1989**, *379*, 139; (b) Auzias, M.; Therrien, B.; Süss-Fink, G. *Acta. Crystallogr. E.*, **2005**, *61*, M2426.

(14) (a) Neumann, F.; Süss-Fink, G. *J. Organomet. Chem.*, **1989**, *367*, 175; (b) Neumann, F.; Stoeckli-Evans, H.; Süss-Fink, G. *J. Organomet. Chem.*, **1989**, *379*, 151.

(15) Langenbahn, M.; Stoeckli-Evans, H.; Süss-Fink, G. *J. Organomet. Chem.*, **1990**, *397*, 347.

(16) Rheinwald, G.; Stoeckli-Evans, H.; Süss-Fink, G. *J. Organomet. Chem.*, **1992**, *441*, 295.

(17) Kepert, C. M.; Deacon, G. B.; Spiccia, L.; Fallon, G. D.; Skelton, B. W.; White, A. H. *J. Chem. Soc., Dalton Trans.*, **2000**, 2867.

(18) Anderson, P. A.; Deacon, G. B.; Haarmann, K. H.; Keene, F. R.; Meyer, T. J.; Reitsma, D. A.; Skelton, B. W.; Strouse, G. F.; Thomas, N. C.; Treadway, J. A.; White, A. H. *Inorg. Chem.*, **1995**, *34*, 6145.

(19) (a) Frediani, P.; Giannelli, C.; Salvini, A.; Ianelli, S. *J. Organomet. Chem.*, **2003**, *667*, 197; (b) Frediani, P.; Bianchi, M.; Salvini, A.; Guarducci, R.; Carluccio, L. C.; Piacenti, F. *J. Organomet. Chem.*, **1995**, *498*, 187.

(20) Salvini, A.; Frediani, P.; Piacenti, F. *J. Mol. Catal. a-Chem.*, **2000**, *159*, 185.

(21) Byerley, J. J.; Rempel, G. L.; Takebe, N.; James, B. R. *J. Chem. Soc. D.*, **1971**, 1482.

(22) (a) Maas, G.; Werle, T.; Alt, M.; Mayer, D. *Tetrahedron*, **1993**, *49*, 881; (b) Werle, T.; Maas, G. *Adv Synth Catal* **2001**, *343*, 37.

(23) (a) Rotem, M.; Shvo, Y. *Organometallics*, **1983**, *2*, 1689; (b) Hua, R. M.; Tanaka, M. *Chem. Lett.*, **1998**, 431.

(24) Salvini, A.; Frediani, P.; Giannelli, C.; Rosi, L. *J. Organomet. Chem.*, **2005**, *690*, 371.

(25) Salvini, A.; Frediani, P.; Rivalta, E. *Inorg. Chim. Acta.*, **2003**, *351*, 225.

(26) Wolfender, J. L.; Neumann, F.; Süss-Fink, G. *J. Organomet. Chem.*, **1990**, *389*, 351.

(27) Schmidt, G. F.; Süss-Fink, G. *J. Organomet. Chem.*, **1989**, *362*, 179.

(28) Matteoli, U.; Menchi, G.; Frediani, P.; Bianchi, M.; Piacenti, F. *J. Organomet. Chem.*, **1985**, *285*, 281.

(29) Bianchi, M.; Menchi, G.; Francalanci, F.; Piacenti, F.; Matteoli, U.; Frediani, P.; Botteghi, C. *J. Organomet. Chem.*, **1980**, *188*, 109.

(30) (a) Matteoli, U.; Bianchi, M.; Menchi, G.; Frediani, P.; Piacenti, F. *J. Mol. Catal.*, **1985**, *29*, 269; (b) Matteoli, U.; Menchi, G.; Bianchi, M.; Piacenti, F. *J. Organomet. Chem.*, **1986**, *299*, 233; (c) Matteoli, U.; Menchi, G.; Bianchi, M.; Piacenti, F.; Ianelli, S.; Nardelli, M. *J. Organomet. Chem.*, **1995**, *498*, 177.

(31) Winkhaus, G.; Singer, H. *J. Organomet. Chem.*, **1967**, *7*, 487.

(32) Zelonka, R. A.; Baird, M. C. *Can. J. Chem.*, **1972**, *50*, 3063.

(33) Bennett, M. A.; Smith, A. K. *J. Chem. Soc., Dalton Trans.*, **1974**, 233.

(34) Canivet, J.; Therrien, B.; Süss-Fink, G. *Acta. Crystallogr. E.*, **2005**, *61*, M1090.

(35) Bennett, M. A.; Huang, T. N.; Matheson, T. W.; Smith, A. K. *Inorg. Synth.*, **1982**, *21*, 74.

(36) Kang, J. W.; Moseley, K.; Maitlis, P. M. *J. Am. Chem. Soc.*, **1969**, *91*, 5970.

(37) White, C.; Yates, A.; Maitlis, P. M.; Heinekey, D. M. *Inorg. Synth.,* **1992**, *29*, 228.

(38) (a) Ibao, A.-F.; Gras, M.; Therrien, B.; Süss-Fink, G.; Zava, O.; Dyson, P. J. *Eur. J. Inorg. Chem.*, **2012**, 1531; (b) Dance, I. G. *Polyhedron,* **1986**, *5*, 1037; (c) Blower, P. J.; Dilworth, J. R. *Coord. Chem. Rev.*, **1987**, *76*, 121.

(39) Schacht, H. T.; Haltiwanger, R. C.; Dubois, M. R. *Inorg. Chem.,* **1992**, *31*, 1728.

(40) Mashima, K.; Mikami, A.; Nakamura, A. *Chem. Lett.*, **1992**, 1795.

(41) Nishio, M.; Matsuzaka, H.; Mizobe, Y.; Hidai, M. *Inorg. Chim. Acta.,* **1997**, *263*, 119.

(42) (a) Chérioux, F.; Therrien, B.; Süss-Fink, G. *Eur. J. Inorg. Chem.*, **2003**, 1043; (b) Cherioux, F.; Therrien, B.; Süss-Fink, G. *Inorg. Chim. Acta.,* **2004**, *357*, 834; (c) Cherioux, F.; Therrien, B.; Sadki, S.; Comminges, C.; Süss-Fink, G. *J. Organomet. Chem.,* **2005**, *690*, 2365.

(43) Gras, M.; Therrien, B.; Süss-Fink, G.; Zava, O.; Dyson, P. J. *Dalton Trans.,* **2010**, *39*, 10305.

(44) Burk, M. J.; Feng, S. G.; Gross, M. F.; Tumas, W. *J. Am. Chem. Soc.,* **1995**, *117*, 8277.

(45) Noyori, R. *Chem. Commun.,* **2005**, 1807.

(46) Jessop, P. G.; Hsiao, Y.; Ikariya, T.; Noyori, R. *J. Am. Chem. Soc.,* **1996**, *118*, 344.

(47) Jessop, P. G.; Ikariya, T.; Noyori, R. *Nature,* **1994**, *368*, 231.

(48) Jessop, P. G.; Hsiao, Y.; Ikariya, T.; Noyori, R. *J. Am. Chem. Soc.,* **1994**, *116*, 8851.

(49) Xiao, J. L.; Nefkens, S. C. A.; Jessop, P. G.; Ikariya, T.; Noyori, R. *Tetrahedron Lett.,* **1996**, *37*, 2813.

(50) Kainz, S.; Koch, D.; Baumann, W.; Leitner, W. *Angew. Chem. Int. Ed.,* **1997**, *36*, 1628.

(51) (a) Ikariya, T.; Noyori, R.; Green chemistry using liquid and supercritical carbon dioxide; Oxford university press: Oxford, U. K, 2003, pp 56-57; (b) Berven, B. M.; Koutsantonis, G. A.; Skelton, B. W.; Trengove, R. D.; White, A. H. *Inorg. Chem.,* **2009**, *48*, 11832.

(52) He, L.-N.; Choi, J.-C.; Sakakura, T. *Tetrahedron Lett.,* **2001**, *42*, 2169.

(53) (a) Johnpeter, J. P.; Therrien, B. *J. Struct. Chem.,* **2011**, *52*, 151; (b) Johnpeter, J. P.; Plasseraud, L.; Schmitt, F.; Juillerat-Jeanneret, L.; Therrien, B. *J. Coord. Chem.,* **2013**, *66*, 1753.

(54) Auzias, M.; Therrien, B.; Süss-Fink, G. *Inorg. Chim. Acta.,* **2006**, *359*, 3412.

(55) Tsuzuki, S.; Honda, K.; Uchimaru, T.; Mikami, M.; Tanabe, K. *J. Am. Chem. Soc.*, **2002**, *124*, 104.

(56) (a) Jessop, P. G.; Ikariya, T.; Noyori, R. *Chem. Rev.*, **1999**, *99*, 475; (b) Ikariya, T.; Kayaki, Y. *Catal. Surv. Jpn.*, **2000**, *4*, 39.

(57) Altinel, H.; Avsar, G.; Yilmaz, M. K.; Guzel, B. *J. Supercrit. Fluids.*, **2009**, *51*, 202.

(58) Hagen, C. M.; Vieille-Petit, L.; Laurenczy, G.; Süss-Fink, G.; Finke, R. G. *Organometallics*, **2005**, *24*, 1819.

(59) Chen, C. W.; Whitlock, H. W. *J. Am. Chem. Soc.*, **1978**, *100*, 4921.

(60) (a) Zimmerman, S. C.; Vanzyl, C. M. *J. Am. Chem. Soc.*, **1987**, *109*, 7894; (b) Zimmerman, S. C.; Wu, W. M. *J. Am. Chem. Soc.*, **1989**, *111*, 8054; (c) Zimmerman, S. C.; Wu, W. M.; Zeng, Z. J. *J. Am. Chem. Soc.*, **1991**, *113*, 196.

(61) (a) Sygula, A.; Fronczek, F. R.; Sygula, R.; Rabideau, P. W.; Olmstead, M. M. *J. Am. Chem. Soc.*, **2007**, *129*, 3842; (b) Hardouin-Lerouge, M.; Hudhomme, P.; Salle, M. *Chem. Soc. Rev.*, **2011**, *40*, 30; (c) Leblond, J.; Petitjean, A. *ChemPhysChem*, **2011**, *12*, 1043; (d) Korendovych, I. V.; Roesner, R. A.; Rybak-Akimova, E. V. *Adv. Inorg. Chem.*, **2006**, *59*, 109.

(62) (a) Gorlich, D.; Kutay, U. *Annu. Rev. Cell Dev. Biol.*, **1999**, *15*, 607; (b) Meyer, E. A.; Castellano, R. K.; Diederich, F. *Angew. Chem. Int. Ed.*, **2003**, *42*, 1210; (c) Klärner, F. G.; Kahlert, B. *Acc. Chem. Res.*, **2003**, *36*, 919.

(63) Wu, J. I.; Dobrowolski, M. A.; Cyrański, M. K.; Merner, B. L.; Bodwell, G. J.; Mo, Y.; Schleyer, P. V. *Mol. Phys.*, **2009**, *107*, 1177.

(64) Randić, M. *Chem. Rev.*, **2003**, *103*, 3449.

(65) Baba, M.; Saitoh, M.; Kowaka, Y.; Taguma, K.; Yoshida, K.; Semba, Y.; Kasahara, S.; Yamanaka, T.; Ohshima, Y.; Hsu, Y. C.; Lin, S. H. *J. Chem. Phys.*, **2009**, *131*.

(66) (a) Winnik, F. M.; Winnik, M. A.; Ringsdorf, H.; Venzmer, J. *J. Phys. Chem.*, **1991**, *95*, 2583; (b) Yamana, K.; Iwai, T.; Ohtani, Y.; Sato, S.; Nakamura, M.; Nakano, H. *Bioconjugate Chem.*, **2002**, *13*, 1266; (c) Yamana, K.; Ohshita, Y.; Fukunaga, Y.; Nakamura, M.; Maruyama, A. *Bioorg. Med. Chem.*, **2008**, *16*, 78; (d) Hu, J.-Y.; Pu, Y.-J.; Nakata, G.; Kawata, S.; Sasabe, H.; Kido, J. *Chem. Commun.*, **2012**, *48*, 8434.

(67) Fernández-Lodeiro, J.; Núñez, C.; de Castro, C. S.; Bértolo, E.; de Melo, J. S. S.; Capelo, J. L.; Lodeiro, C. *Inorg. Chem.*, **2013**, *52*, 121.

(68) (a) Colquhoun, H. M.; Zhu, Z. X.; Williams, D. J. *Org. Lett.*, **2003**, *5*, 4353; (b) Colquhoun, H. M.; Zhu, Z.; Cardin, C. J.; Gan, Y.; Drew, M. G. B. *J. Am. Chem. Soc.*, **2007**, *129*, 16163.

(69) He, X. P.; Xie, J.; Chen, G. R.; Chen, K. X. *Chin. J. Chem.*, **2012**, *30*, 2874.

(70) (a) D`Souza, L. J.; Maitra, U. *J. Org. Chem.*, **1996**, *61*, 9494; (b) Potluri, V. K.; Maitra, U. *J. Org. Chem.*, **2000**, *65*, 7764.

(71) Narita, M.; Mima, S.; Ogawa, N.; Hamada, F. *Anal. Sci.*, **2001**, *17*, 379.

(72) Sahin, O.; Yilmaz, M. *Tetrahedron*, **2011**, *67*, 3501.

(73) Jeon, Y.-M.; Kim, D.; Mirkin, C. A.; Golen, J. A.; Rheingold, A. L. *Tetrahedron*, **2008**, *64*, 8428.

(74) Slagt, M. Q.; Jastrzebski, J. T. B. H.; Gebbink, R. J. M. K.; van Ramesdonk, H. J.; Verhoeven, J. W.; Ellis, D. D.; Spek, A. L.; van Koten, G. *Eur. J. Org. Chem.*, **2003**, 1692.

(75) Cho, H. K.; Lee, D. H.; Hong, J. I. *Chem. Commun.*, **2005**, 1690.

(76) Hu, J.; Nguyen, M. H.; Yip, J. H. K. *Inorg. Chem.*, **2011**, *50*, 7429.

(77) (a) Shoji, Y.; Tashiro, K.; Aida, T. *J. Am. Chem. Soc.*, **2010**, *132*, 5928; (b) Schmittel, M.; He, B.; Mal, P. *Org. Lett.*, **2008**, *10*, 2513; (c) Marois, J. S.; Cantin, K.; Desmarais, A.; Morin, J.-F. *Org. Lett.*, **2008**, *10*, 33; (d) Fukuzumi, S.; Honda, T.; Ohkubo, K.; Kojima, T. *Dalton Trans.*, **2009**, 3880; (e) Gil-Ramírez, G.; Karlen, S. D.; Shundo, A.; Porfyrakis, K.; Ito, Y.; Briggs, G. A. D.; Morton, J. J. L.; Anderson, H. L. *Org. Lett.*, **2010**, *12*, 3544; (f) Tong, L. H.; Wietor, J. L.; Clegg, W.; Raithby, P. R.; Pascu, S. I.; Sanders, J. K. M. *Chem.-Eur. J.*, **2008**, *14*, 3035; (g) Olmstead, M. M.; Costa, D. A.; Maitra, K.; Noll, B. C.; Phillips, S. L.; Van Calcar, P. M.; Balch, A. L. *J. Am. Chem. Soc.*, **1999**, *121*, 7090; (h) Perez, E. M.; Martin, N. *Pure Appl. Chem.*, **2010**, *82*, 523.

(78) Solladié, N.; Aziat, F.; Bouatra, S.; Rein, R. *J. Porphyrins Phthalocyanines*, **2008**, *12*, 1250.

(79) (a) Tashiro, K.; Aida, T. *Chem. Soc. Rev.*, **2007**, *36*, 189; (b) Hosseini, A.; Taylor, S.; Accorsi, G.; Armaroli, N.; Reed, C. A.; Boyd, P. D. W. *J. Am. Chem. Soc.*, **2006**, *128*, 15903; (c) Wu, -. Z. Q.; Shao, X.-B.; Li, C.; Hou, J.-L.; Wang, K.; Jiang, X.-K.; Li, Z.-T. *J. Am. Chem. Soc.*, **2005**, *127*, 17460.

(80) (a) Sun, D. Y.; Tham, F. S.; Reed, C. A.; Chaker, L.; Burgess, M.; Boyd, P. D. W. *J. Am. Chem. Soc.*, **2000**, *122*, 10704; (b) Sun, D. Y.; Tham, F. S.; Reed, C. A.; Chaker, L.; Boyd, P. D. W. *J. Am. Chem. Soc.*, **2002**, *124*, 6604.

(81) Ayabe, M.; Ikeda, A.; Shinkai, S.; Sakamoto, S.; Yamaguchi, K. *Chem. Commun.*, **2002**, 1032.

(82) (a) Fujita, M.; Tominaga, M.; Hori, A.; Therrien, B. *Acc. Chem. Res.*, **2005**, *38*, 369; (b) Severin, K. *Chem. Commun.*, **2006**, 3859; (c) Pluth, M. D.; Raymond, K. N. *Chem. Soc. Rev.*, **2007**, *36*, 161; (d) Northrop, B. H.; Zheng, Y. R.; Chi, K. W.; Stang, P. J. *Acc. Chem. Res.*, **2009**, *42*, 1554; (e) Therrien, B. *Eur. J. Inorg. Chem.*, **2009**, 2445.

(83) (a) Kim, D.; Lee, S.; Gao, G. H.; Kang, H. S.; Ko, J. *J. Organomet. Chem.*, **2010**, *695*, 111; (b) Oliveri, C. G.; Ulmann, P. A.; Wiester, M. J.; Mirkin, C. A. *Acc. Chem. Res.*, **2008**, *41*, 1618.

(84) (a) Boyd, P. D. W.; Reed, C. A. *Acc. Chem. Res.*, **2005**, *38*, 235; (b) Makha, M.; Purich, A.; Raston, C. L.; Sobolev, A. N. *Eur. J. Inorg. Chem.*, **2006**, 507; (c) Chen, C.-F. *Chem. Commun.*, **2011**, *47*, 1674.

(85) (a) Gras, M.; Barry, N. P. E.; Therrien, B.; Suss-Fink, G. *Inorg. Chim. Acta.*, **2011**, *371*, 59; (b) Gladkov, L. L.; Solovyov, K. N. *Spectrosc. Lett.*, **1986**, *19*, 905.

(86) (a) Macchioni, A.; Ciancaleoni, G.; Zuccaccia, C.; Zuccaccia, D. *Chem. Soc. Rev.*, **2008**, *37*, 479; (b) Li, D. Y.; Kagan, G.; Hopson, R.; Williard, P. G. *J. Am. Chem. Soc.*, **2009**, *131*, 5627.

(87) (a) Flamigni, L.; Talarico, A. M.; Ventura, B.; Rein, R.; Solladié, N. *Chem.-Eur. J.* **2006**, *12*, 701; (b) Lyons, D. M.; Mohanraj, J.; Accorsi, G.; Armaroli, N.; Boyd, P. D. W. *New J. Chem.*, **2011**, *35*, 632.

(88) (a) Armaroli, N.; Accorsi, G.; Song, F. Y.; Palkar, A.; Echegoyen, L.; Bonifazi, D.; Diederich, F. *ChemPhysChem*, **2005**, *6*, 732; (b) Bonifazi, D.; Accorsi, G.; Armaroli, N.; Song, F. Y.; Palkar, A.; Echegoyen, L.; Scholl, M.; Seiler, P.; Jaun, B.; Diederich, F. *Helv. Chim. Acta.*, **2005**, *88*, 1839.

(89) (a) Brettar, J.; Gisselbrecht, J. P.; Gross, M.; Solladie, N. *Chem. Commun.*, **2001**, 733; (b) Iengo, E.; Zangrando, E.; Alessio, E.; Chambron, J. C.; Heitz, V.; Flamigni, L.; Sauvage, J. P. *Chem.-Eur. J.*, **2003**, *9*, 5879; (c) Oliva, A. I.; Ventura, B.; Wurthner, F.; Camara-Campos, A.; Hunter, C. A.; Ballester, P.; Flamigni, L. *Dalton Trans.*, **2009**, 4023.

(90) (a) Imahori, H.; Yoshizawa, E.; Yamada, K.; Hagiwara, K.; Okada, T.; Sakata, Y. *J. Chem. Soc., Chem. Commun.,* **1995**, 1133; (b) Satake, A.; Kobuke, Y. *Tetrahedron,* **2005**, *61*, 13.

(91) Benesi, H. A.; Hildebrand, J. H. *J. Am. Chem. Soc.* **1949**, *71*, 2703.

(92) Flamigni, L.; Talarico, A. M.; Ventura, B. *J. Porphyrins Phthalocyanines* **2003**, *7*, 318.

(93) American Cancer Society, Global Cancer - Facts & Figures 2007, p. 1.

(94) Siegel, R.; Naishadham, D.; Jemal, A. *Ca-Cancer J Clin.*, **2013**, *63*, 11.

(95) (a) Sadler, P. J. *Adv. Inorg. Chem.,* **1991**, *36*, 1; (b) Clarke, M. J. *Coord. Chem. Rev.,* **2003**, *236*, 209.

(96) (a) Dyson, P. J.; Sava, G. *Dalton Trans.,* **2006**, 1929; (b) Rosenber.B; VanCamp, L.; Krigas, T. *Nature,* **1965**, *205*, 698.

(97) Boulikas, T.; Vougiouka, M. *Oncol. Rep.,* **2003**, *10*, 1663.

(98) Allardyce, C. S.; Dyson, P. J.; Ellis, D. J.; Heath, S. L. *Chem. Commun.* **2001**, 1396.

(99) Natile, G.; Coluccia, M. *Coord. Chem. Rev.,* **2001**, *216*, 383.

(100) Wong, E.; Giandomenico, C. M. *Chem. Rev.,* **1999**, *99*, 2451.

(101) (a) Köpf-Maier, P.; Köpf, H. *Chem. Rev.,* **1987**, *87*, 1137; (b) Caruso, F.; Rossi, M. *Mini-Rev. Med. Chem.,* **2004**, *4*, 49.

(102) (a) Bergamo, A.; Sava, G. *Dalton Trans.*, **2007**, 1267; (b) Hartinger, C. G.; Jakupec, M. A.; Zorbas-Seifried, S.; Groessl, M.; Egger, A.; Berger, W.; Zorbas, H.; Dyson, P. J.; Keppler, B. K. *Chem. Biodiv.,* **2008**, *5*, 2140.

(103) (a) Mestroni, G.; Alessio, E.; Santi, A. S.; Geremia, S.; Bergamo, A.; Sava, G.; Boccarelli, A.; Schettino, A.; Coluccia, M. *Inorg. Chim. Acta.,* **1998**, *273*, 62; (b) Erck, A.; Rainen, L.; Whileyma.J; Chang, I. M.; Kimball, A. P.; Bear, J. *Proc. Soc. Exp. Biol. Med.*, **1974**, *145*, 1278.

(104) Higgins, J. D.; Neely, L.; Fricker, S. *J. Inorg. Biochem.,* **1993**, *49*, 149.

(105) Elo, H.; Lumme, P. *Inorg. Chim. Acta.,* **1987**, *136*, 149.

(106) (a) Calamai, P.; Carotti, S.; Guerri, A.; Mazzei, T.; Messori, L.; Mini, E.; Orioli, P.; Speroni, G. P. *Anti-Cancer Drug Des.,* **1998**, *13*, 67; (b) Calamai, P.; Carotti, S.; Guerri, A.; Messori, L.; Mini, E.; Orioli, P.; Speroni, G. P. *J. Inorg. Biochem.,* **1997**, *66*, 103.

(107) Dabrowiak, J. C. *Meatls in Medicine*; J. Wiley & Sons, 2009.

(108) Sava, G.; Pacor, S.; Bergamo, A.; Cocchietto, M.; Mestroni, G.; Alessio, E. *Chem.-Biol. Interact.,* **1995**, *95*, 109.

(109) Bergamo, A.; Messori, L.; Piccioli, F.; Cocchietto, M.; Sava, G. *Invest. New Drugs.,* **2003**, *21*, 401.

(110) Reisner, E.; Arion, V. B.; Keppler, B. K.; Pombeiro, A. J. L. *Inorg. Chim. Acta.,* **2008**, *361*, 1569.

(111) Ang, W. H.; Dyson, P. J. *Eur. J. Inorg. Chem.,* **2006**, 4003.

(112) (a) Wang, F.; Chen, H. M.; Parsons, S.; Oswald, L. D. H.; Davidson, J. E.; Sadler, P. J. *Chem.-Eur. J.,* **2003**, *9*, 5810; (b) Peacock, A. F. A.; Sadler, P. J. *Chem.-Asian J.* **2008**, *3*, 1890.

(113) (a) Scolaro, C.; Bergamo, A.; Brescacin, L.; Delfino, R.; Cocchietto, M.; Laurenczy, G.; Geldbach, T. J.; Sava, G.; Dyson, P. J. *J. Med. Chem.,* **2005**, *48*, 4161; (b) Aird, R. E.; Cummings, J.; Ritchie, A. A.; Muir, M.; Morris, R. E.; Chen, H.; Sadler, P. J.; Jodrell, D. I. *Brit. J. Cancer,* **2002**, *86*, 1652.

(114) Süss-Fink, G. *Dalton Trans.,* **2010**, *39*, 1673.

(115) Smith, G. S.; Therrien, B. *Dalton Trans.,* **2011**, *40*, 10793.

(116) (a) Mendoza-Ferri, M.-G.; Hartinger, C. G.; Eichinger, R. E.; Stolyarova, N.; Severin, K.; Jakupec, M. A.; Nazarov, A. A.; Keppler, B. K. *Organometallics,* **2008**, *27*, 2405; (b) Mendoza-Ferri, M.-G.; Hartinger, C. G.; Nazarov, A. A.; Kandioller, W.; Severin, K.; Keppler, B. K. *Appl. Organomet. Chem.,* **2008**, *22*, 326.

(117) Magennis, S. W.; Habtemariam, A.; Novakova, O.; Henry, J. B.; Meier, S.; Parsons, S.; Oswald, I. D. H.; Brabec, V.; Sadler, P. J. *Inorg. Chem.,* **2007**, *46*, 5059.

(118) Giannini, F.; Furrer, J.; Ibao, A.-F.; Süss-Fink, G.; Therrien, B.; Zava, O.; Baquie, M.; Dyson, P. J.; Štěpnička, P. *J. Biol. Inorg. Chem.,* **2012**, *17*, 951.

(119) Gupta, G.; Garci, A.; Murray, B. S.; Dyson, P. J.; Fabre, G.; Trouillas, P.; Giannini, F.; Furrer, J.; Therrien, B. *Dalton Trans.,* **2013**, doi: 10.1039/C3DT51991K.

(120) Letavayová, L.; Vlčková, V.; Brozmanová, J. *Toxicology,* **2006**, *227*, 1.

(121) Rigobello, M. P.; Gandin, V.; Folda, A.; Rundlöf, A. K.; Fernandes, A. P.; Bindoli, A.; Marzano, C.; Björnstedt, M. *Free Radic. Biol. Med.,* **2009**, *47*, 710.

(122) (a) Rosenber.B; Vancamp, L.; Trosko, J. E.; Mansour, V. H. *Nature,* **1969**, *222*, 385; (b) Hoeschele, J. D. *Dalton Trans.,* **2009**, 10648.

(123) Baldew, G. S.; Van den Hamer, C. J. A.; Los, G.; Vermeulen, N. P. E.; Degoeij, J. J. M.; Mc Vie, J. G. *Cancer Res.,* **1989**, *49*, 3020.

(124) (a) Cunha, R. L. O. R.; Gouvea, I. E.; Juliano, L. *An. Acad. Bras. Cienc.* **2009**, *81*, 393; (b) Tiekink, E. R. T. *Dalton Trans.,* **2012**, *41*, 6390.

(125) Giannini, F.; Furrer, J.; Süss-Fink, G.; Clavel M, G.; Dyson, P. J. *J. Organomet. Chem.,* **2013**, *734*, 41.

(126) (a) Chérioux, F.; Thomas, C. M.; Therrien, B.; Süss-Fink, G. *Chem.-Eur. J.*, **2002**, *8*, 4377; (b) Chérioux, F.; Thomas, C. M.; Monnier, T.; Süss-Fink, G. *Polyhedron*, **2003**, *22*, 543; (c) Tschan, M. J. L.; Chérioux, F.; Therrien, B.; Süss-Fink, G. *Eur. J. Inorg. Chem.*, **2004**, 2405; (d) Boudreau, J.; Grenier-Desbiens, J.; Fontaine, F. G. *Eur. J. Inorg. Chem.*, **2010**, 2158.

(127) Mashima, K.; Kaneko, S.; Tani, K.; Kaneyoshi, H.; Nakamura, A. *J. Organomet. Chem.,* **1997**, *545*, 345.

(128) Mosmann, T. *J. Immunol. Methods*, **1983**, *65*, 55.

(129) (a) Harris, A. L.; Yang, X. H.; Hegmans, A.; Povirk, L.; Ryan, J. J.; Kelland, L.; Farrell, N. P. *Inorg. Chem.,* **2005**, *44*, 9598; (b) Therrien, B.; Süss-Fink, G.; Govindaswamy, P.; Renfrew, A. K.; Dyson, P. J. *Angew. Chem. Int. Ed.,* **2008**, *47*, 3773.

(130) Xu, K.; Liang, X.; Wang, F.; Xie, L.; Xu, Y.; Liu, J.; Qian, X. *Anti-Cancer Drugs*, **2011**, *22*, 875.

(131) (a) Taimen, P.; Kallajoki, M. *J. Cell Sci.* **2003**, *116*, 571; (b) Schwartz, L. M.; Smith, S. W.; Jones, M. E. E.; Osborne, B. A. *P. Natl. Acad. Sci. USA.*, **1993**, *90*, 980.

(132) Ramakrishnan, S.; Palaniandavar, M. *J. Chem. Sci.,* **2005**, *117*, 179.

(133) Wang, B. D.; Yang, Z. Y.; Crewdson, P.; Wang, D. Q. *J. Inorg. Biochem.,* **2007**, *101*, 1492.

(134) Arjmand, F.; Aziz, M. *Eur. J. Med. Chem.,* **2009**, *44*, 834.

(135) Parkinson, G. N.; Ghosh, R.; Neidle, S. *Biochemistry*, **2007**, *46*, 2390.

(136) Satyanarayana, S.; Dabrowiak, J. C.; Chaires, J. B. *Biochemistry,* **1993**, *32*, 2573.

(137) Pratviel, G.; Bernadou, J.; Meunier, B. *Adv. Inorg. Chem.,* **1998**, *45*, 251.

(138) Mann, B. E.; Motterlini, R. *Chem. Commun.,* **2007**, 4197.

(139) Mann, B. E. *Top. Organomet. Chem.,* **2010**, *32*, 247.

(140) (a) Johnson, T. R.; Mann, B. E.; Teasdale, I. P.; Adams, H.; Foresti, R.; Green, C. J.; Motterlini, R. *Dalton Trans.,* **2007**, 1500; (b) Smith, H.; Mann, B. E.; Motterlini, R.; Poole, R. K. *IUBMB Life* **2011**, *63*, 363.

(141) Bathoorn, E.; Siebos, D. J.; Postma, D. S.; Koeter, G. H.; van Oosterhout, A. J. M.; van der Toorn, M.; Boezen, H. M.; Kerstjens, H. A. M. *Eur. Respir. J.*, **2007**, *30*, 1131.

(142) (a) Farrer, N. J.; Sadler, P. J. *State of the art, new trends, and a vision of the future, in Bioinorganic Medicinal Chemistry*; Ed. E. Alessio, Wiley-VCH, Weinheim, Germany, 2011, pp. 1-47; (b) Bratsos, I.; Gianferrara, T.; Alessio, E.; Hartinger, C. G.; Jakupec, M. A.; Keppler, B. K. *Ruthenium and other non-platinum anticancer compounds, in Bioinorganic Medicinal Chemistry*; Ed. E. Alessio, Wiley-VCH, Weinheim, Germany, 2011, pp. 151-174; (c) Ang, W. H.; Casini, A.; Sava, G.; Dyson, P. J. *J. Organomet. Chem.*, **2011**, *696*, 989.

(143) (a) Lavigne, G. *Eur. J. Inorg. Chem.*, **1999**, 917; (b) Bruce, M. I. *Coord. Chem. Rev.*, **1987**, *76*, 1.

(144) Gras, M.; Barry, N. P. E.; Therrien, B.; Süss-Fink, G. *Inorg. Chim. Acta.*, **2011**, *371*, 59.

(145) Johnpeter, J. P.; Schmitt, F.; Denoyelle-Di-Muro, E.; Wagnieres, G.; Juillerat-Jeanneret, L.; Therrien, B. *Inorg. Chim. Acta.*, **2012**, *393*, 246.

(146) (a) Enomoto, A.; Kimura, H.; Chairoungdua, A.; Shigeta, Y.; Jutabha, P.; Cha, S. H.; Hosoyamada, M.; Takeda, M.; Sekine, T.; Igarashi, T.; Matsuo, H.; Kikuchi, Y.; Oda, T.; Ichida, K.; Hosoya, T.; Shimokata, K.; Niwa, T.; Kanai, Y.; Endou, H. *Nature*, **2002**, *417*, 447; (b) Detjen, K. M.; Welzel, M.; Wiedenniann, B.; Rosewicz, S. *Int. J. Cancer* **2003**, *107*, 844.

(147) (a) Duffy, C. P.; Elliott, C. J.; O'Connor, R. A.; Heenan, M. M.; Coyle, S.; Cleary, I. M.; Kavanagh, K.; Verhaegen, S.; O'Loughlin, C. M.; NicAmhlaoibh, R.; Clynes, M. *Eur. J. Cancer*, **1998**, *34*, 1250; (b) Rayburn, R. E.; Ezell, S. J.; Zhang, R. *Mol. Cell. pharmacol.*, **2009**, *1*, 29.

(148) (a) Stein, J. A.; Brownell, I. *J. Drugs. Dermatol.*, **2008**, *7*, 175; (b) Lorigan, P.; Eisen, T.; Hauschild, A. *Exp Dermatol* **2008**, *17*, 383; (c) Davids, L. M.; Kleemann, B. *Cancer. Treatment. Rev.*, **2011**, *37*, 468.

(149) (a) Detty, M. R.; Gibson, S. L.; Wagner, S. J. *J. Med. Chem.*, **2004**, *47*, 3897; (b) Schmitt, F.; Juillerat-Jeanneret, L. *Anti-Cancer Agents Med. Chem.*, **2012**, *12*, 500.

(150) (a) Almeida, R. D.; Manadas, B. J.; Carvalho, A. P.; Duarte, C. B. *Biochem. Biophys. Acta* **2007**, *1704*, 59; (b) Buytaert, E.; Dewaele, M.; Agostinis, P. *Biochim. Biophys.*

Acta, **2007**, *1776*, 86; (c) Dolmans, D. E. J. G. J.; Fukumura, D.; Jain, R. K. *Nat. Rev. Cancer* **2003**, *3*, 380.

(151) Vrouenraets, M. B.; Visser, G. W. M.; Snow, G. B.; van Dongen, G. A. M. S. *Anticancer Res.* **2003**, *23*, 505.

(152) Castano, A. P.; Demidova, T. N.; Hamblin, M. R. *Photodiagn. Photodyn.Ther.*, **2004**, *1*, 279.

(153) Figge, F. H. J.; Weiland, G. S.; Manganiello, L. O. J. *Proc. Soc. Exp. Biol. Med.*, **1948**, *68*, 640.

(154) Bonnett, R. *Rev. Contemp. Pharmacother.*, **1999**, *10*, 1.

(155) Wagnières, G.; Hadjur, C.; Grosjean, P.; Braichotte, D.; Savary, J.-F.; Monnier, P.; van den Bergh, H. *Photochem. Photobiol.*, **1998**, *68*, 382.

(156) (a) Kiesslich, T.; Neureiter, D.; Alinger, B.; Jansky, G. L.; Berlanda, J.; Mkrtchyan, V.; Ocker, M.; Plaetzer, K.; Berr, F. *Photochem. Photobiol. Sci.*, **2010**, *9*, 734; (b) Zellweger, M.; Grosjean, P.; Monnier, P.; van den Bergh, H.; Wagnieres, G. *Photochem. Photobiol.*, **1999**, *69*, 605.

(157) (a) Nyman, E. S.; Hynninen, P. H. *J. Photoch. Photobio. B*, **2004**, *73*, 1; (b) Vrouenraets, M. B.; Visser, G. W. M.; Stewart, F. A.; Stigter, M.; Oppelaar, H.; Postmus, P. E.; Snow, G. B.; van Dongen, G. A. M. S. *Cancer Res.*, **1999**, *59*, 1505; (c) Gravier, J.; Schneider, R.; Frochot, C.; Bastogne, T.; Schmitt, F.; Didelon, J.; Guillemin, F.; Barberi-Heyob, M. *J. Med. Chem.*, **2008**, *51*, 3867; (d) El-Akra, N.; Noirot, A.; Faye, J. C.; Souchard, J.-P. *Photochem. Photobiol. Sci.*, **2006**, *5*, 996; (e) Akhlynina, T. V.; Rosenkranz, A. A.; Jans, D. A.; Gulak, P. V.; Serebryakova, N. V.; Sobolev, A. S. *Photochem. Photobiol.*, **1993**, *58*, 45.

(158) Allison, R. R.; Downie, G. H.; Cuenca, R.; Hu, X.-H.; Childs, C. J. H.; Sibata, C. H. *Photodiagn. Photodyn.Ther.*, **2004**, *1*, 27.

(159) Kelland, L. *Nat. Rev. Cancer* **2007**, *7*, 573.

(160) Abu-Surrah, A. S.; Kettunen, M. *Curr. Med. Chem.*, **2006**, *13*, 1337.

(161) (a) Goldhirsch, A.; Greiner, R.; Dreher, E.; Locher, G.; Davis, B. W.; Reinhard, J.-P.; Joss, R.; Brunner, K. W. *Onkologie*, **1985**, *8*, 383; (b) Goldhirsch, A.; Greiner, R.; Dreher, E.; Sessa, C.; Krauer, F.; Forni, M.; Jungi, F. W.; Brunner, K. W.; Veraguth, P.; Engeler, V.; Leyvraz, S.; Siegenthaler, P.; Gloor, E.; Buser, K.; Gelber, R. D.; Cavalli, F. *Cancer*, **1988**, *62*, 40.

(162) (a) Lottner, C.; Bart, K. C.; Bernhardt, G.; Brunner, H. *J. Med. Chem.,* **2002**, *45*, 2079; (b) Lottner, C.; Bart, K. C.; Bernhardt, G.; Brunner, H. *J. Med. Chem.,* **2002**, *45*, 2064.

(163) van Rijt, S. H.; Sadler, P. J. *Drug. Discov. Today,* **2009**, *14*, 1089.

(164) (a) Schmitt, F.; Govindaswamy, P.; Süss-Fink, G.; Ang, W. H.; Dyson, P. J.; Juillerat-Jeanneret, L.; Therrien, B. *J. Med. Chem.,* **2008**, *51*, 1811; (b) Schmitt, F.; Govindaswamy, P.; Zava, O.; Süss-Fink, G.; Juillerat-Jeanneret, L.; Therrien, B. *J. Biol. Inorg. Chem.,* **2009**, *14*, 101.

(165) (a) Davia, K.; King, D.; Hong, Y. L.; Swavey, S. *Inorg. Chem. Commun.,* **2008**, *11*, 584; (b) Sweigert, P.; Xu, Z. M.; Hong, Y. L.; Swavey, S. *Dalton Trans.,* **2012**, *41*, 5201.

(166) (a) Gianferrara, T.; Bratsos, I.; Iengo, E.; Milani, B.; Oštrić, A.; Spagnul, C.; Zangrando, E.; Alessio, E. *Dalton Trans.,* **2009**, 10742; (b) Gianferrara, T.; Bergamo, A.; Bratsos, I.; Milani, B.; Spagnul, C.; Sava, G.; Alessio, E. *J. Med. Chem.,* **2010**, *53*, 4678.

(167) Johnpeter, J. P.; Mohanraj, J.; Armaroli, N.; Therrien, B. *Eur. J. Inorg. Chem.,* **2012**, 3449.

(168) Davids, L. M.; Kleemann, B. *Cancer. Treatment. Rev.,* **2011**, *37*, 465.

(169) (a) Wu, D. H.; Chen, A. D.; Johnson, C. S. *J. Magn. Reson. Ser. A,* **1995**, *115*, 260; (b) Jr Johnson, C. S. *Prog. Nucl. Magn. Reson. Spectrosc.,* **1999**, *34*, 203; (c) Furrer, J. *J. Nat. Prod.,* **2009**, *72*, 1437; (d) Barry, N. P. E.; Furrer, J.; Therrien, B. *Helv. Chim. Acta.,* **2010**, *93*, 1313.

(170) Isaacs, N. S.; Sharp, A.; Safety procedures for high-presure systems. In high-presure techniques in chemstry and physics, W. B. Holzapful, N. S. Isaacs (Eds), Oxford university press, 1997, pp 381-384,.

(171) De Angelis, P. M.; Svendsrud, D. H.; Kravik, K. L.; Stokke, T. *Mol. Cancer.,* **2006**, *5*, 1.

(172) Sheldrick, G. M. *Acta Crystallogr A.,* **2008**, *64*, 112.

(173) Farrugia, L. J. *J. Appl. Crystallogr.,* **1997**, 565.

List of abbreviations

thf = tetrahydrofuran

CCl_4 = carbon tetrachloride

CH_2Cl_2 = dichloromethane

bpy = 2,2'-bipyridine

biisoq = 1,1'-biisoquinoline

dppe = 1,2-bis(diphenylphosphino)ethane

cyclop = 1,2-bis(diphenylphosphinomethyl)cyclohexane

diop = 4,5-bis(diphenyl-phosphinomethyl)-2,2-dimethyl-1,3-dioxolane

$scCO_2$ = supercritical carbon dioxide

STP = standard temperature and pressure

TOF = catalytic turnover frequencies

TON = catalytic turnover number

BARF = tetrakis-{3,5-bis(trifluoromethyl)phenyl}borate

CF_3SO_3 = trifluoromethanesulfonate

binap = 2,2'-bis(diphenylphosphino)-1,1'-binaphthyl

dmpe = $(CH_3)_2P(CH_2)_2P(CH_3)_2$

dppe = $(C_6H_5)_2P(CH_2)_2P(C_6H_5)_2$

dfppe = $\{CF_3(CF_2)_5(p\text{-}C_6H_4)\}_2P(CH_2)_2P\{(p\text{-}C_6H_4)(CF_2)_5CF_3\}_2$

PTA = 1,3,5-triaza-7-phosphatricyclo[3.3.1.1]decane

PPh_3 = triphenylphosphine

pyr = pyridine

C_{60} = fullerene

bpy = 4,4'-bipyridine

bpe = 1,2-bis(4-pyridyl)ethylene

5,10-dpp = 5,10-bis(4-pyridyl)-15,20-di-phenyl-21H,23H-porphyrin

5,15-dpp = 5,15-bis(4-pyridyl)-10,20-diphenyl-21H,23H-porphyrin

ESI-MS = electrospray mass spectrometry

UV-Vis = ultraviolet-visible spectroscopy

DOSY = diffusion ordered spectroscopy

NAMI-A = imidazolium *trans*-[imidazoledimethylsulfoxide-tetrachlororuthenate(III)]

KP1019 = indazolium-*trans*-[tetrachlorobis(1H-indazole)ruthenate(III)]

RAPTA-C = $[(\eta^6\text{-}p\text{-}MeC_6H_4Pr^i)Ru(PTA)Cl_2]$

RM175 = $[(C_6H_5Ph)Ru(en)Cl][PF_6]$

en = ethane-1,2-diamine

Me = methyl group

dpp = 2,3-bis(2-pyridyl)pyrazine

IR = infrared spectroscopy

MTT = 3-(4,5-dimethyl-2-thiazoyl)-2,5-diphenyltetrazolium bromide

IC_{50} = drug concentration necessary for 50% inhibition of cell survival

LD_{50} = laser light dose necessary to inhibit 50 % cell survival

DMSO = dimethyl sulfoxide

FDA = food and drug administration

PDT = Photodynamic therapy

List of Publications

1. $Ru_2(CO)_4\{OOC(CH_2)_nCH_3\}_2L_2$ sawhorse-type complexes containing μ_2-η^2-carboxylato ligands derived from saturated fatty acids. **J. P. Johnpeter**, B. Therrien, *J. Struct. Chem.*, **2011**, *52*, 151.
2. Sawhorse-type tetracarbonyl diruthenium tweezers. **J. P. Johnpeter**, J. Mohanraj, N. Armaroli, B. Therrien, *Eur. J. Inorg. Chem.*, **2012**, *21*, 3449.
3. Photoactive sawhorse-type diruthenium tetracarbonyl complexes. **J. P. Johnpeter**, F. Schmitt, E. Denoyelle-Di-Muro, G. Wagnières, L. Juillerat-Jeanneret, B. Therrien, *Inorg. Chim. Acta*., **2012**, *393*, 246.
4. Sawhorse-type diruthenium tetracarbonyl complexes containing biologically relevant acids. **J. P. Johnpeter**, B. Therrien, *Inorg. Chim. Acta*., **2013**, *394*, 723.
5. Catalytic and anticancer activity of sawhorse-type diruthenium tetracarbonyl complexes derived from fluorinated fatty acids. **J. P. Johnpeter**, L. Plasseraud, F. Schmitt, L. Juillerat-Jeanneret, B. Therrien, *J. Coord. Chem*., **2013**, *66*, 1753.
6. Sawhorse-type diruthenium tetracarbonyl complexes derived from pyrenyl-carboxylic acids. **J. P. Johnpeter**, B. Therrien. *Inorg. Chim. Acta*., **2013**, *405*, 437.
7. Biological studies of chalcogenolato-bridged dinuclear half-sandwich complexes. **J. P. Johnpeter**, G. Gupta, J. M. Kumar, G. Srinivas, N. Nagesh, B. Therrien. *Inorg. Chem*., ***In press***.